

**EXPERIMENTAL INVESTIGATION OF CONCENTRATION  
DEPENDENT NON-IDEAL DIFFUSION IN HYDROCARBON  
SYSTEMS**

by

© Ebubechi Azubuike Evulukwu

A Thesis submitted to the

School of Graduate Studies

In partial fulfillment of the requirements for the degree of

**Masters of Engineering**

**Faculty of Engineering**

Memorial University of Newfoundland

**August 2015**

St. John's

Newfoundland and Labrador

# **ABSTRACT**

Solvent extraction technology (Vapor extraction/VAPEX) has drawn a lot of industry attention due to its potential to be an alternative to Steam assisted Gravity Drainage (SAGD) in heavy oil production. However the mass transfer mechanisms involved is yet to be fully comprehended. Reliable oil production rate data is scarce, hence the reluctance from oil companies to implement the technology on a field/commercial scale. More work is required at the experimental level to fully understand the intricacies of the technology and hence facilitate its commercialization.

Experiments were conducted to evaluate the one-dimensional diffusivity of butane solvent in Athabasca bitumen at varying temperatures. Given diffusion is driven by concentration gradient, the diffusivity cannot be assumed constant throughout the whole diffusion process. Hence the diffusivity was found as a function of butane solvent concentration (mass fraction). Diffusivity functions for ideal mixing and non-ideal mixing were computed. Butane vapor temperature (24.00°C and 34.65 psi) is kept constant while the bitumen temperature is varied at 5 levels (27.00°C, 30.25°C, 33.50°C, 36.75°C and 40.00°C).

Assuming ideal mixing between hydrocarbons in VAPEX experiments is prevalent in the field. This is because finding a parameter in the solvent-bitumen mixing system that accounts for non-ideal mixing without upsetting the system is difficult. This work accounts for non-ideal mixing by constantly measuring the bitumen liquid hydrostatic pressure via pressure differential transmitters as diffusion occurs. With bitumen height change and amount of diffused butane solvent being monitored, the real density reduction (non-ideal density reduction) can be computed. Results showed that assuming ideal mixing over-estimates the density reduction. The deviation between ideal and non-ideal mixing density values increase as temperature increases. This is supported by most literature in the field. As temperature tends to standard temperature (25.00°C), the effects of non-ideal mixing become insignificant.

A MATLAB model is used to predict the ‘bitumen growth’ (bitumen swelling), this is compared to ‘bitumen growth’ observed experimentally. The difference between the two (experimental –

predicted) is minimized by optimizing the diffusivity function coefficients. Results showed that the diffusion values (obtained via diffusivity functions) decreases as temperature increases. There was no ‘live oil’ drainage in this experiment so diffusion is governed by the butane solvent solubility in the bitumen. This butane solvent solubility decreases with increasing temperature.

At equal mass fractions ( $\omega_s$ ) all non-ideal mixing diffusivity functions yielded higher diffusion values than ideal mixing diffusivity functions. This is logical because diffusion is driven by concentration gradient. Ideal mixing scenarios over-estimate density reduction on mixing and hence provide a smaller concentration gradient compared to non-ideal mixing. The assumption of ideal mixing conditions clearly underestimates the real diffusivity values. The deviation between ideal and non-ideal diffusivity functions also increased as temperature increased. This follows the same trend as the deviation between ideal and non-ideal mixing density results.

A macroscopic mass balance was used to independently validate the diffusivity functions. This mass balance predicted the change in solvent height after ‘bitumen growth’ had been resolved for the full experimental time. This is an independent validation because change in solvent height data was not used to obtain the diffusivity functions. All but one of the diffusivity functions (40.00°C) was independently validated. Lack of validation in the 40.00°C run was due to technical issues while running the experiment. For all validation data, the non-ideal diffusivity functions provided a better fit for the experimental data than the ideal diffusivity functions.

Finally, the experimentally determined butane slope decrease, bitumen slope increase and non-ideal mixing coefficients for all varied temperature conditions were used as input values to make models in Design Expert (DE). These models were used to predict the aforementioned parameters at a random bitumen temperature (28.50°C). An extra experiment was run at this temperature (28.50°C) to compare the diffusivity functions coming from the experimental data to those from (DE) predictions. The DE originated diffusivities functions showed a good fit with the experimentally originated diffusivity functions. The model is therefore a robust model and can be used to predict diffusivity of butane at 24.00°C, within a given bitumen temperature range of 27.00°C - 40.00°C, while also accounting for non-ideal mixing and concentration dependency.

# **ACKNOWLEDGEMENTS**

I would first like to thank the Lord God almighty for his guidance. Completing this thesis easily ranks as the most challenging thing I have done to date in my life. So many times I thought I would never be able to complete this work, yet he also somehow gave me the strength and motivation to keep plugging away.

I would also like to thank my family (Mommy, Daddy, Chike, Ugo and Iheanyi), who consistently served as my support system while completing this thesis. I felt a jolt of motivation after every phone call, email and skype video conversation with them.

I would like to thank Lesley (my professor) for her guidance along with her team; Edison, Shervin, Mohammed, Xiaolong and Kim. Would also like to thank the guys from Technical services and Brian at the glass blowing shop for all the help they gave me with putting my equipment together.

I hope this work serves as an inspiration to many and contributes to the eventual development of solvent extraction technology on a commercial scale.

# **TABLE OF CONTENTS**

LIST OF TABLES	vii
LIST OF FIGURES	viii
APPENDIX	xi
NOMENCLATURE	xii
1) INTRODUCTION	1
1.1. World Heavy Oil Overview	2
1.2. Canadian Perspective	5
1.3. In-situ Extraction Methods for Bitumen	8
1.3.1. Cyclic Steam Stimulation	9
1.3.2. SAGD	11
1.3.3. VAPEX	14
1.3.4. N-Solv	16
1.3.5. Hybrid Processes	17
1.4. Technological Impacts	19
1.5. Scope of Research	21
2) LITERATURE REVIEW	23
2.1. History of VAPEX Experiments	23
2.2. Viscosity correlations	46
2.3. Diffusivity/Diffusion coefficient	52
2.2.1. Constant diffusion coefficient methods	54
2.2.1.1. Pressure decay methods	54
2.2.1.2. Dynamic Pendant Drop Shape Analysis (DPDSA)	59
2.2.1.3. Computer Assisted Tomography (CAT)	60
2.2.1.4. Nuclear Magnetic Resonance (NMR)	65
2.2.2. Mutual diffusion coefficient	68
2.2.3. Concentration dependent diffusivity methods	70
2.4. Non-ideal mixing of solvent and oil	78
2.5. This work	85
3) EXPERIMENTAL METHODOLOGY	88

3.1. Experimental overview	88
3.2. Equipment set-up	89
3.2.1. Butane Loading	90
3.2.2. Bitumen Loading	92
3.2.3. Solvent gas phase purity and vacuum creation	96
3.2.4. Run procedure	101
3.2.5. Troubleshooting	103
4) NUMERICAL METHODOLOGIES	104
4.1. Bitumen/Butane Density and Pressure Calculations	104
4.1.1. Non-ideal mixture density	104
4.1.2. Ideal mixture density	107
4.2. Bitumen height analysis	108
4.3. Solvent Continuity and Diffusivity Calculations	115
4.3.1. Diffusivity equations	115
4.3.2. Accounting for non-ideal mixing	116
4.3.3. Butane solvent solubility in bitumen	121
4.4. Using Design Expert	123
5) DISCUSSION OF RESULTS	126
5.1. Butane solvent height changes as a function of time	126
5.2. Bitumen height changes as a function of time	130
5.3. Ideal & non-ideal mixing density results	135
5.4. Diffusivity results	140
5.4.1. Diffusivity functions	141
5.4.2. Butane solvent mass fraction profile and bitumen density profile	142
5.4.3. Ideal and non-ideal mixing comparisons	144
5.4.4. Temperature comparisons	153
5.4.5. Diffusivity results validation	159
5.5. Design expert correlation results	165
5.5.1. Butane solvent decrease results	165
5.5.2. Bitumen increase results	169

5.5.3. Non-ideal mixing results -----	172
5.5.4. Diffusivity results and validation-----	174
5.6. Experimental Error -----	181
6) CONCLUSIONS AND RECOMMENDATIONS -----	188
6.1. Conclusions -----	188
6.2. Recommendations -----	189
7) REFERENCES-----	191
APPENDIX-----	198
APPENDIX A - Bitumen assay characteristics -----	198
APPENDIX B - Troubleshooting -----	201
APPENDIX C - Starting experimental values -----	207
APPENDIX D - Bitumen/Butane density and pressure calculations -----	207
APPENDIX E - Bitumen height analysis table -----	215
APPENDIX F - Specific volume graphs (all temperatures) -----	216
APPENDIX G - Butane/Bitumen changes as function of time calculations -----	218
APPENDIX H - Design expert ANOVA tables -----	222
APPENDIX I - Matlab code & diffusivity function results -----	223
APPENDIX J - Solvent concentration profiles (non-ideal)-----	240
APPENDIX K - Density profiles (non-ideal) -----	244
APPENDIX L - Extra Validation temperatures data -----	248

# **LIST OF TABLES**

Table 1-1 - Heavy Oil Deposits in Utah (Speight 2013b) .....	4
Table 2-1 - Experimental results (Das and Butler 1994) .....	25
Table 2-2 - Total Oil production - Free fall and Diluted Oil (Haghighat and Maini 2013) .....	45
Table 2-3 - Diffusivity of C <sub>3</sub> H <sub>8</sub> in heavy oil at different diffusion time 23.9°C (Tharanivasan <i>et al.</i> 2006)..	57
Table 2-4 - Diffusion coefficient of solvents in oils (Wen <i>et al.</i> 2013) .....	67
Table 2-5 - Results for multi-component fluid at 422k & 15 MPa (Leahy-Dios and Firoozabadi 2007) .....	83
Table 4-1- Sample calculation for non-ideal density .....	104
Table 4-2 - Sample calculations for ideal density .....	107
Table 4-3 - Notation for bitumen height analysis .....	109
Table 4-4 - Difference in left tube pixel points from time t = 0 minutes and t = 660 minutes .....	114
Table 4-5 - Non-ideal mixing specific volume expressions .....	120
Table 4-6 - Full list of solubility limits at different conditions .....	123
Table 5-1 - Tabulated values for butane solvent decrease data (t = 0 and t ≠ 0) .....	129
Table 5-2 - Tabulated values for bitumen increase data (t = 0 and t ≠ 0).....	133
Table 5-3 - SRT graph slope comparisons between James (2009) and this work.....	135
Table 5-4 - Ideal and non-ideal mixing density results .....	139
Table 5-5 - Non-ideal mixing specific volume expressions .....	140
Table 5-6 - Diffusivity functions for all temperatures (ideal and non-ideal) .....	141
Table 5-7 - Table showing % difference between ideal and non-ideal diffusion values .....	147
Table 5-8 - Validation data for butane solvent height decrease at all temperatures .....	164
Table 5-9 - Butane solvent height decrease data (28.50°C) .....	166
Table 5-10 - Comparison of 28.50°C butane decrease graph data to other temperatures.....	169
Table 5-11 - Bitumen height increase graph data (28.50°C).....	170
Table 5-12 - Comparison of 28.50°C bitumen increase graph data to other temperatures.....	172
Table 5-13 - Non-ideal mixing expression (28.50°C) vs other temperatures.....	174
Table 5-14 - Diffusivity results (28.50°C).....	174
Table 5-15 - Comparison of ideal/non-ideal diffusivity function deviation for 28.50°C.....	177
Table 5-16 - Standard deviations for temperature logging of all experimental runs .....	182

# **LIST OF FIGURES**

Figure 1-1 - Resource Pyramid focusing on Unconventional resources (Rajnauth 2012) .....	2
Figure 1-2 - Global heavy oil resources (Law 2011) .....	3
Figure 1-3 - Orinoco Belt Venezuela (EIA 2014a) .....	4
Figure 1-4 - Schematic of Alberta’s Oilsand deposits (Lunn 2013) .....	6
Figure 1-5 - Schematic of Alberta’s and Saskatchewan’s deposits (Nasr and Ayodele 2005) .....	7
Figure 1-6 - Typical CSS system (Lunn 2013) .....	10
Figure 1-7 - Typical SAGD set-up (Lunn 2013) .....	12
Figure 1-8 - Cross sectional schematic of SAGD process (Irani and Gates 2013) .....	13
Figure 1-9 - Cross section of VAPEX system (James 2009) .....	15
Figure 1-10 - N-Solv Process (Stickler 2009) .....	17
Figure 2-1 - Schematic of experimental Set-up (Jiang 1997) .....	26
Figure 2-2 - Change in VAPEX position with time for one of the models (James and Chatzis 2004) .....	30
Figure 2-3 - VAPEX interface and concentration profiles (James <i>et al.</i> 2007) .....	34
Figure 2-4 - VAPEX interface advancement for 92cm High Model (James and Chatzis 2005) .....	35
Figure 2-5 - Dispersion coefficient vs. permeability for all runs (El-Haj 2007) .....	37
Figure 2-6 - Mass transfer coefficient for various models (James and Chatzis 2007) .....	38
Figure 2-7 - Graph of Dispersion coefficient vs mass fraction (Abukhalifeh <i>et al.</i> 2009) .....	40
Figure 2-8 - Diffusion coefficient vs. Kinematic viscosity (Okazawa 2009) .....	42
Figure 2-9 - Oil production via gravity drainage w/wo dissolution (Haghighat and Maini 2013) .....	44
Figure 2-10 - Calculated viscosities vs. observed viscosities (Shu 1984) .....	47
Figure 2-11 - Comparison of viscosity predictions with various correlations (Yazdani and Maini 2010) .....	50
Figure 2-12 - Concentration dependence of viscosity and diffusivity (Das and Butler 1996) .....	51
Figure 2-13 - Concentration dependency of viscosity & diffusivity butane (Yazdani and Maini 2009) .....	52
Figure 2-14 - Pressure decay schematic (Zhang <i>et al.</i> 2000) .....	55
Figure 2-15 - Pressure decay graph (Zhang <i>et al.</i> 2000) .....	55
Figure 2-16 - Schematic diagram of the pressure cell set-up (Behzadfar and Hatzikiriakos 2014) .....	58
Figure 2-17 - DPDSA set-up (Yang and Gu 2006) .....	59
Figure 2-18 - CT images of a sand pack sample (Luo and Kantzas 2008) .....	63
Figure 2-19 - CT Scan at different times (Luo and Kantzas 2008) .....	63
Figure 2-20 - CT converted concentration profile at time 667 minutes (Luo and Kantzas 2008) .....	64
Figure 2-21 - Diffusivity in Heavy oil for bulk fluids and porous fluids (Luo and Kantzas 2008) .....	64
Figure 2-22 - Typical NMR spectra for bitumen, pure solvent and a mixture (Wen <i>et al.</i> 2013) .....	66
Figure 2-23 - Spectra change during diffusion (Wen <i>et al.</i> 2013) .....	67
Figure 2-24 - Solvent decrease (experimental vs model results) (James 2009) .....	78
Figure 2-25 - BIP for bitumen vs. temperature (Saryazdi <i>et al.</i> 2013) .....	81
Figure 2-26 - Infinite dilution diffusivity: experimental & computed (Leahy-Dios and Firoozabadi 2007) .....	84
Figure 2-27 - Ideal/non ideal mixture density vs. solvent volume fraction at 40°C (Etminan <i>et al.</i> 2011) .....	85
Figure 3-1 - Simplified schematic of experiment .....	88

Figure 3-2- Workflow diagram for experiment.....	89
Figure 3-3 - Butane loading set-up.....	90
Figure 3-4 - Schematic of butane side .....	91
Figure 3-5 - Butane side of one-dimensional diffusion experiment .....	92
Figure 3-6 - Schematic of bitumen side .....	93
Figure 3-7 - Schematic of bitumen loading.....	94
Figure 3-8 - Magnified schematic of bitumen loading.....	95
Figure 3-9 - Bitumen side.....	96
Figure 3-10 - Bitumen height pictures during vacuum creation (A) and at start of experiment (B) .....	99
Figure 3-11 - A side by side look at both L-tubes (during A and B) and R-tubes (during A and B) .....	99
Figure 3-12 - Full experimental set-up.....	100
Figure 3-13 - Detailed experimental schematic (butane and bitumen side together) .....	100
Figure 4-1 - Picture of bitumen height at $t = 0$ minutes .....	109
Figure 4-2 - Picture of bitumen height at time $t = 660$ minutes (11 hours).....	113
Figure 4-3 - Bitumen mixture specific volume plots for ideal and non-ideal mixing.....	117
Figure 4-4 - Non-ideal mixing coefficients at varying temperatures .....	120
Figure 4-5 - Solvent solubility at varying experimental conditions .....	122
Figure 5-1- Butane height decrease vs. time (all temperatures) .....	127
Figure 5-2 - Butane solvent decrease vs SRT for $t = 0$ and $t \neq 0$ .....	128
Figure 5-3 - Butane height decrease vs. SRT (all temperatures).....	130
Figure 5-4- Bitumen height increase vs. time (all temperatures).....	131
Figure 5-5 - Bitumen increase vs SRT for $t = 0$ and $t \neq 0$ .....	132
Figure 5-6 - Bitumen height increase vs. SRT (all temperatures) .....	134
Figure 5-7 - Mixture densities vs. time (all temperatures) .....	136
Figure 5-8 - Mixture density vs. solvent mass fraction (40.00°C) .....	137
Figure 5-9 - Mixture density vs. solvent mass fraction (36.75°C) .....	137
Figure 5-10 - Mixture density vs. solvent mass fraction (33.50°C) .....	138
Figure 5-11 - Mixture density vs. solvent mass fraction (30.25°C) .....	138
Figure 5-12- Mixture density vs. solvent mass fraction (27.00°C) .....	139
Figure 5-13 - Butane solvent mass fraction profile at 27.00°C (non-ideal) .....	142
Figure 5-14 - Bitumen density profile at 27.00°C (non-ideal) .....	144
Figure 5-15- Solvent diffusivity functions at 27.00°C.....	145
Figure 5-16 - Solvent diffusivity functions at 33.50°C.....	146
Figure 5-17 - Solvent diffusivity functions at 40.00°C.....	146
Figure 5-18 - Ideal and non-ideal butane solvent mass fraction profile at 27.00°C .....	148
Figure 5-19 - Ideal and non-ideal butane solvent mass fraction profile at 33.50°C .....	149
Figure 5-20 - Ideal and non-ideal butane solvent mass fraction profile at 40.00°C .....	150
Figure 5-21 - Ideal and non-ideal bitumen density profile at 27.00°C.....	151
Figure 5-22 - Ideal and non-ideal bitumen density profile at 33.50°C.....	152
Figure 5-23 - Ideal and non-ideal bitumen density profile at 40.00°C.....	152

Figure 5-24- Non-ideal diffusivity functions at all temperatures.....	153
Figure 5-25 - Solvent mass fraction profile at 60 minutes for all temperatures .....	155
Figure 5-26 - Bitumen density profile at 60 minutes for all temperatures.....	156
Figure 5-27 - Solvent mass fraction profile at 2000 minutes for all temperatures .....	157
Figure 5-28 - Bitumen density profile at 2000 minutes for all temperatures.....	157
Figure 5-29 - Solvent mass fraction profile at 4500 minutes for all temperatures .....	158
Figure 5-30 - Bitumen density profile at 4500 minutes for all temperatures.....	159
Figure 5-31 - Predicted and experimental change in solvent height vs time at 33.50°C.....	160
Figure 5-32 - Predicted and experimental change in solvent height vs SRT at 33.50°C .....	161
Figure 5-33- Predicted and experimental change in solvent height vs time at 27.00°C.....	162
Figure 5-34 - Predicted and experimental change in solvent height vs SRT at 27.00°C .....	162
Figure 5-35 - Predicted and experimental change in solvent height vs time at 40.00°C.....	163
Figure 5-36 - Predicted and experimental change in solvent height vs SRT at 40.00°C .....	163
Figure 5-37 - Butane solvent decrease vs SRT for $t = 0$ and $t \neq 0$ at 28.50°C.....	166
Figure 5-38 - Butane solvent height decrease vs. SRT (28.50°C) .....	167
Figure 5-39 - Butane solvent decrease DE predicted vs experimental values (28.50°C).....	168
Figure 5-40 - Bitumen height increase vs SRT for $t = 0$ and $t \neq 0$ at 28.50°C .....	169
Figure 5-41 - Bitumen height increase vs SRT at 28.50°C .....	170
Figure 5-42 - Bitumen increase DE predicted vs experimental values (28.50°C) .....	171
Figure 5-43 - Bitumen mixture specific volume plots for ideal and non-ideal mixing 28.50°C .....	173
Figure 5-44 - Experimental and DE predicted diffusivity functions 28.50°C (ideal/non-ideal).....	175
Figure 5-45- Comparison of 28.50°C diffusivity function to other temperature (ideal).....	176
Figure 5-46 - Comparison of 28.50°C diffusivity function to other temperature (non-ideal) .....	176
Figure 5-47 - Comparison of 28.50°C solvent profile to other temperatures (non-ideal).....	178
Figure 5-48 - Comparison of 28.50°C density profile to other temperatures (non-ideal).....	179
Figure 5-49 - Predicted and experimental change in solvent height vs SRT at 28.50°C .....	180
Figure 5-50 - Predicted and DE predicted change in solvent height vs SRT at 28.50°C.....	180
Figure 5-51 - Graph of temperature vs time for experiment (27.00°C bitumen and 24.00°C butane) ....	183
Figure 5-52 - Graph of temperature vs time for experiment (33.50°C, 36.75°C and 40.00°C bitumen) ..	184
Figure 5-53 - Smooth pressure decline at 33.50°C .....	185
Figure 5-54 - Pressure spikes at 27.00°C.....	186
Figure 5-55 - Pressure spikes at 40.00°C.....	187

# **APPENDIX**

Appendix - A1: Viscosity correlations .....	199
Appendix - A2: Bitumen Assay .....	200
Appendix - B3: Two sided butane set-up .....	203
Appendix - B4: PVTSim butane solvent temperature vs vapour pressure graph .....	205
Appendix - C5: Starting experimental parameters .....	207
Appendix - D6: Sample calculation for non-ideal density .....	208
Appendix - D7: Sample calculations for ideal density .....	212
Appendix - E8: Bitumen height analysis .....	215
Appendix - F9: Bitumen mixture specific volume plots for ideal and non-ideal mixing 40.00°C .....	216
Appendix - F10: Bitumen mixture specific volume plots for ideal and non-ideal mixing 36.75°C .....	216
Appendix - F11: Bitumen mixture specific volume plots for ideal and non-ideal mixing 33.50°C .....	217
Appendix - F12: Bitumen mixture specific volume plots for ideal and non-ideal mixing 30.25°C .....	217
Appendix - F13: Bitumen mixture specific volume plots for ideal and non-ideal mixing 27.00°C .....	218
Appendix - G14: Butane solvent height decrease graph data (all temperatures) .....	220
Appendix - G15: Bitumen height increase graph data (all temperatures) .....	221
Appendix - J16: Butane solvent mass fraction profile at 30.25°C (non-ideal) .....	240
Appendix - J17: Butane solvent mass fraction profile at 33.50°C (non-ideal) .....	241
Appendix - J18: Butane solvent mass fraction profile at 36.75°C (non-ideal) .....	242
Appendix - J19: Butane solvent mass fraction profile at 40.00°C (non-ideal) .....	243
Appendix - K20: Bitumen density profile at 30.25°C (non-ideal) .....	244
Appendix - K21: Bitumen density profile at 33.50°C (non-ideal) .....	245
Appendix - K22: Bitumen density profile at 36.75°C (non-ideal) .....	246
Appendix - K23: Bitumen density profile at 40.00°C (non-ideal) .....	247
Appendix - L24: Predicted and experimental change in solvent height vs SRT at 30.25°C .....	248
Appendix - L25: Predicted and experimental change in solvent height vs SRT at 36.75°C .....	249
Appendix - L26: Validation data for bitumen height increase at all temperatures .....	250

# NOMENCLATURE

Symbol	Description	Units
A	Area	cm <sup>2</sup> , m <sup>2</sup>
C	Concentration	g/mol
D	Diffusivity	cm <sup>2</sup> /s, m <sup>2</sup> /s
d	Depth	cm, m, mm, μm
g	Gravitational constant	m/s <sup>2</sup> , cm/s <sup>2</sup>
h	Height	cm, m, mm
k	Permeability	Darcy, μm <sup>2</sup>
L	Length	cm, m, mm
m	Mass	g, kg
$\dot{m}$	Mass flow rate	g/min
N	Flux	g/cm <sup>2</sup> .s, kg/m <sup>2</sup> .s
P	Pressure	kPa, MPa, psi
PV	Pore volume	cm <sup>3</sup>
Q	Volumetric flow rate	cm <sup>3</sup> /min, barrels/day (bbp)
S	Saturation	%
t	Time	day, hour, min, s
U	Velocity	m/s, cm/s
V	Volume	m <sup>3</sup> , cm <sup>3</sup> , barrels, bb
$V_m$	Mass average velocity	m/s, cm/s
v	Volume fraction	
w	Width	M, cm

## Greek

δ	Depth of the draining live oil	μm, mm, pores
Δ	change	
φ	Porosity	%
μ	Viscosity	mPa.s, cP
ρ	Density	kg/m <sup>3</sup> , g/cm <sup>3</sup>
σ	Surface tension	N/m, dyne/cm
ω	Mass fraction	

## Subscripts

b	Bitumen
eq	Equivalent
g, G	Gas
i	Interface or nodal position
l, L	Liquid
lo	Live oil
m	Cementation factor
max	Maximum
min	Minimum
mix	Mixture
n	Exponent
o	Oil
p	Pore
s	Solvent
v	Vapor
wb	Water bath
sys	System

## Superscript

*	Solubility limit, i.e. $\omega_s^*$
i	Interfacial
dr	Drainage
x	X-direction

## Acronyms/Definitions

OOIP	Original oil in place
EIA	Energy Information Administration
DE	Design Expert
DE	Design Expert
Diffusivity	Measure of the magnitude of diffusion (usually varies)
Diffusivity function	Mathematical expression for diffusion
Diffusion coefficient	Measure of the magnitude of diffusion (usually constant)
Diffusion value	Numerical values obtained from diffusivity function
One-dimensional diffusivity	Diffusion occurring in one direction and no outside impact

# 1) INTRODUCTION

Canada has the third largest World oil reserves behind Saudi Arabia and Venezuela with 174 billion barrels (bbls) in proven reserves (CAPP 2014), 97% are oil sands. These oil sands are typically extracted through mining or in-situ methods. The in-situ methods predominantly comprise of some form of thermal stimulation. One of such technology is Steam Assisted Gravity Drainage (SAGD).

However, thermal methods are not always ideal for in-situ formations, and can be replaced with more energy efficient mass transfer methods (Vapor Extraction VAPEX or N-Solv). Although some research has been done on the implementation of this technology, the key diffusion mechanism at the crux of the technology is yet to be fully understood.

Oil sands are a natural mixture of sand water, clay and bitumen. Bitumen is oil that is too heavy or thick to flow, or be pumped out thereby needing a form of heat stimulation or dilution (VAPEX or N-Solv) for it to flow. It typically possesses an API of less than 10°, viscosity of greater than 10000 cp and density of about 1000 kg/m<sup>3</sup> (Law 2011). SAGD technology is energy intensive, produces adverse environmental effects, and is not economical for a number of heavy oil rich areas.

The purpose of this research is to evaluate the one – dimensional diffusivity of butane solvent in bitumen at varying temperature conditions, while accounting for changes in concentration and non-ideal mixing of hydrocarbons. Diffusivity function is a mathematical expression for diffusion as a function of another term (mass fraction in this work). It should be noted that one-dimensional diffusivity represents diffusion occurring in one direction and no outside impacts. The difference between diffusivity functions and diffusion values should also be noted. Diffusion values are the numerical values obtained when mass fraction ( $\omega_s$ ) is substituted into the diffusivity function and computed. The study also intends to find a correlation that will predict the diffusivity within the given temperature range.

## 1.1. World Heavy Oil Overview

Heavy oil and bitumen are types of crude oil that fall under the unconventional resource umbrella. The key difference between conventional and unconventional resources is that conventional resources are able to flow in their natural state through production conduits (wells) while being economical for production (Vassilellis 2009). Unconventional resources are unable to be produced at economical rates without assistance from massive stimulation treatments or special recovery processes (Haskett and Brown 2005). **Figure 1-1** shows a resource pyramid for conventional and unconventional resources. It should be noted that in this current day Gas Hydrates technology is still in the works while Shale Oil technology is fully commercial.

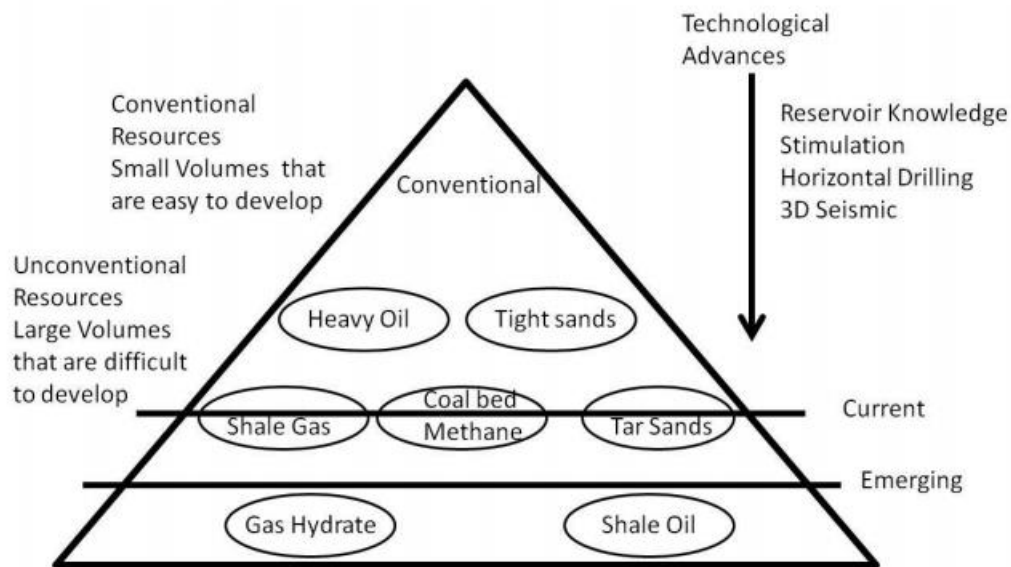


Figure 1-1 - Resource Pyramid focusing on Unconventional resources (Rajnauth 2012)

Most heavy oil reservoirs originated as conventional oil that formed in deep formations that later migrated to the surface. They were then degraded by bacteria and weathering leading to the escape of the lightest hydrocarbons. As a result, heavy oil is deficient in hydrogen and high in carbon, sulphur and heavy metals. This also leads to heavy oil having API gravity of below 22.3° and viscosity of over 1,000 cP (Speight 2013a).

There are conflicting definitions as to what is heavy oil versus bitumen. Technically bitumen is a crude grade that has an API of less than 10° and viscosity of greater than 10,000 cP (Law 2011). It also exists in solid and semi-solid states in the reservoir. Heavy oil is a crude grade with an API of 10° – 22.3° and viscosity of 100 – 10,000 cP. It is predominantly found in a highly viscous liquid state and can also be referred to as ‘extra heavy oil’. For the purpose of this research, the definitions of heavy oil will encompass normal bitumen, heavy oil, and extra heavy oil.

As profitable as heavy oil can be, there are smaller profit margins achieved with its production when compared to conventional oil. This is mainly due to higher production costs, upgrading costs and lower market price for heavier crude oils.

From a location stand point heavy oil is predominantly found in Canada and Venezuela. Other countries include the US, Russia, Brazil, and China. **Figure 1-2** shows a diagram of OOIP (Original Oil in Place) heavy oil resources around the world.

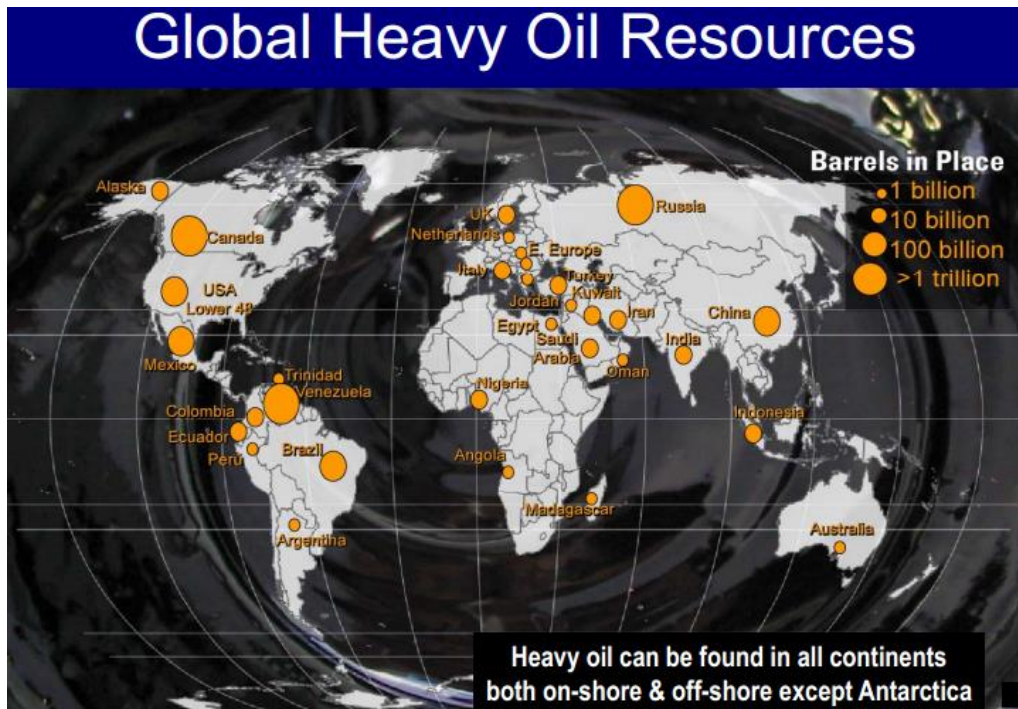


Figure 1-2 - Global heavy oil resources (Law 2011)

Heavy oil deposits in Venezuela are the largest in the world with 298 billion barrels of proved reserves (EIA 2014b). The vast majority are located in the Orinoco heavy oil belt. **Figure 1-3** shows a diagram of the heavy oil deposits. The U.S. Energy Information Administration (EIA) estimates Venezuela produced 2.49 million barrels per day (bpd) of petroleum and other liquids in 2013.



Figure 1-3 - Orinoco Belt Venezuela (EIA 2014a)

Major heavy oil deposit in the US, are found mostly in the Uinta Basin, Utah. These include the Sunnyside, Oil sand triangle, Peor Springs, Asphalt Ridge and Sundry deposits. **Table 1-1** shows a list of these deposits along with their reserves.

Table 1-1 - Heavy Oil Deposits in Utah (Speight 2013b)

<b>Deposit</b>	<b>Known Reserves (bbl×10<sup>6</sup>)</b>	<b>Additional Probable Reserves (bbl×10<sup>6</sup>)</b>
Sunnyside	4,400	1,700
Tar Sand Triangle	2,500	420
PR Spring	2,140	2,230
Asphalt Ridge	820	310
Circle Cliffs	590	1,140
Other	1,410	1,530
<b>Total</b>	<b>118,060</b>	<b>7,330</b>

Brazil possessed 13 billion bbls of proven oil reserves as of January 2013 (EIA 2013). The offshore Campos and Santos Basins, located off the country's southeast coast, hold the vast majority of Brazil's proved reserves, 90% of which are heavy oil. In China four natural heavy oil accumulations are located in the Junggar basin with resources of about 1.6 billion bbls (USGS 2010). In Russia, large resources are present in the east Siberia platform inside the Tunguska basin. The area is conservatively estimated to contain 51 billion bbls of oil reserves (USGS 2010). The area, however, is very remote and unlikely to be exploited in the near future due to Russia's large conventional oil and gas resources.

## 1.2. Canadian Perspective

Canada, with 1.7 trillion bbls of original oil in place OOIP, is estimated to have 168 billion barrels of oil sands (Alberta Energy 2010). The main locations are in the provinces of Alberta and Saskatchewan.

Alberta's heavy oil deposits are located in Athabasca, Peace River and Cold Lake. These deposits combined, occupy an area of 54,000 square miles (139,860 km<sup>2</sup>) (Alberta, Energy Resources Conservation Board 2013). This is just over half the size of the entire United Kingdom (243,610 km<sup>2</sup>). **Figure 1-4** shows a schematic of Alberta's heavy oil deposits.



Figure 1-4 - Schematic of Alberta's Oilsand deposits (Lunn 2013)

Athabasca deposits are the largest and most accessible reserve of bitumen. It underlies a 16000 m<sup>2</sup> area and contains 812 billion bbls of bitumen in place (Alberta, Energy Resources Conservation Board 2013). The rich bitumen accumulation is covered by overburden between 5 – 100 m typically with an average pay zone of 20 m. 7% of the deposits lie under less than 5 – 100 m of overburden making it accessible to surface mining techniques and 33 billion barrels are estimated to be recoverable by mining methods (Speight 2013b). Also worth mentioning is the Wabasca oil sand deposit, which is usually indicated as part of the Athabasca reserve. It is estimated to have 42.5 billion bbls of OOIP and at 490 – 1500 ft (149.35 – 457.2 m) of overburden (Speight 2013b) it is only recoverable by in-situ methods.

Cold lake deposits are the second largest of the three and have four separate reservoir deposits – one each in McMurray, Clearwater, Lower Grand Rapids and Upper Grand Rapids. Given depth varies from 984 – 1969 ft (299.92 – 600.15 m) with surface mining not possible, the deposits are

suitable for in-situ methods. Cold lake holds approximately 178 billion barrels of oil reserves (Speight 2013b).

The Peace River deposit has bitumen at a depth of 1000 to 2500 ft (304.8 – 762 m) in the Blue-sky and Gething formation. With an area of 3000 m<sup>2</sup> there are 71.7 billion barrels of bitumen in place.

In Saskatchewan, oil sands are found in McMurray formation sediments equivalent to those of the Athabasca deposits. Bitumen-bearing sands in the McMurray formation extend from Alberta into Saskatchewan and are estimated to contain 20.5 billion bbls OOIP (Speight 2013b). These oil sands are known as ‘shallow in-situ oil sands’. This is because there is substantial difficulty in driving and producing the bitumen while managing water flows in the reservoir. They are found between 75 – 200 m making extraction with both mining and normal in-situ methods difficult. VAPEX technology currently represents the best opportunity to recover these reserves. **Figure 1-5** shows a schematic of Alberta’s and Saskatchewan’s deposits.



Figure 1-5 - Schematic of Alberta’s and Saskatchewan’s deposits (Nasr and Ayodele 2005)

### 1.3. In-situ Extraction Methods for Bitumen

Extraction methods can be classified under mining or in-situ methods. Mining methods are typically used when the heavy oil is close enough to the surface with about 75 m of over-burden (Schramm *et al.* 2010) . This process typically gives a recovery factor of 95% or greater. In-situ methods are used when depths are greater than 200 m of over-burden with recovery factors ranging from 50% – 60% (Speight 2013a) 75 – 200 m fall under ‘shallow in-situ’ reserves as stated above.

Surface Mining Methods - This is the excavation (surface or sub-surface) of petroleum resources for subsequent removal of the bitumen via washing, floatation or restoring treatments. Athabasca deposits are the only ones that are shallow enough to be extracted via mining methods. Of Alberta’s 167 billion bbls of oil reserves 81% are recoverable via in-situ methods while the remaining 19% are close enough to the surface and can be mined (Alberta, Energy Resources Conservation Board 2013). About 1.2 million bbls per day are produced via surface mining methods, almost exclusive to Canada (Vassilellis 2009).

A typical mining operation removes one and a half ton of over-burden, mines two tonnes of oil sands and processes it to yield one bbl of bitumen after extraction. With increasing depth, the grade of oil sand decreases and additional tonnes must be mined and processed to yield the same amount of bitumen. Commercial mining operations therefore, have economic depth limits and economic grade limits. Both of these are dictated by the trade-off between mining and processing costs vs. the value of the bitumen (Schramm *et al.* 2010).

After extraction the bitumen is separated from the sand through the ‘Hot Water Process’. This utilizes linear and the non-linear variations of bitumen density and water density, respectively, with temperature, so that the bitumen that is heavier than water at room temperature becomes lighter than water at 80°C (Speight 2013b). To date, hot water processes are still the only commercially viable way to separate bitumen from the sand.

In-situ methods – In Latin terms, the word in-situ stands for ‘in position’. When this is used in heavy oil production scenarios, it stands for extraction done underground. This means extraction is occurring in the place where the oil resources are located. Deep oil sand reservoirs (greater than 200 m in depth) lend themselves to this form of extraction.

In-situ extraction methods encompass thermal (Cyclic processes, SAGD and Hybrid processes) and non-thermal methods (VAPEX and N-Solv). For this thesis, Solvent technology will encompass VAPEX and N-Solv methods. Thermal methods, as the name suggest, requires a form of heat stimulation for extraction. It is, therefore, water and energy intensive, while still being the most economical of all the processes. Non–thermal methods usually use solvents to dilute the bitumen, reducing its viscosity and leading to extraction. This thesis will exclusively cover in-situ methods that are used for bitumen where the viscosity reduction is first required.

### **1.3.1. Cyclic Steam Stimulation**

Cyclic Steam Stimulation (CSS) involves alternating between injecting the well with steam and producing the same well using the condensed steam (Speight 2013a). This cycling occurs with a single vertical well which serves as both an injector and producer well (this is sometimes referred to as “huff and puff”). An alternative incorporates steam drive between injectors and producers. These processes originally depended on vertical wells, but a combination of vertical and horizontal wells are now used. CSS can be used for bitumen, heavy and extra heavy oil grades. **Figure 1-6** shows a schematic of a typical CSS system.

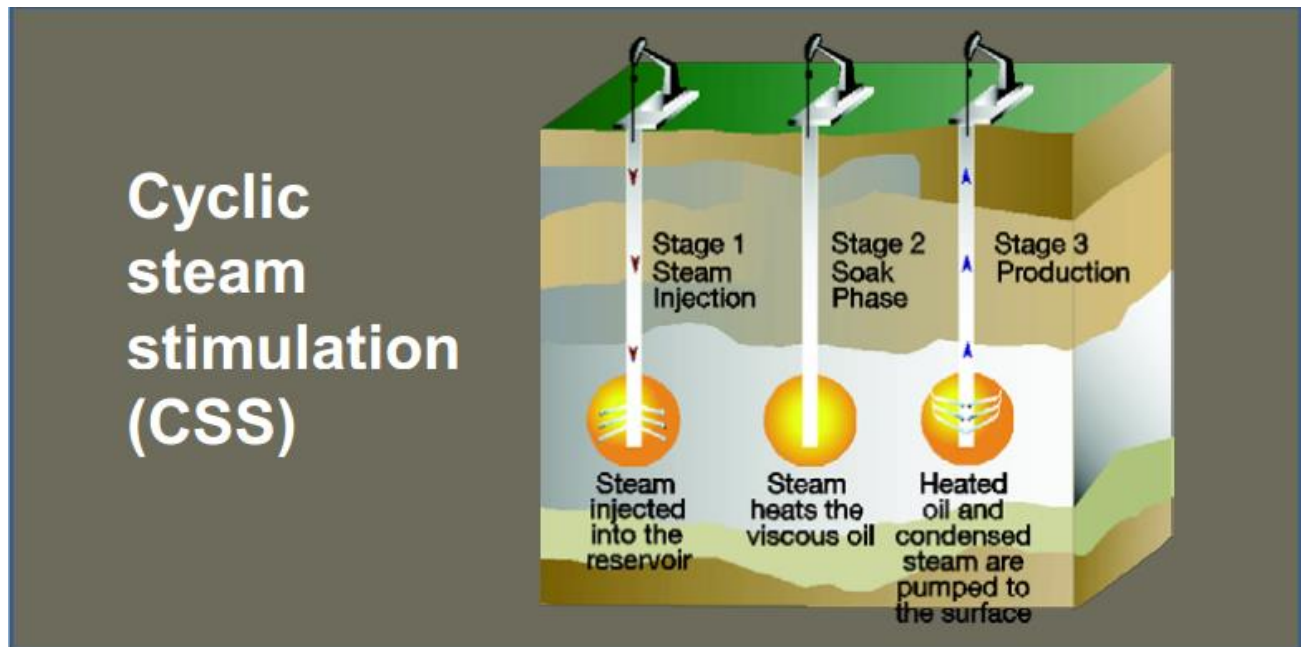


Figure 1-6 - Typical CSS system (Lunn 2013)

As shown above, CSS is a three-stage process: first, high-pressure steam is injected into the vertical well for a period of time; second, the reservoir is shut in to soak; and third, the well is put into production. Production rate decline prompts the start of another cycle of steam injection. The injection-production cycle is repeated a number of times over the life of the well. The time required to steam and produce the wells varies from well to well with each cycle, typically, between 6 and 18 months.

Steam generated is injected into the formation through the wellbore at a temperature of about 300°C and pressures averaging 11,000 kPa. This pressure is sufficient to cause parting of the unconsolidated oil sands formation, creating paths for fluid flow (Speight 2013a). The recovery factors for CSS range from about 20 – 25% of original bitumen-in-place.

Typical steam-to-oil ratios, the major economic factor, are 3:1 – 4:1. Although CSS is characterized by higher steam-oil ratios than with SAGD, the quality of steam used is much lower and requires less energy to produce. In CSS operations, natural gas requirements can be

met through produced solution gas from the process. The same is not applicable SAGD operations, because of the low amount of solution gas produced.

Bitumen produced by CSS tends to have a higher API gravity and is less viscous; therefore, diluent costs are reduced when compared with bitumen produced by the SAGD process. A key focus in a CSS operation is to increase the total recovered bitumen by increasing the quantity of bitumen recovered in each cycle and increasing the number of cycles for which bitumen recovery is economical. The steam–oil ratio, and therefore, gas costs for steam generation, is typically at its lowest point during early cycles. After this it begins to rise until the point at which bitumen production is no longer economical and the well is abandoned (Speight 2013b).

The CSS process is a well-developed process; the major limitation is its unfavorable recovery rate (usually less than 20%) of the initial oil-in-place. The process is particularly effective in reservoirs with limited vertical permeability and is best suited to operations in the Cold Lake area and the Peace River heavy oils.

### **1.3.2. SAGD**

Steam-assisted gravity drainage (SAGD) is currently the most commercially successful heavy oil in-situ extraction method in Canada. Alberta produces approximately 1.4 million bbls per day of heavy oil via this technology (Alberta, Energy Resources Conservation Board 2013). The key element of SAGD is that the two wells need to be in parallel and horizontal form. The development of horizontal drilling in 1992 was a key break-through that led to the commercialization of SAGD technology. **Figure 1-7** shows a schematic of a typical SAGD set-up.

This technology involves drilling two parallel horizontal wells along the reservoir itself. The top well is known as the injector well and used to inject hot steam into oil sands. The bottom well is known as the producer well and used to produce the oil and pump it up to the surface. Steam from the injector well builds up a steam chamber in the reservoir. Once this steam chamber reaches the bitumen source, it heats up the immobile bitumen leading to viscosity reduction of

the oil. With viscosity reduced by 10,000 cP, the oil becomes mobile, and drains into the producer well before being pumped to the surface.

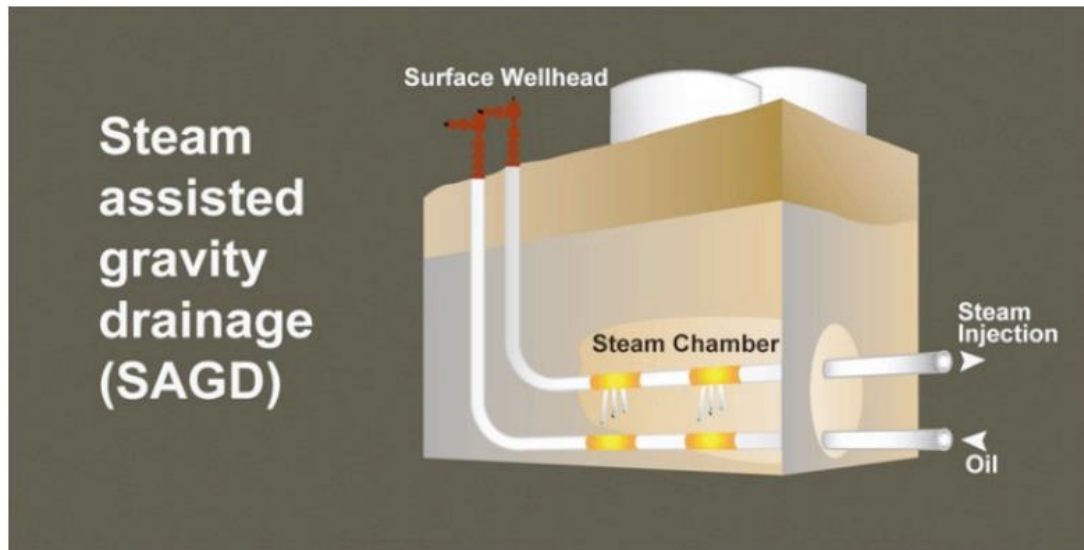


Figure 1-7 - Typical SAGD set-up (Lunn 2013)

**Figure 1-8** represents a cross sectional schematic of the SAGD process. Section A represents the initial circulation phase, where thermal communication is established between the wells. Section B is the early production stage in which the steam chamber has yet to come in contact with the oil formation (cap-rock). Section C is the lateral growth stage, where steam has fully come in contact with the oil and reduced its viscosity, leading to production. Some by-products of the production include non-condensable gases like methane.

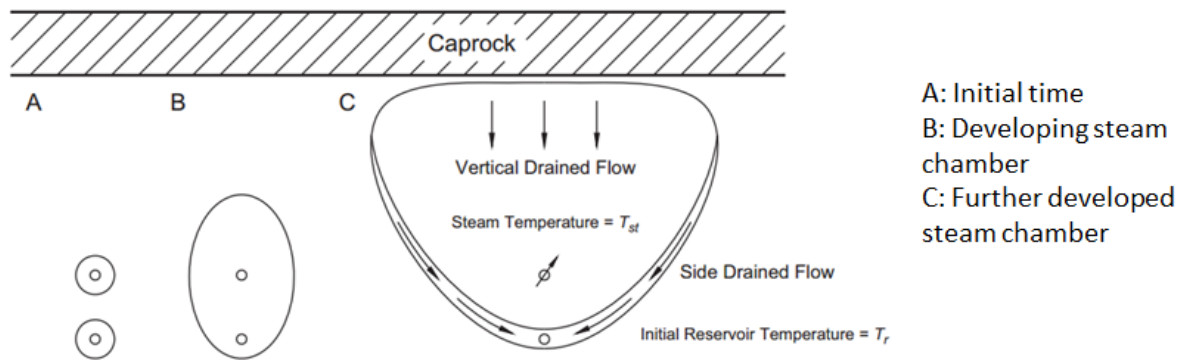


Figure 1-8 - Cross sectional schematic of SAGD process (Irani and Gates 2013)

Even though the injection and production wells can be very close (between 5 – 7 m), the mechanism causes the steam-saturated zone to rise to the top of the reservoir, expand gradually sideways, and eventually allow drainage from an increase area. Operating the production and injection wells at approximately the same pressure as the reservoir pressure eliminates viscous fingering and coning processes, and also suppresses water influx or oil loss through permeable streaks (Speight 2013a, Speight 2013b) . This keeps the steam chamber interface relatively sharp and reduces heat losses considerably. Injection pressures are much lower than the fracture gradient, which means that the chances of breaking into a thief zone, an instability problem which plagues all high-pressure steam injection processes, are essentially zero.

Heat losses and deceleration of lateral growth mean that there is an economic limit to the lateral growth of the steam chamber. This limit is thought to be a chamber width of four times the vertical zone thickness. For thinner zones, the horizontal well pairs would need to be put in closer proximity leading to cost increase as well as lower total resource per well pair. Consequently, the zone thickness limit (net pay thickness) must be defined for all reservoirs.

SAGD is widely known to recover 50 – 70% of OOIP (Mukhametshina *et al.* 2014) and is therefore the most efficient thermal recovery method. The key benefits of the SAGD process are an improved steam-oil ratio and high ultimate recovery (on the order of 60 – 70%). Key issues still troubling the technology relate to low initial oil rate, artificial lifting of bitumen to the

surface, horizontal well operation, and the extrapolation of the process to reservoirs having low permeability, low pressure, or bottom water (aquifers). The cost of heat is also still a major economic constraint on all thermal processes. Currently, steam is generated with natural gas, and when the cost of natural gas rises, operating costs rise considerably.

### **1.3.3. VAPEX**

VAPEX (Solvent Vapor Assisted Petroleum Extraction) technology can be summarized as SAGD technology with solvent vapor replacing the steam used. The solvent vapor ranges from ethane, propane to butane depending on circumstances. The key is that this solvent, given its significantly lower viscosity, would dilute the highly viscous bitumen leading to overall viscosity reduction and therefore the flow of oil. The bitumen viscosity reduction factor using these solvents is not as much as that seen in thermal-based methods, but the hope is that it becomes comparable enough for the technology to have a viable future.

The key parameter to this dilution occurring is mass transfer of the solvent into the bitumen through diffusion. The more soluble the solvent is in the bitumen, the more diffusion occurs and subsequent viscosity reduction of the bitumen.

Parallel horizontal wells are drilled with about 15 ft (4.57 m) of vertical separation in similar fashion to SAGD technology (Speight 2013b). The injected vapor forms a vapor chamber (analogous to SAGD's steam chamber), through which the solvent travels to the immobile oil face where it diffuses into the immobile liquid. The viscosity reduced oil become mobile and drains to the production well via gravity drainage, where it is pumped to the surface. **Figure 1-9** shows a cross sectional area schematic of a typical VAPEX system.

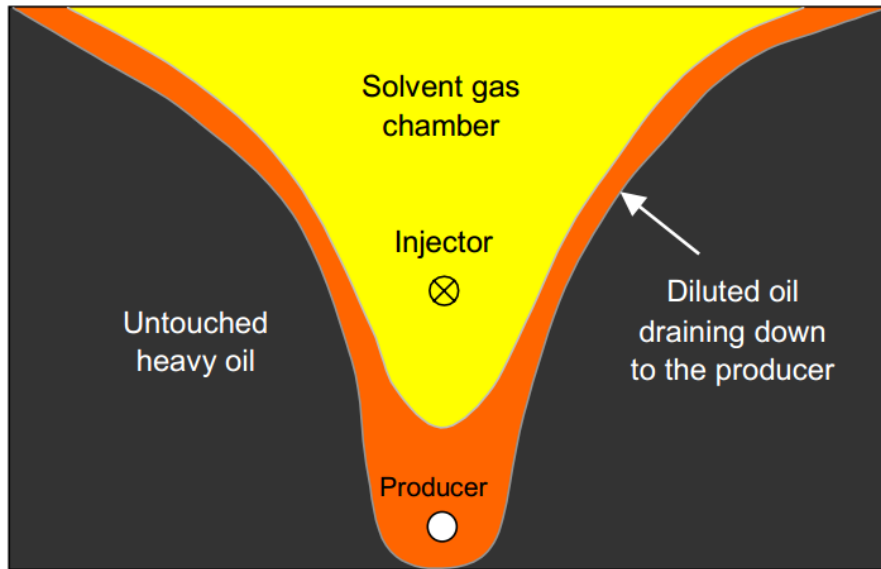


Figure 1-9 - Cross section of VAPEX system (James 2009)

VAPEX can be applied in paired horizontal wells, single horizontal wells, or a combination of vertical and horizontal wells. The mechanism of the VAPEX process is essentially the same as for the SAGD as said earlier, as is the configuration of the wells. The key benefits are claimed to be significantly lower energy costs, the potential for in-situ upgrading and the application to thin reservoirs with bottom water or reactive mineralogy. VAPEX also does not require water processing or recycling, offers lower carbon dioxide emissions and can be operated at deposit temperatures with no loss of heat. From a numbers perspective, VAPEX capital costs are about 75% of SAGD costs and 50% of SAGDs operating costs (Vargas-Vasquez and Romero-Zeran 2007). Research carried out thus far suggests that up to 90% of the solvent used can be recovered and recycled, offering the potential for dramatic cost savings over other extraction methods (Speight 2013b). Also, more wells are needed to achieve similar production rates and rates of recovery compared to SAGD.

There is also the chance of asphaltene precipitation. This can be an advantage as it reduces the viscosity of the drained oil, but conversely some feel that the precipitated asphaltene may clog portions of the pore space leading to lower production rates (Speight 2013b). However James (2009) work proves otherwise because: the upgraded oil sells at a higher price and

environmental/energy implications required by surface upgrading of the oil are reduced if the asphaltene are left in-situ.

Because of the slow diffusion of gases and liquids into viscous oils, this approach, would insufficient for use in its own, unless use for less viscous oils. Preliminary tests indicate, however, that there are micro-mechanisms that act, which indicate that the VAPEX dilution process is not diffusion-rate limited. This means the process may be suitable for the highly viscous heavy oil and tar sands.

#### **1.3.4. N-Solv**

This is a patented in-situ technology (Nenniger and Dunn 2008) that uses warm solvent to extract bitumen from oil sands. The concept of N-Solv is a fairly new type of technology and relative to other in-situ techniques could be seen as a mix between VAPEX and SAGD technology. N-Solv uses the same kind of solvents used in VAPEX, but adds a much bigger thermal aspect compared to VAPEX.

This process uses the proven horizontal well technology developed for SAGD, but differs as it substitutes water (steam) for a warm solvent (propane/butane). This is injected as vapor and condenses at the immobile bitumen interface, washing the valuable compounds out of the bitumen. A key benefit of the process is that it produces lighter, partially upgraded and more valuable oil products. It may also recover more resource from each well at lower capital and operating costs than existing in-situ processes. Environmental benefits like reduced CO<sub>2</sub> emissions are also present.

While in VAPEX viscosity reduction mainly comes from diluting the bitumen with solvent through diffusion, N-Solv involves viscosity reduction through dilution (diffusion and convective mixing) with solvent and raising the temperature of the bitumen. It is a best of both worlds scenario and as a result it gives a much faster viscosity reduction factors compared to VAPEX. Also the solvent vapor is intentionally kept at lower pressure (or higher temperature) to stop it condensing to liquid in VAPEX systems. N-Solv conversely requires the condensation of

the solvent vapor for its latent heat to be given off. The sensible heat given to the bitumen to aids viscosity reduction, however, James, (2009) proves that the solvent mixing plays the biggest role in speeding up the N-Solv process.

Like in SAGD and VAPEX, the vapor flows from the injection well to the colder perimeter of the chamber, where it condenses. This delivers heat and fresh solvent directly to the bitumen extraction interface. The extraction conditions are mild compared to in-situ steam processes, so the valuable components in the bitumen are preferentially extracted. **Figure 1-10** shows a schematic of your typical N-Solv process

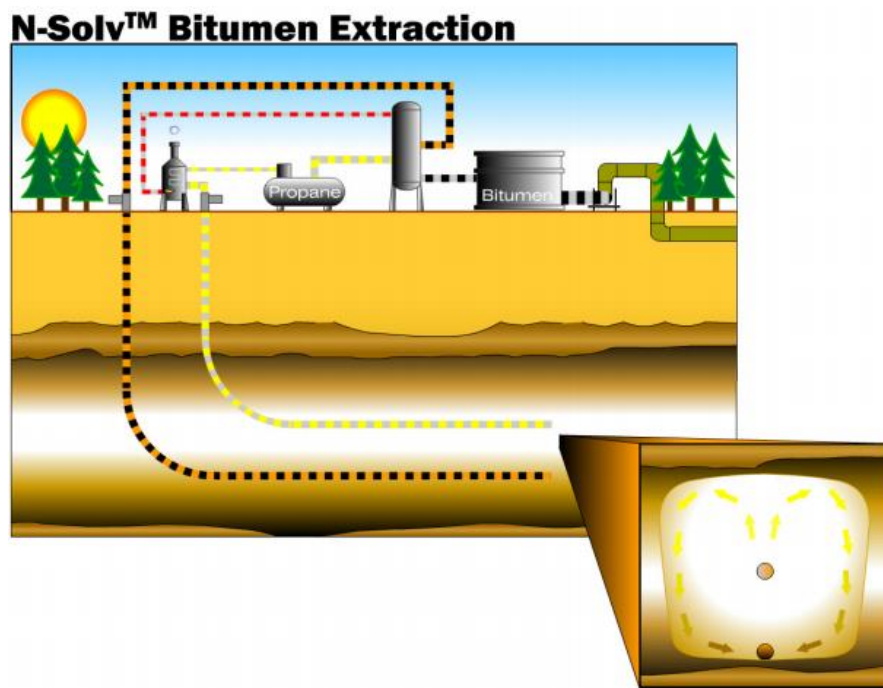


Figure 1-10 - N-Solv Process (Stickler 2009)

### 1.3.5. Hybrid Processes

These are processes that involve the simultaneous use of several technologies for extraction and these processes are seen to hold significant promise for recovering worldwide reserves (Speight 2013a).

In addition to hybrid approaches, the new production technologies, along with older, pressure-driven technologies, will be used in successive phases to extract more oil from reservoirs, even from reservoirs that have been abandoned after primary exploitation. Old reservoirs can be redeveloped with horizontal wells, even linking up the wells to bypassed oil because of the physics of oil film spreading between water and gas phases.

For example, in a SAGD–VAPEX or ES–SAGD hybrid process, a mixture of steam and miscible (non-condensable) hydrocarbons is used. 5 – 10% solvent is injected as a liquid and vaporizes when it encounters the steam. The solvent vapor and steam travel up to the oil interface at the edge of the vapor chamber and condense. The solvent dissolves in the oil. The diluted oil is reduced in viscosity and flows down the edge of the production well. The vaporized solvent is flashed out of the oil as it enters the heated area near the production well. This vaporized solvent then returns to the vapor chamber, where it mobilizes additional oil (Frauenfeld *et al.* 2013). A long-term challenge with the process is how much solvent can be recovered over time as it is necessary to recover more than 70% of the solvent to make the process viable and environmentally friendly (Speight 2013a).

Well placement changes provide a viable option for SAGD-related processes. A single horizontal laterally offset well can be operated as moderate-pressure cyclic steam stimulation well in combination with SAGD pairs to widen the steam chamber and reduce steam-oil ratios by about 20%.

Another process is the simultaneous use of SAGD and CHOPS (Cold Heavy Oil Production with Sand). CHOPS is used as a production approach in unconsolidated sandstones. The process results in the development of high-permeability channels (wormholes) in the adjacent low-cohesive-strength sands, facilitating the flow of oil foam that is caused by solution gas drive. The immobile oil sand bitumen that is amenable to CHOPS methods is usually heavier than typical heavy oil (which has mobility in the reservoir) but lighter than the oil sand bitumen that is recovered through mining or thermal stimulation methods. The key benefits of the process are

improved reservoir access, order-of-magnitude higher production rates (as compared to primary recovery), and lower production costs.

CHOPS (when paired with SAGD) offset wells until steam breakthrough occurs. CHOPS wells are then converted to slow gas and hot-water (or steam) injection wells to control the process. The high-permeability zones generated by CHOPS accelerate the SAGD recovery process. In addition to hybrid approaches, the new production technologies and older, pressure-driven technologies will be used in successive phases to extract more oil from reservoirs.

## 1.4. Technological Impacts

The purpose of this section is to outline some of the negative impacts of heavy oil technology (mostly SAGD). It should be noted that these impacts are not prevalent with VAPEX systems, thereby making the implementation of this technology crucial to the sustainability of the heavy oil industry.

**Water Usage** – Has the biggest negative impact of the above mentioned technologies and applies to both thermal in-situ and mining methods. Water requirements for oil sands projects range from 2.5 – 4.0 bbls of water for each barrel of bitumen produced (Speight 2013a). The primary challenge for process water is that no large-scale water treatment facilities exist near the oil sands, and as a result, process water must be recycled. Groundwater aquifers are used as the source of process water and the typical operating procedure involves the disposal of process-affected water to deep aquifers. The decision to use groundwater or surface water is dependent on whether a source of surface water is available, or if it is necessary to drill a well to access subsurface aquifers.

For mining operations, pollutants leakage and dewatering of the formation/deposit, as well as diversion of water flow are major issues related to water use. The removal of water from nearby aquifers can lower the overall water level in the area and may affect other aquifers and surface water bodies, including wetlands that are dependent on groundwater recharge.

For in-situ processes, the water requirement to produce a barrel of recovered bitumen/oil may be less than 1 bbl (even as little as 0.2 bbls) (Lunn 2013), depending on how much water is recycled. In-situ facilities require freshwater for the following: to generate steam, for various utility functions throughout the plant, separation of the bitumen from sand, hydro-transportation of bitumen slurry, and upgrading of the bitumen into lighter forms of oil for transport.

The demand for freshwater for in-situ oil sands projects is projected to more than double to 82 million barrels by 2015 (Speight 2013a). In SAGD operations, 90 – 95% of the water used for steam to recover bitumen is reused, but for every 6.3 bbl of bitumen produced, approximately 1.3 bbls of additional groundwater must be used. Thus, even with the recycled water, large amounts of freshwater are still required.

**Surface Disturbance** – The surface disturbance from mining operations and processing of bitumen includes land clearing, and disturbance of surface strata and soil. These activities result in the deforestation of forests and woodlands, as well as having negative impacts on fish and wildlife populations. The open-pit mining of the Athabasca oils sand deposits destroys the boreal forest and muskeg, as well as bringing about changes to the natural landscape (Morrow *et al.* 2014).

In-situ processes are much less harmful in terms of surface damage and result in limited negative environmental impact on forests, wildlife, and fisheries.

**Green House Gas Emissions** – It has been estimated that for every barrel of synthetic oil produced at oil sand facilities in Alberta, more than 35 lbs (15.88 kg) of greenhouse gases (GHGs) are released into the atmosphere and between 2 – 4 bbls of wastewater are sent to the tailings ponds, which are highly toxic (Speight 2013a).

Emissions of GHGs are one of the most complicated future environmental issues for the oil sands industry. Development of oil sand leases causes the emissions of carbon dioxide (CO<sub>2</sub>),

methane ( $\text{CH}_4$ ), and nitrous oxide ( $\text{N}_2\text{O}$ ). These are members of the group of GHGs that have profound effects on global climate.

A major Canadian initiative—the Integrated Carbon Dioxide Network (ICO<sub>2</sub>N), whose members represent a group of industry participants providing a framework for carbon capture and storage development in Canada—has proposed a system for the large-scale capture, transport, and storage of carbon dioxide ( $\text{CO}_2$ )

## 1.5. Scope of Research

Having reviewed SAGD, VAPEX and N-Solv technology, we now look at what this research can add to the information that is currently available. As already stated, solvent technology (VAPEX and N-Solv) has yet to be fully commercialized, due to lack of reliable information on its key mechanisms (mass transfer particularly). Getting reliable concentration dependent diffusion values is at the very heart of the issue. Diffusivity function is the mathematical expression for diffusion as a function of another term (mass fraction in this work). Diffusion values are the numerical values obtained when mass fraction ( $\omega_s$ ) is substituted into the diffusivity function. This study will exclusively examine the molecular diffusion of solvent in bitumen without reservoir characteristics (permeability etc.) and study diffusion in one-dimensional. As previously stated one-dimensional diffusivity represents diffusion occurring in one direction (in this case vertically downwards). Also it is important to note that we only consider butane diffusing into bitumen and not bitumen diffusing into butane. Below is a list of the expected research deliverables:

- Obtain concentration dependent diffusivity. Most diffusion calculations in the field assume the solvent concentration in the bitumen remains constant through the whole diffusion process and hence diffusion remains constant. This leads to erroneous diffusion values. The simple logic behind this is that diffusion is driven by concentration. Hence lower concentration at any points in the fluid lead to lower concentration gradients and lower values for diffusivity.
- Account for ideal and non-ideal mixing in the diffusion process. Most literature that has calculated diffusivity assumes that ideal mixing occurs between the solvent and the bitumen.

This is normally done to simplify experiments as parameters that can account for non-ideality without upsetting the experiments are hard to measure. This research we will account for the non-ideality by utilizing pressure differential transmitters to consistently find the density of the butane and bitumen mixture. This is then used in conjunction with numerical calculations to get diffusivity.

- Vary Bitumen tube temperature ( $27^{\circ}\text{C} - 40^{\circ}\text{C}$ ) and acquire the given diffusivities at these temperatures. Random conditions are picked and run based on a one factor design in Design expert software. The bitumen temperature is varied with the help of water temperature in the water bath. This thesis will however side step how the temperature of the reservoir (bitumen deposits) will be raised in actual field conditions.
- Use the experimental data to predict diffusivity within the given temperature range. The above data should be enough to generate an experimental model that can be used to predict diffusivity for any given bitumen temperature.

The value and impact of this research will be enhancing comprehension of the mechanism involved when butane solvent diffuses into bitumen. This work represents the only experiment up to date to calculate diffusivity functions in VAPEX systems while accounting for concentration dependence and non-ideal mixing of butane solvent and bitumen

## **2) LITERATURE REVIEW**

The purpose of this section is to review previous experimental work related to this study. This section will focus on the mass transfer related aspects of diffusion, concentration dependency and non-ideality. Note that Solvent technology and Solvent extraction process will be used interchangeably and both refer to VAPEX and N-Solv technology

As previously stated, solvent technology has drawn considerable industry attention in recent years due to its potential to be a viable alternative to SAGD technology in problematic reservoirs by minimizing heat losses and energy requirements. Solvent extraction has potential for down-hole upgrading and could be applied in reservoirs that are not suitable for SAGD production (reservoirs with aquifers). Also Solvent extraction opens the door to the possible sequestration of greenhouse gases Upreti *et al.* (2007). Hence researchers have been motivated to fully understand Solvent extraction processes and the driving mechanisms behind them.

Majority of the research performed in Solvent extraction processes have focused on the VAPEX part. The work done so far shows there are several factors that affect the rate of live oil production using VAPEX method. Excluding the mass transfer aspect, the porosity, permeability, possible asphaltene precipitation, heterogeneity, pay zone height (gravity drainage height) and dip angle of the injection/production well play a key role in live oil production. The research conducted on some these factors are reviewed next.

### **2.1. History of VAPEX Experiments**

The initial idea for the VAPEX process is attributed to J.C Allen in 1974. He varied the cyclic steam stimulation (CSS) process by alternating steam and solvents (butane and propane). However, Butler and Mokrys (1991) made the first significant breakthrough in VAPEX history. They sought inspiration from the extensive heavy oil deposits in Saskatchewan and Alberta that could only be recovered with low recovery efficiency via conventional methods at the time.

The rate of oil recovery was measured in experiments with vertical hele-shaw cells immersed in an atmosphere of saturated propane. This represented a form of investigating the porosity and permeability aspects of VAPEX oil production. Propane vapor contacted the oil along a vertical edge of the cell and the same diluted oil drained from the exposed edge. When this work was tested at field scale, a mixture of hot water with propane vapor was used, and high recovery rates were achieved. Propane requirements were on the order of 0.5 kg (or less) per kg of oil recovered. In addition, nearly all the injected propane was recovered. The oil production rate could be calculated via the following equation;

$$Q = \sqrt{2kg\phi\Delta S_oHN} , m^3d^{-1} \quad 2-1$$

where  $Q$  is flowrate ( $m^3d^{-1}$ ),  $k$  is absolute permeability (darcy),  $g$  is acceleration due to gravity ( $ms^{-2}$ ),  $\phi$  is porosity,  $\Delta S_o$  is the change in oil saturation,  $H$  is the reservoir height (m) and  $N$  is a dimensionless number defined for SAGD processes as;

$$N = \int_{T_{min}}^{T_s} \frac{\alpha\Delta\rho}{\mu} \cdot \frac{dT}{(T - T_R)} \quad 2-2$$

Parameter  $\alpha$  is thermal diffusivity ( $m^2d^{-1}$ ),  $\Delta\rho$  is bitumen density minus steam density ( $kgm^{-3}$ ),  $\mu$  is bitumen viscosity ( $kgm^{-1}d^{-1}$ ),  $T$  is temperature ( $^{\circ}C$ ),  $T_s$  is steam temperature ( $^{\circ}C$ ) and  $T_{min}$  is temperature above reservoir temperature  $T_R$  ( $^{\circ}C$ ). For the solvent process,  $N$  would be analogously described as;

$$N = \int_{c_{smin}}^1 \frac{D_s(1 - c_s)\Delta\rho}{\mu} \cdot \frac{dc_s}{(c_s)} \quad 2-3$$

where  $D_s$  is the intrinsic solvent diffusivity ( $m^2d^{-1}$ ),  $\Delta\rho$  is solution density minus solvent density ( $kgm^{-3}$ ),  $C_s$  is solvent concentration (volume fraction),  $\mu$  is solution viscosity ( $kgm^{-1}d^{-1}$ ) and  $C_{smin}$  is the minimum solvent concentration in the oil (volume fraction).

Das and Butler (1994) went a step further to test the effect of asphaltene deposition in the VAPEX process. Asphaltene precipitate from heavy oil when the operating conditions depart from phase equilibrium conditions. When the asphaltene content is reduced from 16% by mass to zero, the heavy oil viscosity (even at low temperatures) is reduced to over twenty orders of magnitude. This upgrades the quality of the oil in-situ and reduces environmental and operating costs for the VAPEX process.

Das and Butler (1994) using Hele-Shaw cells with propane and heavy crude oil concluded that asphaltene deposition takes place if the injected solvent (propane) is very close to its saturated vapor pressure at reservoir temperature, and that asphaltene deposition does not prevent the flow of oil for the production scheme. In another set of experiments in Hele-Shaw cells, the drainage profiles of heavy oil were studied to estimate the “VAPEX Parameter” and, hence predict field flow rates. **Table 2-1** shows a summary of experimental results obtained. At higher temperatures with asphaltene precipitation occurring, predicted oil production rates are doubled illuminating the potential benefits of asphaltene precipitation in the reservoir.

Table 2-1 - Experimental results (Das and Butler 1994)

Cell Temp. °C	Saturation pressure at cell temp. (MPa)	Propane Bath temp. °C	Propane Pressure (MPa)	Vapex Parameter $m^{1.5}/hr \times 10^{-3}$	Deposition	Production Rates ( $m^3/d$ )
21.0	0.8639	21.0	0.8639	1.95	Yes	9.25
25.0	0.9588	25.0	0.9588	2.77	Yes	13.15
25.0	0.9588	24.7	0.9514	2.73	Yes	12.96
30.0	1.0879	30.0	1.0879	3.20	Yes	15.19
30.0	1.0879	29.0	1.0611	3.06	Yes	14.52
30.0	1.0879	28.9	1.0348	2.34	No	11.11
35.0	1.2292	35.0	1.2292	4.08	Yes	19.36
35.0	1.2292	32.4	1.1541	2.58	No	12.26
35.0	1.2292	28.0	1.0348	2.35	No	11.15

Yildirim (2003) also conducted research on asphaltene precipitation of heavy oil. Carbon dioxide, propane and butane solvents were injected at varying injection rates (20, 40 and 80 ml/min) into Hele-Shaw cells containing light (Garzan crude), medium (Raman crude) and heavy (Bati Raman) oils.

20 experiments were conducted in total: 9 for propane at room temperature for the three injection rates with the three different oils, 9 for butane at room temperature for the three injection rates with the three different oils, one for butane with steam at injection rate 40 ml/min with Garzan crude and one for CO<sub>2</sub> at injection rate 40 ml/min with Garzan crude. All solvent had a pressure equivalent to their vapor pressure at the given experimental temperatures.

Results confirmed that propane (compared to butane) injection shows better extraction performance. The propane also showed better upgrading (asphaltene precipitation) for the light and medium oil while butane makes for better upgrading of the heavy oil. The CO<sub>2</sub> experiment showed the best extraction performance while the butane/steam 40 ml/min experiment showed similar extraction performance to the propane experiment at 40 ml/min

Jiang (1997) looked extensively at VAPEX technology in homogeneous and heterogeneous reservoirs. Butane and propane solvents were utilized in packed models in the Tangle-Flags, Peace River and Atlee Buffalo heavy crudes. **Figure 2-1** shows a schematic of the experimental set-up.

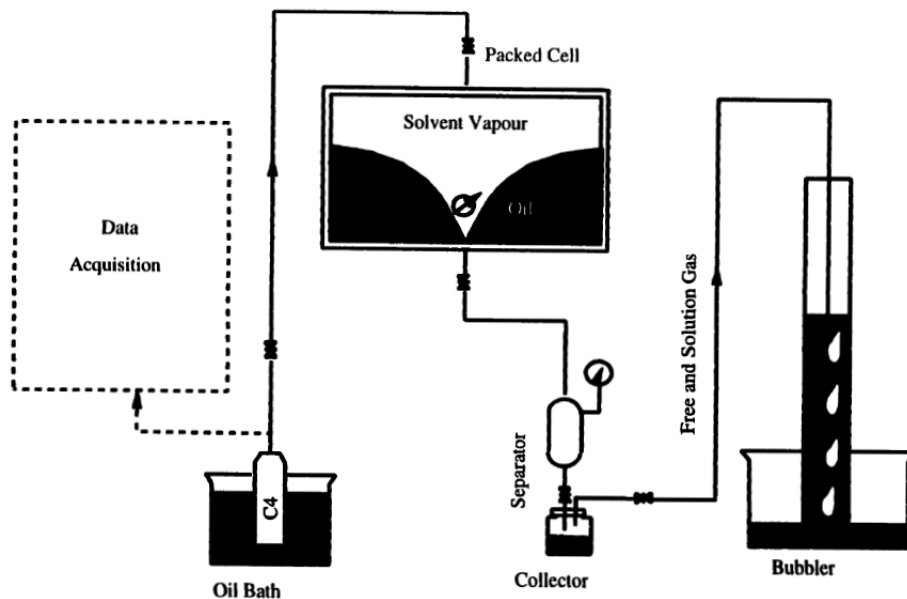


Figure 2-1 - Schematic of experimental Set-up (Jiang 1997)

The packed cell was two dimensionally scaled with a cavity 14 inches wide, 9 inches high and 1.25 inches thick (356 x 229 x 32 mm). A heterogeneous reservoir was simulated by packing the model in horizontal or vertical regions using two different sized sands: 20-30 mesh (coarse sand) and 30-50 mesh (fine sand). On experimental start-up, the packed cell was injected with water from the bottom. Oil saturation was then established by displacing water downwards with oil from a container. The oil and cell were heated to 60°C before injection, due to the crudes high viscosity. Once the packed cell was uniformly filled with oil, it was allowed to cool down to room temperature overnight.

Butane was then injected into the model at a pressure slightly below vapor pressure. The temperature of the butane container was maintained 1°C below the model temperature. Cumulative butane injection was measured from weights from an electric load cell that weighed the solvent cylinder with time and the data was recorded by a computer. The oil, diluted with butane, was recovered from the well located at the bottom of the model. Injector locations were varied to model different well configurations. The solution and free gas from the produced fluids were separated at the production outlet at atmospheric pressure. The volume of the produced gas was measured by the displacement of water in the cylinder labeled the "bubbler". Produced oil was collected in a 250 ml sample bottle at suitable time intervals. At the end of each experiment, the model was blown down to atmospheric pressure to recover the solvent left in the vapor chamber and those dissolved in the oil.

The effects of well spacing, well configurations, permeability, temperature, viscosity of oil and solvent injection rate were investigated with the above procedure. The following was discovered:

- Reservoir heterogeneity is more important in VAPEX than in SAGD systems
- The use of mixed solvents (solvent and non-condensable gas) gives similar performance to the use of pure solvents. The effects adding NCG is addressed later
- The optimal injection rates are highly dependent on the well configuration, spacing and permeability.

By the early 2000s, VAPEX experiments were in full swing. Cuthiell *et al.* (2006) investigated the porosity and permeability effects on VAPEX through capillarity. An experiment was carried out in a 2D rectangular cell, using a 4.3 darcy ( $4.24 \times 10^{-6} \mu\text{m}^2$ ) sand-pack partially saturated with heavy oil and n-butane as the solvent (injected at constant pressure). Oil was diluted by the solvent and drained into the lower part of the pack while a CT scanner monitored the oil. Capillary pressure was shown to have a major role in the VAPEX process. When its effects are ignored, the CT saturation profiles cannot be matched. Ayub (2009) similarly explored the effects of capillary pressure in VAPEX systems and found that capillarity acts in favor of VAPEX by shaping the vapor chamber, reducing free gas production and increasing drainage rate by increasing the effective area of molecular diffusion.

James (2003) carried out VAPEX extraction using consolidated and unconsolidated media macro-models. Consolidated media experiment was used to investigate the effect of dip angle and length of the system on oil production. The unconsolidated experiment was used to investigate the VAPEX solvent chamber growth.

Live oil production rates for consolidated media were also found to be constant for a given system and production rates varied linearly with the length of the system and were proportional to sine of the dip angle ( $\sin \theta$ ). The live oil density and solvent concentration were independent of length and dip angle with a density ranging from  $0.81 - 0.82 \text{ g/cm}^3$  and the solvent concentration ranging from  $0.27 - 0.32$  mass fraction. The residual oil saturation decreased from 22% to 10% percentage volume as the length of the system increased

James *et al.* (2003) investigated the effects of consolidated media on live oil production rates compared to unconsolidated media. Also the shape of the VAPEX with its evolution during production is examined in unconsolidated media. The live oil production trends in consolidated and unconsolidated media were similar. However live production rates from consolidated media were less than those from equivalent unconsolidated media. Live oil production rates for consolidated media were also found to vary linearly with the length of the system

The unconsolidated media experiments showed that the solvent chamber grows in a parabolic way where the live oil drains from the top of the formation. It is not until most of the live oil from the highest part of the model is drained that the interface advances further into the heavy oil at points below. The growth of the solvent chamber indicated that the rate limiting step in VAPEX was the gravity drainage of the live oil.

James and Chatzis (2004) investigated the characteristics of gravity drainage in the VAPEX process using rectangular models of porous media. They developed a model for describing the evolution of the VAPEX chamber growth as a function of time. Butane was used as a solvent and micro-models of pore networks were etched on glass plates for pore scale flow visualization. The butane was provided at constant pressure and the vapour uptake was monitored during the experiments as well as the advancement of the VAPEX interface.

Several glass micro-models with different pore structure characteristics were used to investigate this process in order to discern pore scale events and compare interface velocities between different models. The interface velocity is defined as the speed at which the moving VAPEX interface boundary moves into the bitumen in the horizontal direction at any vertical location in the system. This parameter helps clarify the dependence between oil production rates and height of the system (drainage height). **Figure 2-2** shows the changes in the interface position of VAPEX chamber with time for one of the models.

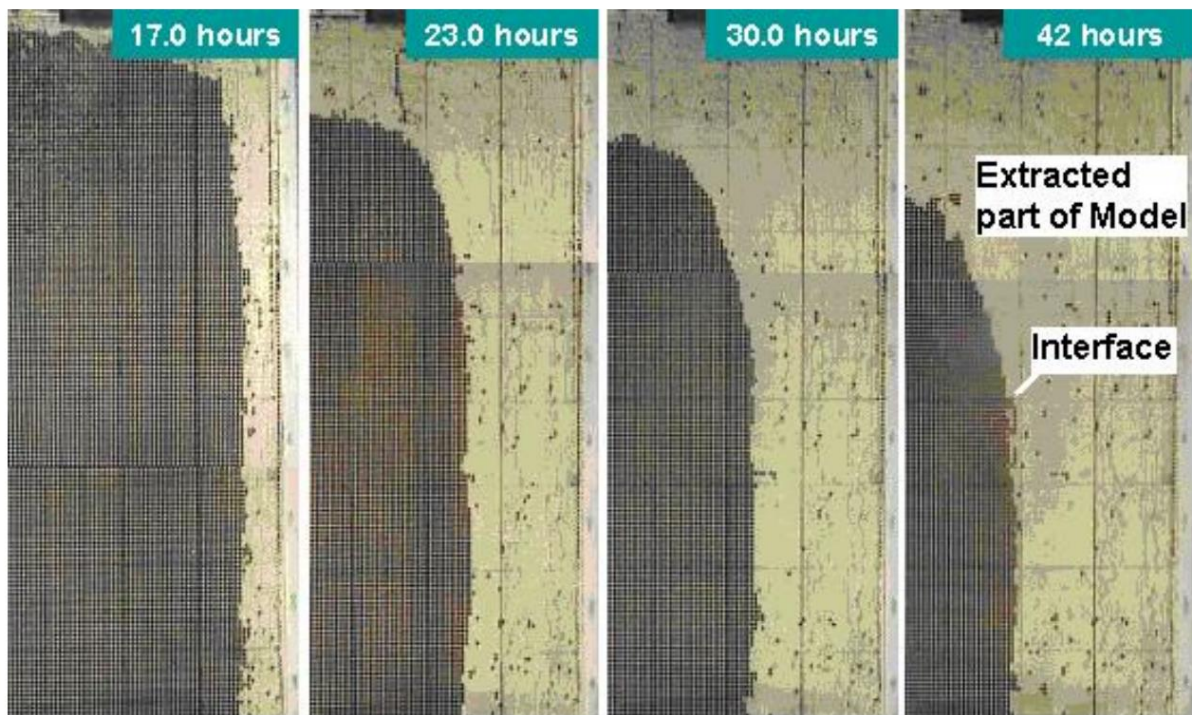


Figure 2-2 - Change in VAPEX position with time for one of the models (James and Chatzis 2004)

The following observations were discovered:

- The rate at which the VAPEX interface advances depends on porous media characteristics; permeability, diffusion distance and drainage flow path
- The VAPEX interface advancement is linear with time for a given cross-section.
- Drainage of live oil (solvent rich oil) occurs in one or two pores at a time
- The velocity of the VAPEX interface can be used to predict live oil flow rates in similar systems

Yang and Gu (2005) designed a set-up to calculate the Bond numbers for methane, ethane, propane and carbon dioxide. The Bond number is the ratio of gravity to capillary forces and this plays a significant role in the gravity drainage flow in porous matrix. Two sand packed models were used; One with permeability  $3 \mu\text{m}^2$  and porosity 32% and another with permeability (k)  $830 \mu\text{m}^2$  and porosity 35%. The Bond number was found to increase with pressure (all pressures

were below respective vapor pressures of solvents). The increasing bond number indicated a large effect of gravity on the VAPEX and thus enhanced oil recovery.

Rezaei *et al.* (2014) investigated the use of vuggy porous media in VAPEX extraction with n-pentane to recover Cold lake bitumen. Vuggy porous media was investigated because despite the enormous quantities of heavy oil deposits (2 trillion bbl) in vuggy carbonate reservoirs, there has not been enough attention drawn to EOR techniques applicable to these reserves.

Seven different sintered glass-bead models were utilized: 3 homogeneous and 4 vuggy porous all with different vuggy to total pore volume ratios. The live oil sample weights were converted to cumulative live-oil production basis vs. sampling time. The performance of the VAPEX process in each vuggy medium was compared with that of the homogeneous medium with the same matrix glass-bead size.

It was concluded that the presence of vuggy porous media improved production performance compared to the equivalent homogeneous media. Oil production rate increased and residual oil saturation decreased with the vuggy porous media. Also unlike the homogeneous models, the dead oil production rate was not constant in the vuggy models. An increase in oil-production rate was observed when several vugs were simultaneously invaded.

Addition of a non-condensable gas (NCG) like  $\text{CO}_2/\text{N}_2$  to the VAPEX process has been considered. The possible benefits include raising total gas pressure while maintaining the solvent in gaseous form and lowering amount of expensive pure solvent used in the process thereby reducing cost. Friedrich (2006) examined the effect of using non-condensable gas (NCG) with the solvent in the VAPEX process. As stated earlier, maintaining the solvent in gaseous form can be done by co-injecting solvent with a NCG. This increases total gas pressure but reduces partial pressure of the solvent gas.

The experimental set-up used consisted of a porous media saturated with bitumen and put inside acrylic housing. The non-condensable gas (air) was present in the housing before liquid pentane

was added. Pentane vapor evolved from the liquid pentane, which was being maintained at constant temperature. Partial pressure of the liquid butane was varied by varying the temperature of the liquid butane.

The diffusive flux of the solvent through the stagnant air and at the bitumen/solvent interface was described via **Equation 2-4**:

$$N_{sz(z=z_1)} = \frac{PD_{sa}}{RT(z_2 - z_1)} \left( \frac{\bar{P}_{ai} - \bar{P}_{a0}}{(P_a)_M} \right), \quad 2-4$$

Where  $N_{sz}$  is the molar flux of solvent in direction  $z$  (mole.cm<sup>-2</sup>.min),  $P$  is pressure (Pa),  $D_{sa}$  is the diffusivity of solvent in air (cm<sup>2</sup>/s),  $R$  is the molar gas constant (m<sup>3</sup>.Pa.mol<sup>-1</sup>k<sup>-1</sup>),  $T$  is temperature (k),  $z$  represents interface position and  $P_a$  with its subscripts represents the pressure of the air at varying positions (Pa). The molar flow-rate of pentane in live oil can be given as **Equation 2-5**

$$Q_s(t) = N_s(t)A_s = \frac{x_z^v \rho_s}{M_s} \frac{dV_{total,cum}}{dt}, \quad 2-5$$

where  $A_s$  is interfacial surface area (cm<sup>2</sup>),  $V_{total}$  is cumulative volume (cm<sup>3</sup>),  $x$  is mass fraction,  $t$  is time (s). Substituting  $N_s(t)$  in **Equation 2-4** into **Equation 2-5** and re-arranging to solve for the diffusivity of solvent in air ( $D_{sa}$ ) yielded:

$$D_{sa,eff} = \frac{x_z^v \rho_s}{A_s M_s} \left( \frac{dV_{total,cum}}{dt} \right) \frac{RT(\Delta z)(P_a)_m}{P(\bar{P}_{ai} - \bar{P}_{a0})}. \quad 2-6$$

Results showed that in the presence of NCG, the rate of interface advancement is proportional to the square root of time instead of just being proportional to time. The average steady state effective diffusion coefficient was found to be 0.166 cm<sup>2</sup>/s.

Chatzis *et al.* (2006) and James (2009) also investigated the effect of non-condensable gas in the production history of VAPEX. Results showed that the accumulation of NCG near the boundary reduced the rate of advancement of the VAPEX chamber. This is because the NCG became an extra boundary the solvent had to diffuse through. Also the reduction in solvent partial pressure due to the NCG leads to a reduction of solvent solubility in the heavy oil. However, progression of the VAPEX front (compared to the source of the vapor) was also found to be proportional to the square root of time.

James *et al.* (2007) compared various enhanced oil recovery techniques and included different solvent choices. VAPEX, warm VAPEX and hybrid VAPEX technology were investigated. Warm VAPEX involves giving sensible heat to the solvent so that it condenses on contact with the bitumen. Hybrid VAPEX involves the co-injection of solvent vapor with steam. Both these methods reduce bitumen viscosity with a combination of solvent dissolution and heat. **Figure 2-3** shows the bitumen & solvent interface profiles for all 3 methods.

The mobile oil film  $\delta_m$  is the part of the oil that has had its viscosity sufficiently reduced to mobilize the oil under gravity. Ignoring temperature effects, the oil film is thicker for VAPEX and warm VAPEX due to higher solvent concentrations at the interface.

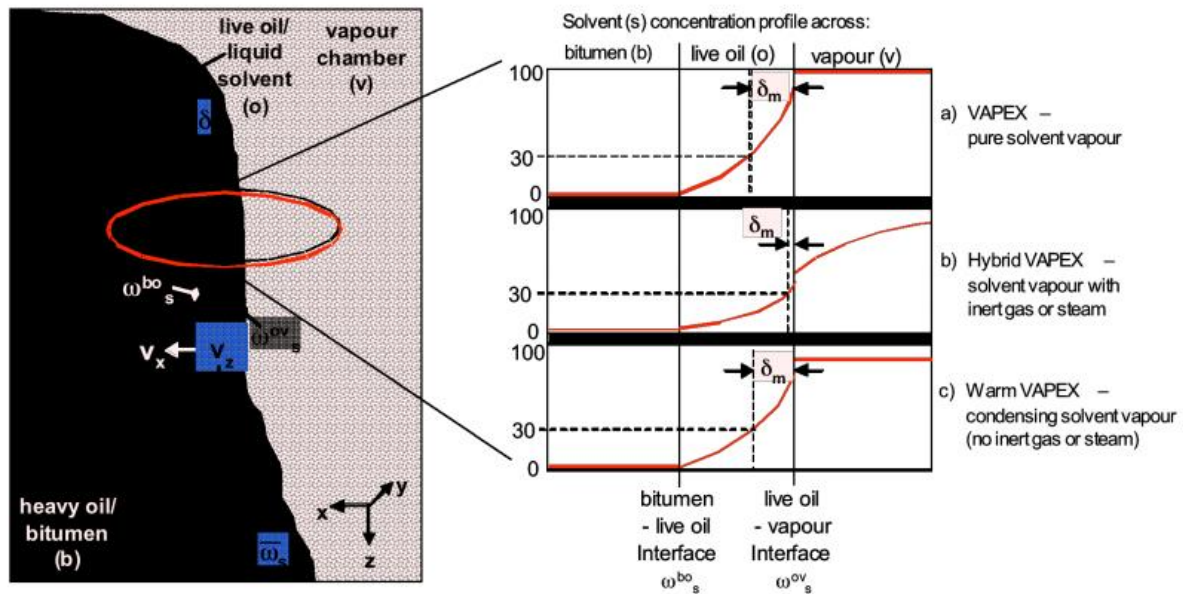


Figure 2-3 - VAPEX interface and concentration profiles (James *et al.* 2007)

In spite of the success of most of the aforementioned experiments, field applications of the VAPEX process have been limited amid concerns that the favorable laboratory recoveries may not scale up to the field. James and Chatzis (2005) reviewed various VAPEX work to collect lab scale data and scaled them up to field conditions. They did find some difficulty comparing lab scale results between different research groups. A big problem was the difference in injection rates. Some researchers inject solvent at a constant rate where as others delivered it at its vapor pressure. Constant rate injection could lead to condensation and hence the need to mix the solvent with NCG and thereby reducing mass transfer rate compared to injection rate. Also different researchers have different methods of recording oil production rates. The core analysis and testing of process conditions has yet to be standardized.

Nevertheless, James and Chatzis (2005) examined the VAPEX interface advancement using various models and **Figure 2-4** shows that constant interface advancement is consistent between models.

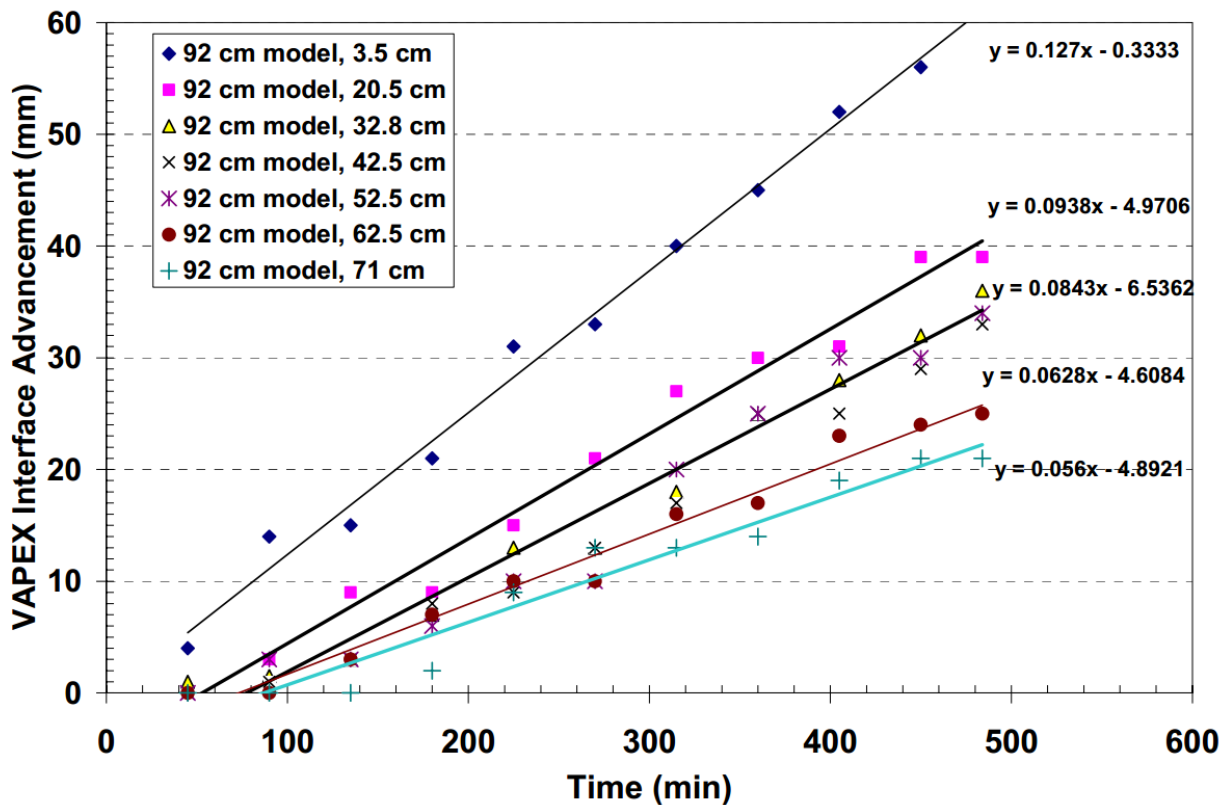


Figure 2-4 - VAPEX interface advancement for 92cm High Model (James and Chatzis 2005)

It was concluded that heavy oil experiments in long enough models are desirable for predicting production rates. Also analysis of production history shows that diffusion coefficient measured in stagnant heavy oil was orders of magnitude smaller than the dispersion coefficient measured in the same oil.

The major transport mechanism involved in VAPEX is well known to be dispersion while the major transport mechanism in SAGD is heat transfer. SAGD uses thermal conduction as the driving force to reduce heavy oil viscosity and hence facilitate production. This technology is well understood and is widely used in the heavy oil industry. The complexities behind dispersion in VAPEX are yet to be fully comprehended and as a result the technology has yet to be fully embraced by oil companies.

The dispersion in VAPEX is a combination of mass transfer of solvent into the heavy oil and then subsequent gravity drainage of the solvent enhanced live oil. Solvent is transferred into the heavy oil to reduce the viscosity of the heavy oil till gravity forces overcome capillary forces enabling drainage of the live oil. The mass transfer occurs through a combination of diffusion and convection. Having already covered some of the gravity drainage characteristics, understanding the individual contribution of each mass transfer mechanism (diffusion and convection) is crucial to predicting the possible oil production rates that can be obtained from VAPEX.

Diffusion is analogous to heat conduction in heat transfer but the driving force is not temperature difference but difference in concentration (concentration gradient), for convection the driving force is movement or mixing of the fluids. This can easily be influenced externally by density difference, gravity and pressure difference. A number of papers have made efforts to review the mass transfer involved in the VAPEX.

Boustani and Maini (2001) used effective diffusion coefficient that included Taylor dispersion coefficient and diffusivity to find the overall mass transfer parameter ( $N_S$ ) from **Equation 2-2**. They found that fluid flow (convection) has a strong effect on overall mass transfer in VAPEX and hence the convection always needs to be accounted for.

El-Haj (2007) investigated the dispersion of butane gas solvent as a linear function of its concentration in heavy oil based on previously carried out VAPEX experiments. A cylindrical wire mesh (cavity 21 cm high and 6 cm diameter) packed with homogeneous porous media saturated with Athabasca heavy oil was used as the physical model for the heavy oil vapor interface. 3 different sizes of glass beads with different permeability's (180, 157 and 110 Darcy) were used as the packing for the experiments. For each experiment, temperature was kept at room temperature and pressure at the butane dew point. **Figure 2-5** shows a histogram of the resulting dispersion coefficients at the varying permeability.

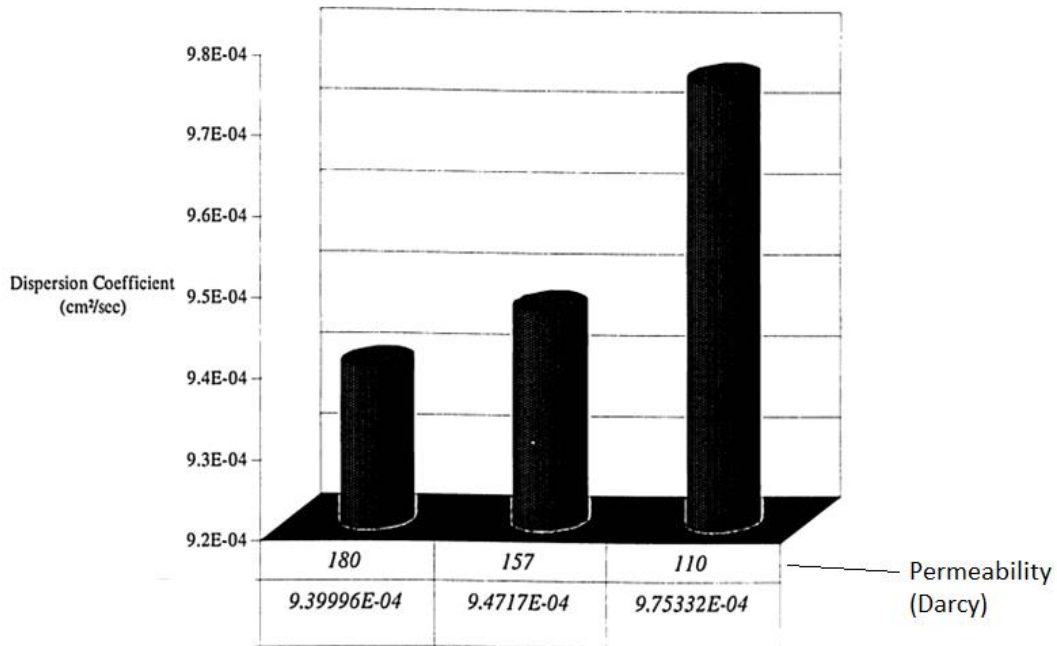


Figure 2-5 - Dispersion coefficient vs. permeability for all runs (El-Haj 2007)

James and Chatzis (2007) designed an experimental set-up to investigate overall mass transfer coefficient as a function of height, permeability, different solvents and solvent flow rates. The porous media used included a consolidated and unconsolidated glass bead packing model. The mass transfer coefficient is flux and concentration dependent, as indicated in **Equation 2-7**

$$k = \frac{N_A}{\Delta\omega_A} = \frac{\dot{m}_B}{A_{yz}(\omega_{BZ} - \omega_{B0})} \left( \frac{g}{cm^2 s} \right) \quad 2-7$$

Where,  $k$  = mass transfer coefficient ( $g \cdot cm^{-2} s^{-1}$ ),  $N_A$  = mass flux ( $g \cdot cm^{-2} s^{-1}$ ),  $\omega$  = mass fraction of component and  $\dot{m}$  = mass flowrate ( $g \cdot s^{-1}$ ).

The mass transfer coefficient from the various experiments is shown in **Figure 2-6** below. The slope of the mass based graphs represent the mass transfer coefficient for each experimental set-up divided by cross sectional area.

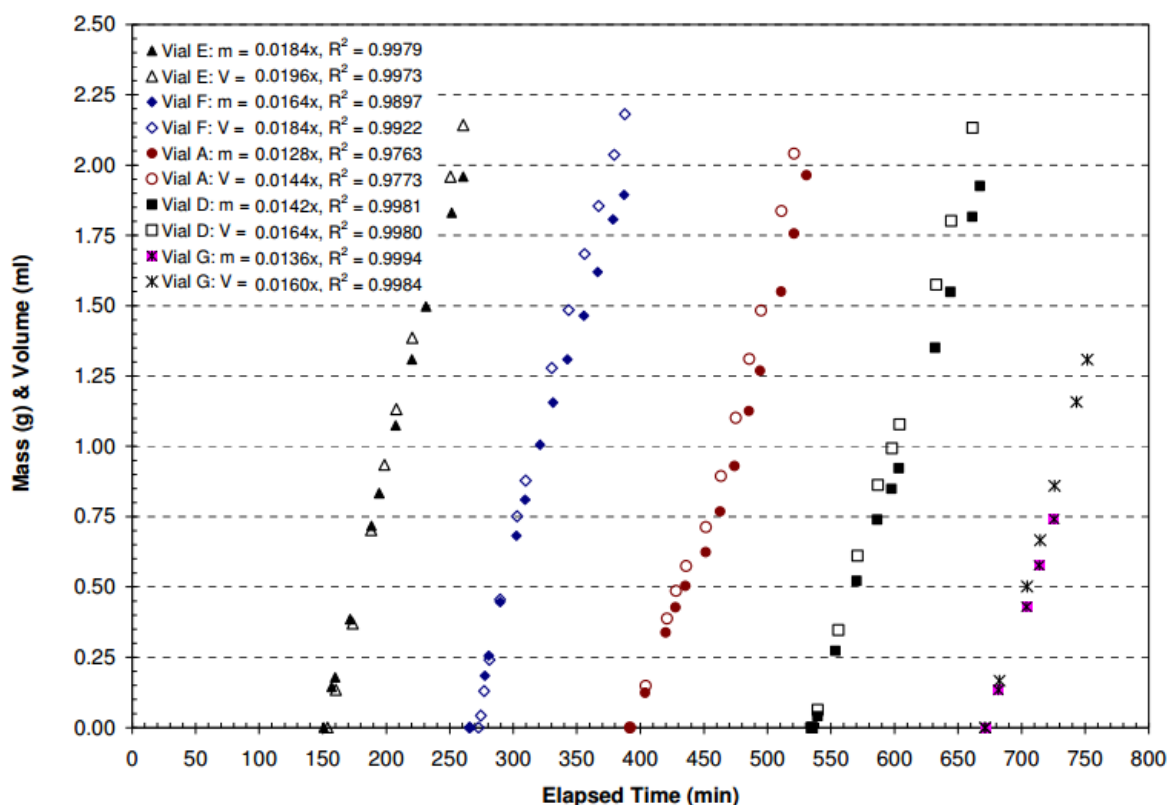


Figure 2-6 - Mass transfer coefficient for various models (James and Chatzis 2007)

It was concluded that the VAPEX interface advances at constant velocity for a given position and the solvent concentration in the live oil is affected by the injection flow rate and the matrix permeability. The diffusion coefficient contribution to mass transfer is discussed in more detail in **Section 2.2**.

All these studies so far show that convection has an effect on the mass transfer of solvent molecules into the bitumen. Heavy oil viscosity reduction is the core of oil production in heavy oil systems. Quicker heavy oil viscosity reduction leads to increased oil production. Mixing of the heavy oil and solvent via mass transfer (diffusion and convection) is the rate limiting step for viscosity reduction. It is therefore important to quantify the contribution of convection and diffusion. A failure to account for convection leads to an overestimation of the diffusion contribution to the mass transfer mechanisms and hence does not reflect the overall mass transfer.

Abukhalifeh *et al.* (2009) investigated a technique to experimentally determine the concentration dependent dispersion coefficient of a solvent in the VAPEX process. The principles of variational calculus were utilized in conjunction with a mass transfer model of the VAPEX process. A computational algorithm was then developed to optimally compute solvent dispersion as a function of its concentration in heavy oil.

The mathematical model used to describe the mass transfer process based on vapor extraction, involved the following assumptions:

- VAPEX is carried out at constant temperature and pressure
- Solvent dispersion is along the radial direction only
- The velocity of live oil along the vertical direction is governed by Darcy's law in a porous medium
- The porous medium has uniform porosity and permeability
- There are no chemical reactions and any volume changes result from drainage of live oil
- Heavy oil is non-volatile

The main feature of this work was that it didn't impose any functional form on dispersion as a function of concentration, but allows its realistic determination. During the mathematical development, the concentration-dependent dispersion function is left undetermined. When the function is incorporated into the mass transfer model, the calculated mass of oil produced is expected to be equal to its experimental value.

The technique was applied to VAPEX with propane as the solvent and results show dispersion of propane as a unimodal function of its concentration in bitumen. **Figure 2-7** shows a graph of dispersion coefficient versus propane mass fraction at 21°C and 0.689 MPa (99.9 psi). The optimal dispersion coefficient is found to be  $4.048 \times 10^{-5} \text{ m}^2/\text{s}$ . The corresponding propane mass fraction is 0.336.

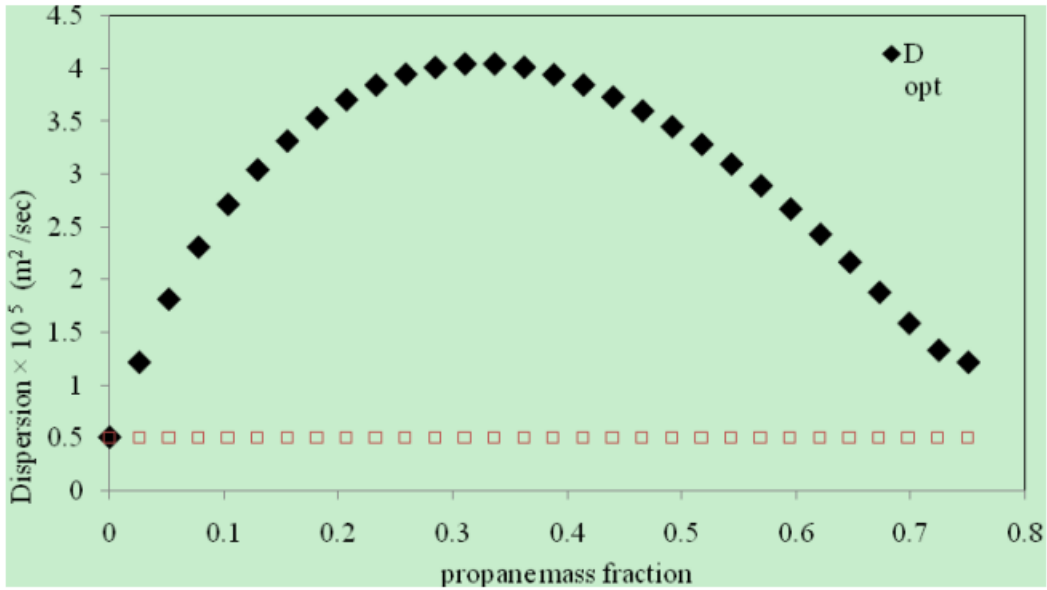


Figure 2-7 - Graph of Dispersion coefficient vs mass fraction (Abukhalifeh *et al.* 2009)

However, the process of obtaining  $J$ , the augmented objective function is complex. The mathematical model possesses a moving bitumen/butane boundary which is always complicated to resolve and assumes all bitumen volume changes (swelling) immediately result into live oil drainage. This is not necessarily the case given there is a bitumen/solvent mixture viscosity threshold (minimum value) for live oil drainage to occur.

Okazawa (2009) extended the Butler and Mokrys (1991) VAPEX analytical model to include situations when diffusion coefficients are dependent on concentration during the gravity drainage process (hence dispersion), as extreme viscosity reduction occurs from solvent dissolution in the bitumen. The model also covers situations where the diffusion coefficient and viscosity relate to each other under the Stokes-Einstein Law. The diffusion coefficient is expressed as a function of kinematic viscosity through **Equation 2-8**;

$$D(v) = \frac{\left( n A v_s^{\frac{n}{m}} \right)}{\left( v^{-\frac{n}{m}} \right)} \quad 2-8$$

Where  $D$  is the diffusion coefficient,  $\nu$  is kinematic viscosity,  $\nu_s$  is kinematic viscosity at bitumen interface,  $A$  is a constant for concentration dependent diffusion,  $m$  is an exponent to concentration for kinematic viscosity and  $n$  is an exponent to concentration for the diffusion coefficient. **Equation 2-8** satisfies Stokes-Einstein's law when  $n = m$  or  $n < m$ . The most fundamental mechanism of the process is the gravity drainage caused by the density difference between the liquid heavy oil and injected solvent vapor. The final bitumen gravity drainage rate is as **Equation 2-9**:

$$Q_B = \sqrt{\frac{2\bar{C}'_B K g \phi \Delta S_o (H-y)}{m * \nu_s}} \quad 2-9$$

$$\bar{C}'_B = 1 - C_s \left( \frac{m}{m+1} \right)$$

Where  $H$  is vertical coordinate at the top of the formation,  $y$  is vertical coordinate increasing upwards,  $\bar{C}'_B$  is bitumen average flow fraction,  $C_s$  is solvent concentration at interface and  $\nu_s$  is interface viscosity. Comparing the above **Equation 2-9** to the original VAPEX model equation in **Equation 2-1**, it is noticed that;

$$h \equiv H - y \quad 2-10$$

$$N_s = \frac{\bar{C}'_B}{m * \nu_s} \quad 2-11$$

The dimensionless value  $N_s$  in Butler and Mokrys (1991)'s model is therefore related to the concentration dependent diffusion coefficient. Okazawa (2009) found the concentration dependent diffusion coefficient as a function of kinematic viscosity and plotted the graph in **Figure 2-8**. The diffusion coefficient (thus oil drainage rate) is seen to decrease with increasing kinematic viscosity, hence supporting the notion that VAPEX is applicable for reservoirs with naturally low bitumen viscosities.

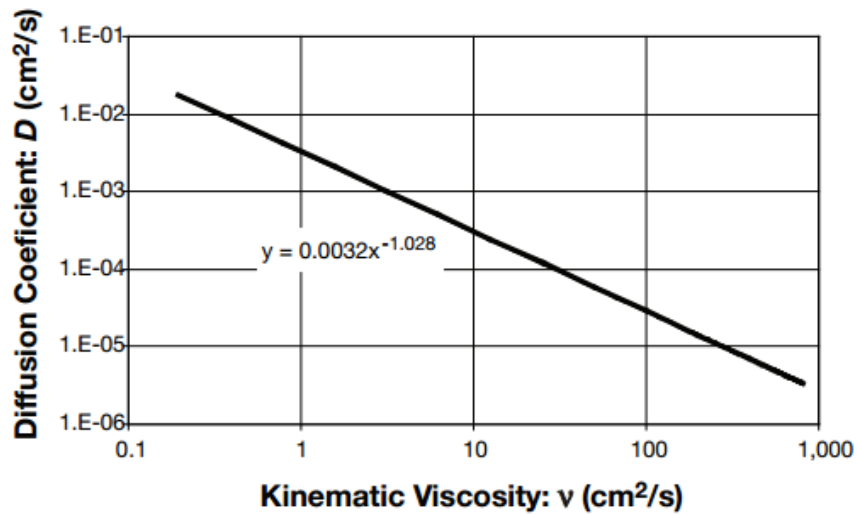


Figure 2-8 - Diffusion coefficient vs. Kinematic viscosity (Okazawa 2009)

The kinematic viscosity of the bitumen  $\nu_s$  at the interface is the key parameter to the process. However it is a difficult quantity to nail down due to its dependency on solvent concentration, which in turn is dependent on pressure and temperature.

Temperature conditions are a huge part of this work given the experiment will be conducted at varying temperatures to compare results. There are correlations that can be used to investigate the effect of temperature on diffusion coefficient. The Wilke - Chang correlation (**Equation 2-12**) for small molecules diffusing through large molecules can be used to estimate the infinite dilution diffusivity of solvent into bitumen.

$$D_{AB} = \frac{1.173 \times 10^{-16} (\phi M_B)^{\frac{1}{2}} T}{\mu V_A^{0.6}} \quad 2-12$$

Where,  $\phi$  = association parameter of solvent,  $M_B$  = molecular weight of liquid fluid,  $T$  = absolute of temperature (k),  $\mu$  = viscosity of the liquid fluid (kg/ms),  $V_A$  = solvent specific molar volume at its normal boiling point ( $\text{m}^3/\text{kg mol}$ ). Using this correlation, at  $15^\circ\text{C}$  the diffusivity of propane into bitumen is estimated to be  $5.3 \times 10^{-1} \text{ cm}^2/\text{s}$  yet at  $0^\circ\text{C}$  it is estimated to be  $5.2 \times 10^{-9} \text{ cm}^2/\text{s}$ .

The Stokes-Einstein equation quantitatively describes diffusion of spherical particles through a liquid with low Reynolds number Bird *et al.* (2002). The equation is given as;

$$D_{AB} = \frac{kT}{6\pi R_A \mu_B} \quad 2-13$$

Where  $k$  is the Boltzmann constant,  $T$  is absolute temperature,  $R_A$  is the radius of the spherical particle and  $\mu$  is the viscosity of the given liquid component. Using the Stokes-Einstein equation to predict the infinite dilution of bitumen into the diffusion coefficients at 15°C and 50°C are estimated to be  $6.1 \times 10^{-5}$  and  $6.8 \times 10^{-5}$  cm<sup>2</sup>/s respectively.

These correlations insinuate that increasing the temperature increases the diffusion of solvent into the bitumen (by huge orders of magnitude for Wilke – Chang). This would be expected since temperature increase significantly reduces bitumen viscosity and thus immobilizing the oil (live oil) for drainage. After drainage, the bitumen immediately has a fresh new surface (large concentration gradient) for diffusion to occur. This work however will not have any oil drainage hence the impact of the reduced viscosity of the oil on diffusion will be minimal. Also the Stokes-Einstein theory is true for large molecules diffusing into a dilute solution. Butane solvent vapor is considered a small molecule diffusing into large molecular weight bitumen.

There is some literature that has looked at the effects of temperature on the VAPEX process as a whole. Haghghat and Maini (2013) took an in depth look at the effect temperature has on the VAPEX process. Experiments were conducted in a large high-pressure physical model packed with 250 Darcy ( $2.45 \times 10^{-4}$  μm<sup>2</sup>) sand, Mackay River oil (300 Pa.s viscosity at 23°C, 0.988 kg/m<sup>3</sup> at 50°C) and propane as the solvent. The model was preheated to 40, 50 and 60°C before propane was injected at the same temperature, but different injection pressures.

Six experiments were run under different operating conditions. For the first four experiments, solvent pressure was kept constant (0.817 MPa or 105 psig) and pre-heated temperature values were 22, 40, 50 and 60°C. For experiments 5 and 6 injection pressure was increased to 1.23 MPa

(165 psig) at  $T = 40^{\circ}\text{C}$  and 1.55 MPa (212 psig) at  $T = 50^{\circ}\text{C}$ . To eliminate the effect of solvent dilution on viscosity reduction, nitrogen as a NCG was injected for a 7<sup>th</sup> experimental run at  $50^{\circ}\text{C}$  and 1.55MPa. A free-fall gravity drainage test was also conducted at  $50^{\circ}\text{C}$  to estimate the additional oil production caused by free-fall-gravity drainage beyond the vapor chamber in the absence of solvent dissolution.

Each experiment was left to run for 60 hours before the system pressure was depleted and produced blow-down gas was collected and measured. Oil production rates were then measured to evaluate VAPEX performance. To quantify the contribution of free fall gravity drainage and solvent dissolution the total oil production rate, the results from experiment 7 (Nitrogen experiment) and experiment 6 (propane,  $50^{\circ}\text{C}$  and 1.55MPa) were compared as shown in **Figure 2-9**.

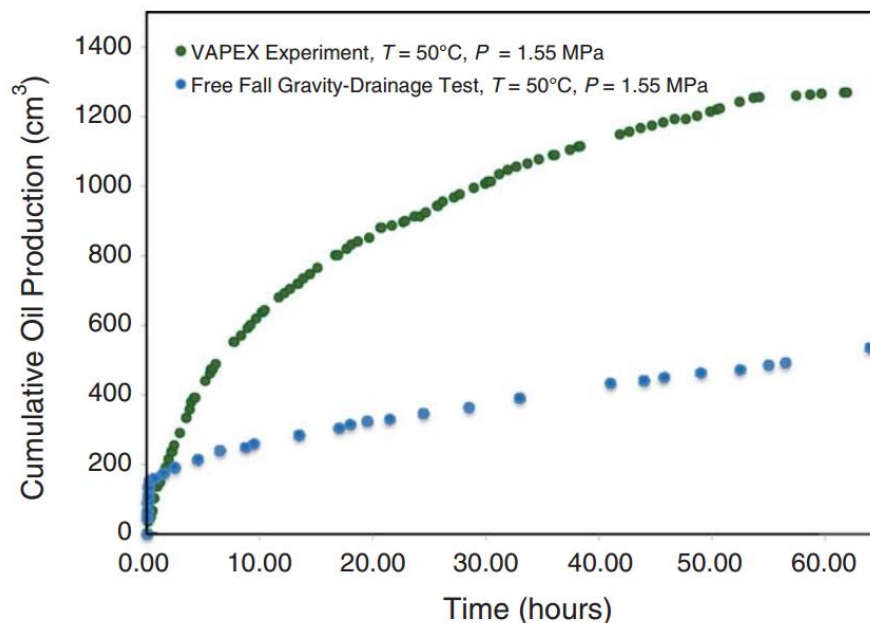


Figure 2-9 - Oil production via gravity drainage w/wo dissolution (Haghighat and Maini 2013)

With the above data, they were then able to differentiate between oil production rate due to free-fall gravity drainage and oil production rate due to diluted oil drainage as shown in **Table 2-2**.

Table 2-2 - Total Oil production - Free fall and Diluted Oil (Haghighat and Maini 2013)

Experiment #	T (°C)	P (MPa)	Total Rate of Oil Production (cm <sup>3</sup> /h)	Rate of Free Fall Gravity Drainage (cm <sup>3</sup> /h)	Rate of Diluted Oil Drainage (cm <sup>3</sup> /h)
1	22	0.817	9	0.0	9.0
2	40	0.817	13	2.5	10.5
3	50	0.817	23	7.8	15.2
4	60	0.817	44	17.0	23.0
5	40	1.230	25	3.0	22.0
6	50	1.550	45	10.0	35.0

Haghighat and Maini (2013)'s results showed an increasing oil production rate with increasing temperature. This is due to the significant viscosity reduction (hence higher gravity drainage) at higher temperatures. The total rate of oil production was 70% higher at 50°C and 200% higher at 60°C compared to the oil production rate at 40°C when the pressure was kept constant at 0.817MPa. The increased injection pressure led to an increased total oil production rate due to the higher solubility of solvent in bitumen (greater dilution drainage) when comparing experiments at the same temperature (40°C and 50°C) but at different pressures (0.817 – 1.23 or 1.55MPa).

Haghighat *et al.* (2013) went a step further to add a numerical simulation to the temperature experiments. The experimental results were simulated with a commercial compositional simulator to model the phase behavior and properties of propane/Athabasca systems. With history matching experimental production data, the temperature range was extended to 70°C, 80°C and 90°C. Viscosity of dead oil reduced drastically (favoring free fall gravity drainage production) but the solubility of solvent in the bitumen became far too low (unfavorable for diluted oil drainage). At 90°C the system therefore converges to the thermal-based end of the hybrid-solvent spectrum like ES-SAGD.

## 2.2. Viscosity correlations

This section reviews viscosity correlations in bitumen and solvent systems. Given viscosity is dependent on temperature, it is important to know the impact the viscosity will have on Solvent extraction mass transfer mechanism. Shu (1984) is a very popular viscosity model. It presents a generalized correlation for calculating viscosities of mixtures of heavy and light oil solvents. Using an Einstein-like relationship for viscosities of infinitely dilute solutions, a power law mixing rule was generalized. The density along with viscosity of both fluids is needed to predict mixture viscosity and accurate predictions have been achieved with heavy oil/solvents systems compared to experimental data.

$$\mu_{mix} = \mu_s^{f_s} \mu_b^{f_b} \quad 2-14$$

Where  $f_s$  and  $f_b$  both stand for the specie's weighting factor. They also account for the difference in viscosity and specific gravity of both terms.

$$f_b = \frac{\alpha C_{vb}}{\alpha C_{vb} + C_{vs}} \quad 2-15$$

Where  $C_{vb}$  and  $C_{vs}$  are both volume fractions of the heavy oil and solvent respectively. The summation of  $f_s$  and  $f_b$  is 1 as is the summation of  $C_{vb}$  and  $C_{vs}$ . The constant  $\alpha$  is an empirical parameter and calculated as:

$$\alpha = \frac{17.04 \Delta \rho^{0.5237} \rho_b^{3.2745} \rho_s^{1.6316}}{\ln\left(\frac{\mu_b}{\mu_s}\right)} \quad 2-16$$

$$\Delta \rho = \rho_b - \rho_s \quad 2-17$$

Shu (1984) tested this correlation by mixing bitumen with light petroleum fractions at temperatures varying from 23.9 - 27.8°C and achieved an excellent fit, as shown in **Figure 2-10**

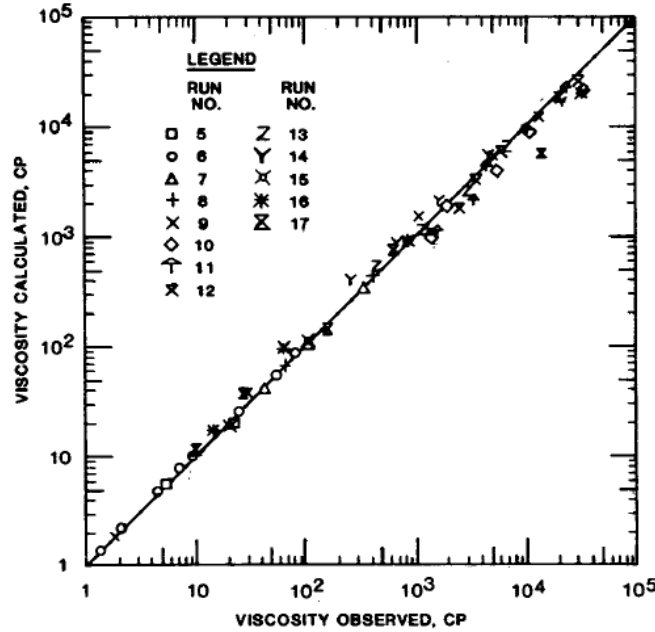


Figure 2-10 - Calculated viscosities vs. observed viscosities (Shu 1984)

Lobe (1973) is another popular viscosity model. It takes the following form:

$$\mu_m = \theta_s \mu_s \exp(\theta_o \alpha_o) + \theta_o \mu_o \exp(\theta_s \alpha_s) \quad 2-18$$

where  $\theta_s$  and  $\theta_o$  both represent the volume fractions of the solvent and volume fraction of oil respectively. Parameters  $\alpha_o$  and  $\alpha_s$  are given as:

$$\alpha_o = 0.27 \ln\left(\frac{\mu_o}{\mu_s}\right) + \left[1.3 \ln\left(\frac{\mu_o}{\mu_s}\right)\right]^{0.5} \quad 2-19$$

$$\alpha_s = -1.7 \ln\left(\frac{\mu_o}{\mu_s}\right) \quad 2-20$$

However, Lobe's model is predominantly a viscosity reduction model for liquid-liquid systems. The Cragoe (1933) model is based on the fact that the mixture viscosity behavior is not a linear function of the solvent fraction. Mixing rules are incorporated into the model as shown below:

$$L = \frac{1000 \ln 20}{\ln \mu - \ln(5 \times 10^{-4})} \quad 2-21$$

For a mixture of oil and solvent:

$$L_m = f_1 L_1 + f_2 L_2 \quad 2-22$$

$$f_2 = 1 - f_1 \quad 2-23$$

Wen and Kantzas (2006) compared an NMR (Nuclear Magnetic Resonance) model, Shu's model and Cragoe's model with experimental data, which were obtained from four heavy oil samples mixed with six solvent in varying ratios. Based on the NMR model, viscosity has a strong relationship with relative hydrogen index (RHI) and  $T_{2gm}$ . RHI is the oil  $A_I$  divided by water  $A_I$ , and  $T_{2gm}$  is the geometric mean of the  $T_2$  spectral distribution. The  $A_I$  is the signal amplitude per unit sample mass derived from the NMR. Viscosity is shown as;

$$\mu = \frac{\alpha'}{RHI^\beta T_{2gm}} \quad 2-24$$

Where  $\alpha'$  and  $\beta$  are both empirical constants and are estimated for different solvent and oil data sets. All three models (Shu, Cragoe and NMR) use a fixed form to predict viscosities of oil and solvent mixture. Viscosity, density and concentration are needed for Shu's and Cragoe's model. There are therefore limitations when the concentrations of the component mixtures are unknown. This is not the case with the NMR model. It was concluded that Shu's model is similar to the NMR model, and both are superior to Cragoe's model.

Yazdani and Maini (2010) designed a set-up to perform PVT experiments and viscosity measurements. The PVT experiments were conducted with Frog Lake heavy oil and butane as a solvent. The measurements included solvent solubility in oil, mixture density and viscosity at four different saturation pressures. In a mixing vessel, the mixture of oil/butane was made by placing an arbitrary volume of oil in the vessel and pressuring the oil with butane to near its dew point (210 kPa or 30.45 psi) for room temperature. Mixing was continued until no solvent decrease was observed from solvent dissolution. Lower pressure mixtures were prepared by releasing the gas from a mixture saturated until saturation pressure was achieved and no pressure rise was observed.

The data obtained from the experiment are used to tune an equation of state (EOS) to numerically simulate (WINPROP simulator) the VAPEX experiment. Two-phase flash and saturation pressure calculations were performed during the tuning process. Peng-Robinson was found to be the most representative EOS for the oil/butane phase behavior.

Viscosity changes are correlated by applying mixing type relationships. This correlation is based on the Kendall model in which mixture viscosity is calculated from individual component viscosities as shown in **Equation 2-25**,

$$\mu_{mix}^n = \sum_{i=1}^{i=m} c(i) * \mu(i)^n , \quad 2-25$$

where  $n$  is an adjustable parameter in this correlation and  $c$  is the mole fraction of each component. The exponent  $n$  was determined to be 0.09 and **Figure 2-11** shows a comparison of the viscosity experimental results, EOS tuned model, and other viscosity correlations. A clear pattern is the reduction of viscosity with increasing butane volume fraction.

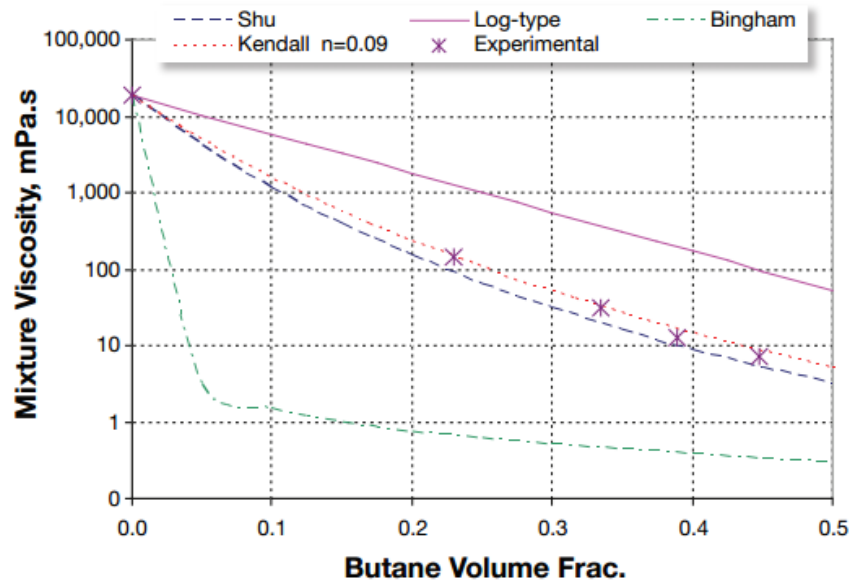


Figure 2-11 - Comparison of viscosity predictions with various correlations (Yazdani and Maini 2010)

Das and Butler (1996) uses results of a Hele-Shaw cell VAPEX experiments to obtain empirical correlations for propane and butane in Peace River bitumen. Solubility of the solvent in bitumen and a correlation for the viscosity of solvent mixture is added to the experimental data to estimate diffusivity. Das and Butler (1996) applied Hayduk and Cheng (1971)'s expression as the general form for evaluating diffusivity. The equation is:

$$D_s = \alpha(\mu^{-\beta}) \quad 2-26$$

where  $\mu$  is mixture viscosity,  $\alpha$  and  $\beta$  are constants for each diffusive substance. The dependency of diffusivity on temperature and composition appears through the viscosity, which is a strong function of both. Das and Butler (1996) eventually found the diffusivity of propane in Peace River bitumen to be as follows:

$$D_s = 1.306 \times 10^{-9}(\mu^{-0.46}) \quad 2-27$$

**Figure 2-12** shows the concentration dependence of viscosity and diffusivity using the above expression.

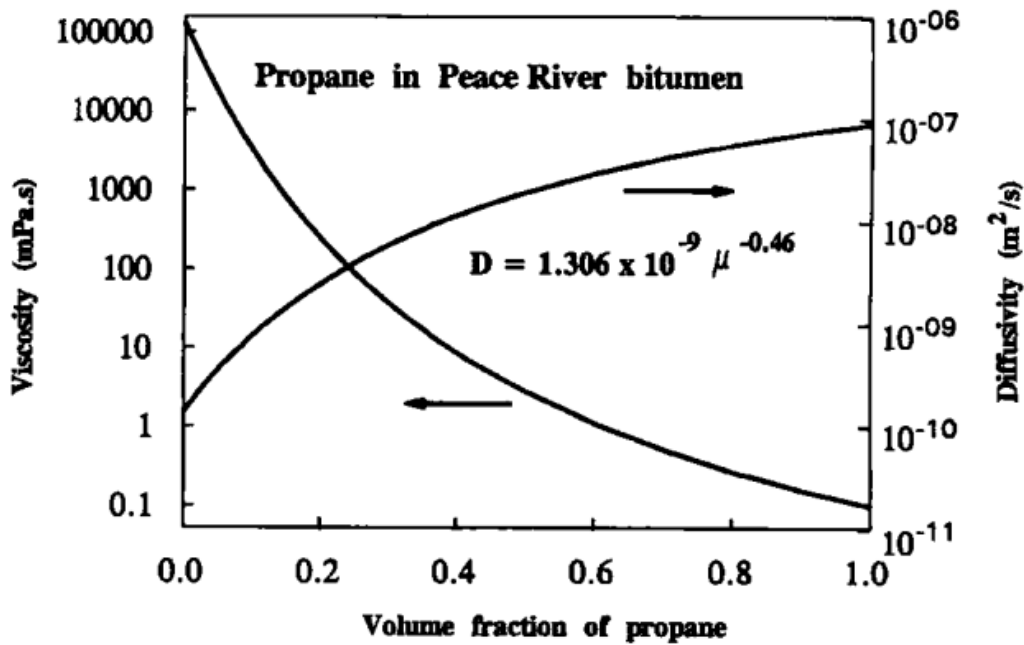


Figure 2-12 - Concentration dependence of viscosity and diffusivity (Das and Butler 1996)

Using the same principles, the butane expression was found to be as follows:

$$D_s = 4.13 \times 10^{-10} (\mu^{-0.46})$$

2-28

Yazdani and Maini (2009) applied the expression for frog-lake oil and the graph is shown in **Figure 2-13**. One to two orders of magnitude change in diffusivity is observed in the entire concentration domain of the graph, thus showing a strong concentration dependency.

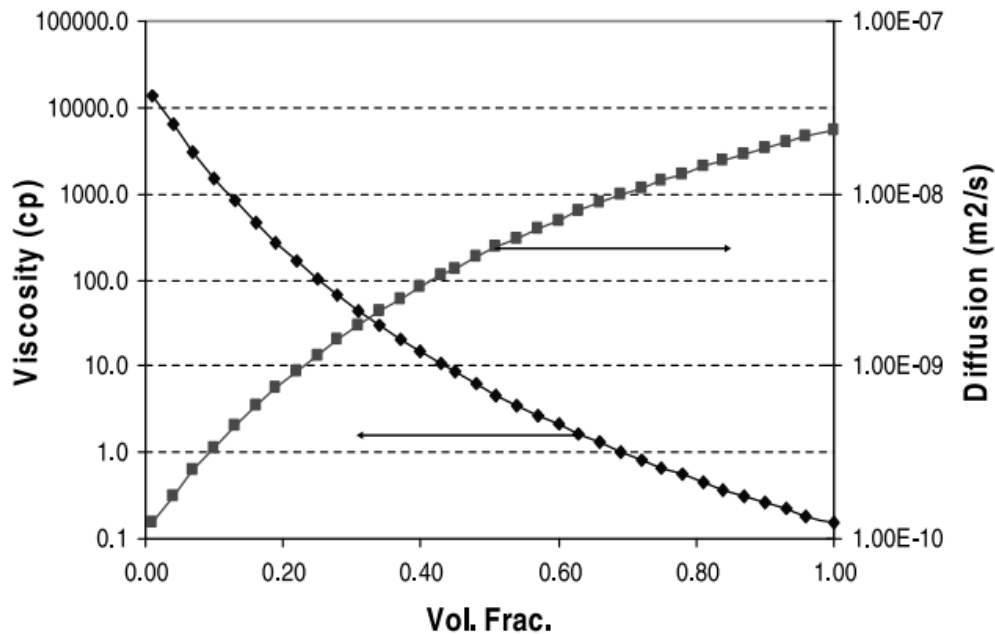


Figure 2-13 - Concentration dependency of viscosity & diffusivity butane (Yazdani and Maini 2009)

The literature shows that diffusivity/diffusion coefficient increase as viscosity reduces. This would be expected since temperature increase significantly reduces bitumen viscosity and thus immobilizing the oil (live oil) for drainage. After drainage, the bitumen immediately has a fresh new surface (large concentration gradient) for diffusion to occur. This work however will not have any oil drainage hence the impact of the reduced viscosity of the oil on diffusion will be minimal

### 2.3. Diffusivity/Diffusion coefficient

Please note that for the purpose of this work, diffusivity and diffusion coefficient are used interchangeably. However in technical terms diffusion coefficient would represent a constant numerical value while diffusivity varies with another independent variable (say for example concentration). Diffusivity is usually represented as a function. Both are a measure of the magnitude of the mass transfer occurring between two fluids via diffusion.

Among momentum, heat and mass transport processes, heat conduction and viscosity have standardized techniques for measurements. However, this is not the case for the mass transfer characteristics. Measurements of mass transfer characteristics are often more challenging, specifically due to difficulties in measuring point values of concentration and other issues like: phase equilibrium, effect of convective transport and having a mixture rather than a pure fluid. Experimental techniques specifically for VAPEX systems are also inhibited due to the opacity of the bitumen and the volatility of the light hydrocarbon solvents mostly used.

Measuring the diffusivity of light hydrocarbon solvents in heavy oil has been of great interest due to its direct link to oil production rates in VAPEX systems. Butler and Mokrys (1991) and Das (1995) concluded that a much higher diffusion coefficient than estimated by theoretical predictions was required to match production rates from laboratory scale VAPEX experiments. Until diffusion values (obtained from diffusivity functions) are reliable, oil companies will continue to be reluctant to implement VAPEX technology on a field/commercial scale.

In the past two decades, majority of the experimental methods developed to determine the diffusion coefficient of a gas in bitumen have relied on Fick's law as the basis of their work (Bird *et al.* 2002). It states that flux goes from a region of high concentration to a region of low concentration depending on the concentration gradient. It relates diffusive flux to concentration of a component under steady state conditions. The Fick's 1<sup>st</sup> law equation takes the following form;

$$j_A = -\rho D_{AB} \nabla w_A \quad 2-29$$

Where  $j_A$  is the diffusive flux of component  $A$  in component  $B$ ,  $\rho$  is the density that when multiplied with parameter  $w_A$  (mass fraction) gives mass concentration of component  $A$ .  $D_{AB}$  is the diffusion coefficient,  $\nabla$  indicates the direction of diffusion in concentration gradient. With no chemical reaction occurring, Fick's 1<sup>st</sup> Law equation can be differentiated to give Fick's 2<sup>nd</sup> law as given:

$$\frac{\partial C_A}{\partial t} = D_{AB} \nabla^2 C_A$$

2-30

Where  $C_A$  is the concentration of component A found by multiplying density and mass fraction. This equation is applicable to diffusion in solids or stationary liquids when the concentration is dilute enough for the diffusivity to be constant.

It must be stated that Fick's 1<sup>st</sup> law works on the assumption that density of diffusing fluids is equal and constant (Chordia and Trivedi 2010). This is not the case when gas diffuses into heavy oil. This work will account for the changing fluid density by making diffusivity a function of solvent mass fraction (solvent concentration). The next sections will constant diffusion coefficient measurement methods and concentration dependent diffusivity measurement methods.

## 2.2.1. Constant diffusion coefficient methods

### 2.2.1.1. Pressure decay methods

This method, as the name suggests, involves pressuring gas solvent into an enclosed vessel filled with bitumen, and recording the system pressure reduction over time to evaluate the diffusion coefficient. The system pressure declines as the gas solvent continuously diffuses into the bitumen, hence increasing the bitumen's solvent concentration. This method was initially developed by Riazi (1996) to determine diffusion coefficients of methane in pentane liquids using a PVT cell. Riazi (1996)'s method was simple and did not require any expensive or time-consuming compositional analysis.

Zhang *et al.* (2000) adapted Riazi (1996)'s methodology for heavy oil systems and specifically looked at the diffusion coefficient of carbon-dioxide and methane in high pressure window cells. Fick's law of diffusion, along with gas material balance equations, was then used to history match the gas absorption data. The diffusion coefficient was made an adjustable parameter. **Figure 2-14** shows a simple schematic of the experiment and **Figure 2-15** shows a graph of the subsequent pressure decay.

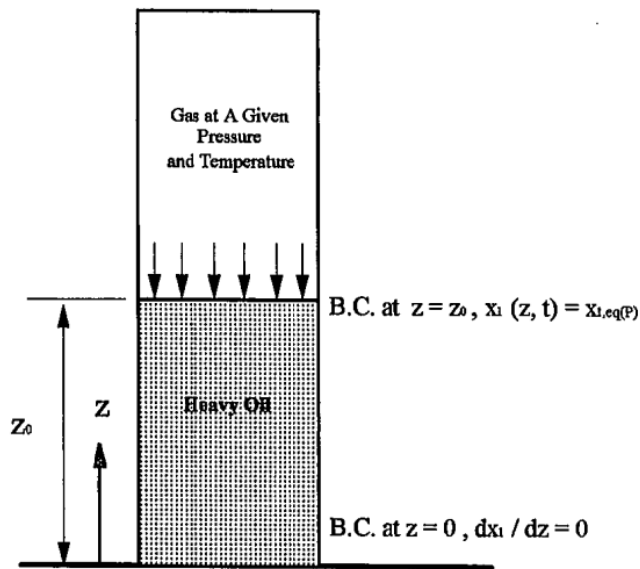


Figure 2-14 - Pressure decay schematic (Zhang *et al.* 2000)

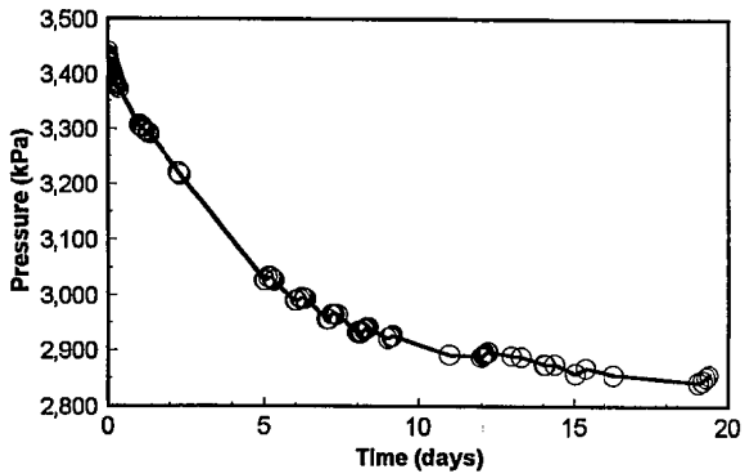


Figure 2-15 - Pressure decay graph (Zhang *et al.* 2000)

Some of the assumptions made by Zhang *et al.* (2000) are listed below;

- 1) Swelling of the liquid phase is negligible and the gas/bitumen interface height is constant through the full experiment. It is hard to justify this assumption from a logical stand point. Mass can neither be created nor destroyed so all the diffusing solvent must go

somewhere in the heavy oil fluid. The heavy oil is thick and not particularly porous so the fluid will have to swell as diffusion occurs. The occurrence of bitumen swelling was later definitively proved by Chatzis (2002)

- 2) The concentration of gas at the interface and temperature of the system remains constant through the experiment. This is also hard to justify given the concentration at the interface (solubility) is pressure dependent. The pressure of the system clearly declines as they experiment progresses so the concentration should equally decline as such.
- 3) Diffusion coefficient is constant through the whole experiment regardless of gas concentration. This assumption is linked to point 2) of constant gas concentration at the interface. Diffusion is driven by concentration gradient so it just isn't logical for it to remain the same at varying concentrations. Concentration dependency is further discussed in **Section 2.2.3**.
- 4) Oil is non-volatile and the gas is a pure gas.

For Zhang *et al.* (2000)'s work, modest pressures of about 3500 kPa were used with methane and 2900 kPa for carbon-dioxide to evaluate the diffusion coefficient. Diffusion coefficient values ranged from **9.8393–6.1726 ( $10^{-9}$ )  $m^2/s$**  for methane and **4.7254– 4.4241 ( $10^{-9}$ )  $m^2/s$**  for carbon-dioxide. Both trends did show that higher gas pressures gave higher diffusion coefficient values.

A big issue developing a diffusion model based on pressure decay is the problem of boundary conditions between the solvent and bitumen. A lot of literature assumes that the heavy oil and solvent vapor instantaneously reach equilibrium concentration on contact with each other at the given thermodynamic conditions. But this concentration of the solvent (solubility) at the bitumen interface is dependent on pressure so any decreases in pressure will inevitably lead to decrease in interface concentration. Tharanivasan *et al.* (2006) attempted tackle this problem associated with pressure decay methods by utilizing special boundary conditions. Based on previous work, three boundary conditions were feasible;

- 1) the interface assumes the saturated solvent concentration at equilibrium pressure regardless of whether or not equilibrium is reached Zhang *et al.* (2000),

- 2) the interfacial concentration is equal to the solubility concentration dependent on pressure hence the interfacial concentration is constantly changed to match the declining pressure. This method was used by Upreti and Mehrotra (2002) and is a sort of ‘quasi-equilibrium’.
- 3) the interface is not at equilibrium, hence proving resistance to mass transfer. This method was first introduced by Civan and Rasmussen (2011). It is however an incredibly complex method to use and is therefore rarely utilized by researchers

Tharanivasan *et al.* (2006) applied all three boundary conditions to these heavy oil solvent systems and diffusion coefficients were found for each boundary condition by finding the minimum objective function (minimum average pressure difference between theoretically calculated and experimentally measure pressures). The most suitable boundary condition was then found by comparing all minimum objective functions, and history matching is used to determine the solvent diffusivity. The non-equilibrium boundary condition worked best for a CO<sub>2</sub>-heavy oil system, equilibrium boundary condition worked best for methane-heavy oil system and the quasi-equilibrium worked for best for a propane-heavy oil system. **Table 2-3** below shows the diffusivities obtained for the propane heavy oil system.

Table 2-3 - Diffusivity of C<sub>3</sub>H<sub>8</sub> in heavy oil at different diffusion time 23.9°C (Tharanivasan *et al.* 2006)

diffusion time (day)	boundary condition	$D$ (10 <sup>-9</sup> m <sup>2</sup> /s)	$k_D$	$\Delta P_{ave}$ (kPa)
5	equilibrium	2.53		23.6
	quasi-equilibrium	1.10		16.1
	nonequilibrium	2.55	500	23.7
10	equilibrium	2.01		28.8
	quasi-equilibrium	0.92		22.0
	nonequilibrium	2.02	> 500	<28.9
20	equilibrium	1.78		27.7
	quasi-equilibrium	0.80		23.4
	nonequilibrium	1.79	> 450	<27.8
23.5	equilibrium	1.76		25.8
	quasi-equilibrium	0.79		22.0
	nonequilibrium	1.78	> 300	<26.0

Behzadfar and Hatzikiriakos (2014) combined the pressure decay technique with rheological experiments to measure equilibrium pressure precisely and determine diffusion based on the final equilibrium state. Experiments were performed at three different temperatures (30, 50, 70°C) using two different pressures levels for each temperature (~2 MPa and ~4 MPa) within a CO<sub>2</sub>-bitumen system. The experimental schematic is shown in **Figure 2-16**.

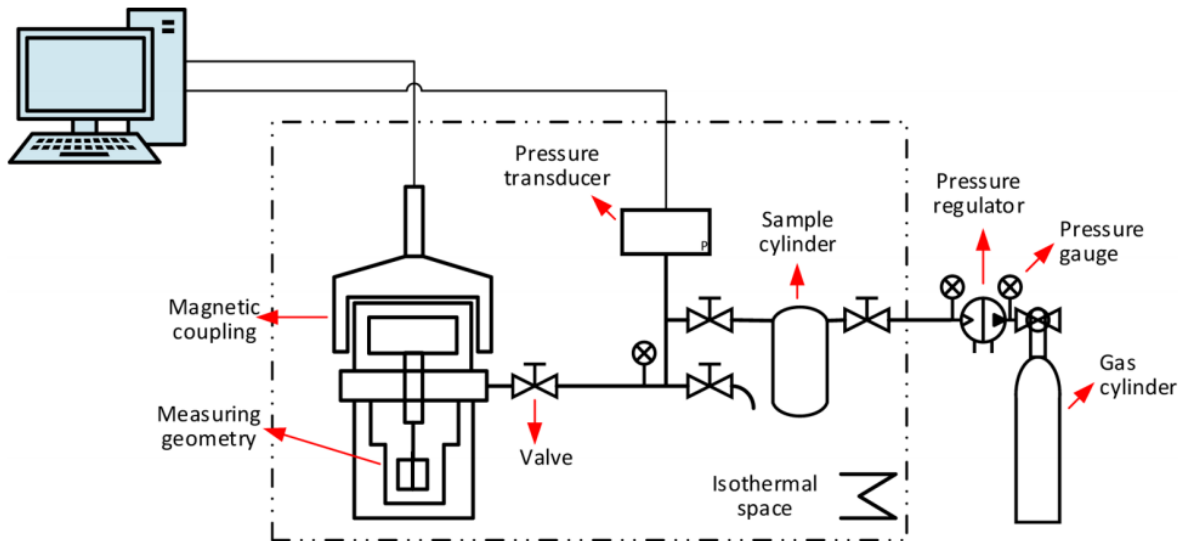


Figure 2-16 - Schematic diagram of the pressure cell set-up (Behzadfar and Hatzikiriakos 2014)

The liquid cup incases the measuring geometry and is the part of schematic where the CO<sub>2</sub> and bitumen mixing takes place. The measuring geometry facilitates the mixing (using shear) of the CO<sub>2</sub> and bitumen while being connected directly to the torque measuring system of a rheometer. Experiments are conducted using three steps:

- 1) First CO<sub>2</sub> is allowed into the liquid to mix with bitumen while no shearing is applied to capture the static diffusion thoroughly
- 2) The measuring geometry is then allowed to spin gently at shear rates 10-30s<sup>-1</sup>
- 3) Saturation takes place by diffusion which is facilitated by shear. Higher shear rates of 10-50s<sup>-1</sup> are applied to ensure equilibrium state of the system

Mixing due to shear imposed by rheometry allows rapid direct measurements of equilibrium pressure with a high degree of accuracy. This is achieved by monitoring both the viscosity and

pressure of the system at the shearing step to ensure the system reaches equilibrium. Results showed that diffusion of a CO<sub>2</sub>-bitumen system can be described by the Arrhenius equation (effect of temperature). The diffusion increases with temperature (30-70°C) by 88% at equilibrium pressure of 2 MPa and 54% at equilibrium pressure 4 MPa. The calculated diffusion increase with pressure suggests in the case of diffusion in the presence of more CO<sub>2</sub> molecules but this increase is clearly more dominant in lower temperatures.

This method is advantageous as it calculates diffusion directly from measured equilibrium pressure with no assumptions. It is easy to apply and eliminates the errors from the uncertainty of estimating the equilibrium pressure. However the forced mixing of the CO<sub>2</sub> and bitumen through shearing really is not applicable in real reservoir scenarios. The method like other pressure decay methods also neglects the swelling of the bitumen liquid due to the diffusion of the CO<sub>2</sub>.

### 2.2.1.2. Dynamic Pendant Drop Shape Analysis (DPDSA)

Yang and Gu (2003) and Yang and Gu (2006) formulated a method that involves a pendant drop of bitumen formed in a transparent high pressure cell. This cell will be filled with solvent (butane or propane) at the desired temperature and pressure. The bitumen sample is then injected into the system via a syringe to form a pendant drop inside the pressure cell. The diffusion that takes place leads to the bitumen sample shape and volume to change until equilibrium is reached. At equilibrium, the bitumen is completely saturated with solvent. Digital images of the bitumen droplet are acquired over the experiment and analyzed with digital image processing. Below is a schematic of the system setup **Figure 2-17**.

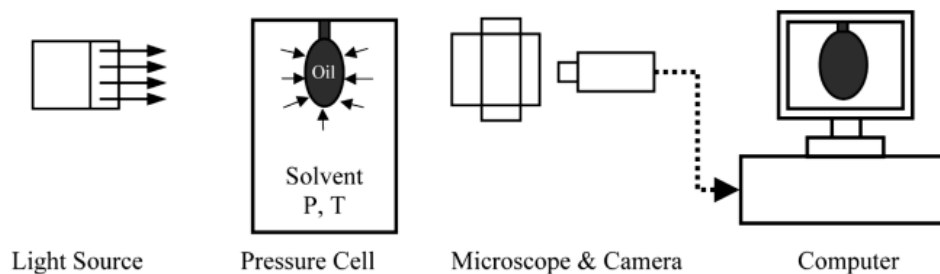


Figure 2-17 - DPDSA set-up (Yang and Gu 2006)

The physical changes noticed in the bitumen droplet are a result of interfacial tension reduction. Convergence between the experimentally observed and numerically predicted profiles is obtained by constructing an objective function. Once the minimum objective function is reached, the solvent diffusion in heavy oil and mass transfer Biot number are determined. A finite-element method is employed to simulate the unsteady 2D solvent concentration distribution within the droplet. The drop profile is predicted by numerically solving the Laplace equation of capillarity. A single diffusion measurement can be completed within an hour and only a small amount of oil is needed. This method was applied to diffusion of CO<sub>2</sub> in brine and diffusion of CO<sub>2</sub> in heavy oil. The diffusion coefficient values obtained agreed with literature data;  $1.81 \cdot 10^{-9} \text{ m}^2/\text{s}$  for CO<sub>2</sub> (3.6 MPa and 25°C) in brine and  $1.14 \cdot 10^{-9} \text{ m}^2/\text{s}$  for CO<sub>2</sub> (2.9 MPa and 25°C) in heavy oil.

However, the impact of the shape/volume of the pendant drop on diffusion was neglected. Also, introducing the needed brine/bitumen into the system was difficult because it had to be spread evenly on the drop surface. This is very difficult to achieve given the volume of the droplet is constantly changing. Also, the surface profiles are analyzed under the assumption that surface tension is the same as the surface tension of a static droplet shape. Also another issue is the difference in diffusion driving force at the top and bottom of the droplet. At the top of the droplet, diffusion occurs into the drop but with hardly any solvent remaining there due to lack of solvent accumulates. Solvent falls and accumulates the bottom of the droplet leading to a completely different concentration driving force compared to the top.

### **2.2.1.3. Computer Assisted Tomography (CAT)**

This method involves the use of x-ray tomography with a CT scanner to generate 2D images of the solvent-oil mixture. Higher density regions (bitumen rich) will typically have higher CT numbers compared to lower density regions (solvent rich). The CT scanner is therefore used for comprehensive analysis of the solvent diffusion into the bitumen. Wen *et al.* (2004) examined a range of solvents in different heavy oils using CT scanning and Nuclear Magnetic Resonance. Luo and Kantzas (2008) presented diffusion experiments of liquid solvents in heavy oil saturated sand using this CT scanning method while considering porosity variation of media

and volume changes of mixing. The inclusion of porous media leads to a differentiation of effective diffusivity ( $D_e$ ) and bulk diffusivity ( $D_o$ );  $D_e$  represents diffusivity in porous media while  $D_o$  represents diffusivity in bulk fluids. **Equation 2-31** and **Equation 2-32** give an approximation of how both parameters are related.

$$D_e = \frac{D_o}{\sqrt{2}} \quad 2-31$$

Or

$$D_e = \frac{D_o}{F} \quad 2-32$$

$$F = \phi^{-m} \quad 2-33$$

Where  $F$  is the formation electrical resistivity factor,  $\phi$  is porosity and  $m$  being cementation factor (different values in different packing).

Luo and Kantzas (2008) outlined the following assumptions for their work:

- No chemical reaction occurring
- The system is contained in a static cell
- Porosity variation of the media is considered
- Volume changes occur due to mixing
- Only one-dimensional diffusion is considered
- Temperature and pressure are constant

For a heterogeneous porous media, the rates at which the concentrations of two components  $C_A$  and  $C_B$  change at a given point are given by:

$$\emptyset \frac{\partial C_A}{\partial t} = \frac{\partial}{\partial x} \left( D \emptyset \frac{\partial C_A}{\partial x} \right) - \frac{\partial}{\partial x} \left\{ C_A \int_{-\infty}^x \frac{D \emptyset}{V_B C_A} \left( \frac{\partial V_B}{\partial C_A} \right) \left( \frac{\partial C_A}{\partial x} \right)^2 dx \right\}, \text{ and} \quad 2-34$$

$$\emptyset \frac{\partial C_B}{\partial t} = \frac{\partial}{\partial x} \left( D \emptyset \frac{\partial C_B}{\partial x} \right) - \frac{\partial}{\partial x} \left\{ C_B \int_{-\infty}^x \frac{D \emptyset}{V_B C_A} \left( \frac{\partial V_B}{\partial C_A} \right) \left( \frac{\partial C_A}{\partial x} \right)^2 dx \right\} \quad 2-35$$

For a homogeneous porous media, the rates at which the concentrations of two components  $C_A$  and  $C_B$  change are simplified to:

$$\frac{\partial C_A}{\partial t} = \frac{\partial}{\partial x} \left( D \frac{\partial C_A}{\partial x} \right) - \frac{\partial}{\partial x} \left\{ C_A \int_{-\infty}^x \frac{D}{V_B C_A} \left( \frac{\partial V_B}{\partial C_A} \right) \left( \frac{\partial C_A}{\partial x} \right)^2 dx \right\}, \text{ and} \quad 2-36$$

$$\frac{\partial C_B}{\partial t} = \frac{\partial}{\partial x} \left( D \frac{\partial C_B}{\partial x} \right) - \frac{\partial}{\partial x} \left\{ C_B \int_{-\infty}^x \frac{D}{V_B C_A} \left( \frac{\partial V_B}{\partial C_A} \right) \left( \frac{\partial C_A}{\partial x} \right)^2 dx \right\} \quad 2-37$$

The parameter  $V_A/V_B$  represents volume at constant pressure and temperature for the given component. For a bulk fluid (porosity is one),  $D$  would represent molecular diffusivity  $D_o$ ; for porous media (porosity  $< 1$ ),  $D$  would represent effective diffusivity  $D_e$ . Applying the Boltzmann substitution to **Equation 2-36** gives an evaluation for  $D$ ;

$$D = - \frac{1}{2t} \frac{dx}{dC_A} \left\{ \int_0^{C_A} x dC_A + C_A V_B \int_0^{C_A} \frac{\int_0^{C_A} x dC_A}{C_A V_B^2} \left( \frac{\partial V_B}{\partial C_A} \right)_{P,T} dC_A \right\} \quad 2-38$$

The diffusion process was monitored by a GE9800 CT scanner and x-ray tomography techniques were employed to generate 2D images of the solvent-oil mixture. These scans were then averaged and converted to solvent and bitumen concentration profiles. **Figure 2-18** below shows CT images of a sand pack sample filled with solvent and heavy oil. **Figure 2-19** shows CT sand-pack images at different times.

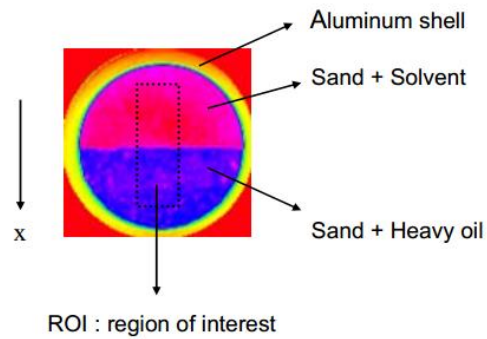


Figure 2-18 - CT images of a sand pack sample (Luo and Kantzas 2008)

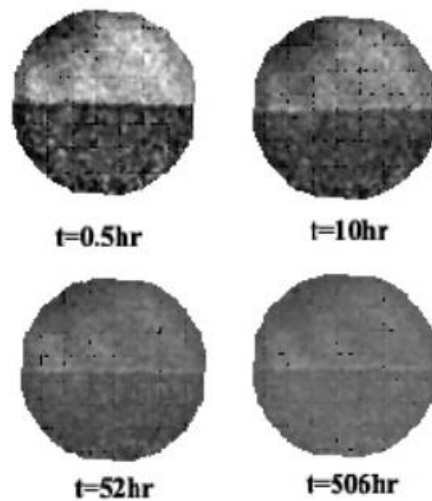


Figure 2-19 - CT Scan at different times (Luo and Kantzas 2008)

To process the CT scan, a Region of Interest (ROI) was selected, porosity variation was analyzed, the CT number of the ROI in the horizontal direction was averaged (giving CT number profiles) and these CT number profiles were converted to density profiles. Density profiles were then later converted to concentration profiles. **Figure 2-20** shows an example of such concentration profiles at varying times.

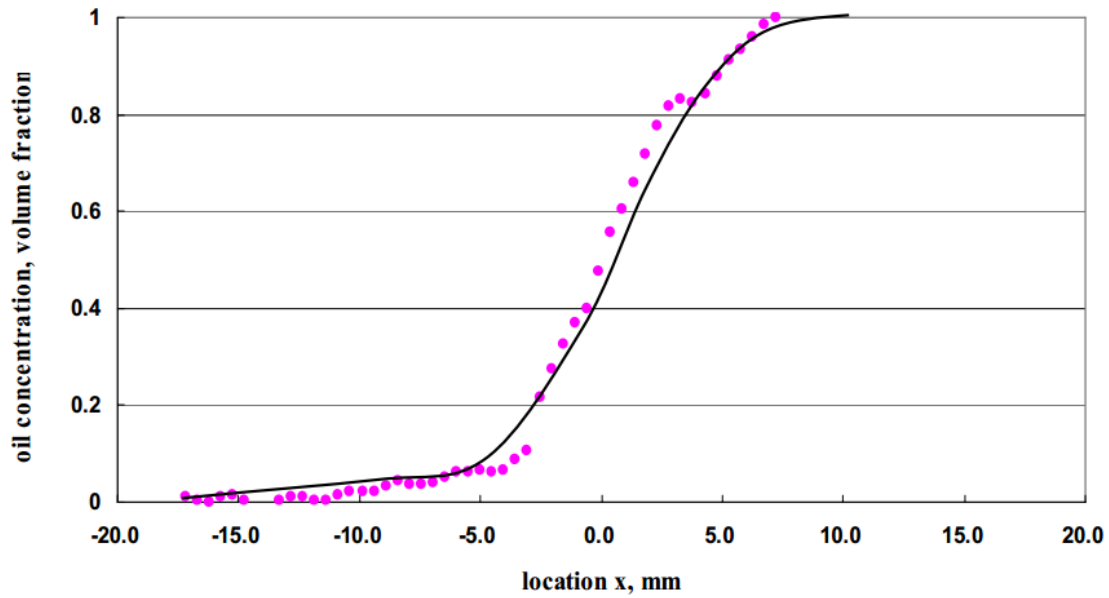


Figure 2-20 - CT converted concentration profile at time 667 minutes (Luo and Kantzas 2008)

Results showed that the time dependency of the diffusivity is reduced by taking into account the volume change on mixing. The mutual concentration diffusion coefficient was found to be dependent on concentration in both homogeneous and heterogeneous porous media. **Figure 2-21** shows the diffusion coefficient relationship with concentration for bulk fluids and porous media.

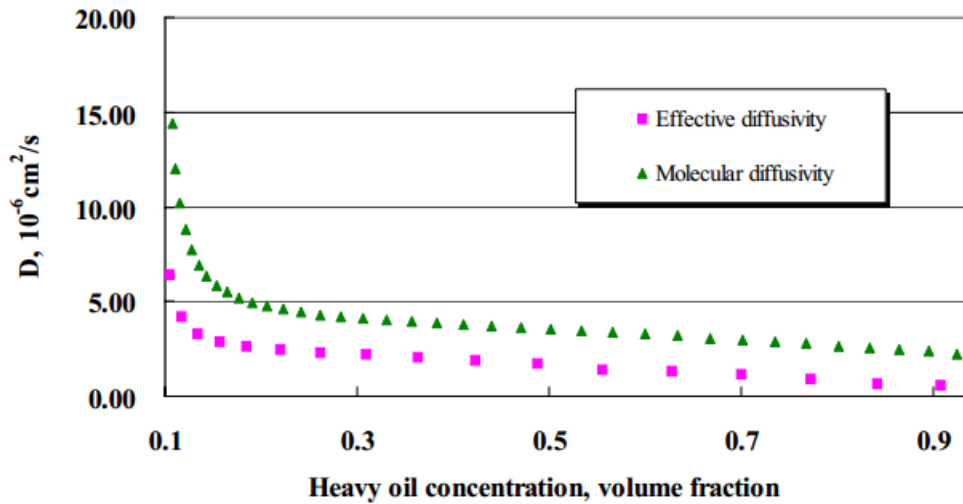


Figure 2-21 - Diffusivity in Heavy oil for bulk fluids and porous fluids (Luo and Kantzas 2008)

#### 2.2.1.4. Nuclear Magnetic Resonance (NMR)

Wen *et al.* (2004) and Wen *et al.* (2013) applied low field NMR to determine solvent content and viscosity reduction in heavy oil mixtures. The mobility of the hydrogen molecules changed when the solvent came in contact with the bitumen. These changes were detectable through changes in the NMR relaxation characteristics for the solvent and heavy oil. The relaxation changes were then correlated to mass flux and concentration changes.

The diffusion coefficient calculated was via Fick's 2<sup>nd</sup> law **Equation 2-30** and is independent of concentration and the approach tested against a variety of oil/solvents. Some of the following assumptions were made:

- The system is in a static vial having a constant volume
- The solvent is above the heavy oil and the heavy oil is one pseudo-component
- One-dimensional mass transfer occurs
- Infinite medium and no volume change on mixing
- Constant temperatures and pressure through the full experiment

The changes in concentration along the x-axis are expressed as below:

$$C = \frac{1}{2} C_0 \operatorname{erfc} \left( \frac{x}{2\sqrt{Dt}} \right) \quad 2-39$$

During the NMR experiments, the concentration determined NMR spectra change is the overall concentration, 'C' in the mixture area, which is a function of time and diffusion coefficient. The parameter 'x' is the distance of unsteady diffusion. With some pre-determined boundary conditions, the correlation between concentration, time and *D* is given as:

$$C = f(x, t, D) \quad 2-40$$

$$\int_0^l C dx = \int_0^l f(x, t, D) dx = f(t, D) \quad 2-41$$

At a given t,

$$\bar{C} = \frac{\int_0^l C dx}{\int_0^l dx} = \frac{\int_0^l f(x, t, D) dx}{l} = f(t, D) \quad 2-42$$

The basis for using NMR is the fact that the relaxation spectrum of heavy oil is distinctly different than that of the solvent. **Figure 2-22** shows this difference in spectra. **Figure 2-23** shows the difference in spectra during diffusion.

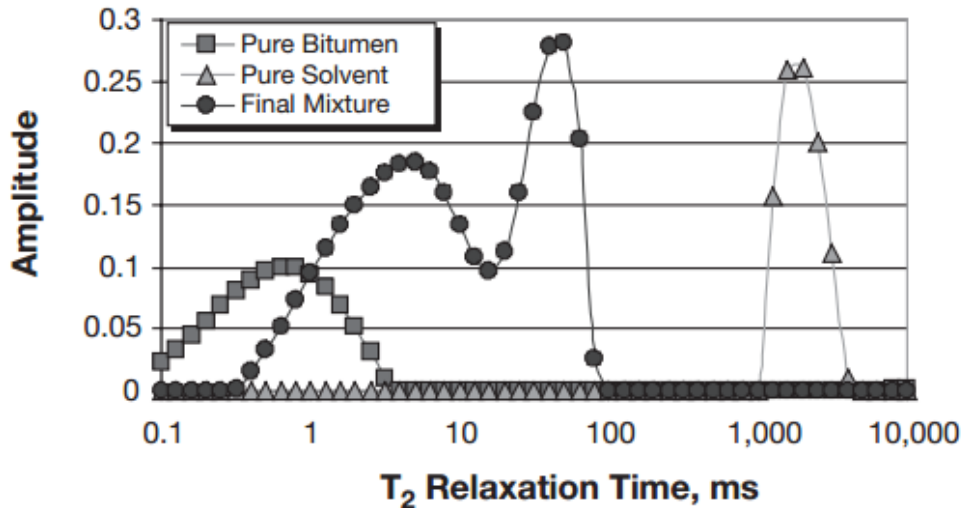


Figure 2-22 - Typical NMR spectra for bitumen, pure solvent and a mixture (Wen *et al.* 2013)

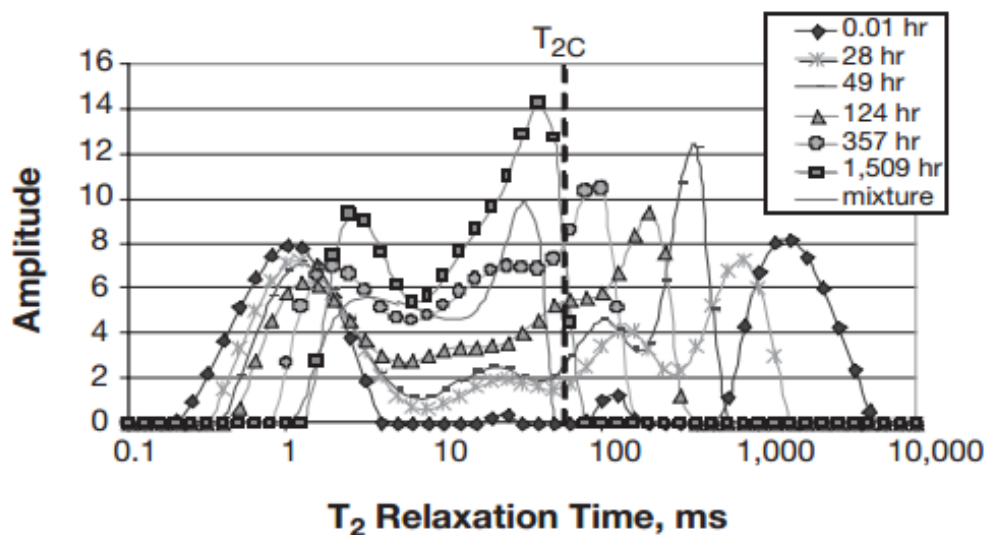


Figure 2-23 - Spectra change during diffusion (Wen *et al.* 2013)

Below in **Table 2-4** is a list of diffusion coefficient values obtained from the various experimental conditions.

Table 2-4 - Diffusion coefficient of solvents in oils (Wen *et al.* 2013)

Solvent	Bitumen	% of Solvent to Solution	$D$ ( $10^{-6}$ cm <sup>2</sup> /s)	
Heptane	Cold Lake oil	5%	2.93	
		10%	4.16	
		15%	4.92	
		20%	5.06	
		30%	5.1	
		50%	5.39	
Pentane	Cold Lake oil	20%	8.89	
Hexane			8.32	
Naphtha			5.64	
Toluene			9.26	
Kerosene			4.08	
Heptane			Atlee Buffalo	7.81
Heptane			Peace River oil	4.95

The NMR method is great because it can also be used to understand the relationship between asphaltene precipitation Wen *et al.* (2003), density and viscosity Wen and Kantzas (2004) in solvent-heavy oil systems. However it does rely on the assumption of no swelling of bitumen as the diffusion occurs (already disproved). The assumption of an infinite medium for diffusion to occur is also hard to justify. The infinite medium assumptions maybe applicable while simulating a reservoir but in a closed system like the one used for this the experiment, the wall effects and finite limitation may apply dominantly hence introducing deviations in the model. Also the experiment is run for four weeks but only data for the first two days is accounted for when calculating the diffusion coefficient. This is because the interface between the solvent and oil could only be maintained for a short period of time. This represents a huge approximation as the distance traversed by the solvent front is unknown and thus the effects of the boundary walls on the interface may have been judged poorly.

### 2.2.2. Mutual diffusion coefficient

Mutual diffusion coefficient is not directly relevant to this work but is related to general Solvent extraction processes. Mutual diffusion occurs mainly liquid-liquid or gas-gas systems when the rate of diffusion of species A in B is equal to the rate of diffusion of species B in A. As the VAPEX technology advances, different solvent options will be explored. There will therefore be the possibility of including of liquid hydrocarbons as solvents. Given the foundational definition of VAPEX involves the using a solvent ‘vapor’ (gas), using liquid solvents would generally be termed as a ‘Solvent assisted recovery’ process. In liquid-liquid systems the diffusion occurring is typically known to be mutual diffusion given both liquid diffuse into each at fairly similar rates (unlike gas-liquid systems). However data for such systems are scarce, limited to ambient conditions and show apparent inconsistencies.

Ghanavati *et al.* (2014a) reported all the mutual diffusion coefficient measurements in two general cases of concentration independency and concentration dependency. The report showed that literature suffers from experimental limitations and difficulties in analysis that make their interpretation a challenging task. Asphaltene precipitation is also very prevalent at the liquid-liquid interface hence forming a barrier that hinders the mutual diffusion. It was concluded that

for significant progress to be made in liquid-liquid mutual diffusion calculations, new measuring techniques need to be implemented. These measuring techniques must not be limited by practical restrictions nor sensitive to calculation procedures.

Ghanavati *et al.* (2014b) applied Taylor dispersion technique to find reliable mutual diffusion coefficients in a hexane-bitumen mixture. The infinite-dilution molecular diffusion coefficients of bitumen in hexane were measured in both the presence and relative absence of asphaltene precipitates at atmospheric pressures with temperatures 303.15 K, 310.15 K and 317.15 K.

In a Taylor dispersion experiment, a minute amount of solvent, called a pulse, is injected into a laminar carrier stream of a slightly different composition of fluid flowing in a long capillary tube. As the pulse travels through the tube, it spreads out into a nearly Gaussian profile under the combined actions of molecular diffusion and convection. The shape of the dispersed peak measured by an adequate detector, commonly at the end of the tube, is used to determine the molecular diffusion coefficient  $D$  from the dispersion coefficient  $K$ . The following equation is applied:

$$K = D + \frac{R^2 \bar{u}^2}{48D} \quad 2-43$$

Where  $R$  is the internal radius and  $\bar{u}$  is the average velocity of the laminar flow in the tube. The acquired dispersion profiles (refractometer voltages) are then analyzed using the nonlinear least square method based on a normal distribution equation assuming concentration and voltage are linearly correlated as:

$$V^E(t) = V_0^E + V_{max}^E \exp\left(-0.5 \left(\frac{t - t_R}{\sigma_t}\right)^2\right) \quad 2-44$$

Where  $V_{max}^E$  is the peak height relative to the baseline voltage  $V_0^E$ ,  $t_R$  is the residence time and  $\sigma_t$  is the peak variance in unit time. Dispersion coefficient  $K$  is correlated to  $t_R$  and  $\sigma_t$  through  $\sigma_t^2 = 2 \frac{K t_R}{\bar{u}^2}$  as long as the distribution is spatially Gaussian in the detector. Finally molecular diffusion coefficient is calculated from the following:

$$D = \frac{R^2 t_R}{24 \sigma_t^2} \quad 2-45$$

Taylor dispersion was selected for its convenient short run experiments and reliable data analysis. Results showed mutual diffusion coefficients are strongly concentration dependent within the concentration range studied (0-34% volumetric bitumen). Thus any assumption of constant molecular diffusion coefficient for such a liquid solvent-bitumen system would lead to considerable errors in designing solvent assisted recover processes.

### 2.2.3. Concentration dependent diffusivity methods

This section reviews diffusion work that accounts for concentration dependency (diffusivity). Most diffusivity calculations assume the solvent concentration in the bitumen remains constant through the whole diffusion process and hence diffusion coefficient remains constant. This could not be further from the truth, and leads to erroneous diffusion values. The simple logic behind this as explained before is that diffusion is driven by concentration. Hence lower concentration lead to lower concentration gradients and hence lower values for diffusion.

According to Upreti *et al.* (2007), accurate concentration-dependent diffusivity data is necessary to determine: the amount/flow rate of solvent required to mobilize the heavy oil, the extent of heavy oil reserves that would undergo viscosity reduction, the time required to mobilize the heavy oil for drainage under gravity and production rate of live oil. This has led to more researchers taking into consideration the concentration dependency of diffusivity. Some key findings over time include the following:

- The solubility of light hydrocarbons is sufficiently high so that assumptions for dilute conditions are invalid.
- The high solubility of the light hydrocarbon in heavy causes the bitumen phase to swell in time so that swelling of the oil cannot be ignored.
- The solubility of the light hydrocarbon in the heavy oil is proportional to the partial pressure of the solvent in the gas phase and the overall system pressure.
- The viscosity of the oil phase decreases exponentially when mixed with a light hydrocarbon solvent.
- There are large density gradients between the light solvent and the dense heavy oil.

Etminan *et al.* (2009) developed a modified version of the pressure decay method that maintains constant concentration at the gas-liquid interface and measures the amount of gas transferred to the liquid as a function of time. This constant concentration is maintained by having a supply cell to continuously inject gas into the decay cell hence, making the measurements easier and a simple analysis can be performed to determine the equilibrium concentration and diffusion coefficient. The constant pressure helped eliminate some of the complexities in modeling the physics of the interface caused by declining pressure in the original pressure decay method. An infinite and finite acting analytical solution is derived to fit the boundary conditions. The concentration dependency of diffusivity is studied with a stepwise increase in pressure starting from a low pressure. Diffusion coefficient is measured for each gas saturation pressure, going from low pressure to near gas dew point pressure in 5-6 steps.

The first experiment was conducted at 26 psig with test fluids Athabasca bitumen and CO<sub>2</sub>. Temperature disturbances did occur due to a malfunction in the supply cell water bath. The diffusion was determined to be  $1.45 \cdot 10^{-6} \text{ cm}^2/\text{sec}$  with a saturation concentration of  $C_{g1}^* = 0.019 \text{ g/cm}^3$ . The second experiment could not be completed due to the gas dissolution in bitumen being extremely slow.

Etminan *et al.* (2009) method for the most part ignores the continuous swelling of bitumen due to the dissolution of gas in it during each step. It does try to account for swelling by updating

bitumen height at each starting pressure step but this is not adequate enough. Also the pressure supply cell and diffusion cell are connected by electronic valves. The connection is intermittent and hence there is a pressure build up every time gas goes into the diffusion cell. Etminan *et al.* (2009) accounted for this by assuming, all the gas leaving the pressure cell dissolves into the liquid but this assumption may have induced further errors.

James (2003) investigated the concentration dependence of diffusion coefficient of butane in heavy oil, swelling effects at the pore scale and mass transfer rates were addressed for characterizing the rate of mass transfer of a hydrocarbon vapor in heavy oils. Experimental procedures were developed for investigating the transient behavior of butane solubility in heavy oil and heavy oil swelling as a function of time. Results showed that when the linear dependence between the diffusivity and solvent mass fraction was used, the model adequately predicted the overall change in height of both the butane and bitumen compared to experimental results.

James (2009) used similar principles to investigate the one-dimensional diffusion of butane (24.9°C) in Athabasca bitumen (26.3°C) while accounting for bitumen swelling and assuming ideal mixing between butane and bitumen. Diffusivity of butane in bitumen was found as a function of butane mass concentration by, utilizing a mathematical model (solvent continuity equations) to predict the ‘bitumen growth’. This is the swelling of the bitumen fluid that occurs due to the diffusion of butane vapor into the bitumen. The ‘bitumen growth’ determined mathematically is compared to the ‘bitumen growth’ observed experimentally and the difference between the two (experimental – predicted) is minimized by optimizing the diffusivity function coefficients. James (2009) solvent continuity equation comprises of three main terms:

$$\frac{\partial(\rho_s)}{\partial t} + \frac{\partial}{\partial x}(\rho_s V^m) - \frac{\partial}{\partial x} \left( \rho D_{sb} \frac{\partial \omega_s}{\partial x} \right) = 0 \quad 2-46$$

Where  $\rho_s$  (g/cm<sup>3</sup>) is mass concentration of the solvent,  $t$  (s) is time,  $V^m$  (g\*cm/s) is mass average velocity,  $\rho$  (g/cm<sup>3</sup>) is overall phase density,  $D_{sb}$  (cm<sup>2</sup>/s) is solvent (s) diffusivity in bitumen (b),  $\omega_s$  is solvent mass fraction and  $x$  is the direction of diffusion. The first term is the solvent

accumulation term, the second is the convection term and, the third the diffusion term. **Equation 2-46** yields three main equations;

First is an expression for change of solvent mass fraction in bitumen over time.

$$\frac{\partial \omega_s}{\partial t} = \frac{\partial \omega_s}{\partial x} \left[ \frac{D_{sb}}{\rho} \frac{\partial \rho}{\partial x} + \frac{\partial D_{sb}}{\partial x} - V^m \right] + D_{sb} \frac{\partial^2 \omega_s}{\partial x^2} \quad 2-47$$

where  $\omega_s$  is the solvent mass fraction,  $D_{sb}$  is solvent diffusivity in bitumen,  $\rho$  is bitumen phase density,  $V^m$  is mass averaged velocity of the mixture,  $t$  is time.

The second is an expression for the mass averaged velocity of the fluid mixture  $V^M$ . Please note James (2009) assumes ideal mixing of bitumen and butane

$$V^m(x, t) = (v_s^* - v_b^*) \int_0^x \left( D_{sb} \frac{\partial \rho}{\partial x} \frac{\partial \omega_s}{\partial x} + \rho \frac{\partial D_{sb}}{\partial x} \frac{\partial \omega_s}{\partial x} + \rho D_{sb} \frac{\partial^2 \omega_s}{\partial x^2} \right) dx \quad 2-48$$

where  $v_s^*$  and  $v_b^*$  are the solvent and bitumen specific volumes ( $\text{cm}^3/\text{g}$ ) respectively. The final is an expression describes the bitumen height increase (bitumen swelling) with time

$$\frac{dx_s}{dt} = \left( D_{sb} \frac{\partial \omega_s}{\partial x} \right) \Big|_{x=x_s} - \frac{(v_b^* - v_s^*) x_s}{\rho(x_s, t)} \int_0^{(t)} \rho^2 \frac{\partial \omega_s}{\partial t} \Big|_x dx \quad 2-49$$

**Equations 2-47, 2-48 and 2-49** are transformed (to give dimensionless positions) using a front fixing method first proposed by Landau 1950. Without the dimensionless transformation, the interface position would change with time and resolving time derivatives with respect to changing spatial coordinate is more complicated. The x-dimension is made dimensionless by introducing a dimensionless variable ' $\xi'$ '

$$\xi = \frac{x}{x_s(t)} \quad 2-50$$

using this transformation, bitumen interface ( $\xi$ ) is always equal to one and the following derivatives are acquired

$$dx = x_s d\xi, \quad \frac{d\omega_s}{dx} = \frac{1}{x_s(t)} \frac{d\omega_s}{d\xi}, \quad \text{and} \quad \frac{d^2\omega_s}{dx^2} = \frac{1}{x_s(t)} \frac{d^2\omega_s}{d\xi^2} \quad 2-51$$

The method of lines is used to discretize the dimensionless  $\xi$  and transform to an approximate set of ordinary differential where the remaining independent variable is time to give the following 3 sets of equations

1) **Solvent continuity equation:**

$$\begin{aligned} \frac{d\omega_s}{dt} \Big|_i &= \left[ \frac{(i-1)\Delta\xi}{x_s} \right] \left[ \frac{\omega_s^{i+1} - \omega_s^{i-1}}{2\Delta\xi} \right] \frac{dx_s}{dt} + \frac{1}{x_s} \left[ \frac{\omega_s^{i+1} - \omega_s^{i-1}}{2\Delta\xi} \right] \\ &\quad * \left\{ \left( \frac{D_{sb}(\omega_s^i)}{\rho(w_s^i) \cdot x_s} \right) \left( \frac{\rho(\omega_s^{i+1}) - \rho(\omega_s^{i-1})}{2\Delta\xi} \right) + \frac{1}{x_s} \left( \frac{D_{sb}(\omega_s^{i+1}) - D_{sb}(\omega_s^{i-1})}{2\Delta\xi} \right) \right. \\ &\quad \left. - V^m(\xi) \right\} + \left( \frac{D_{sb}(\omega_s^i)}{(x_s)^2} \right) \left( \frac{\omega_s^{i+1} - 2\omega_s^i + \omega_s^{i-1}}{(\Delta\xi)^2} \right) \end{aligned} \quad 2-52$$

No flux boundary,  $\xi = 0, i = 1$

$$\frac{d\omega_s}{dt} \Big|_{i=1} = \left( \frac{2D_{sb}(\omega_s^i)}{(x_s)^2} \right) \left( \frac{\omega_s^{i+1} - \omega_s^i}{(\Delta\xi)^2} \right) \quad 2-53$$

At the bitumen-solvent vapor interface,  $\xi = 1, i = n+1$

$$\left. \frac{d\omega_s}{dt} \right|_{i=n+1} = 0 \quad 2-54$$

2) **Mass average velocity,  $V^m$ :**

$$\int_a^b f(x)dx \cong \left(\frac{h}{2}\right) (f(a) + f(b)) + h \sum_{i=1}^n f(x)_n \quad \text{where } h = \frac{b-a}{n} \quad 2-55$$

$$V^m \cong (v_s^* - v_b^*) \left(\frac{(i-1)\Delta\xi}{2(i-1)}\right) (f(a) + f(b)) + \left(\frac{(i-1)\Delta\xi}{(i-1)}\right) \sum_{i=1}^n f(\xi_i) \quad 2-56$$

$$f(a) = f(0) = 0 \quad 2-57$$

$$\begin{aligned} f(\xi^i) = & \left(\frac{D_{sb}(\omega_s^i)}{x_s}\right) \left(\frac{\rho(\omega_s^{i+1}) - \rho(\omega_s^{i-1})}{2\Delta\xi}\right) \left(\frac{\omega_s^{i+1} - \omega_s^{i-1}}{2\Delta\xi}\right) \\ & + \left(\frac{\rho(\omega_s^i)}{x_s}\right) \left(\frac{D_{sb}(\omega_s^{i+1}) - D_{sb}(\omega_s^{i-1})}{2\Delta\xi}\right) \left(\frac{\omega_s^{i+1} - \omega_s^{i-1}}{2\Delta\xi}\right) \\ & + \left(\frac{\rho(\omega_s^i)D_{sb}(\omega_s^i)}{x_s}\right) \left(\frac{\omega_s^{i+1} - 2\omega_s^i + \omega_s^{i-1}}{(\Delta\xi)^2}\right) \end{aligned} \quad 2-58$$

$$\begin{aligned} f(1) = & \left(\frac{D_{sb}(\omega_s^{n+1})}{x_s}\right) \left(\frac{3\rho(\omega_s^{n+1}) - 4\rho(\omega_s^n) + \rho(\omega_s^{n-1})}{2\Delta\xi}\right) \left(\frac{3\omega_s^{n+1} - 4\omega_s^n + \omega_s^{n-1}}{2\Delta\xi}\right) \\ & + \left(\frac{\rho(\omega_s^{n+1})}{x_s}\right) \left(\frac{3D_{sb}(\omega_s^{n+1}) - 4D_{sb}(\omega_s^n) + D_{sb}(\omega_s^{n-1})}{2\Delta\xi}\right) \\ & * \left(\frac{3\omega_s^{n+1} - 4\omega_s^n + \omega_s^{n-1}}{2\Delta\xi}\right) \\ & + \left(\frac{\rho(\omega_s^{n+1})D_{sb}(\omega_s^{n+1})}{x_s}\right) \left(\frac{\omega_s^{n+1} - 2\omega_s^n + \omega_s^{n-1}}{(\Delta\xi)^2}\right) \end{aligned} \quad 2-59$$

3) **Increase in bitumen height:**

$$\frac{dx_s}{dt} = \left( \frac{D_{sb}(\omega_s^{n+1})}{x_s} \right) \left( \frac{3\omega_s^{n+1} - 4\omega_s^n + \omega_s^{n-1}}{2\Delta\xi} \right) - \frac{x_s(v_b^* - v_s^*)}{\rho(\omega_s^{n+1})} * Integral \quad 2-60$$

$$Integral \cong \left( \frac{1}{2n} \right) (f(a) + f(b)) + \left( \frac{1}{n} \right) \sum_{i=2}^n f(\xi_i) \quad 2-61$$

Node 1

$$f(a) = f(0) = \rho(\omega_s^1)^2 \left( \frac{\partial \omega_s}{\partial t} \Big|_{\xi=0} \right) \quad 2-62$$

Node n+1

$$f(b) = f(1) = \rho(\omega_s^{n+1})^2 \left[ \frac{-1}{x_s} \left( \frac{dx_s}{dt} \right) \left( \frac{3\omega_s^{n+1} - 4\omega_s^n + \omega_s^{n-1}}{2\Delta\xi} \right) + \left( \frac{\partial \omega_s}{\partial t} \Big|_{\xi=1} \right) \right] \quad 2-63$$

Node i = 2 : n

$$f(\xi^i) = \rho(\omega_s^i)^2 \left[ \left( \frac{-(i-1)\Delta\xi}{x_s} \right) \left( \frac{dx_s}{dt} \right) \left( \frac{\omega_s^{i+1} - \omega_s^{i-1}}{2\Delta\xi} \right) + \left( \frac{\partial \omega_s}{\partial t} \Big|_{\xi=1} \right) \right] \quad 2-64$$

James (2009) assumes the following:

- At the solvent/bitumen interface, the solvent concentration remains constant (0.6 mass fraction solvent solubility at given temperature and pressure) and this concentration is reached instantaneously.
- Ideal mixing occurs between the bitumen and butane solvent.
- The initial form of the diffusivity function is guessed

The transformation and discretization yields **Equations 2-52 to 2-64** which are all input and solved simultaneously in MATLAB using “lsqnonlin-least squares nonlinear” optimization

option. This optimization automatically minimizes the objective function (difference between experimental and predicted ‘bitumen growth’). The coefficients of the proposed diffusivity function are set as the parameters for which to optimize.

James (2009) found the diffusivity of butane (24.9°C) in bitumen (26.3°C) to be  $(4.78\omega_s+4.91)*10^{-6}$  cm<sup>2</sup>/s where  $\omega_s$  is the solvent mass fraction. The diffusivity result was independently validated by utilizing a macroscopic mass balance to predict the change in solvent height after ‘bitumen growth’ has been resolved for the full time duration. This counts as an independent validation because the experimental solvent height change values are not used in the model to determine the diffusivity. The summation of the solvent concentration profile resolved throughout the depth of the bitumen phase gives mass of solvent in bitumen at a given time.

$$m_s(t) = A_b \int_0^{x_s(t)} \rho \omega_s dx = 0 \quad 2-65$$

where ‘ $m_s(t)$ ’ is mass of solvent (g) at time ‘ $t$ ’, ‘ $A_b$ ’ is cross sectional area of bitumen tube (cm<sup>2</sup>), ‘ $\rho$ ’ is density of the bitumen phase (g/cm<sup>3</sup>), ‘ $\omega_s$ ’ is mass fraction of solvent and ‘ $x_s(t)$ ’ is increase in bitumen height (cm) due to swelling from diffusing solvent at time ‘ $t$ ’. With this mass of solvent, the height change of solvent in the solvent tube can be found as;

$$h_s(t) = \frac{m_s}{\rho_s A_s} = 0 \quad 2-66$$

where ‘ $h_s(t)$ ’ is height change of solvent (cm) in the solvent tube at time ‘ $t$ ’, ‘ $m_s$ ’ is mass of solvent (g), ‘ $\rho_s$ ’ is density of solvent (g/cm<sup>3</sup>) at solvent temperature and ‘ $A_s$ ’ is cross sectional area (cm<sup>2</sup>) of solvent tube. A good fit was found between the experimental decrease in butane solvent height and predicted decrease in butane solvent height as shown in **Figure 2-24** hence validating the obtained diffusivity function.

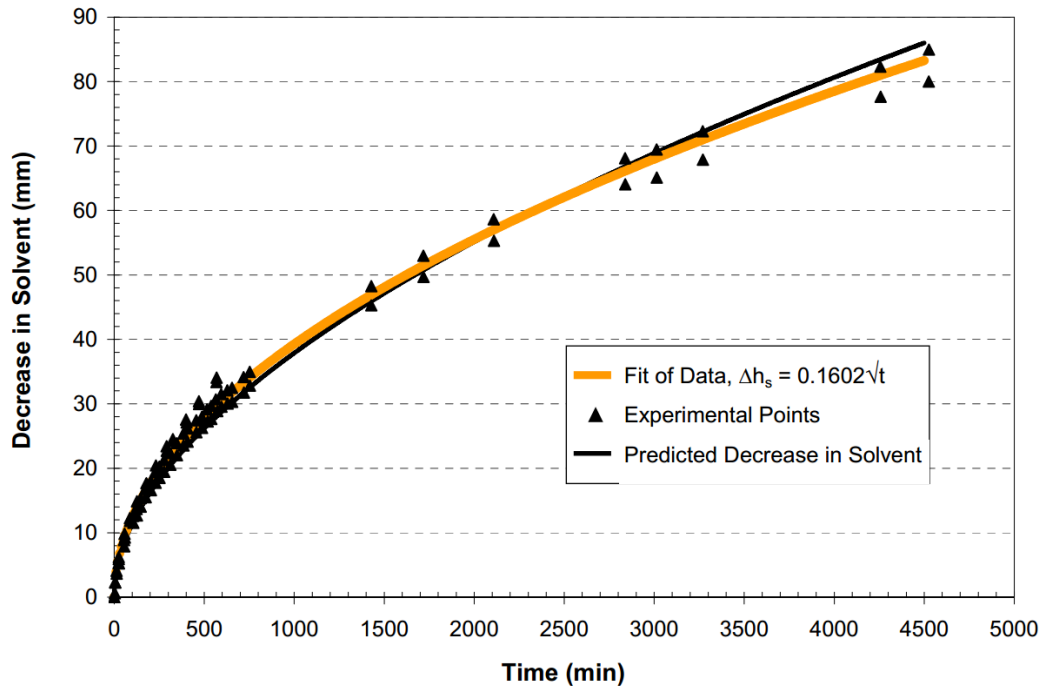


Figure 2-24 - Solvent decrease (experimental vs model results) (James 2009)

## 2.4. Non-ideal mixing of solvent and oil

The majority of VAPEX diffusion coefficient studies assume that bitumen and butane mix in equal proportions. In simple terms, this means it is assumed that a mixture of 2 m<sup>3</sup> of bitumen and 4 m<sup>3</sup> of butane should equate to a 6 m<sup>3</sup> overall mixture. This is not the case given both fluids are hydrocarbons and mix in a non-ideal fashion. Mass can neither be created nor destroyed; hence the assumption of ideal mixing will either overestimate or underestimate density values used in our solvent continuity equations. It is therefore imperative to seek out methods to account for this non-ideality, and, hence enhance accuracy of diffusivity function and subsequent diffusion values.

However accounting for the non-ideal of hydrocarbons in VAPEX system is challenging because finding a reliable and easily measurable parameter within the solvent-bitumen mixing system that can consistently account for non-ideal mixing (non-ideality) without upsetting the system (sampling) is very difficult. A popular way of accounting for non-ideal mixing in hydrocarbon

fluids is through the use of Peng -Robinson's equations of state Peng and Robinson (1976). This is given by;

$$P = \frac{RT}{V - b} - \frac{a}{V^2 + 2bV - b^2} , \quad 2-67$$

where  $P$  is pressure,  $T$  is absolute temperature,  $R$  is the universal gas constant, and  $V$  is the molar volume. The coefficient  $b$  is the co-volume given by:

$$b = \frac{0.0777969RT_c}{P_c} . \quad 2-68$$

The coefficient 'a' is defined as

$$a = a_c \alpha(T) , \quad 2-69$$

where

$$a_c = \frac{0.457235R^2T_c^2}{P_c} , \quad 2-70$$

And  $T_c$  and  $P_c$  are the critical temperature and pressure respectively and,  $\alpha(T)$  is an empirical dimensionless scaling function of temperature. This empirical function is the correlated to acentric factor for non-polar or slightly pure components, such as hydrocarbons as,

$$\alpha = [1 + f_w(1 - \sqrt{T_r})]^2 , \quad 2-71$$

where  $T_r$  is the reduced temperature and  $f_w$  is given by:

$$f_w = 0.37464 + 1.54226w - 0.26992w^2 \quad \text{for } w < 0.5, \quad \text{and} \quad 2-72$$

$$f_w = 0.3796 + 1.4850w - 0.1644w^2 + 0.01666w^3 \quad \text{for } w \geq 0.5. \quad 2-73$$

The parameters  $a$  and  $b$  are calculated for the mixtures using the following mixing rules:

$$a = \sum_i \sum_j (1 - k_{ij}) \sqrt{a_i a_j x_i x_j} , \quad 2-74$$

and

$$b = \sum_i x_i b_i , \quad 2-75$$

where  $x_i$  is the mole fraction of component  $i$  and  $k_{ij}$  is the binary interaction parameter (BIP) between components  $i$  and  $j$ . The BIP specifically accounts non ideal mixing and has a value of zero during ideal mixing conditions. **Equations 2-67 to 2-75** can be used to calculate the molar volume  $V$  of a bitumen/solvent mixture. The inverse of molar volume can then be converted to density by multiplying it with the mixture molar mass.

Using the equation of state method is an indirect way of account for non-ideality. There are a large number of parameters that have to be estimated using this method. Each parameter estimated comes with its own error and when density needs to be eventually calculated, the error in the density values would have grown exponentially. Still it is one of the only ways available in the industry to account for non-ideality.

BIP values are affected by temperature and Deo *et al.* (1993) looked into its effects by determining the optimum BIP for a number of paraffinic, naphthenic and aromatic hydrocarbons. Using Peng-Robinson EOS, trends with respect to temperature and molecular size were examined. It was discovered that for components lighter than heptane, the interaction parameter increases slightly with temperature. However this work did not address the interaction specifically between bitumen and butane. Saryazdi *et al.* (2013) achieved this and found that BIP increases with increasing temperature. The red line in **Figure 2-25** below shows the regression line of BIP vs temperature for bitumen and butane.

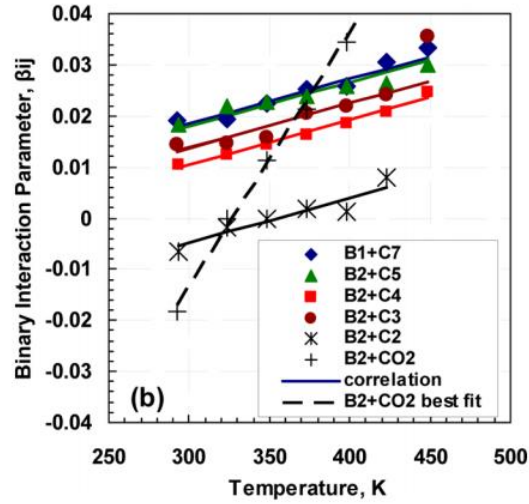


Figure 2-25 - BIP for bitumen vs. temperature (Saryazdi *et al.* 2013)

Leahy-Dios and Firoozabadi (2007) attempted to calculate diffusivity while taking into account non-ideality in gas and liquid states of multi-component fluids. The non-ideality is described by fugacity derivatives evaluated by the volume-translated Peng-Robinson equation of state. For a non-ideal n-component mixture, the mole based Stefan-Maxell (SM) diffusive flux is given by,

$$\mathbf{J}^M = -c(\mathbf{B}^M)^{-1} \Gamma \nabla x \quad 2-76$$

where  $c$  is the molar density of the mixture and  $\nabla x$  is a vector of composition gradient. The elements of the  $(n-1)$  square matrix  $\mathbf{B}^M$  are given by;

$$B_{ii}^M = \frac{x_i}{\mathcal{D}_{im}} + \sum_{\substack{k=1 \\ i \neq k}}^n \frac{x_k}{\mathcal{D}_{ik}}, \quad i = 1, \dots, n-1 \quad 2-77$$

$$B_{ij}^M = -x_i \left( \frac{1}{\mathcal{D}_{ij}} - \frac{1}{\mathcal{D}_{im}} \right), \quad i = 1, \dots, n-1, i \neq j \quad 2-78$$

The parameters  $D_{ij}=D_{ji}$  are the Stefan-Maxwell diffusion coefficients for each i-j binary pair in the mixture and  $x_i$  is the mole fraction of component  $i$ . The elements of the mixture  $\Gamma$  of thermodynamics factors;

$$\Gamma_{ij} = x_i \left. \frac{\partial \ln f_i}{\partial x_j} \right|_{x_j, T, P}, \quad i, j = 1, \dots, n-1 \quad 2-79$$

Where  $f_i$  is the fugacity of the component and  $\Gamma$  represents system non-ideality and is calculated using Peng-Robinson's equation of state. The mole-based multicomponent Fickian diffusive flux is shown as;

$$\mathbf{J}^M = -c(\mathbf{D}^M)\nabla x \quad 2-80$$

Similarly to the previously mentioned Fick's 1<sup>st</sup> law of diffusion in **Equation 2-29**, where  $\mathbf{D}^M$  is a square matrix of mole based fickian diffusion coefficients, and comparing **Equation 2-76** and **Equation 2-80** gives

$$\mathbf{D}^M = (\mathbf{B}^M)^{-1}\Gamma \quad 2-81$$

At infinite dilution limit, all molecular diffusion coefficients become equal and the notation becomes  $D^\infty$ . With  $D_{ij}$  found from **Equation 2-82** below,  $\mathbf{D}^M$  can be calculated from **Equation 2-81**.

$$D_{ij} = (D_{ij}^\infty)^{x_j} (D_{ji}^\infty)^{x_i} \prod_{\substack{k=1 \\ k \neq i, j}}^n (D_{ik}^\infty D_{jk}^\infty)^{x_k/2}, \quad i, j = 1, \dots, n, i \neq j \quad 2-82$$

Leahy-Dios and Firoozabadi (2007) developed a correlation based on 889 experimental data on  $D^\infty$  for non-polar mixtures from the literature. Experimental pressures (0.1-920 MPa), temperatures (154-958K),  $D^\infty$  (**0.46\*10<sup>-9</sup> to 6.8\*10<sup>-4</sup> m<sup>2</sup>/s**) and experimental values of density

with viscosity of the concentrated component were used. The correlation is based on a non-linear square minimization of the following general expression;

$$\frac{cD^\infty}{(cD)^0} = f\left(\frac{\mu}{\mu^0}, T_r, P_r, \omega\right) \quad 2-83$$

For an n-component mixture,  $(n-1)^2 D^M$  from binary pairs  $D^\infty$  is calculated as follows;

- Find  $D_{ij}^\infty$  from **Equation 2-83**
- Find  $D_{ij}$  from **Equation 2-82**
- Find  $B^M$  from **Equation 2-77** and **Equation 2-78**
- Find  $D^M$  from **Equation 2-79** and **Equation 2-81**

**Figure 2-26** and **Table 2-5** below show some of the results of the correlation.

Table 2-5 - Results for multi-component fluid at 422k & 15 MPa (Leahy-Dios and Firoozabadi 2007)

Liquid Phase $D^M$ ( $10^{-9}$ m <sup>2</sup> /s)									
Component	CO <sub>2</sub>	C <sub>1</sub>	C <sub>2</sub>	C <sub>3</sub> -C <sub>4</sub>	C <sub>5</sub> -C <sub>6</sub>	C <sub>7</sub> -C <sub>10</sub>	C <sub>11</sub> -C <sub>12</sub>	C <sub>15</sub> -C <sub>20</sub>	C <sub>21</sub> -C <sub>29</sub>
CO <sub>2</sub>	85.61	-61.25	16.01	-19.26	-9.819	-21.48	-9.019	-8.446	-2.683
C <sub>1</sub>	-29.93	22.15	-27.31	-16.14	-4.734	-7.901	-4.379	-4.105	-2.176
C <sub>2</sub>	-9.340	-43.22	60.99	-14.49	-6.521	-13.58	-5.771	-5.391	-1.735
C <sub>3</sub> -C <sub>4</sub>	-9.440	-0.4549	-6.873	35.53	0.2821	1.898	0.6778	0.6081	0.1871
C <sub>5</sub> -C <sub>6</sub>	-4.885	8.431	-1.873	1.338	9.495	4.113	1.664	1.526	0.4980
C <sub>7</sub> -C <sub>10</sub>	-13.70	26.99	-4.716	4.381	4.504	17.07	4.893	4.451	1.356
C <sub>11</sub> -C <sub>12</sub>	-6.283	17.56	-1.134	3.602	2.992	7.746	7.880	2.876	0.9418
C <sub>15</sub> -C <sub>20</sub>	-5.527	16.39	-0.8028	3.480	2.818	7.307	2.985	7.636	0.9175
C <sub>21</sub> -C <sub>29</sub>	-3.164	16.08	0.8123	3.896	2.677	6.633	2.743	2.501	4.279

Gas Phase $D^M$ ( $10^{-9}$ m <sup>2</sup> /s)									
Component	CO <sub>2</sub>	C <sub>1</sub>	C <sub>2</sub>	C <sub>3</sub> -C <sub>4</sub>	C <sub>5</sub> -C <sub>6</sub>	C <sub>7</sub> -C <sub>10</sub>	C <sub>11</sub> -C <sub>12</sub>	C <sub>15</sub> -C <sub>20</sub>	C <sub>21</sub> -C <sub>29</sub>
CO <sub>2</sub>	864.3	88.38	0.5227	11.21	5.6452	3.855	2.141	2.145	1.354
C <sub>1</sub>	-774.9	-953.0	-765.7	-376.0	-66.56	-38.82	-22.29	-22.95	-13.18
C <sub>2</sub>	-29.03	338.7	764.3	38.54	17.93	12.05	6.030	5.915	3.772
C <sub>3</sub> -C <sub>4</sub>	-31.59	295.3	3.399	315.6	12.44	8.578	3.326	3.063	1.944
C <sub>5</sub> -C <sub>6</sub>	-16.39	38.28	-9.86	-0.8911	29.12	0.7755	0.0665	-0.0087	0.0083
C <sub>7</sub> -C <sub>10</sub>	-13.92	30.50	-8.712	-1.354	0.5443	14.01	-0.0670	-0.1375	-0.0758
C <sub>11</sub> -C <sub>12</sub>	1.34	69.11	7.562	6.693	1.905	1.365	14.31	0.0266	-0.0067
C <sub>15</sub> -C <sub>20</sub>	4.59	109.22	14.00	11.30	3.059	2.172	0.2407	15.67	0.0015
C <sub>21</sub> -C <sub>29</sub>	4.14	85.91	11.43	9.026	2.410	1.707	0.1925	0.0568	9.903

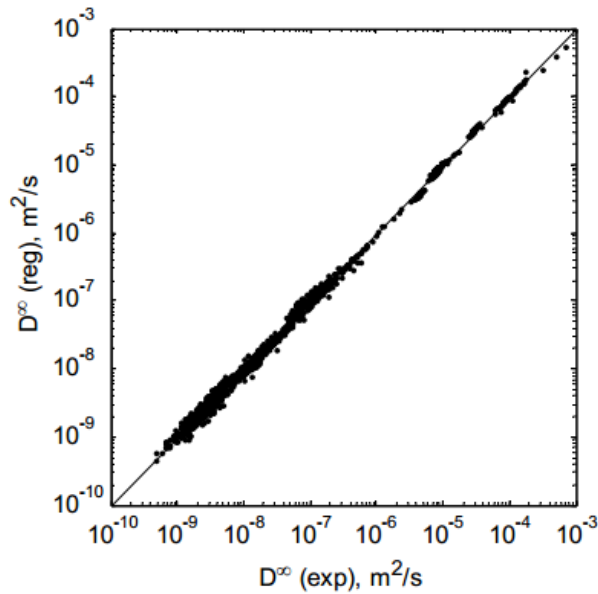


Figure 2-26 - Infinite dilution diffusivity: experimental & computed (Leahy-Dios and Firoozabadi 2007)

Predictions for highly non-ideal gas and liquid multi-component mixtures show this method works. However it is complex and hard to follow and again there would be too much error associated with the final values.

Etminan *et al.* (2011) conducted three sets of experiments with propane, Mackay oil and Athabasca bitumen to determine the effective of molecular diffusion and dispersion coefficient on VAPEX systems while accounting for non-ideality. The first experiment used the modified pressure decay technique from Etminan *et al.* (2009) to determine molecular diffusion of propane in Athabasca bitumen. However, unlike Etminan *et al.* (2009) the first experiment accounts for bitumen swelling during the experiment. The second experiment involves using a physical sand pack model to run a VAPEX experiment at 40°C and 165 psig. Using propane and Mackay oil, dead oil production rate data were collected over 70 hours and introduced into the VAPEX model from **Equation 2-1**. The dimensionless  $N$  value is back calculated with this model.

Finally a set of PVT measurements were conducted to obtain expressions for density and viscosity at varying propane concentrations. These expressions are substituted into the equation

for  $N$  in **Equation 2-3** to obtain dispersion coefficient ( $1.0397 \times 10^{-9} \text{ m}^2/\text{s}$ ). Mixture density versus solvent volume fraction graphs is shown in **Figure 2-27**.

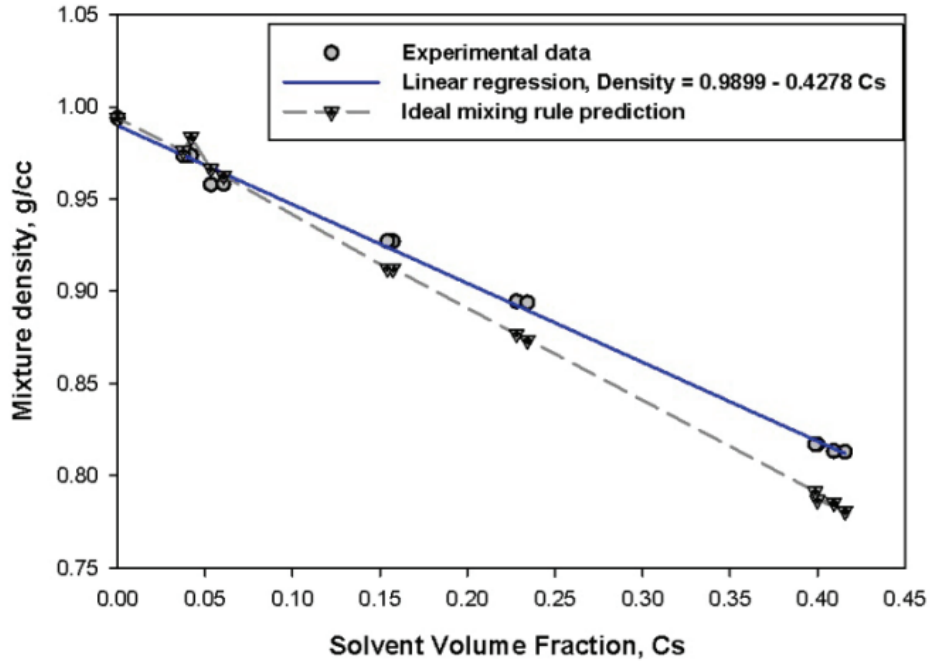


Figure 2-27 - Ideal/non ideal mixture density vs. solvent volume fraction at 40°C (Etminan *et al.* 2011)

From the figure above, there is a clear distinction between the ideal mixing graph (dashed lines) and non-ideal mixing graph (blue line/linear regression line). Hence using the ideal mixing graph to calculate any mass transfer parameters would have given erroneous results.

## 2.5. This work

The literature review shows that accounting for concentration dependency gives significantly more accurate diffusivity functions (and subsequent diffusion values) in VAPEX systems. However there is barely any work that accounts for the non-ideal mixing of the hydrocarbons. This thesis accounts for non-ideality using a density related parameter (pressure), which is continuously measurable over the duration of the experiment. This is achieved using a pressure differential transmitter. Pressure differential transmitters were selected because the pressure changes were expected to be extremely small and difficult to track per minute by a normal

pressure transmitter. A high precision pressure transmitter was needed and only differential transmitters offer such high precision. The basis of this application is the pressure, density and height equation below.

$$P = \rho * g * h \quad 2-84$$

$$\rho = \frac{P}{g * h} \quad 2-85$$

With a camera tracking height changes of bitumen and differential transmitter tracking hydrostatic pressure changes of the fluid, the density changes in the bitumen mixture as the experiment progresses can be computed from **Equation 2-85**. Differential transmitters are only necessary with the bitumen mixture due to the changing density. Butane liquid density remains constant through the experiment so tracking height changes is all that is needed. The changing bitumen density values can then substituted into the solvent continuity equations to obtain much more accurate values of diffusivity.

This work represents the only experiment up to date to calculate diffusivity functions in VAPEX systems while accounting for concentration dependence and non-ideal mixing of solvent-bitumen. James (2009) work will form the basis for accounting for both these factors. James (2009) experimental work achieved the following:

- The design and perfection of a simple one dimensional diffusion experiment to measure and independently validate the uptake of n-butane into bitumen and the swelling of the bitumen phase in time.
- An improved mathematical description of the diffusion of n-butane into heavy oil from first principles, without oversimplified assumptions. This was accomplished by considering:
  - the diffusivity and density are functions of the solvent concentration and cannot be assumed constant, and

- the solvent concentration was assumed to be a function of position and time and numerically calculated
- Determination that the concentration dependent molecular diffusivity of n-butane in heavy oil is a linear function of concentration.
- Validation of the mathematical model with experimental results

This work will form an extension of the work done by James (2009) while accounting for the following:

- Bitumen temperature variation. Bitumen temperature is varied on five levels (27.00°C, 30.25°C, 33.50°C, 36.75°C and 40.00°C) to compare diffusivity functions obtained from all five. The main effect these temperature variations will have is a reduction of butane solubility in bitumen. Higher temperatures also considerably reduce the viscosity of the bitumen but given the absence of gravity drainage in the system, the effects of viscosity on the diffusion will be minimal.
- Non-ideal mixing between the bitumen and butane solvent. As stated above one of James (2009) assumptions was ideal mixing between the two fluids. This may not have affected the accuracy of the diffusivity function James (2009) obtained because literature suggests that the effects of non-ideality are minimal as temperature tends to standard conditions (25.00°C). This work however will have temperatures as high as 40.00°C so the effects of non-ideal mixing are expected to be significant. Both ideal and non-ideal diffusivity functions are found for comparison sake.
- A model is designed using Design Expert software to predict the diffusivity function (ideal/non-ideal) for any temperature within the experimental range (27.00°C - 40.00°C). The values obtained with this model are compared to experimental values obtained at the same temperature to test robustness of the model. Details and results are discussed in **Section 4.4** and **5.5**

### 3) EXPERIMENTAL METHODOLOGY

#### 3.1. Experimental overview

This section gives a simplified overview of the experiment. **Figure 3-1** is a schematic of the experiment in its simplest form. Butane liquid at 24°C has a vapor pressure of 34.65 psi. The bitumen temperature is varied at five different temperature levels (27.00°C, 30.25°C, 33.50°C, 36.75°C and 40.00°C). Each level represents one experimental run and the ‘PT’ is a pressure transmitter. The butane vapor diffuses into the bitumen with time. The height decrease of butane and increase (growth) of bitumen, along with pressure and temperature readings are recorded.

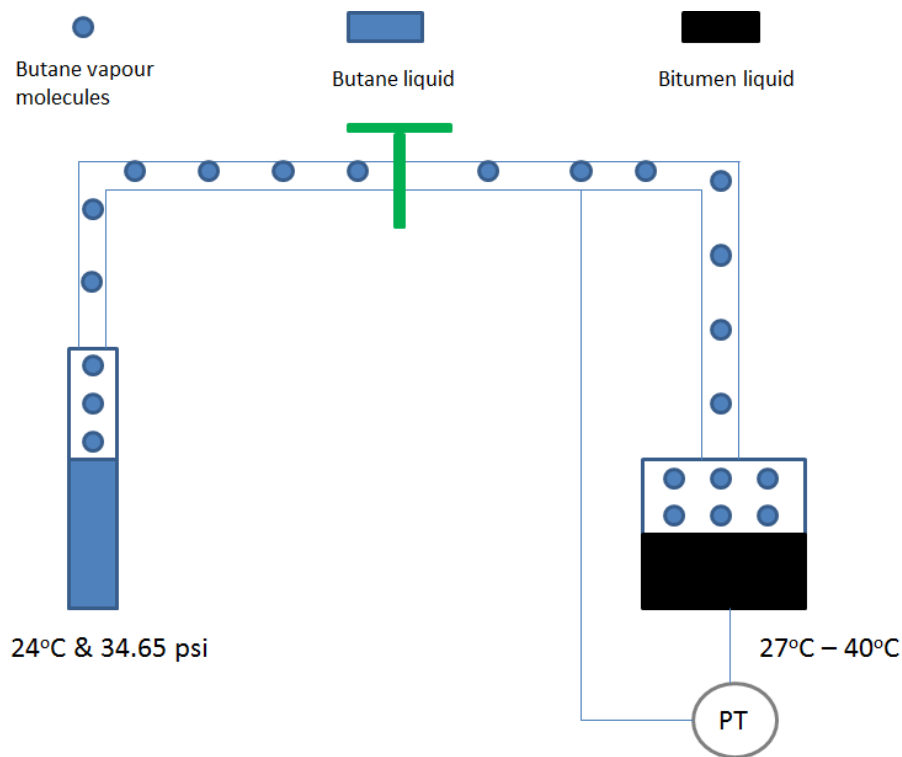


Figure 3-1 - Simplified schematic of experiment

There are five key steps in conducting the experiment: Equipment loading, Equipment assembly, Pre-Experiment, Experiment and Post-Experiment. The sixth step is data analysis and is covered extensively in **Section 4**. **Figure 3-2** gives a brief description of what each component entails. Detailed information about the experiment is provided in the next section.

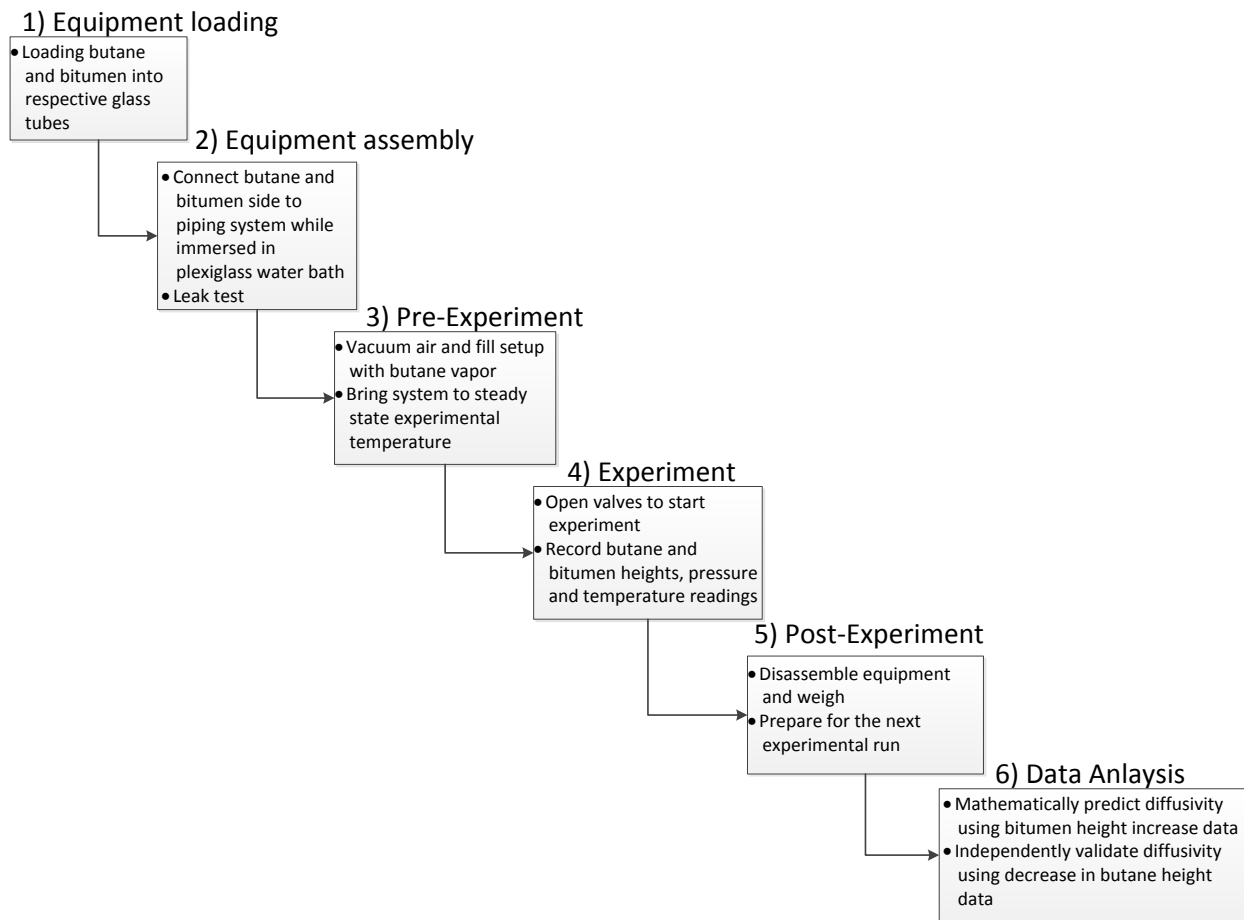


Figure 3-2- Workflow diagram for experiment

## 3.2. Equipment set-up

The purpose of this experimental set-up is to indirectly determine the concentration dependent diffusivity when butane vapor diffuses into bitumen, while also accounting for ideal and non-ideal mixing scenarios. This is done using diffusion apparatus that allows butane vapor to diffuse into bitumen while the bitumen mixture density and height changes are monitored. The steps and procedures involved in setting up the experiment are outlined in this section. All experimentally analyzed parts of the set-up are explained in detail and the section ends with a troubleshooting section that details the pit-falls of putting the experimental set-up together.

### 3.2.1. Butane Loading

**Figure 3-3** below illustrates the set-up for the butane loading. The set-up is a combination of an L-shaped  $\frac{1}{4}$ " OD (outer diameter) glass tube (internal diameter ID 0.15") and a  $\frac{1}{4}$ " OD stainless steel (SS) 2-way valve (internal diameter ID 0.16"). A vacuum pump is used to remove air from the set-up while the  $\frac{1}{4}$ " (SS) 2-way valve is open. The  $\frac{1}{4}$ " (SS) 2-way valve is then closed to maintain the vacuum. Vacuum creation ensures the butane condenses in the set-up as the presence of air makes dew point temperature much lower than can be attained. With the butane set-up connected to the butane source, the butane set-up is dipped in a container of ice. After a few minutes, the butane  $\frac{1}{4}$ " (SS) 2-way valve is opened for butane vapor from the source to flow into the butane set-up. The lower temperature ensures the butane vapor condenses as the temperature of the glass tube is lower than butane dew point temperature. The loading is allowed to continue until a specified butane liquid height is reached. The  $\frac{1}{4}$ " (SS) 2-way valve is then closed and the butane set-up is disconnected from the source.

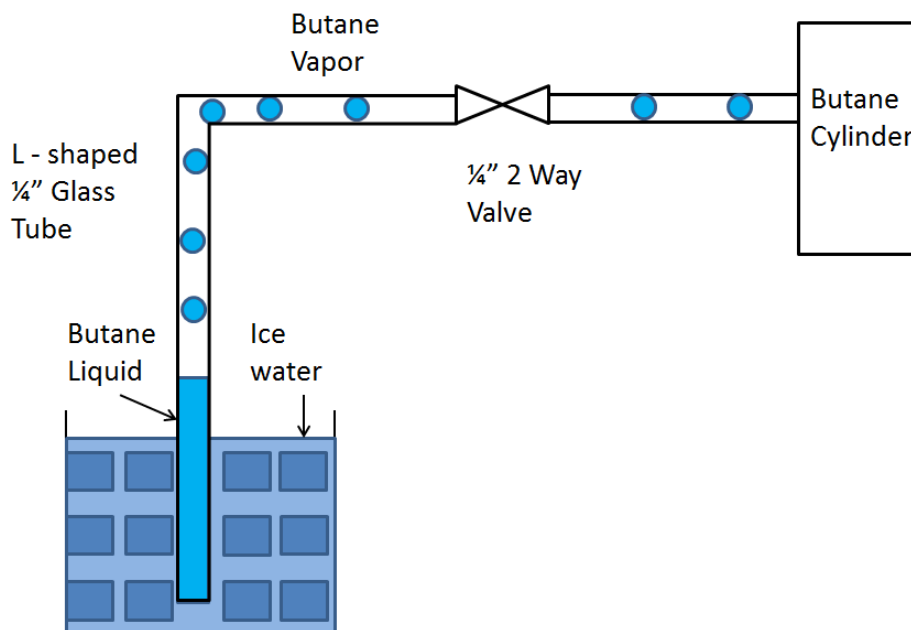


Figure 3-3 - Butane loading set-up

**Figure 3-4** shows a schematic of the butane side during the experiment. The right end of the side is eventually connected to the bitumen side.

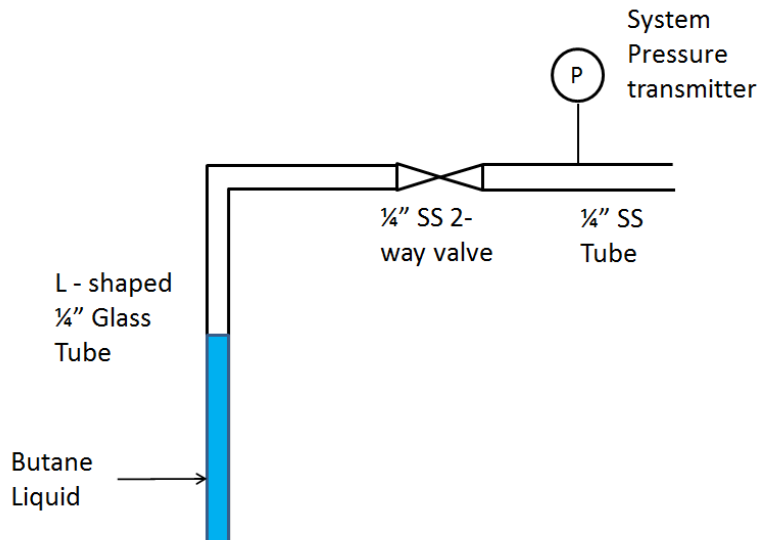


Figure 3-4 - Schematic of butane side

**Figure 3-5** shows a photograph of the butane set-up during the experiment. Note that the set-up is duplicated (front and back) to perform replicate experiments at the same time. Constant temperature is maintained using a circulatory water bath (Cole-Parmer, Polystat water bath) and a custom made visual Plexiglass water bath. The butane is housed in the custom Plexiglass water bath to allow for visualization and ensure that the diffusion apparatus is removed from any vibrations caused from the circulatory water bath motor. Thermocouple wires are used to monitor the system temperature.

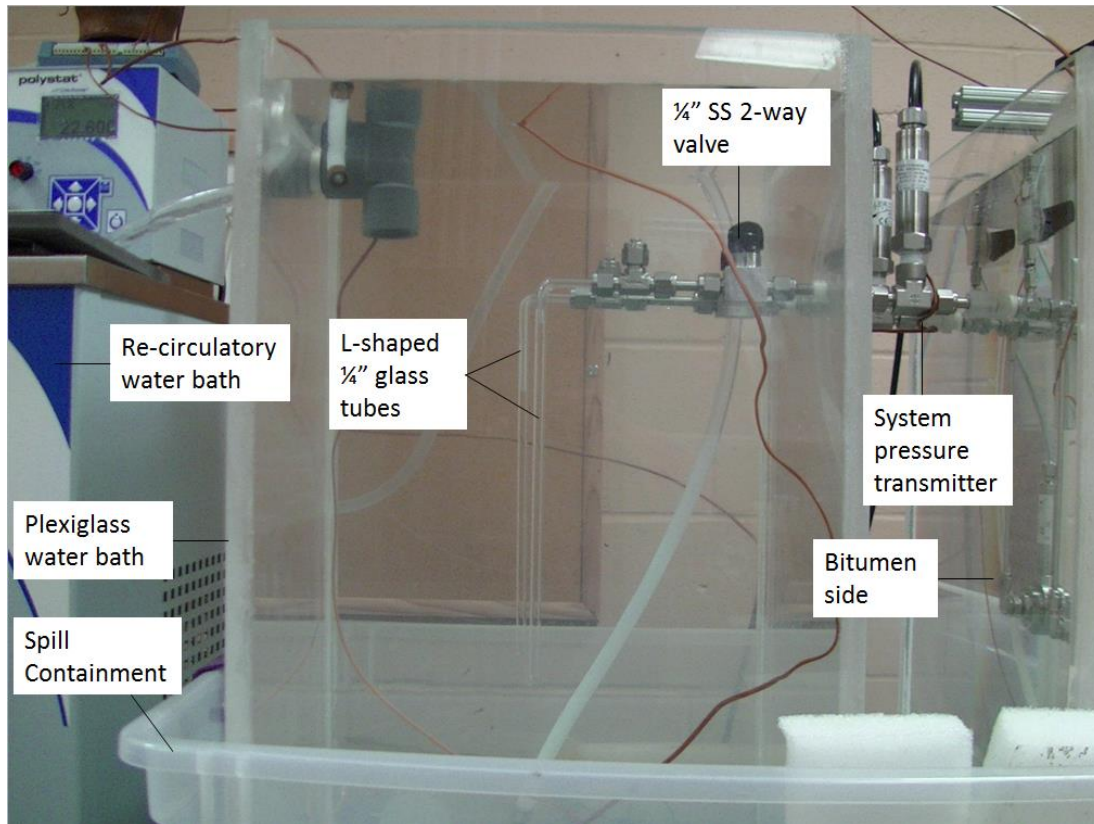


Figure 3-5 - Butane side of one-dimensional diffusion experiment

### 3.2.2. Bitumen Loading

The butane is connected to the bitumen side via SS tubing and valves. The bitumen is housed in a 15 mm OD glass tube (12.4 mm ID) to allow for the interface height tracking. The interface height is tracked visually with a cathetometer and using a differential pressure transmitter. **Figure 3-6** shows a final schematic of the bitumen side set-up. Gel is initially loaded from the bottom right side of a differential Keller pressure transmitter (Model PD-33X), through the 1/4" OD SS male tube union, the 1/4" OD SS T-union, the 1/4" SS tube-15 mm connection and a little bit into the 15 OD mm glass tube (12.4 mm ID). The purpose of this gel is to translate pressure readings through to the Keller transmitter while separating the bitumen from the sensitive keller pressure transmitter diaphragm. The inertness and low viscosity of the gel (toothpaste) makes it perfect for this purpose. Care is taken while loading the gel to ensure no air bubbles. The intention is to fill the bitumen from the top of the 15 mm glass tube allowing it to sit neatly on

the gel. The gel has a density of  $1300 \text{ kg/m}^3$  compared to the bitumen's  $1010 \text{ kg/m}^3$  which is important for gravity stability. The bottom part of the  $\frac{1}{4}$ " SS T-union is closed with a tube cap.

After the gel is properly loaded, the bottom right hand side of the set-up is disconnected. This includes: the  $\frac{1}{4}$ " SS male BSPP-tube union,  $\frac{1}{4}$ " SS T-union,  $\frac{1}{4}$ " SS tube-15 mm connection 15 mm glass tube. Note that all these parts are all still linked to each other and can very easily be reconnected back to the set-up.

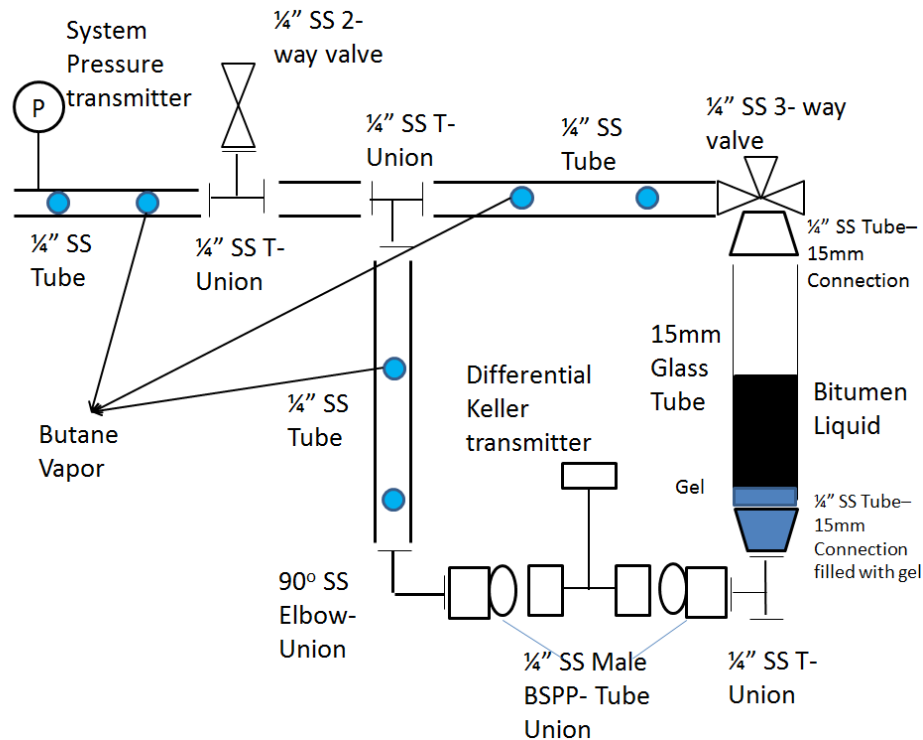


Figure 3-6 - Schematic of bitumen side

**Figure 3-7** shows the set-up used to load the bitumen into the aforementioned disconnected set-up. The bitumen cell is filled with bitumen, heated to  $60^\circ\text{C}$  and pressurized to 2 atm (29.39 psia) to push the bitumen into the bitumen tube. The 2-way  $\frac{1}{8}$ " inch valves serve to regulate the flow of the bitumen into the disconnected set. **Figure 3-8** shows a magnified image of the loading operation. Note that it is important that bitumen does not contact the walls of the 15 mm glass tube. After a specified height of bitumen is reached, the 2-way  $\frac{1}{8}$ " valves are closed. The disconnected set-up is weighed just before and just after the bitumen loading to evaluate the

mass of bitumen loaded. The disconnected bitumen tube set-up is then reconnected to the rest of the one-dimensional diffusion apparatus to prepare for the experiment. Characteristics of the bitumen used can be found in **APPENDIX A**.

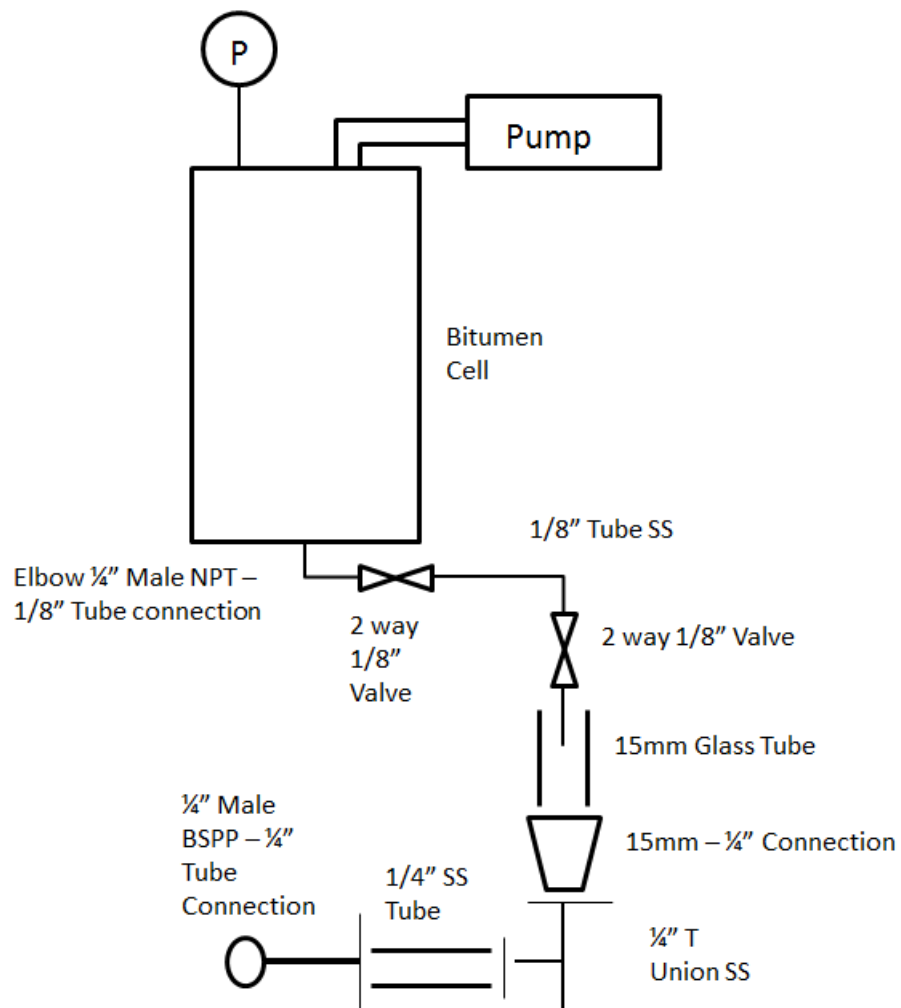


Figure 3-7 - Schematic of bitumen loading

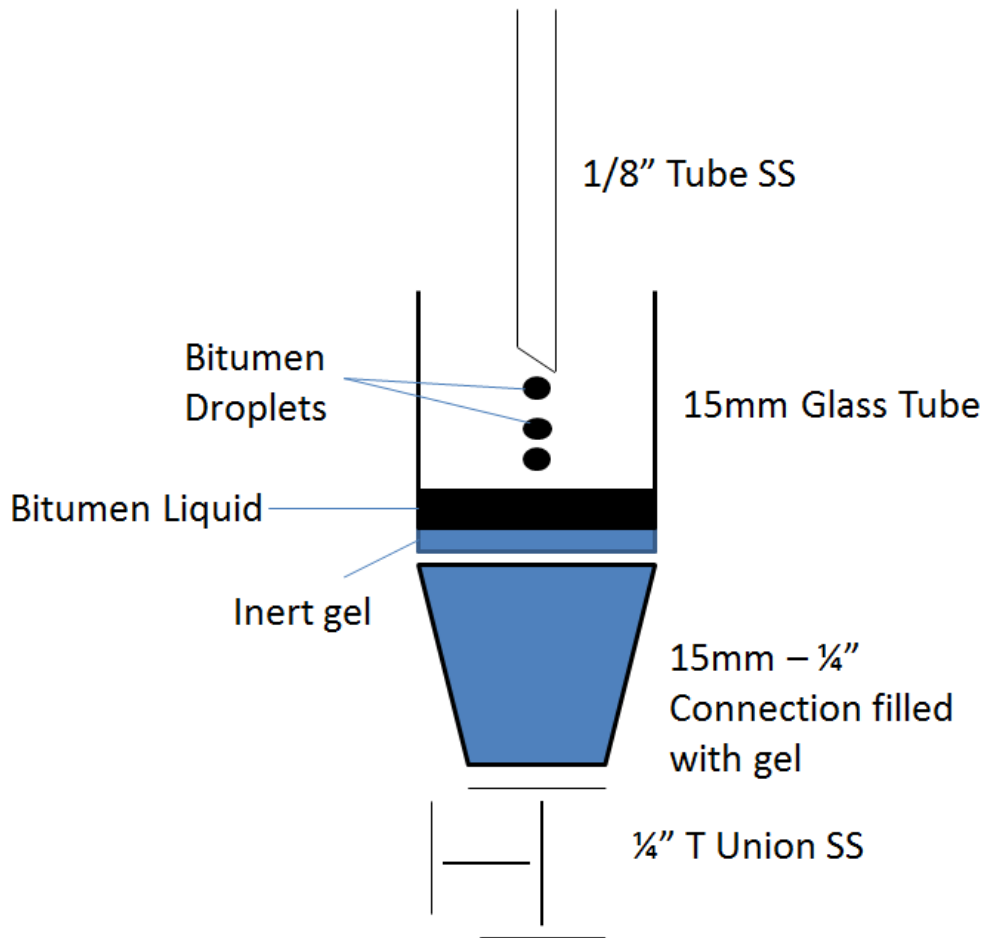


Figure 3-8 - Magnified schematic of bitumen loading

**Figure 3-9** shows a picture of the bitumen side (duplicated) when it is ready for the experiment. Note that the front duplicate contains only gel for illustration purposes while the back duplicate contains gel and bitumen. For all experimental runs, both duplicates contain gel and bitumen at similar (recorded) heights and masses. The full bitumen set-up is connected to the full butane set-up via the system pressure transmitter.

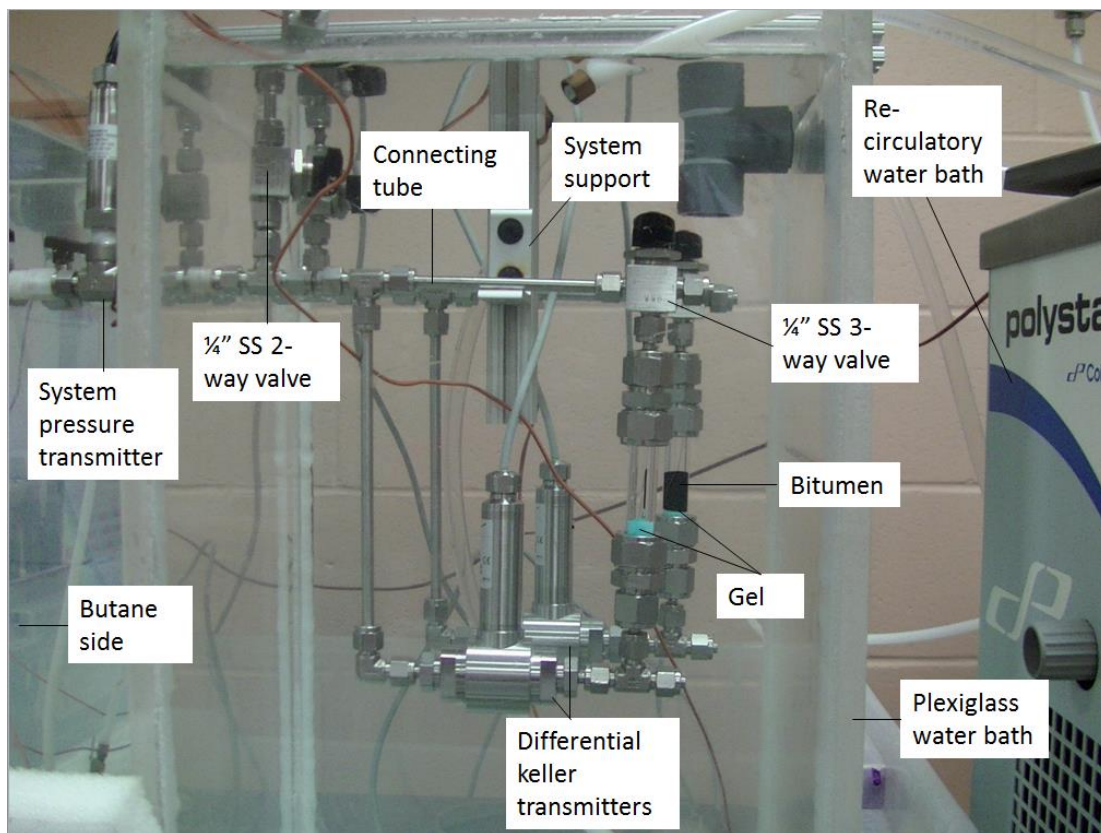


Figure 3-9 - Bitumen side

### **3.2.3. Solvent gas phase purity and vacuum creation**

Ensuring a pure, 100% solvent gas phase is critical to obtaining reliable and repeatable diffusion measurements. James (2009) showed that the presence of air or non-condensable gas (NCG) serves as barrier to diffusion due to the butane having to diffuse through the air/NCG first before diffusing into bitumen. Hence the presence of air/NCG would prolong the diffusion process and lead to erroneous diffusion values. Vacuum creation is achieved for the bitumen side and butane side. For the butane side, it ensures a 100% butane fluid (liquid and gas) during butane loading. The butane 1/4" (SS) 2-way valve is simply connected to an industrial vacuum pump, air is pulled from the tubing and then the 1/4" (SS) 2-way valve is closed. It must be noted that the industrial vacuum pump pulls a very strong vacuum (0.025 atm and below).

Vacuum creation in the bitumen side is more difficult. Pulling vacuum direct from the bitumen pulls up the bitumen fluid, thereby staining the walls of the 15 mm bitumen glass tube. It is more important to saturate the space above the bitumen with pure solvent vapor than to create a vacuum. Therefore a detailed process was perfected to ensure the experimental lines were filled with pure solvent vapor. Please note that prior to set-up for vacuum creation, the butane and bitumen tubes are weighed on a mass balance to record the initial mass of butane and bitumen contained in their respective tubes. While prepping the experiment, the butane height will change but the new height can be used to estimate the new butane mass (when it is submerged in water and inaccessible for measurement) as long as the starting butane mass was recorded.

Referring back to **Figure 3-9**, the system pressure on the bitumen side is typically begins at atmospheric conditions (1 atm). The following steps are taken to create the bitumen side vacuum;

- **Step 1-** This involves voiding air from the 1/4" connecting tube. With the 15 mm glass tubing filled with bitumen, the 1/4" SS 3-way valve is closed and a light vacuum (0.3 atm or 4.4 psi) is pulled from the bitumen side via the opened 1/4" SS 2-way valve to achieve vacuum in the 1/4" connecting tube. Note that at this time, the vacuum has no impact on the 15mm bitumen glass tube. Also note that this vacuum will not affect the butane side either given that its 1/4" SS 2-way valve is closed. The system pressure at this time, read from the system pressure transmitter, is about 0.3 atm (4.4 psi) but this does not account for the air in the bitumen glass tube.
- **Step 2-** The bitumen side's 1/4" SS 2-way valve is closed followed by the switching off of the vacuum pump.
- **Step 3-** The bitumen side 1/4" SS 3-way valve is now opened and this redistributes the air just above the bitumen leading to a system pressure increase to approximately 0.7 atm (10.29 psi). This is the real system. The vacuum causes the bitumen interface to rise momentarily but the interface quickly settles back to normal. This creates a very small stain on the bitumen glass walls but this stain quickly disappears as the experiment starts due to butane vapour pressure acting on the bitumen and the temperature of the bitumen side Plexiglass water bath. **Figure 3-10** shows a before and after picture of the bitumen

interface height leading to minimal wall stain. **Figure 3-11** shows a side by side look of the left and right tubes during vacuuming creation and experimental start time. The time elapsed between time A and B is 60 minutes

- **Step 4-** The butane side  $\frac{1}{4}$ " SS 2-way valve is then opened for 30 seconds and closed. This leads to the system pressure jumping to approximately 2 atm (29.38 psi) and saturates the whole bitumen side with butane vapour. A little diffusion also occurs but the amount is considered negligible. The changing height of the butane liquid is recorded via the cathetometer.
- **Step 5-** The bitumen side  $\frac{1}{4}$ " SS 3-way valve is once again closed and a vacuum of pulled from the system (0.3 atm), again via the bitumen side's  $\frac{1}{4}$ " SS 2-way valve.
- **Step 6-** The bitumen side's  $\frac{1}{4}$ " SS 2-way valve is closed followed by the switching off of the vacuum pump.
- **Step 7-** The bitumen side  $\frac{1}{4}$ " SS 3-way valve is now opened once again leading to the redistribution of air but this time, the system pressure drops to about 0.5 atm (7.39 psi). This is because the starting system pressure before vacuum was pulled was 0.7 atm (10.29 psi). Also, vapor in the bitumen side now consists of air and butane.
- **Step 8-** Step 1-7 is repeated until the final system pressure reached is about 0.3 atm. Note that the more the process is repeated, the higher the ratio of butane vapor to air in the system. By the time the final system pressure is at 0.3 atm, the percentage of air in the system is as low as 1%. The vapor in the system is now predominantly butane vapor and the experiment can be started. **Figure 3-12** shows a picture of the full experimental set-up. The bulk of the experimental set-up (butane and bitumen side Plexiglass water baths) is mounted on a vibration resistant table to eliminate any convective mixing due to vibration. **Figure 3-13** shows a detailed schematic of the experimental setup.

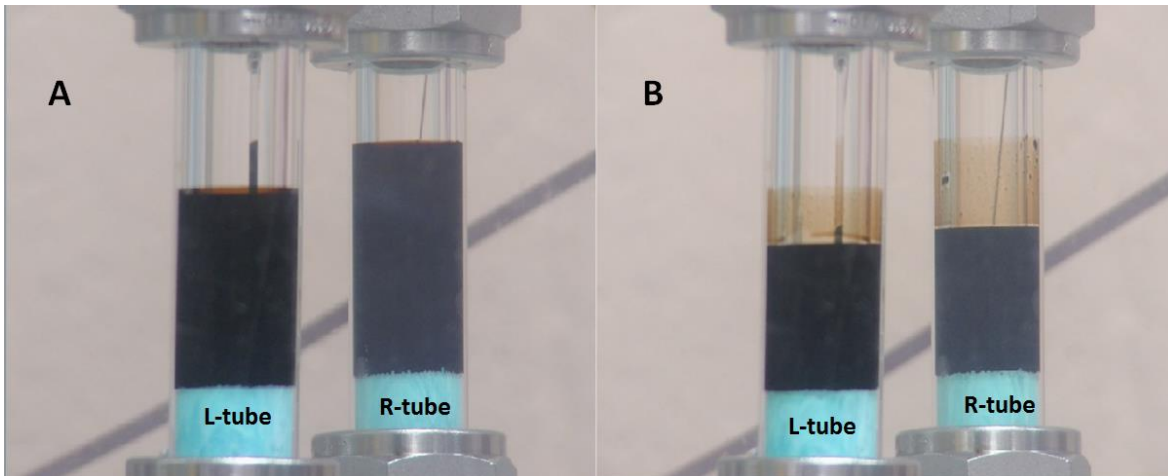


Figure 3-10 - Bitumen height pictures during vacuum creation (A) and at start of experiment (B)

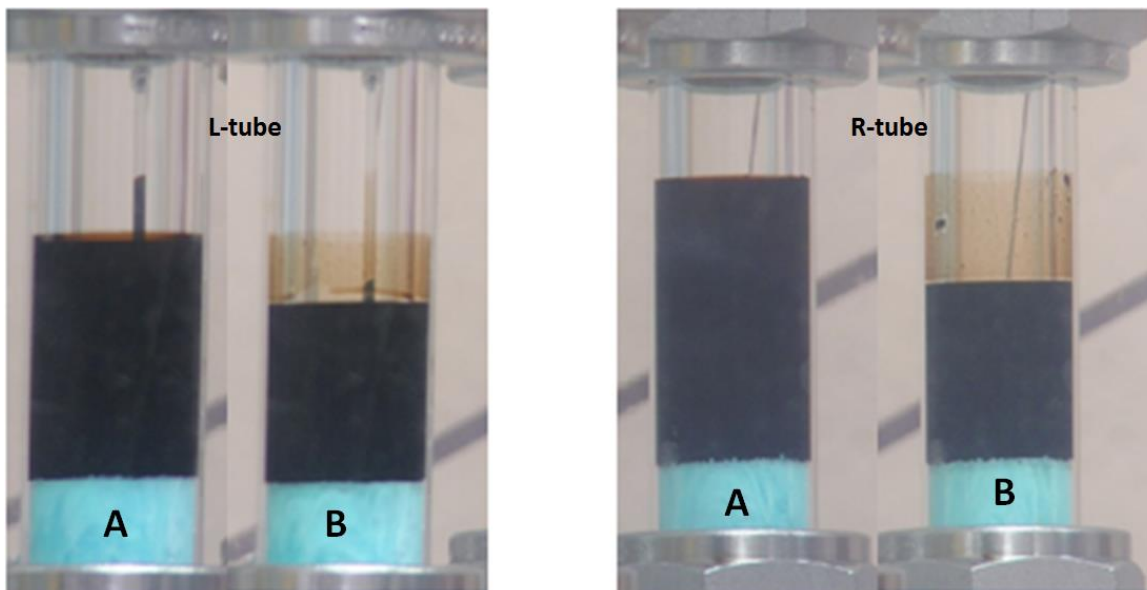


Figure 3-11 - A side by side look at both L-tubes (during A and B) and R-tubes (during A and B)

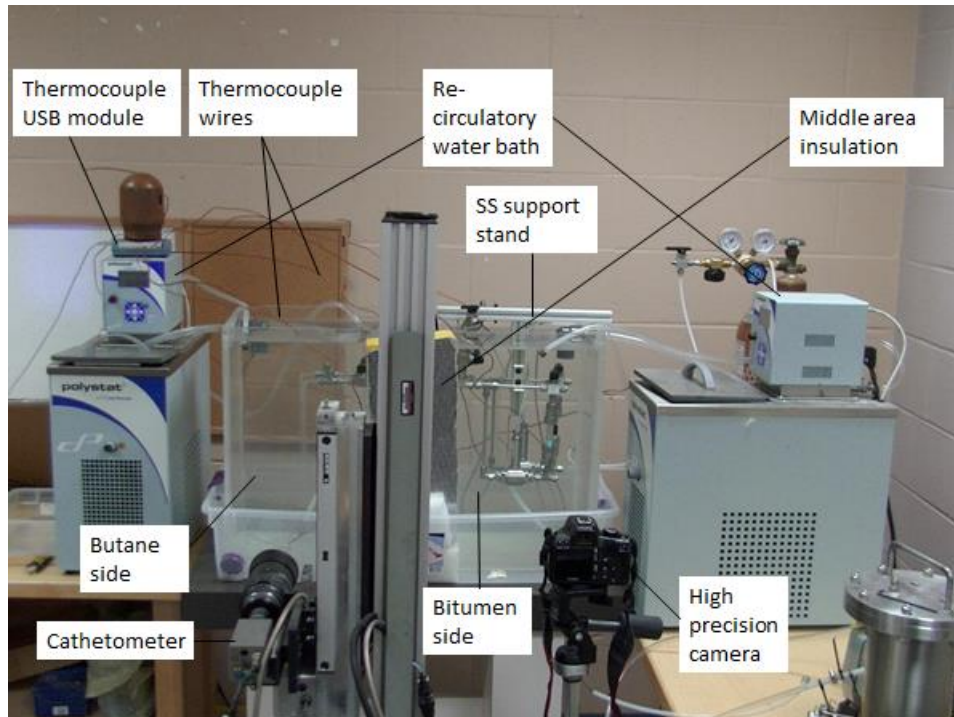


Figure 3-12 - Full experimental set-up

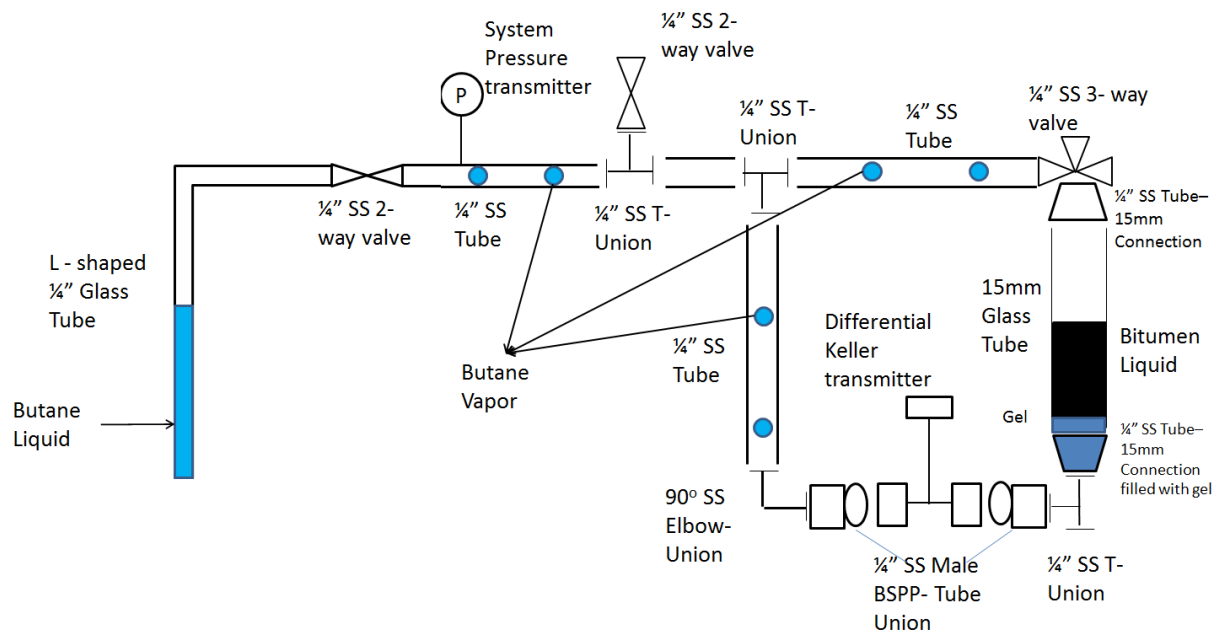


Figure 3-13 - Detailed experimental schematic (butane and bitumen side together)

## Main Equipment and material list

- Re-circulatory water baths (\*2)
- Plexiglass water baths (\*2)
- Vibration resistant table
- Thermocouples for monitoring water bath temperatures
- Thermocouple USB module (Omega Data acquisition board)
- Cathetometer (Schlumberger Charged-Coupled Device Measurement device)
- High precision camera (Nikon digital D5500)
- Bitumen side set-up
- Butane side set-up
- Insulation
- Stainless steel (SS) support stands.
- 99% Butane (Praxair, Canada)
- Athabasca Bitumen
- Gel (Colgate toothpaste)
- Keller differential pressure transmitters (Model PD-33X)

### 3.2.4. Run procedure

Below is the list of procedures taken over the course of an experimental run to get the best possible readings. Please note these come after already following steps 1-8 in **Section 3.2.3**:

- The experimental set-up is given four hours to reach steady state temperature on the bitumen side for the required run. The various temperature runs are 27.00, 30.25, 33.50, 36.75 and 40.00°C. These various constant temperatures are achieved using the re-circulatory water baths. The butane side temperature is held constant at 24°C through all the experimental runs.
- The butane and bitumen heights are recorded before the butane side ¼” SS 2-way valve and bitumen ¼” SS 3-way valves are opened. As soon as the valves are opened the butane saturates the bitumen side with butane vapor until butane vapor pressure reaches 2.36 atm (34.65 psi). Note that this leads to a sudden reduction in butane height that has

to be recorded. The bitumen height changes at this point are negligible. This system pressure is maintained through the whole experiment. Differential pressure however, will change over the course of the experiment. As the butane diffuses into the bitumen, the bitumen phase swells causing a change in differential pressure.

- The experiment is about start and all experimental recording devices are switched on: thermocouple recording devices, Keller transmitters (System and differential), cathetometers, and the high precision camera e.t.c.
- The Keller differential transmitter is zero'd just before the experiment starts. This is to ensure that any pressure changes from then on are solely due to the changing bitumen density and eliminates the need to account for the toothpaste density.
- The experiment now officially starts with the 2-way butane valve and 3-way bitumen valves being opened. The system pressure reaches and stabilizes at 2.36 atm.
- Taking a reading involves: recording butane height with the cathetometer, taking a picture of bitumen height with the high precision camera and logging system/differential pressure values (using Keller transmitter logging software). Thermocouple measuring device automatically logs temperature readings every 10 minutes. The high precision camera pictures are later analysed to determine bitumen height changes.
- Readings are taken every 30 minutes for the first hour, every hour for the next 2 hours and finally every 3 hours. A stop clock is used for this. An experimental run lasts for 4320 minutes (3 days).
- The butane height changes are easily recorded from a monitor system linked to the cathetometer. The pictures taken by the High precision camera for the bitumen height changes are analysed using pixels in Microsoft "Paint" software. Further explanation of this analysis is found in **Section 4.2**. For both height readings, the lower meniscus is taken as the height.
- The system temperatures (the plexiglass water) on both sides are consistently monitored to ensure they are within  $\pm 0.5^{\circ}\text{C}$  of what is specified using the thermocouple measuring device. Tweaks in temperature if needed can be done using the re-circulatory water bath
- The water in the re-circulatory water bath evaporates over time. This could lead to the bath's low level alarm going off. The water is therefore topped over time. This however,

leads to spikes in temperature of the system which also leads to spikes in differential pressure readings. The pressure values stabilise over time so in case of any pressure spikes, readings are not taken until the pressure value stabilizes.

- At the end of the experiment, final values are taken and the system is disconnected. The butane and bitumen sides are weighed to evaluate the final butane and bitumen masses in the system. There is no need to clean any of the SS tubing. The butane glass tube is refilled with butane and the bitumen glass tube is replaced with a new glass tube before being topped up with gel and filled with bitumen.
- Due to both bitumen and butane sides being immersed in water, gas leaks are easy to detect (bubbles showing up in tubing connections).

### 3.2.5. Troubleshooting

The experimental set-up used in this work is unique and has never really been tried by any researcher in the field. Hence there were a lot of issues encountered while putting the set-up together to ensure repeatable results. A list of these issues is as follows:

- Measuring the non-ideality
- Monitoring the butane height
- Purity of butane
- Butane vapour pressure vs. bitumen temperature
- Bitumen and gel interaction

All these issues are addressed in **APPENDIX B**.

## 4) NUMERICAL METHODOLOGIES

The purpose of this section is to outline the mathematical techniques used to analyze the data obtained from this experiment. Symbols used, as well as descriptions, are outlined in the nomenclature section. **APPENDIX C** contains starting conditions for each experiment.

### 4.1. Bitumen/Butane Density and Pressure Calculations

#### 4.1.1. Non-ideal mixture density

Shown below in **Table 4-1** is table used to calculate non-ideal density/real density, real specific volume and equivalent mass over a certain time period for the experiment. The highlighted row is used in our sample calculation. Note that full calculations for all the highlighted columns is available in **APPENDIX D** under the “Non-ideal mixture density”.

Table 4-1- Sample calculation for non-ideal density

Column Number	1	2	3	4	5	6	7	8	9	10	11	12	13
	Given Time	Minutes	Diff pressure (atm)	Diff Pressure (Pa)	$\Delta$ Pressure (Pa)	Real Pressure (Pa)	Bitumen Height (cm)	Full Hydrostatic Height (cm)	$\Delta$ Bitumen Height (cm)	$\Delta$ Bitumen Density ( $\text{g}/\text{cm}^3$ )	Real bitumen density ( $\text{g}/\text{cm}^3$ )	Real bitumen specific volume ( $\text{cm}^3/\text{g}$ )	Real Mass Bitumen (g)
DAY 1	7pm	0	0.00019	19	0	0	1.6169	6.4169	0.0000	0.000	0.999	1.001	1.950
	7.30pm	30	0.00016	16	-3	0	1.6245	6.4245	0.0076	-0.001	0.998	1.002	1.957
	8pm	60	-0.00001	-1	-20	-1	1.6320	6.4320	0.0151	-0.002	0.997	1.003	1.964
	9pm	120	-0.00029	-29	-49	-3	1.6434	6.4434	0.0265	-0.004	0.996	1.004	1.975
	10pm	180	-0.00056	-57	-76	-5	1.6510	6.4510	0.0341	-0.004	0.995	1.005	1.982
	11pm	240	-0.00093	-94	-113	-8	1.6586	6.4586	0.0417	-0.005	0.994	1.006	1.990
	12am	300	-0.00111	-112	-132	-9	1.6661	6.4661	0.0492	-0.006	0.993	1.007	1.997
	6am	660	-0.00222	-225	-244	-17	1.6964	6.4964	0.0795	-0.010	0.989	1.011	2.026

Column 3 shows a reduction in differential pressure values as the experiment progresses. One would expect differential pressure values to increase given bitumen height increase as time proceeds. But the increase in bitumen height is more than offset by the reduction in bitumen density due to diffusion of the butane solvent hence making the differential pressure decrease as the experiment progresses.

The change in bitumen density or  $\Delta$  density, (in column 10) represents the change in density due to the hydrostatic pressure change and increase in bitumen height. Using **Equation 2-84**:

$$P_1 = \rho_1 g h_1 \quad 4-1$$

$$P_2 = \rho_2 g h_2 \quad 4-2$$

Subtracting both sides from each other,

$$P_1 - P_2 = \rho_1 g h_1 - \rho_2 g h_2$$

$$\frac{P_1 - P_2}{g} = \rho_1 h_1 - \rho_2 h_2 ,$$

Knowing that  $(\rho_2 = \rho_1 + \Delta\rho)$  and  $(h_2 = h_1 + \Delta h)$  we get,

$$\frac{P_1 - P_2}{g} = \rho_1 h_1 - [(\rho_1 + \Delta\rho)(h_1 + \Delta h)]$$

$$\frac{P_1 - P_2}{g} = \rho_1 h_1 - (\rho_1 h_1 + \rho_1 \Delta h + \Delta\rho h_1 + \Delta\rho \Delta h)$$

$$\frac{P_1 - P_2}{g} = \rho_1 h_1 - \rho_1 h_1 - \rho_1 \Delta h - \Delta\rho h_1 - \Delta\rho \Delta h$$

$$\frac{P_1 - P_2}{g} = -\rho_1 \Delta h - \Delta\rho h_1 - \Delta\rho \Delta h$$

$$\frac{P_1 - P_2}{g} = -\rho_1 \Delta h - \Delta\rho (h_1 + \Delta h)$$

$$\Delta\rho = \left( \frac{1}{h_1 + \Delta h} \right) \left[ -\rho_1 \Delta h - \left( \frac{P_1 - P_2}{g} \right) \right] \quad 4-3$$

Where,  $h_1$  = hydrostatic height of the gel and bitumen at time 0 minutes (6.4169 cm)

$\Delta h$  = height change at given time (0.0795 cm)

$\rho_1$  = initial bitumen density at time 0 minutes (0.999 g/cm<sup>3</sup>)

$g$  = acceleration due to gravity ( $981 \text{ cm/s}^2$ )

$P_1 - P_2$  = real differential pressure change at given time ( $-17.29 \text{ Pa}$ )

$\Delta\rho$  = Changing density values. Note that the toothpaste density is not used because it is assumed to remain constant while bitumen density changes due to the diffusion. Also the differential transmitter is zero'd at the start of experiment so any pressure change is solely due to changing bitumen density

$$\Delta\rho = \left( \frac{1}{6.4169 \text{ cm} + 0.0795 \text{ cm}} \right) [(-0.999 \text{ gcm}^{-3} * 0.0795 \text{ cm}) - \left( \frac{-17.29 \text{ Pa}}{981 \text{ cm/s}^2} \right)]$$

$$\Delta\rho = -0.01 \text{ gcm}^{-3}$$

Column 11 is the real or non-ideal density of the bitumen mixture at time 't'. This bitumen mixture density is given as the addition of  $\Delta\rho$  at time (t) and Bitumen mixture density at time (t=0):

$$\text{Real bitumen mixture density} = \Delta\rho + \text{Bitumen mixture density (t = 0)}$$

$$\rho_{mix (non-ideal)} = \Delta\rho + \rho_B \quad 4-4$$

$$-0.01 + 0.999 = 0.989 \text{ gcm}^{-3}$$

Column 12 is the real or non-ideal specific volume of the bitumen mixture at time 't'. This bitumen mixture is given as the inverse of the real bitumen mixture density:

$$\text{Real bitumen mixture specific volume} = \frac{1}{\text{Real bitumen mixture density}}$$

$$v_{mix (non-ideal)} = \frac{1}{\rho_{mix (non-ideal)}} \quad 4-5$$

$$\frac{1}{0.989} = 1.011 \text{ cm}^3 \text{g}^{-1}$$

### 4.1.2. Ideal mixture density

**Table 4-2** for this section covers the way to calculate ideal density of the bitumen. Note that full calculations for all the highlighted columns is available in **APPENDIX D** under the “Ideal mixture density”.

Table 4-2 - Sample calculations for ideal density

13	14	15	16	17	18	19	20	21	22
Real Mass Bitumen (g)	$\Delta$ Butane heighty (cm)	Area butane tube (cm <sup>2</sup> )	Volume butane diffused (cm <sup>3</sup> )	Moles butane diffused	Mass butane diffused (g)	Mass fraction butane ( $\omega_s$ )	Mole fraction butane $w_s$	Ideal bitumen Mixture density (g/cm <sup>3</sup> )	Ideal bitumen specific volume (cm <sup>3</sup> /g)
1.950	0.0000	0.112	0.000	0.000	0.000	0.000	0.000	0.999	1.001
1.957	0.1360	0.112	0.015	0.000	0.009	0.004	0.041	0.997	1.003
1.964	0.2230	0.112	0.025	0.000	0.014	0.007	0.065	0.996	1.004
1.975	0.3620	0.112	0.041	0.000	0.023	0.012	0.101	0.994	1.006
1.982	0.4680	0.112	0.052	0.001	0.030	0.015	0.127	0.993	1.008
1.990	0.5650	0.112	0.063	0.001	0.036	0.018	0.150	0.991	1.009
1.997	0.6540	0.112	0.073	0.001	0.041	0.021	0.169	0.990	1.010
2.026	1.0700	0.112	0.120	0.001	0.068	0.034	0.250	0.984	1.016

The ideal bitumen mixture density (column 21) of the bitumen and butane is computed as follows:

*Ideal mixture density*

$$= (\text{Butane density} * \text{Butane mass fraction}) + (\text{Bitumen density} * \text{Bitumen mass fraction})$$

$$\rho_{mix(ideal)} = (\rho_s * \omega_s) + (\rho_B * (1 - \omega_s)) \quad 4-6$$

$$\begin{aligned} \rho_{mix(ideal)} &= (0.557 \text{ g cm}^{-3} * 0.034) + (0.999 \text{ g cm}^{-3} * (1 - 0.034)) \\ &= \mathbf{0.984 \text{ g cm}^{-3}} \end{aligned}$$

Finally, the ideal bitumen mixture specific volume (column 22) is computed as:

$$\text{Ideal bitumen specific volume} = \frac{1}{\text{Ideal mixture density}}$$

$$v_{mix(ideal)} = \frac{1}{\rho_{mix(ideal)}} \quad 4-7$$

$$\frac{1}{0.984} = 1.016 \text{ cm}^3 \text{ g}^{-1}$$

Note: All values from column 11 (real/non-ideal mixture density  $\rho_{mix (non-ideal)}$ ), column 12 (real/non-ideal mixture specific volume  $v_{mix (non-ideal)}$ ), column 19 (solvent mass fraction  $\omega_s$ ), column 21 (ideal mixture density  $\rho_{mix(ideal)}$ ) and column 22 (ideal mixture specific volume  $v_{mix(ideal)}$ ) are later used to plot graphs applied in **Section 4.3.2** and **5.3**

## 4.2. Bitumen height analysis

The purpose of this section is to outline the methodology used to compute bitumen changes as the experiment progresses. As stated in **Section 3**, the bitumen height changes are tracked using pictures taken with a high precision camera (Nikon digital D5500). These pictures are then analyzed using pixels in Microsoft ‘Paint’ software. The smallest movement of the camera between pictures can lead to erroneous bitumen height values. The camera is therefore mounted on a tripod stand and its position is not altered through the whole experiment. **Figure 4-1** shows a picture of a typical bitumen height at the start of an experimental run (time  $t = 0$  mins). **Table 4-3** further explains the notation for the terms used.

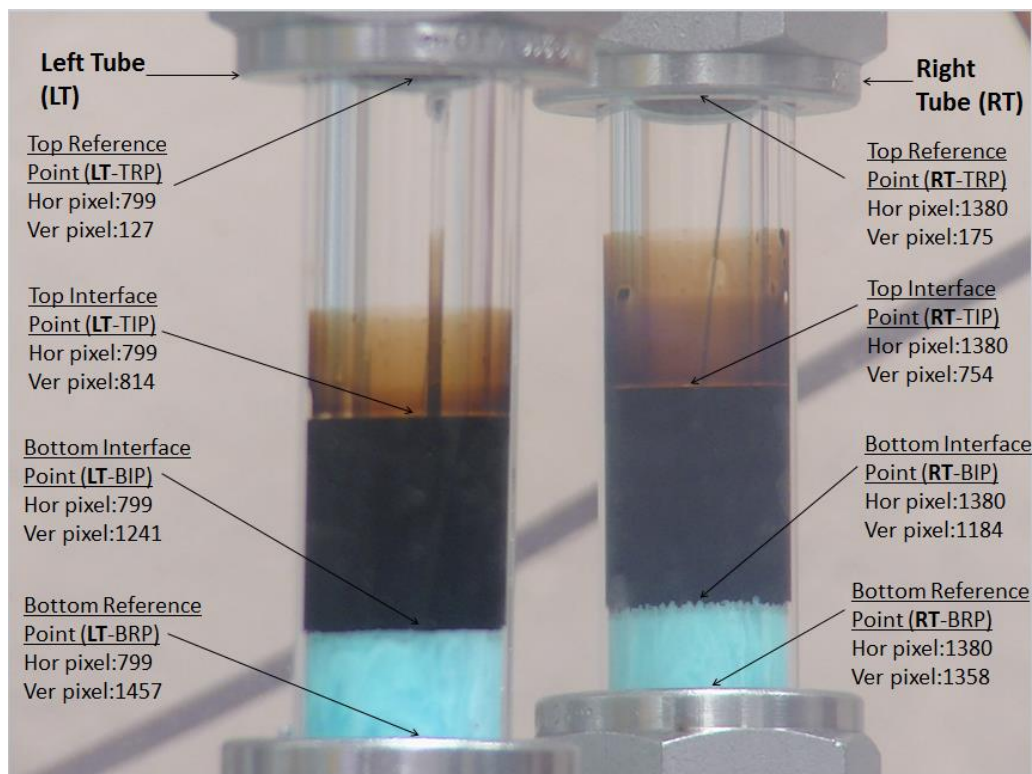


Figure 4-1 - Picture of bitumen height at t = 0 minutes

Table 4-3 - Notation for bitumen height analysis

<b>Acronym</b>	<b>Full meaning</b>	<b>Acronym</b>	<b>Full meaning</b>
<b>LT-TRP</b>	Left tube top reference point	<b>RT-TRP</b>	Right tube top reference point
<b>LT-TIP</b>	Left tube top interface point	<b>RT-TIP</b>	Right tube top interface point
<b>LT-BIP</b>	Left tube bottom interface point	<b>RT-BIP</b>	Right tube bottom interface point
<b>LT-BRP</b>	Left tube bottom reference point	<b>RT-BRP</b>	Right tube bottom reference point
Hor pixel	Horizontal pixel	Ver pixel	Vertical pixel

Four reference points are used when analyzing the bitumen heights in ‘Paint’ software. There are two reference points for the left tube: **LT-TRP** for the top and **LT-BRP** for the bottom. There are

also two reference points for the right tube: **RT-TRP** for the top and **RT-BRP** for the bottom. Each point will have a horizontal pixel and vertical pixel value (Hor pixel and Ver pixel). The values for the reference points should ideally remain constant throughout the experiment. However, there is the slight possibility of a shift in vertical pixel values between readings (usually by  $\pm 1$  or 2 pixels). This could occur if the flash button on the camera is pressed a little too hard while taking the picture leading to a slight elevation in the camera eye-level while taking the picture. Having two reference points for each tube prevents this from being an issue because a vertical pixel point +1 shift for the top reference point (**LT-TRP** or **RT-TRP**) will equally lead to a vertical pixel point +1 shift for the bottom reference point (**LT-BRP** or **RT-BRP**) and vice versa. Hence the vertical pixel point difference between the two positions remains constant. The horizontal pixel points remains constant for all experimental values.

There are four interface points used to compute the bitumen height at any given time. Each tube has two interface points used which represent top and bottom of the bitumen fluid. The left tube has interface points: **LT-TIP** for the top and **LT-BIP** for the bottom. The right tube has interface points: **RT-TIP** for the top and **RT-BIP** for the bottom. The top interface points (**LT-TIP** and **RT-TIP**) are the main points used to track the changing bitumen height as their vertical pixel point values change over the course of the experiment. Ideally, the bottom interface points (**LT-BIP** and **RT-BIP**) remain constant though the whole experiment. However, as stated earlier, a slight increase in camera elevation (usually  $\pm 1-2$  pixels) will similarly lead to a shift in these vertical pixel points. The top interface points (**LT-TIP** and **RT-TIP**) will equally shift vertically by the same amount thereby eliminating these issues. The horizontal pixel points will also remain constant for all experimental values.

For this section, the left tube (**LT**) bitumen height will be analyzed. The whole procedure used is directly applicable to the right tube bitumen height. The lower meniscus is used for all height readings.

There are two key ways of computing the starting bitumen height in **Figure 4-1**. The 1<sup>st</sup> way utilizes the bitumen mass, volume, density and area of the bitumen tube. The mass of bitumen is

measured before the start of the experiment (1.95 g for the left tube and 2.25 g for the right tube). The density of the bitumen at the given experimental run temperature is also known (0.999g/cm<sup>3</sup>). The volume of the bitumen is then found as:

$$Volume = \frac{Mass}{Density} \quad 4-8$$

$$Volume = \frac{1.95}{0.999} = 1.9516 \text{ cm}^3$$

The cross sectional area of the bitumen tube is given as:

$$Area = \pi r^2$$

$$Area = 3.14 * 0.62^2 = 1.207 \text{ cm}^2$$

The height of the bitumen can now be found as:

$$Height = \frac{Volume}{Area} \quad 4-9$$

$$Height = \frac{1.9516}{1.207} = \mathbf{1.6169 \text{ cm}}$$

The second method involves scaling of the bitumen height. It is used to compute the starting bitumen height and the subsequent bitumen heights as the experiment progresses. It is executed as follows:

- Prior to the start of the experiment, the distance between the top reference points (**LT-TRP** or **RT-TRP**) and bottom reference points (**LT-BRP** or **RT-BRP**) is measured with the Cathetometer.
- For the left tube this distance with the cathetometer was found to be 5.036 cm. Hence in terms of real vertical distance

$$\text{Tube vertical distance} = \text{Bottom reference point} - \text{Top reference point} \quad 4-10$$

$$\text{LT-BRP} - \text{LT-TRP} = 5.036 \text{ cm}$$

- From **Figure 4-1**, we can also find the difference between the top (LT-TRP) and bottom (LT-BRP) reference points based on vertical pixel points as;

$$\text{Tube vertical pixel diff} = \text{Bottom reference point} - \text{Top reference point} \quad 4-11$$

$$\text{LT-BRP} - \text{LT-TRP} = 1457 - 127$$

$$= 1330 \text{ pixels}$$

- We now know that 1330 pixels is equivalent to 5.036 cm in real height. We now find the difference in vertical pixel points for the bitumen height (LT-BIP minus LT-TIP) from **Table 4-1** as;

$$\text{Bitumen vertical pixel diff} = \text{Bottom interface point} - \text{Top interface point} \quad 4-12$$

$$\text{LT-BIP} - \text{LT-TIP} = 1241 - 814$$

$$= 427 \text{ pixels}$$

- Therefore finding the real bitumen height or vertical distance can be given as;

$$\text{Bitumen height} = \frac{\text{Bitumen vertical pixel diff}}{\text{Tube vertical pixel diff}} * \text{Tube vertical distance} \quad 4-13$$

$$\text{LT-BIP} - \text{LT-TIP} = \frac{427}{1330} * 5.036 \text{ cm}$$

$$= \underline{\underline{1.6169 \text{ cm}}}$$

- This is exactly the same height value calculated from **Equation 4-9**. If ever the values obtained are not exactly the same, an average is taken. The value also corresponds with bitumen height at time  $t = 0$  minutes from **Figure 4-1** column 7.

- **APPENDIX E** has a table of all initial bitumen heights calculated using both methods for all temperatures

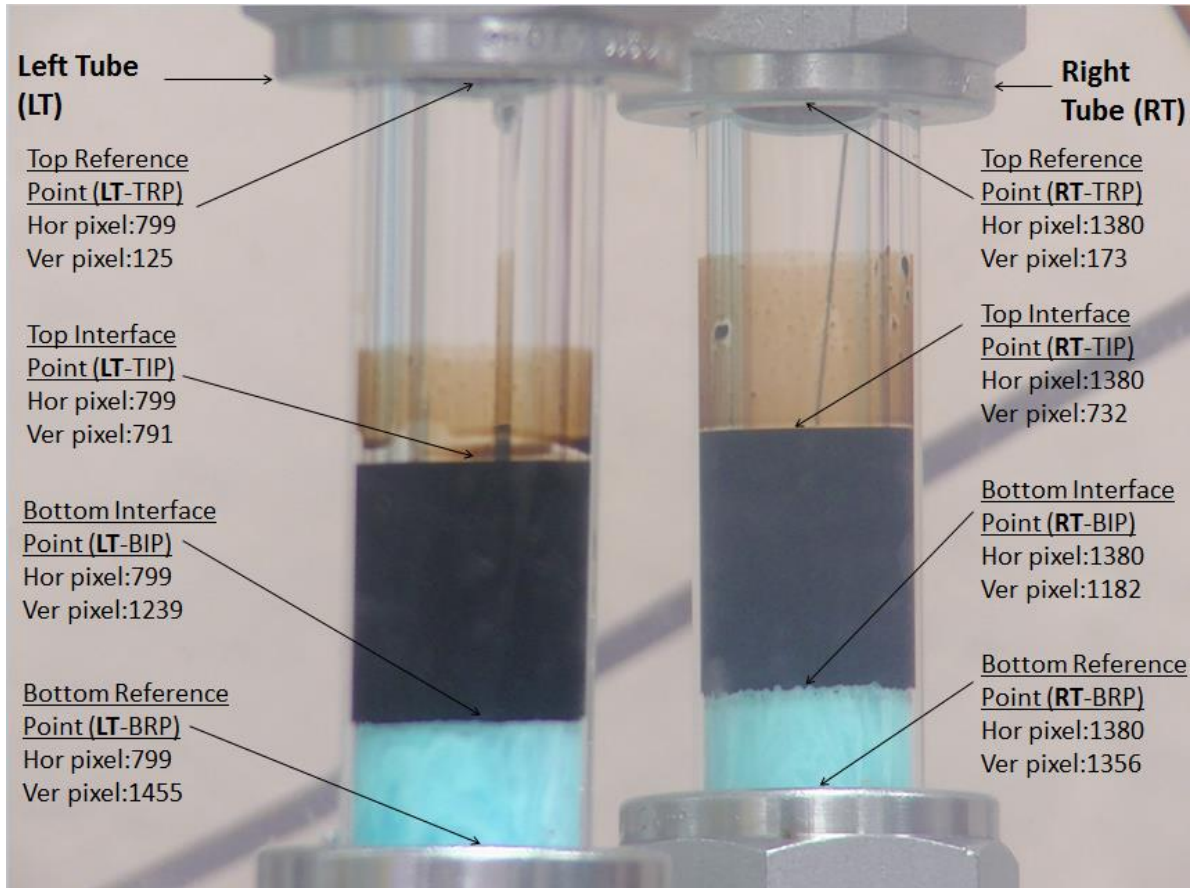


Figure 4-2 - Picture of bitumen height at time  $t = 660$  minutes (11 hours)

**Figure 4-2** shows a picture taken of the bitumen height for the same experiment at time  $t = 660$  minutes (11 hours). This is also the highlighted time in **Table 4-1**. Note there has been a shift in all the reference and interface vertical pixel points compared to those at time  $t = 0$  minutes from **Figure 4-1**. The differences in points for the left tube (LT) are tabulated below in **Table 4-4**;

Table 4-4 - Difference in left tube pixel points from time t = 0 minutes and t = 660 minutes

		Time t = 0 min	Time t = 660 min	Difference
<b>LT-TRP</b>	Vertical pixel	127	125	-2
	Horizontal pixel	799	799	0
<b>LT-TIP</b>	Vertical pixel	814	791	-23
	Horizontal pixel	799	799	0
<b>LT-BIP</b>	Vertical pixel	1241	1239	-2
	Horizontal pixel	799	799	0
<b>LT-BRP</b>	Vertical pixel	1457	1455	-2
	Horizontal pixel	799	799	0

From **Table 4-4**, note that all horizontal pixel points for t = 0 min and t = 660 min are constant. This remains the same through the full duration of the experiment. From t=0mins and t=600mins the left tube top reference point (**LT-TRP**) experiences a vertical pixel point shift (difference) of -2 pixels. As stated earlier, when such a shift occurs, it will also apply to the left tube bottom reference point (**LT-BRP**) and left tube bottom interface point (**LT-BIP**). Note: that looking at **Figure 4-1** and **Figure 4-2**, the right tube vertical pixel values from t = 0 mins and t = 600 mins also experience this -2 pixel shift.

The left tube top interface point (**LT-TIP**) will equally experience the -2 pixel shift combined with an increase in bitumen height (due to diffusion of butane) leading to a difference of -23 pixels. The bitumen height at time t = 660 minute is then calculated using **Equation 4-13**:

$$\begin{aligned}
 \text{Bitumen height} &= \frac{\text{New bitumen pixel vertical diff}}{\text{Tube pixel vertical diff}} * \text{Tube vertical distance} \\
 &= \frac{1239-791}{1330} * 5.036 \text{ cm}
 \end{aligned}$$

$$\begin{aligned}
&= \frac{448}{1330} * 5.036 \text{ cm} \\
&= \underline{\underline{1.6964 \text{ cm}}}
\end{aligned}$$

This value corresponds with the highlighted value in **Table 4-1** column 7.

### 4.3. Solvent Continuity and Diffusivity Calculations

The purpose of this section is to review the differential equations used to eventually calculate concentration dependent diffusivity of the butane solvent in the bitumen. James (2009) carefully explains how these equations are acquired (**Section 2.2.3**). The only tweak needed for the purpose of this thesis is the incorporation of non-ideality and temperature dependent solubilities.

#### 4.3.1. Diffusivity equations

The equations used to evaluate diffusivity functions are discussed in literature review of James (2009) work in **Section 2.2.3**. As stated earlier, the numerical results are independently validated. Trial and error was used to select the type of diffusivity function where the predicted ‘bitumen growth’ and butane solvent decrease were compared to experimental results. The coefficients of the proposed diffusivity function were set as the parameters to optimize. The difference in experimental and predicted growth of the bitumen is used as the objective function and minimized to optimize the linear diffusivity coefficients  $p_1$  and  $p_2$ .

Using the ‘lsqnonlin – least squares nonlinear’ optimization option in Matlab, the objective function is minimized automatically. The butane solvent decrease is not used in the objective function and is utilized as an independent validation of the butane solvent diffusivity.

$$D_{sb} = p_1 \omega_s + p_2 \tag{4-14}$$

$$f_{objective} = \frac{(h_{bitumen})_{experimental} - (h_{bitumen})_{predicted}}{(h_{bitumen})_{experimental}} \tag{4-15}$$

Lower and upper bounds on the diffusivity coefficients are initially set at  $1 \times 10^{-9}$  and  $1 \times 10^{-4}$  before being constantly adjusted depending on results obtained. The aim is to obtain a result with first order optimality of about  $1 \times 10^{-3}$  and sum of squared residuals of about  $1 \times 10^{-2}$ .

One key difference with this work compared to James (2009) is the different temperature used give different solvent mass fractions/concentration  $\omega_s^*$  at the bitumen solvent interface (solubility of solvent in bitumen). This is discussed in **Section 4.3.3**. The full Matlab code used in is **APPENDIX I**. The other key difference between this work and James (2009) work is the accounting for the non-ideal mixing of bitumen and butane solvent. This is discussed next.

### 4.3.2. Accounting for non-ideal mixing

James (2009) assumed ideal mixing of bitumen and butane solvent to give an overall mixture density with the following,

$$\rho_{mix} = \left[ \frac{1}{v_s \omega_s + v_b (1 - \omega_s)} \right] \quad 4-16$$

Where  $\rho_{mix}$  is overall bitumen mixture density ( $\text{g}/\text{cm}^3$ ),  $\omega_s$  is the butane solvent mass fraction/concentration,  $v_s$  and  $v_b$  are butane solvent and bitumen specific volumes ( $\text{cm}^3/\text{g}$ ) at the given butane solvent and bitumen temperatures. The overall bitumen mixture density obtained using **Equation 4-16** ( $\rho_{mix}$ ) is the ideal bitumen mixture density ( $\rho_{mix (ideal)}$ )

$$\frac{1}{\rho_{mix}} = \frac{1}{\rho_{mix (ideal)}} = \left[ \frac{1}{v_s \omega_s + v_b (1 - \omega_s)} \right]^{-1}$$

$$\frac{1}{\rho_{mix (ideal)}} = v_{mix (ideal)} = v_s \omega_s + v_b (1 - \omega_s)$$

$$v_{mix (ideal)} = v_s \omega_s - v_b \omega_s + v_b \quad 4-17$$

where  $v_{mix(ideal)}$  is the overall ideal bitumen mixture specific volume ( $\text{cm}^3/\text{g}$ ). The bitumen mixture specific volume can be based on ideal or non-ideal mixing. James (2009) work based all mixing values on ideal mixing, while this work will account for ideal and non-ideal mixing. In both density and specific volume calculations, non-ideal values give the best estimate of what experimental values actually are. For the sample calculation in **Section 4.1** with bitumen at  $30.25^\circ\text{C}$ , the ideal specific volume  $v_{mix(ideal)}$  values are obtained from **Table 4-2** column 22. The non-ideal volume  $v_{mix(non-ideal)}$  values are obtained from **Table 4-1** column 12. The butane solvent mass fraction/concentration  $\omega_s$  values are obtained from **Table 4-2** column 19. Refer to **APPENDIX D** for comprehensive information on how  $v_{mix(ideal)}$  and  $v_{mix(non-ideal)}$  values were obtained. **Figure 4-3** shows a plot of  $v_{mix(non-ideal)}$  and  $v_{mix(ideal)}$  vs the solvent mass fraction.

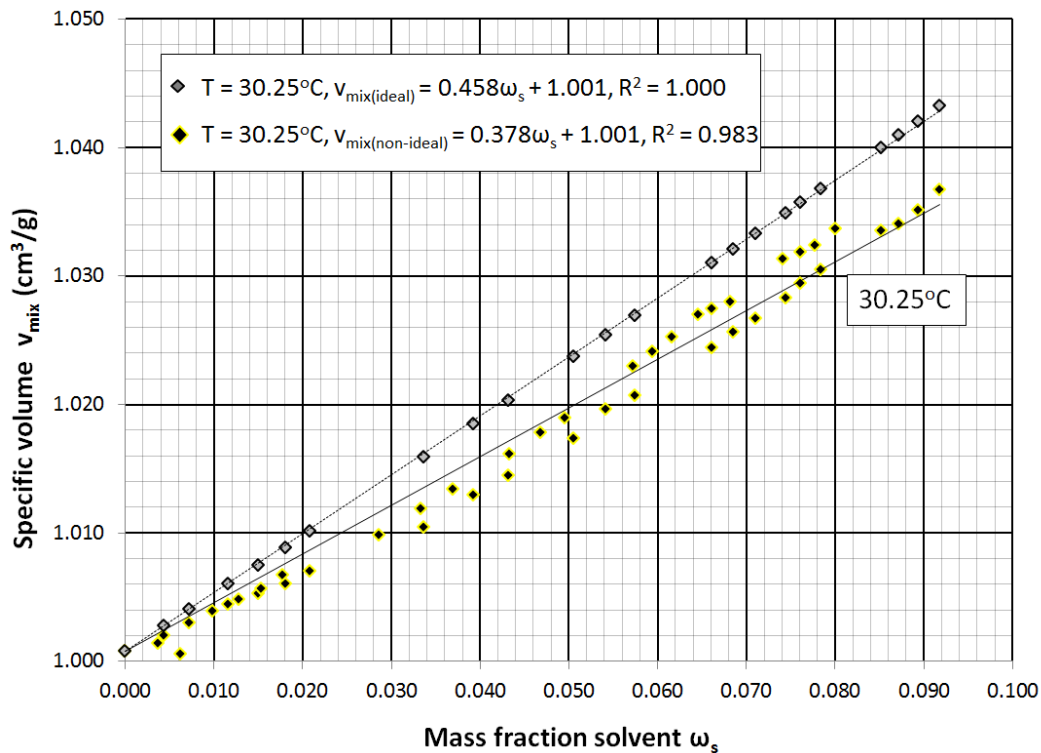


Figure 4-3 - Bitumen mixture specific volume plots for ideal and non-ideal mixing

**APPENDIX F** contains all the specific volume graphs for all temperatures. From **Figure 4-3** plotting a graph of values for  $v_{mix(ideal)}$  against  $\omega_s$  gives an equation representation for the ideal specific volumes as a function of butane solvent mass fraction/concentration. This is given as:

$$v_{mix(ideal)} = 0.458\omega_s + 1.001$$

Organizing the equation in the same form as **Equation 4-17**;

$$\frac{1}{\rho_{mix(ideal)}} = v_{mix(ideal)} = 1.459\omega_s - 1.001\omega_s + 1.001 \quad 4-18$$

where ideal butane solvent specific volume  $v_s$  is 1.459 cm<sup>3</sup>/g and ideal bitumen specific volume  $v_b$  is 1.001 cm<sup>3</sup>/g for the given experimental temperature (30.25°C).

From **Figure 4-3** plotting a graph of values for  $v_{mix(non-ideal)}$  against  $\omega_s$  gives an equation representation for the real or experimental determined specific volumes as a function of solvent mass fraction/concentration. This equation is given as:

$$v_{mix(non-ideal)} = 0.378\omega_s + 1.001$$

Note that the values plotted are for sample 1 and sample 2 of bitumen. Organizing the equation in the same form as **Equation 4-17**;

$$\frac{1}{\rho_{mix(non-ideal)}} = v_{mix(non-ideal)} = 1.379\omega_s - 1.001\omega_s + 1.001 \quad 4-19$$

where non-ideal butane solvent specific volume  $v_s$  is 1.379 cm<sup>3</sup>/g. Non-ideal bitumen specific volume  $v_b$  is 1.001 cm<sup>3</sup>/g for the given experimental temperature (30.25°C). Note that the  $v_s$  and  $v_b$  non-ideal terms are arbitrary terms only used for comparison sake to ideal conditions.

James (2009) differentiates **Equation 4-17** with respect to  $\omega_s$  while trying to simplify the expression for mass average velocity ( $V^m$ ) in **Equation 2-48**. This differentiation follows;

$$\frac{\partial \left( \frac{1}{\rho_{mix}} \right)}{\partial \omega_s} = \frac{\partial (v_{mix})}{\partial \omega_s} = \frac{\partial}{\partial \omega_s} \left[ \frac{1}{v_s \omega_s - v_b \omega_s + v_b} \right]^{-1}$$

$$\frac{\partial \left( \frac{1}{\rho_{mix}} \right)}{\partial \omega_s} = \frac{\partial (v_{mix})}{\partial \omega_s} = \frac{\partial}{\partial \omega_s} (v_s^* \omega_s + v_b^* - v_b^* \omega_s)$$

$$\frac{\partial \left( \frac{1}{\rho_{mix}} \right)}{\partial \omega_s} = \frac{\partial (v_{mix})}{\partial \omega_s} = (v_s^* - v_b^*)$$

Therefore differentiating the ideal specific volume expression in **Equation 4-18** gives;

$$\frac{\partial \left( \frac{1}{\rho_{mix(ideal)}} \right)}{\partial \omega_s} = \frac{\partial (v_{mix(ideal)})}{\partial \omega_s} = [1.459 - 1.001] \quad 4-20$$

And differentiating the non-ideal specific volume expression in **Equation 4-19** gives;

$$\frac{\partial \left( \frac{1}{\rho_{mix(non-ideal)}} \right)}{\partial \omega_s} = \frac{\partial (v_{mix(non-ideal)})}{\partial \omega_s} = [1.379 - 1.001] \quad 4-21$$

The differentiated non-ideal specific volume **Equation 4-21** can be re-expressed in terms of the differentiated ideal specific volume **Equation 4-20**:

$$\frac{\partial \left( \frac{1}{\rho_{mix(non-ideal)}} \right)}{\partial \omega_s} = \frac{\partial (v_{mix(non-ideal)})}{\partial \omega_s} = [0.947(1.459) - 1.001]$$

Hence in non-ideal form, the equation can be expressed as:

$$\frac{\partial \left( \frac{1}{\rho_{mix(non-ideal)}} \right)}{\partial \omega_s} = \frac{\partial (v_{mix(non-ideal)})}{\partial \omega_s} = [0.947v_s - v_b] \quad 4-22$$

The added coefficient is what is used to account for non-ideal mixing for the solvent continuity equations. The value of the coefficient will vary for different temperatures but it can be added straight into the solvent continuity equations in MATLAB to solve for diffusivity. **Equations 2-**

**56 and 2-60** both have the  $v_s$  term and the coefficient is put as above right beside them when calculating non-ideal mixing. **Table 4-5** gives a full list of non-ideal expressions for each experimental run.

Table 4-5 - Non-ideal mixing specific volume expressions

	Non-ideal mixing specific volume expressions ( $\text{cm}^3/\text{g}$ )
27.00°C	$0.992v_s - v_b$
30.25°C	$0.947v_s - v_b$
33.50°C	$0.900v_s - v_b$
36.75°C	$0.849v_s - v_b$
40.00°C	$0.824v_s - v_b$

**Figure 4-4** shows a plot of all the above non-ideal mixing coefficients against temperature.

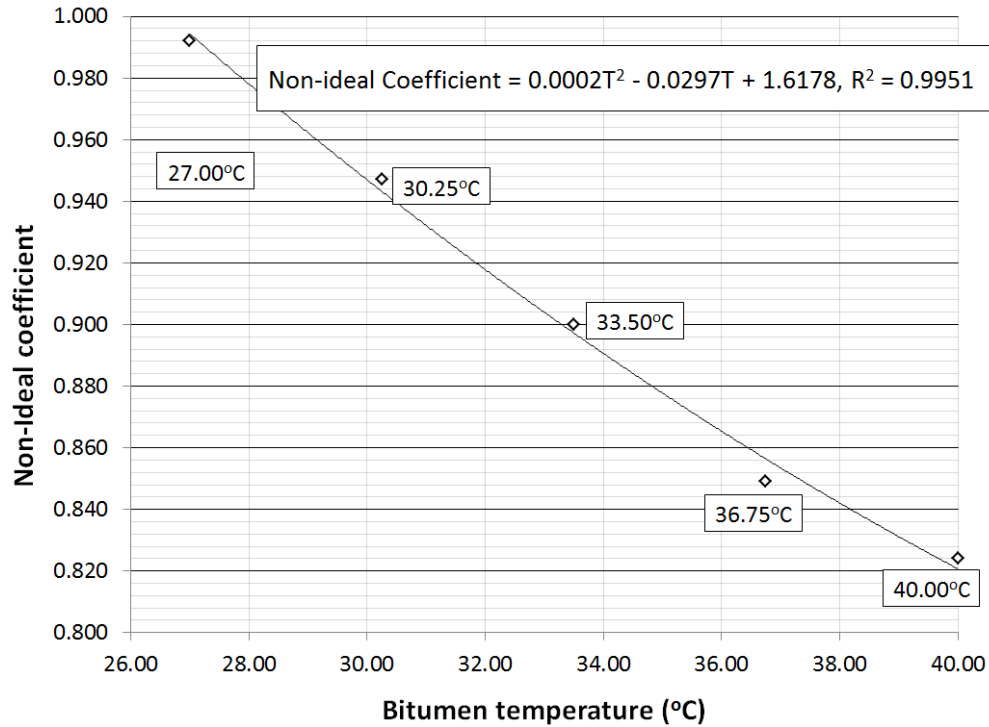


Figure 4-4 - Non-ideal mixing coefficients at varying temperatures

The non-ideal mixing coefficient values reduce with increasing temperature and a second order polynomial equation best describes its relationship to temperature.

$$\text{Coefficient} = 0.0002T^2 - 0.0297T + 1.6178$$

The  $R^2$  value is 0.9951 which signifies a good fit. By making the non-ideal mixing coefficient one (1), we can find the temperature at which the effects of non-ideal mixing are zero.

$$1 = 0.00027T^2 - 0.0297T + 1.6178$$

$$0 = 0.0002T^2 - 0.0297T + 1.6178 - 1$$

$$0 = 0.0002T^2 - 0.0297T + 0.6178$$

$$T = \mathbf{25.02^\circ C}$$

The significance of this temperature is that it is close to standard temperature (25.00°C). All literature says that the effects of non-ideal mixing are at minimum at standard temperature conditions. Note that the non-ideality coefficient used here is analogous to the binary interaction parameter (BIP) discussed in **Section 2.4**. The BIP is used to account for non-ideality when hydrocarbons mix. BIP is zero at ideal mixing conditions while the non-ideality coefficient used in this work is 1 at ideal mixing conditions. BIP deviates from zero as non-ideal mixing becomes more significant while the coefficient in this work deviates from 1 as non-ideal mixing becomes significant.

### **4.3.3. Butane solvent solubility in bitumen**

Another condition at the bitumen-solvent vapor interface is that the interfacial concentration ( $\omega_s^{n+1}$ ) is assumed to have reached equilibrium immediately after times greater than zero. The concentration at the interface is assumed to be the solubility ( $\omega_s^*$ ) of solvent in bitumen at the temperature of the bitumen and the vapor pressure of the solvent.

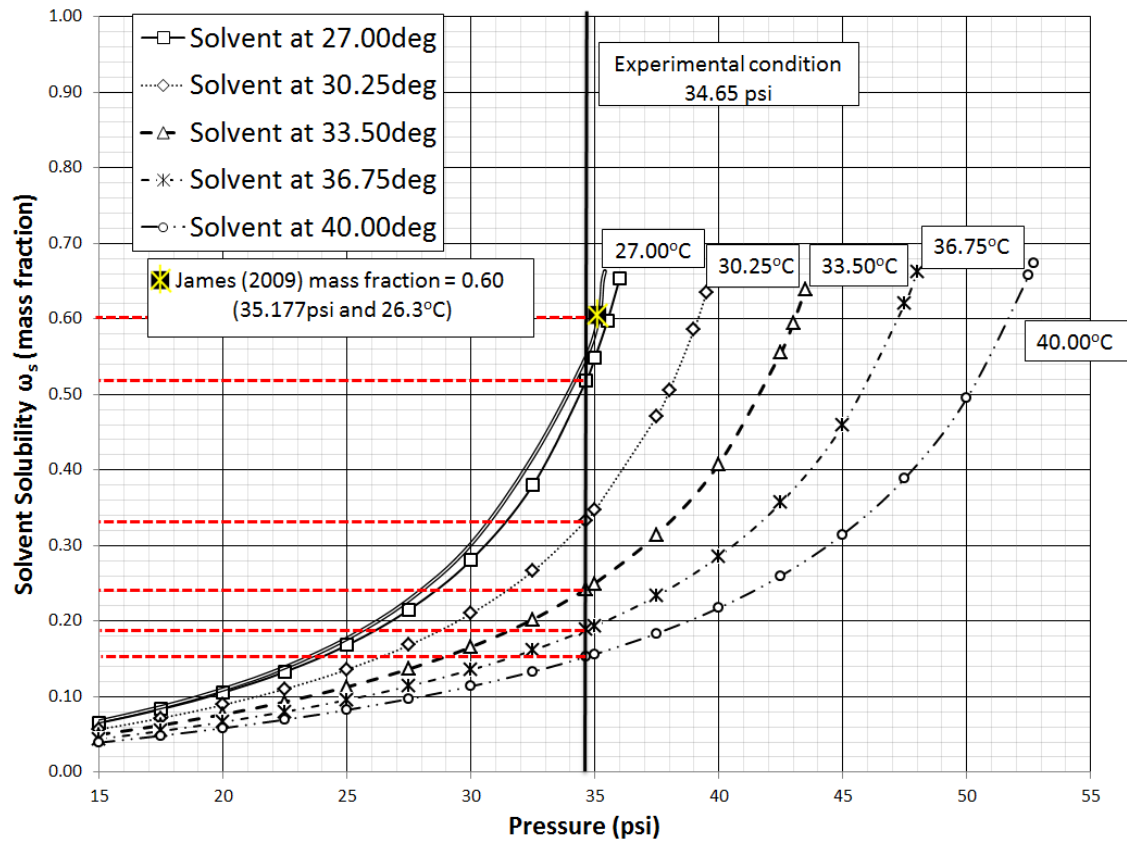


Figure 4-5 - Solvent solubility at varying experimental conditions

The solubility limit was estimated using the Peng-Robinson equation of state (PR EOS) in PVTsim. An assay for Athabasca bitumen closely approximating the bitumen used was entered in PVTsim and the solubility of n-butane in the bitumen was found at 34.65 psi and varying experimental temperatures as shown in **Figure 4-5**. **Figure 4-5** also shows the solvent conditions used by James (2009). James (2009) conditions led to higher butane solvent solubility due to the lower bitumen temperature (26.3°C) and higher butane vapor pressure (35.177psi). **Table 4-6** shows a full list of all solubility values used

Table 4-6 - Full list of solubility limits at different conditions

	<b>Bitumen temperature (°C)</b>	<b>Butane vapor pressure (psi)</b>	<b>Solubility limit (<math>\omega_s^*</math>)</b>
<b>This work</b>	27.00°C	34.650	0.52
	30.25°C	34.650	0.33
	33.50°C	34.650	0.24
	36.75°C	34.650	0.19
	40.00°C	34.650	0.15
<b>James (2009)</b>	26.30°C	35.177	0.60

## 4.4. Using Design Expert

The purpose of this section is the review technique used to incorporate Design Expert (DE) into the experiment. DE is analytical software that can be used to find possible trends and correlations in experimental data. If for instance the experimental values for 28.50°C were needed, normally the experiment would then have to be run at 28.50°C. However, every experimental run takes three days and time/cost constraints might prevent one from performing the experiment. Design Expert (DE) is able to take current experimental data and find a correlation that can be used to find experimental values for any temperature in the given range.

The nature of the experimental parameters creates problems when finding a full-fledged diffusivity prediction model in DE. Below is a list of the main experimental parameters and their inter-dependencies.

1. Diffusivity =  $f(\text{concentration, temperature, solubility, viscosity})$
2. Viscosity =  $f(\text{concentration, temperature})$
3. Solubility or maximum concentration =  $f(\text{temperature})$

The two independent variables are concentration and temperature however, maximum concentration (solubility limit  $\omega^*$ ) is dependent on temperature as well. Trying to analyze the

data in DE to give a model that can predict diffusivity function is beyond the capabilities of the software we have available. Hence the best course of action was not to create a diffusivity model directly in DE, but to create 3 models that can predict key parameters need to compute diffusivity functions in MATLAB.

This experiment has one main independent factor (temperature), at five different levels (27.00, 30.25, 33.50, 36.75 and 40.00°C) with 2 replicates. Given those conditions, the best design for the experiment is using a general factorial design. The three key parameters needed to compute diffusivity functions are;

- Slope of the Butane decrease (cm) vs. Square root time (SRT) ( $s^{0.5}$ ) (**Figure 5-3**)
- Slope of the Bitumen increase (cm) vs. Square root time (SRT) ( $s^{0.5}$ ) (**Figure 5-6**)
- Deviation from ideal mixing (coefficients from **Table 4-5**)

After each model is obtained, it is tested with a value within the experimental range (28.50°C). The experiment is re-run (28.50°C) and all experimental values are compared to predicted values from the DE model. If a good fit is obtained, the model can be used to acquire the above stated output data and subsequently compute diffusivity functions for any temperature value within the given temperature range (27.00°C to 40.00°C).

After analysis was performed in DE, the following models were obtained to compute the output data:

$$\begin{aligned}
 (\text{Butane slope})^{0.5} &= 0.379 - [0.013 \times T] + [5.093 \times (10^{-5}) \times T^2] && 4-23 \\
 &+ [1.728 \times (10^{-6}) \times T^3]
 \end{aligned}$$

$$(\text{Bitumen slope})^{0.5} = 0.123 - [4.955 \times (10^{-3}) \times T] + [5.543 \times (10^{-5}) \times T^2] \quad 4-24$$

$$(Ideality)^3 = -2.13554 + [0.36648 \times T] - [0.013102 \times T^2] + [1.40606 \times (10^{-4}) \times T^3] \quad 4-25$$

where  $T$  is the input temperature ( $^{\circ}\text{C}$ ) within the experimental range ( $27.00^{\circ}\text{C} - 40.00^{\circ}\text{C}$ ) and is used to compute all the output values. The output data *butane slope* is used to obtain butane solvent decrease over time, *bitumen slope* is used to obtain bitumen solvent increase over time and *ideality* is used with the help of ideal mixing densities to obtain non-ideal mixing density. The aforementioned data, along with solubility values at the given temperature and starting bitumen mass, is input into the Matlab code and used to compute diffusivity functions and subsequent diffusion values.

## 5) DISCUSSION OF RESULTS

The purpose of this section is to perform a complete analysis and discussion of the experimental results obtained. Please note that experimental values for butane sample 1 and 2 are plotted together to give an average for every computed value. The same applies for experimental values for bitumen sample 1 and 2.

### 5.1. Butane solvent height changes as a function of time

**Figure 5-1** shows a graph of butane height decrease over time at varying temperatures. The highest bitumen temperature (40.00°C) corresponds to the lowest diffusion of butane, while the lowest bitumen temperature (27.00°C) corresponds to the highest diffusion of butane. Given butane temperature is constant for all the runs (24.00°C), the vapor pressure of butane is constant and the solubility of butane in bitumen is strictly dependent on the bitumen temperature. We find that the solubility decreases with increasing temperature, the trend makes sense as more butane dissolves in bitumen at lower temperatures compared to higher, leading to a greater reduction in butane height at lower temperatures.

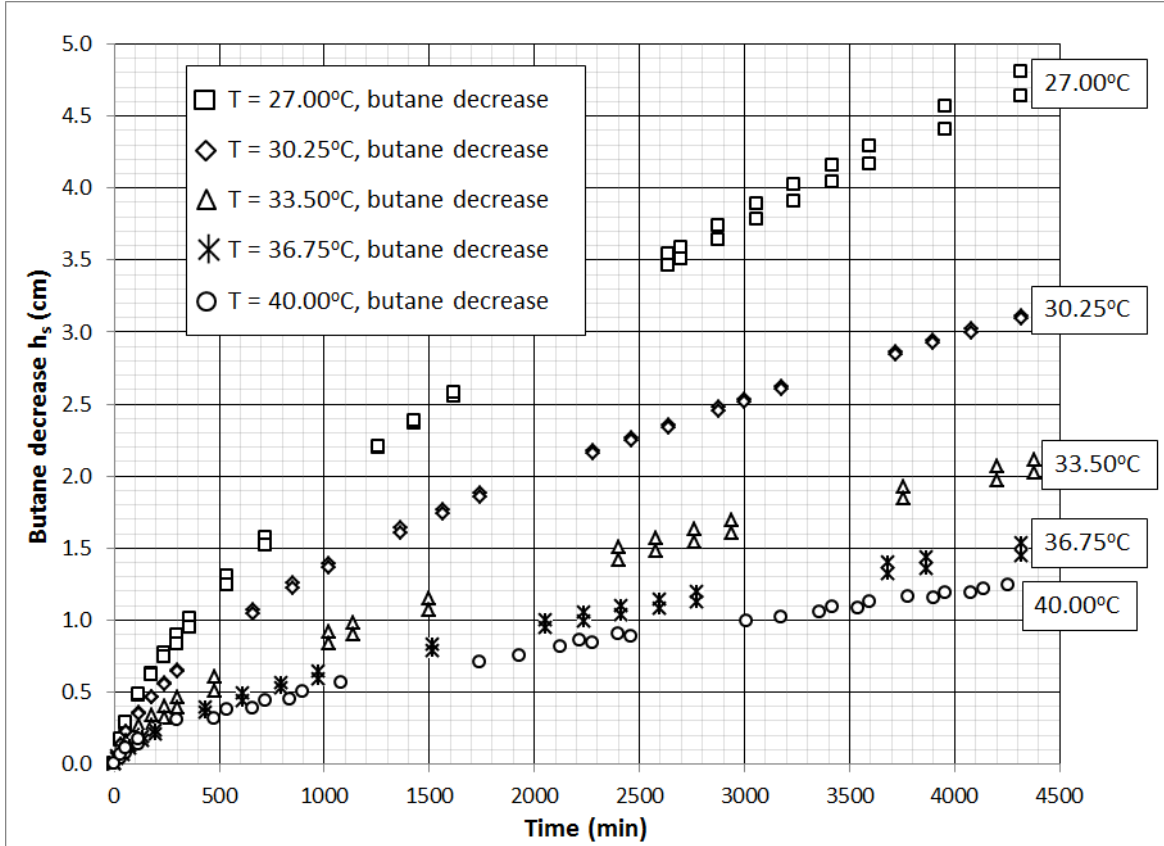


Figure 5-1- Butane height decrease vs. time (all temperatures)

As determined by James (2009), there is a linear relationship between the change in butane height and the square root of time ( $s^{0.5}$ ). The butane height decrease vs. square root time (SRT) graph shown in **Figure 5-2** follows a similar trend. The slopes of the straight trendline graphs are much greater for lower temperatures than for higher temperatures. This is expected given solubility (directly proportional to magnitude of the slopes) is inversely proportional to temperature. **Figure 5-2** also clearly shows 2 straight line graphs drawn for each set of experimental temperatures. The dashed line shows the trendline being forced to pass through time  $t = 0$  while the other allows a time  $t \neq 0$  (a start time that best suits the graph). The  $R^2$  values (fit of the graph) is significantly lower when the trendline is forced to pass through time  $t = 0$  compared to when the trendline is not ( $t \neq 0$ ). The highlighted part of **Table 5-1** further confirms this.

This occurs due to the delicacy of determining the start time of the experiment when creating a vacuum. As stated in **Section 3.2.4** it is extremely hard to pin point the start time of the experiment after creating a vacuum due to the sensitivity of the differential pressure transmitter. Ideally, experiments start when the system pressure (system pressure transmitter) side reaches 2.36 atm (34.65 psi) and plateaus while both the butane 2-way and bitumen 3-way valves are open. However, the sensitivity of the pressure transmitter leads to fluctuations in these values of  $\pm 0.002$  atm. The point at which the differential pressure transmitter value is 0.00 atm could also be used as a reference point for the start of the experiment. However, its value also fluctuates due to the transmitter sensitivity. The bottom line is it takes time to equilibrate the system due to the combination of the pressure transmitter sensitivity and pressure differences from the butane to bitumen side.

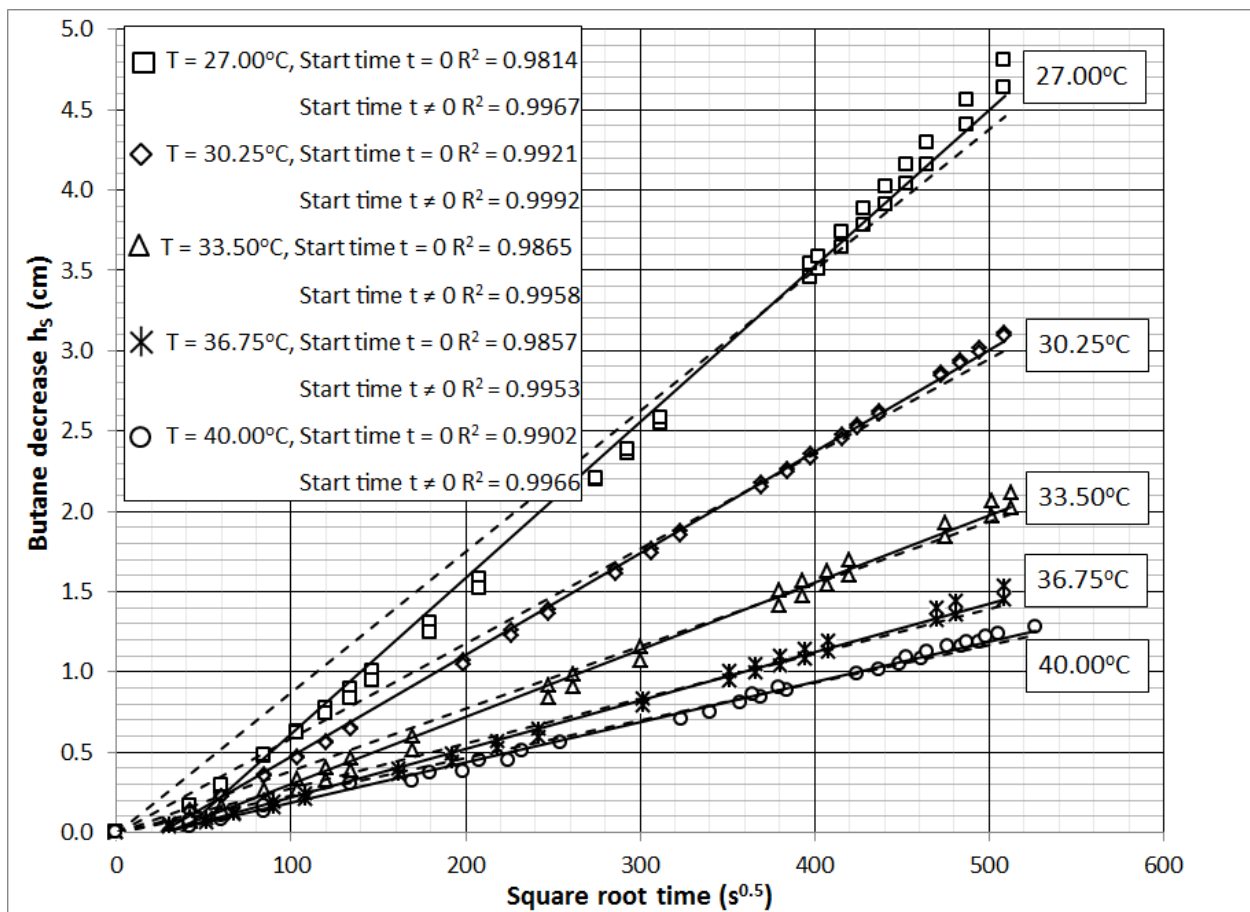


Figure 5-2 - Butane solvent decrease vs SRT for  $t = 0$  and  $t \neq 0$

Table 5-1 - Tabulated values for butane solvent decrease data ( $t = 0$  and  $t \neq 0$ )

Butane height decrease vs. SRT graph data						
Temperature (°C)	Experimental Start time (min)	Slope of graph (cm/s <sup>0.5</sup> )	R <sup>2</sup>	y intercept	x intercept	Start time (min)
27.00	t = 0	0.0088	0.9814	0.0000	0.00	0.00
	t ≠ 0	0.0097	0.9967	-0.3517	36.26	21.91
30.25	t = 0	0.0059	0.9921	0.0000	0.00	0.00
	t ≠ 0	0.0063	0.9992	-0.1604	25.46	10.80
33.50	t = 0	0.0039	0.9865	0.0000	0.00	0.00
	t ≠ 0	0.0042	0.9958	-0.1131	26.93	12.09
36.75	t = 0	0.0028	0.9857	0.0000	0.00	0.00
	t ≠ 0	0.0030	0.9953	-0.0824	27.46	12.56
40.00	t = 0	0.0023	0.9902	0.0000	0.00	0.00
	t ≠ 0	0.0025	0.9966	-0.0617	24.66	10.14

The start times for  $t \neq 0$  were re-calculated according **APPENDIX G (butane)** such that they start at time  $t = 0$ . The new graph with all trendlines passing through zero is shown in **Figure 5-3**. This data is what is used to eventually calculate diffusivity.

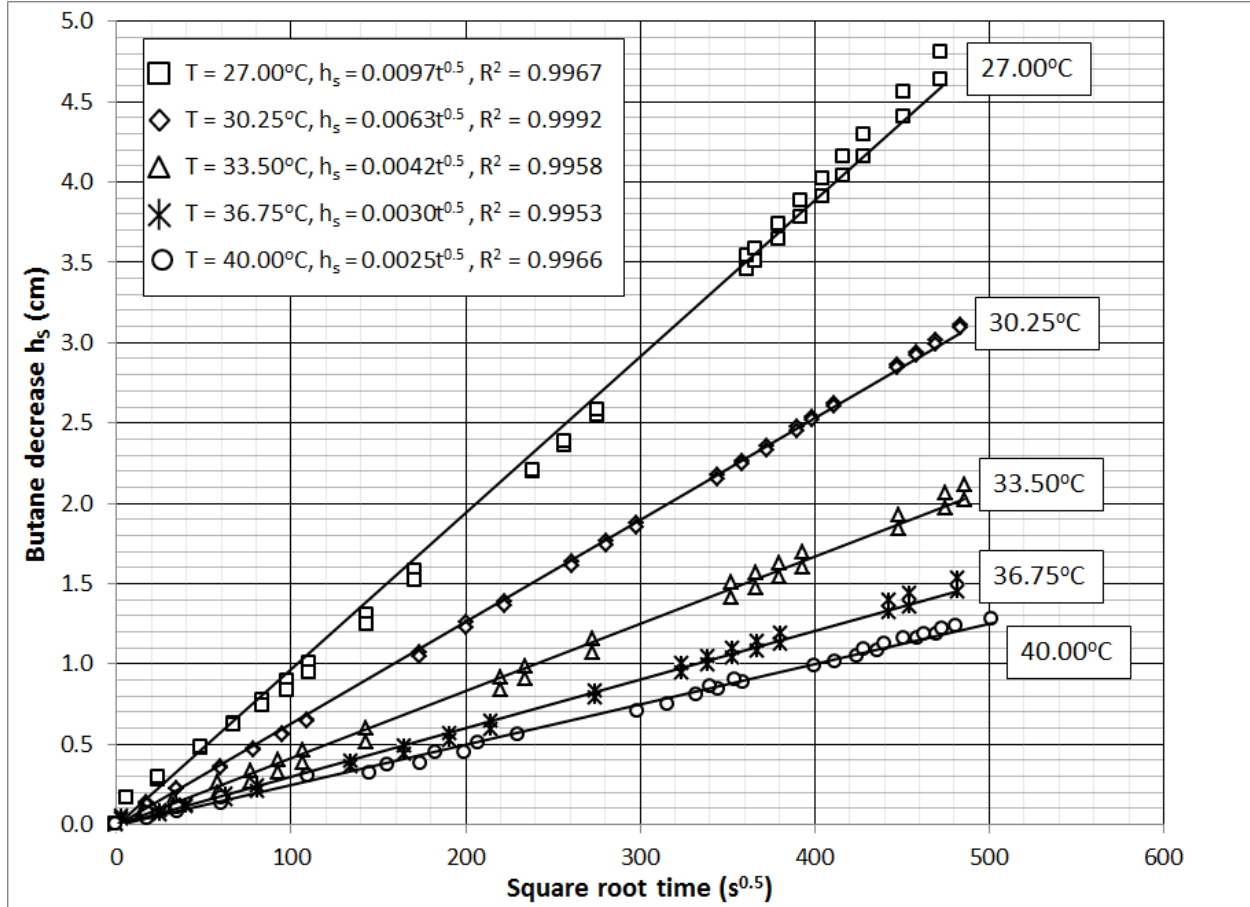


Figure 5-3 - Butane height decrease vs. SRT (all temperatures)

**Figure 5-3** shows all the new trendlines at various temperatures going through zero. It should be noted that all  $R^2$  values are greater than 0.99 thereby showing a great fit for the data. These slopes are also later used in Design Expert (DE) software (**Section 5.5**) for further analysis.

## 5.2. Bitumen height changes as a function of time

**Figure 5-4** shows a graph of bitumen increase (swelling) over time at varying temperatures. The highest bitumen temperature (40°C) sees the lowest diffusion of butane into bitumen (lowest swelling of bitumen), while the lowest bitumen temperature (27°C) sees the highest diffusion of butane into bitumen (highest swelling of bitumen). As stated earlier, the solubility of butane in bitumen is strictly dependent on bitumen temperature given butane vapor pressure is fixed (34.65

psi) for all experimental runs. This solubility decreases with increasing temperature. Hence, lower temperatures lead to more swelling (bitumen increase) compared to higher temperatures.

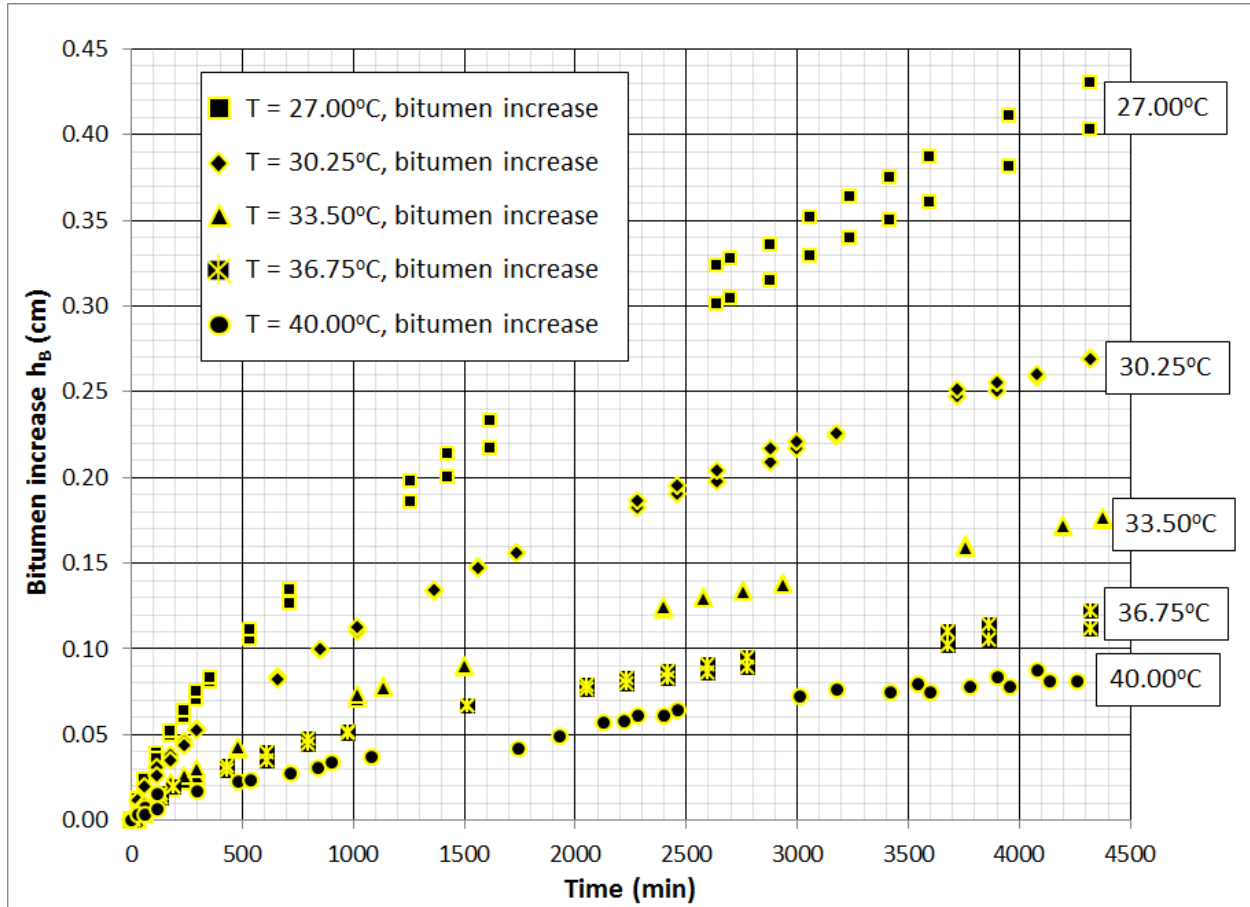


Figure 5-4- Bitumen height increase vs. time (all temperatures)

**Figure 5-5** illustrates the changes in bitumen height in relation to Square root time (SRT). The slopes of the straight trendline graphs are much greater for lower temperatures than for higher temperatures. **Figure 5-5** also clearly shows two straight line graphs drawn for each set of experimental temperatures. The dashed line shows the trendline being forced to pass through time  $t = 0$  while the other allows a time  $t \neq 0$  (a start time that best suits the graph). Just like the butane changes in **Section 5.1** the  $R^2$  values (fit of the graph) is significantly lower when the trendline is forced to pass through time  $t = 0$  compared to when the trendline is not ( $t \neq 0$ ). The

highlighted part of **Table 5-2** further confirms this. This occurs for the same reason stated in **Section 5.1** (fluctuation of pressure differential values due to its high sensitivity).

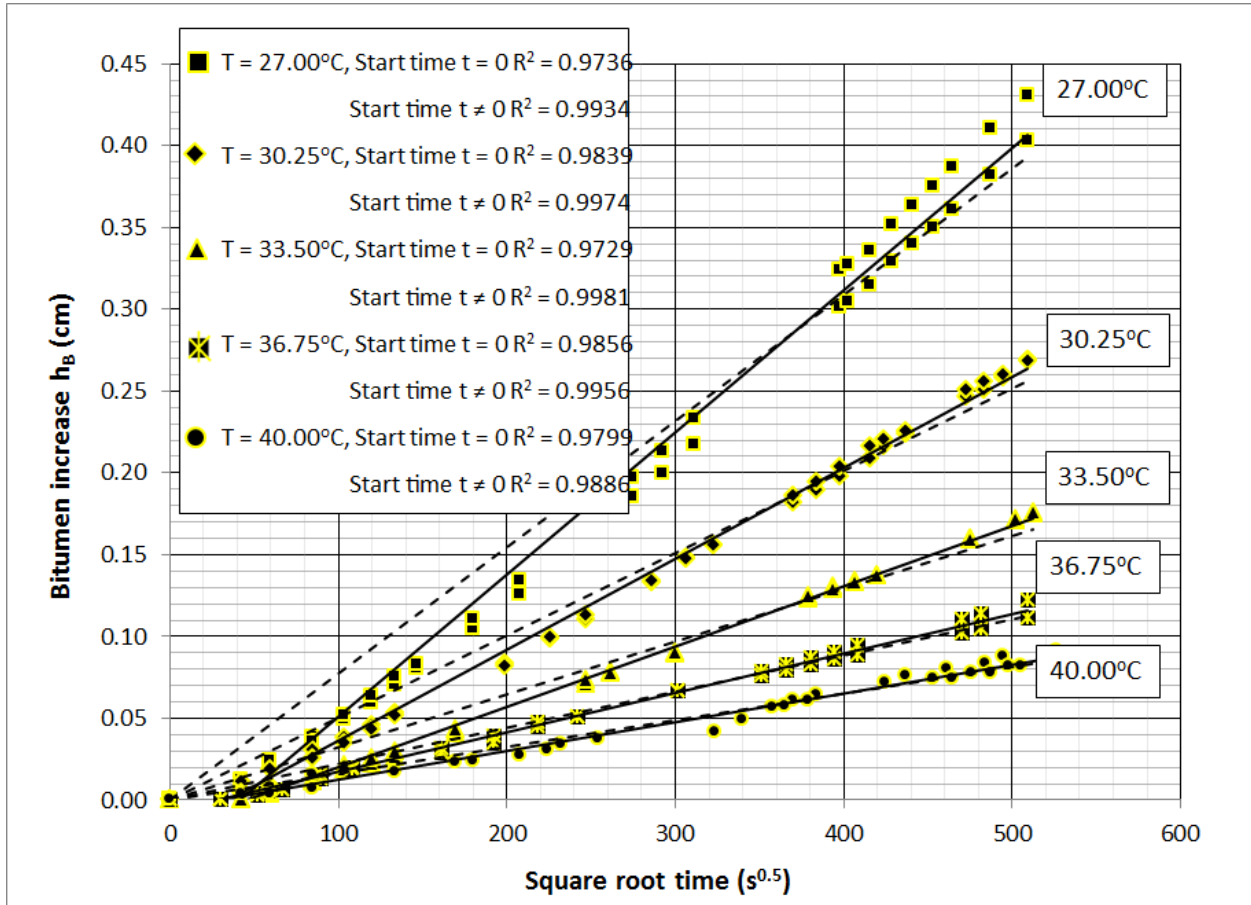


Figure 5-5 - Bitumen increase vs SRT for t = 0 and t ≠ 0

Table 5-2 - Tabulated values for bitumen increase data ( $t = 0$  and  $t \neq 0$ )

Bitumen height increase vs. SRT graph data						
Temperature (°C)	Experimental Start time (min)	Slope of graph (cm/s <sup>0.5</sup> )	R <sup>2</sup>	y intercept	x intercept	Start time (min)
27.00	t = 0	0.00077	0.9736	0.0000	0.00	0.00
	t ≠ 0	0.00087	0.9934	-0.0360	41.33	28.47
30.25	t = 0	0.00050	0.9839	0.0000	0.00	0.00
	t ≠ 0	0.00056	0.9974	-0.0194	34.61	19.96
33.50	t = 0	0.00032	0.9727	0.0000	0.00	0.00
	t ≠ 0	0.00037	0.9981	-0.0167	45.14	33.95
36.75	t = 0	0.00022	0.9857	0.0000	0.00	0.00
	t ≠ 0	0.00024	0.9956	-0.0066	27.50	12.60
40.00	t = 0	0.00016	0.9799	0.0000	0.00	0.00
	t ≠ 0	0.00018	0.9886	-0.0051	28.33	13.38

The start times for  $t \neq 0$  were re-calculated according **APPENDIX G (bitumen)** such that they start at time  $t = 0$ . The new graph with all trendlines passing through zero is shown in **Figure 5-6**. This data is what is used to eventually calculate diffusivity.

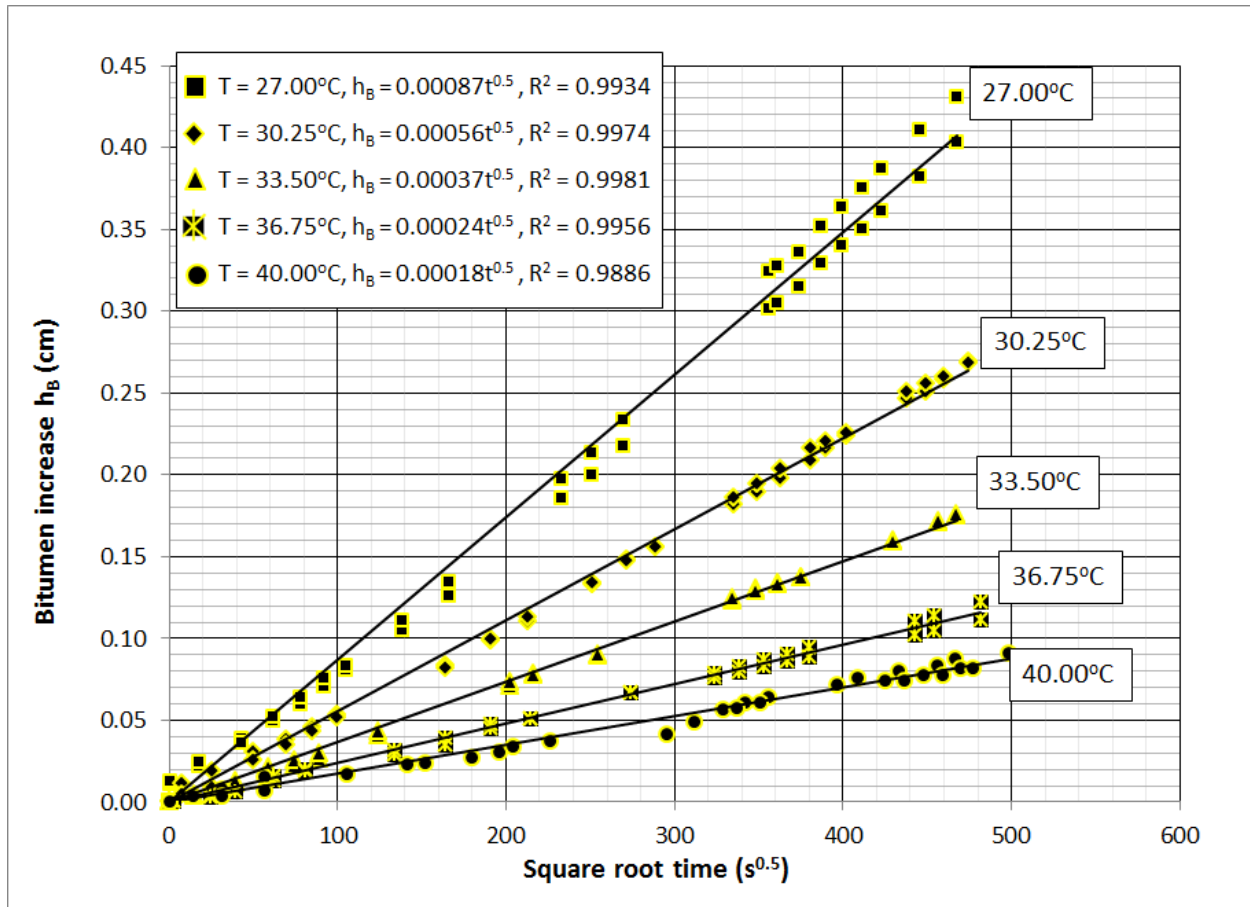


Figure 5-6 - Bitumen height increase vs. SRT (all temperatures)

**Figure 5-6** shows all the new trendlines at various temperatures going through zero. It should be noted that all  $R^2$  values are greater than 0.99 (apart from at 40.00°C) thereby showing a great fit for the data. These slopes are also later used in Design Expert (DE) software (**Section 5.5**) for further analysis.

James (2009) performed this experiment at a butane temperature of 24.9°C and a bitumen temperature of 26.3°C. The experimental run for butane (24°C) in bitumen (27°C) is the closest match to James (2009) conditions. James (2009) obtained a slope of 0.01602 cm/s<sup>0.5</sup> for the butane decrease vs SRT graph and a slope of 0.00244 cm/s<sup>0.5</sup> for the bitumen increase vs SRT graph. Those values are higher than the ones obtained for the 27°C condition for this thesis (0.00971 cm/s<sup>0.5</sup> for butane and 0.00087 cm/s<sup>0.5</sup> for bitumen). This is illustrated in **Table 5-3**.

The lower values in this experiment can be explained as James (2009) operating conditions ensuring higher solubility of butane in bitumen (higher butane vapor pressure and lower bitumen temperature). The raw purity of the butane solvent James (2009) used was 99.5% while the purity used in this work was 99%. Individually these three reasons (higher butane vapor pressure, lower bitumen temperature and higher butane purity) would not be enough to lead to significant differences in solubility limits but combined they are more than enough to do so. As example, in PVTsim keeping all parameters constant (butane vapor pressure at 35.177 psi and purity) but changing bitumen temperature from 26.3°C to 27°C decreases the solubility from 0.60 to 0.56 mass fraction. The combined effects of all parameters lead to greater solubility limit differences.

Table 5-3 - SRT graph slope comparisons between James (2009) and this work

	Temperature Conditions	Butane vapour pressure (psi)	Butane solubility limit $\omega_s^*$	Slope of Butane SRT graph (cm/s <sup>0.5</sup> )	Slope of Bitumen SRT graph (cm/s <sup>0.5</sup> )
James (2009)	24.9°C butane and 26.3°C bitumen	35.177	0.60	0.01602	0.00244
This work	24.0°C butane and 27.0°C bitumen	34.650	0.52	0.00971	0.00087

### 5.3. Ideal & non-ideal mixing density results

The calculations in **Section 4.1** and **APPENDIX D** outline how ideal and non-ideal mixing density values are compiled for this experiment. **Figure 5-7** shows a graph of density vs. time at various temperatures for ideal mixing and non-ideal scenarios (based on pressure transmitter readings). As the experiment progresses, butane diffuse into the bitumen, diluting it and hence reducing the density of the bitumen/butane mixture. The highest bitumen temperature (40.00°C) corresponds to the lowest value of density decrease, while the lowest bitumen temperature (27.00°C) corresponds to the highest value of density decrease. As stated earlier, lower bitumen temperatures give higher butane solubility's and hence more dilution of butane in the bitumen. Also the difference between ideal and non-ideal density values increase as temperature increases from 27.00°C to 40.00°C. This is because the effects of ideality also increase with temperature rises in this bitumen-butane system. This is discussed further in later sections.

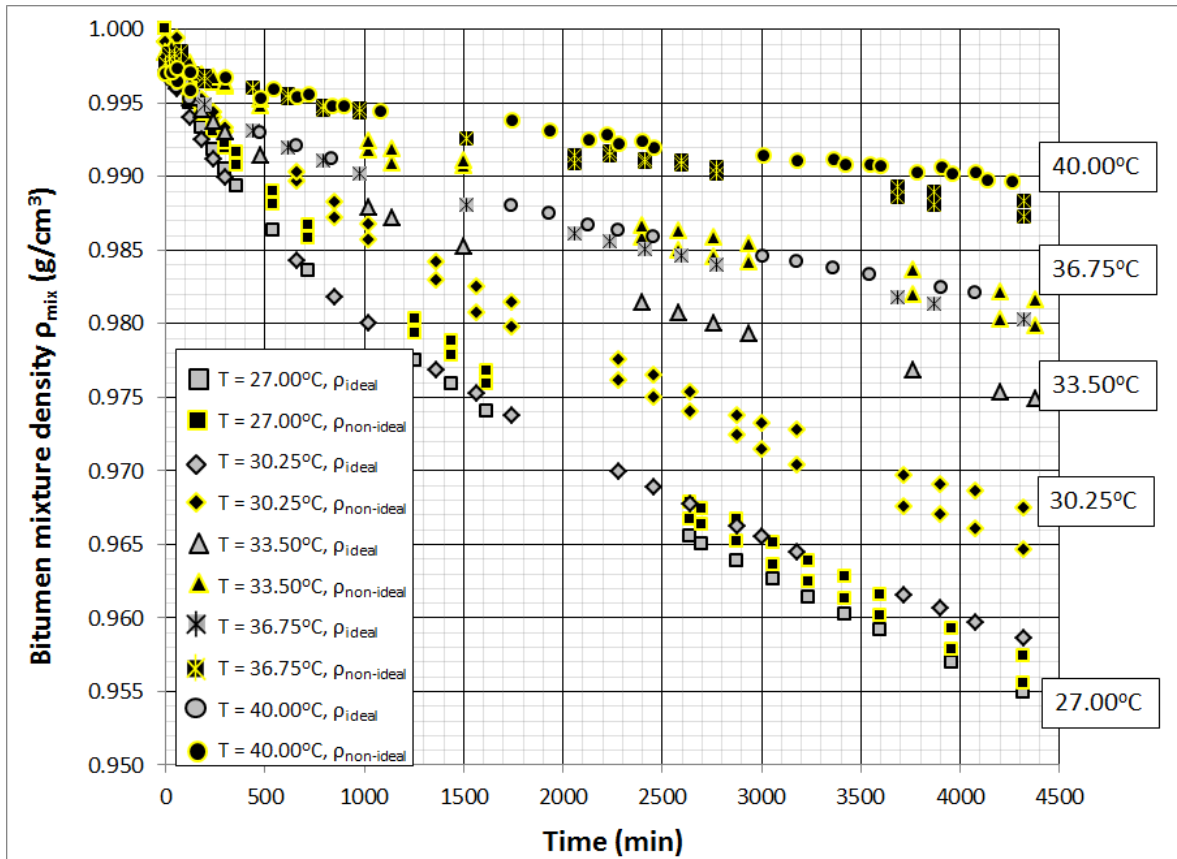


Figure 5-7 - Mixture densities vs. time (all temperatures)

Figures 5-8 to 5-12 show graphs of bitumen/butane mixture density vs. mass fraction of solvent dissolved in bitumen for all temperatures. All graphs are plotted on the same scale for comparison purposes. The black filled markers represent experimental data and subsequently have the  $\rho_{\text{mix (non-ideal)}}$  line drawn through them. The gray filled markers represent calculated ideal densities and subsequently have the  $\rho_{\text{mix (ideal)}}$  line drawn through them. The  $R^2$  value for the  $\rho_{\text{mix (ideal)}}$  line is always one (1), while this value varies for the  $\rho_{\text{mix (non-ideal)}}$  line depending on fit. As expected, the the 40.00°C graph shows the lowest reduction in mixture density over the duration of the experiment. It also shows the lowest increase in solvent mass fraction due to the low solubility at that temperature. The 27.00°C graph conversely shows the highest reduction in mixture density over the duration of the experiment. It also shows the highest increase in solvent mass fraction due to the high solubility at that temperature. All non-ideal linear ( $\rho_{\text{mix (non-ideal)}}$  line) graphs show a good fit with experimental data.

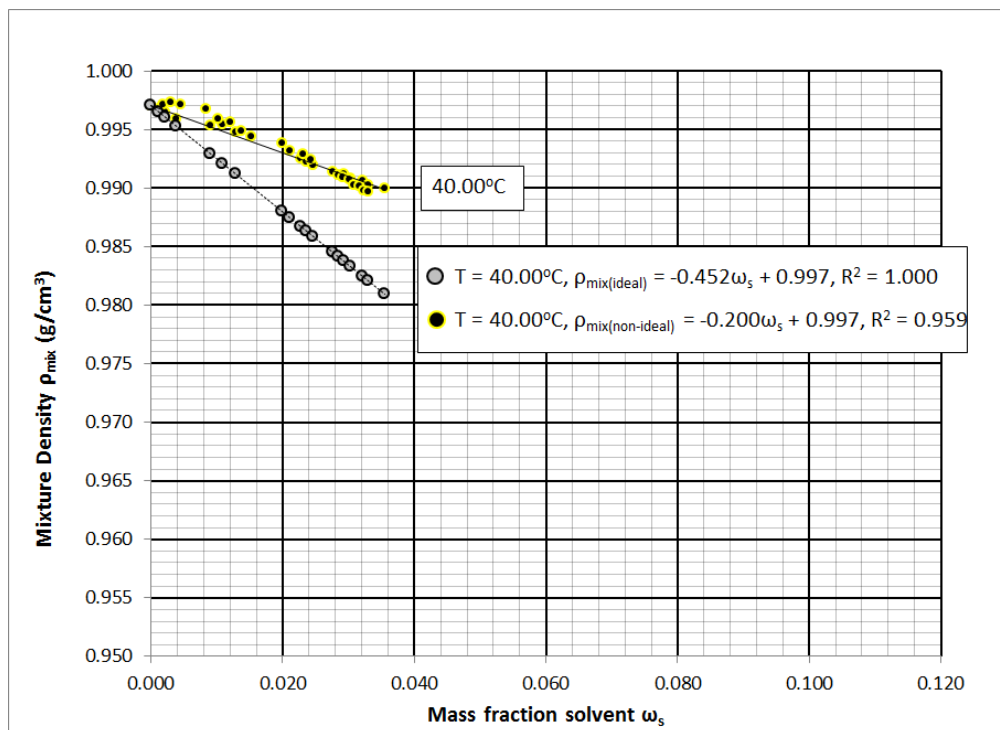


Figure 5-8 - Mixture density vs. solvent mass fraction (40.00°C)

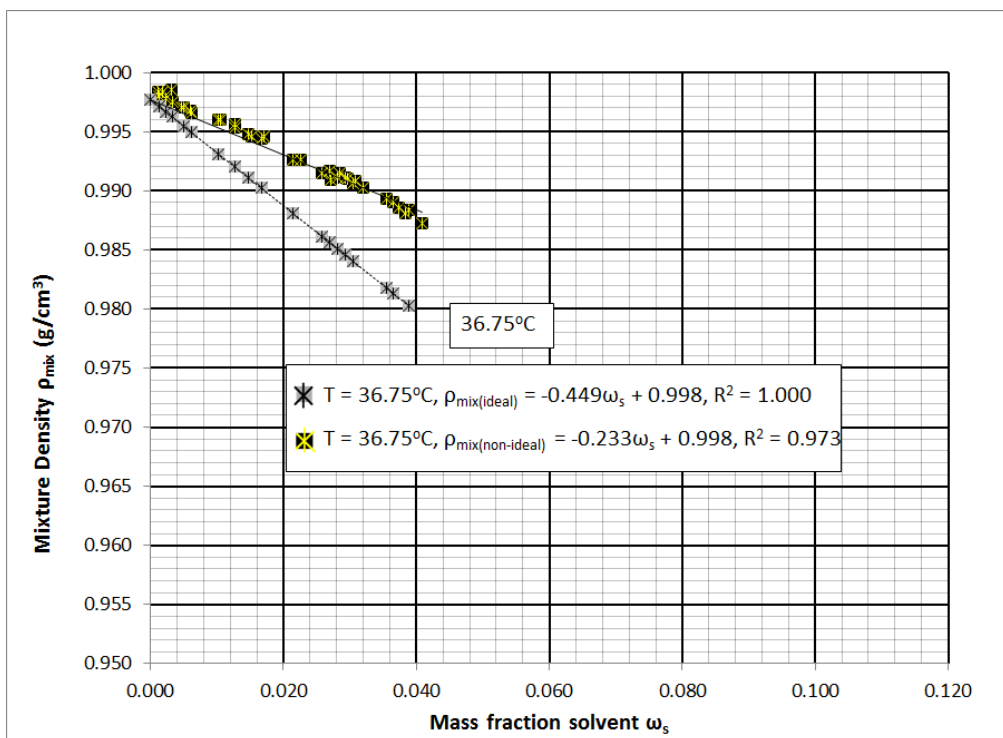


Figure 5-9 - Mixture density vs. solvent mass fraction (36.75°C)

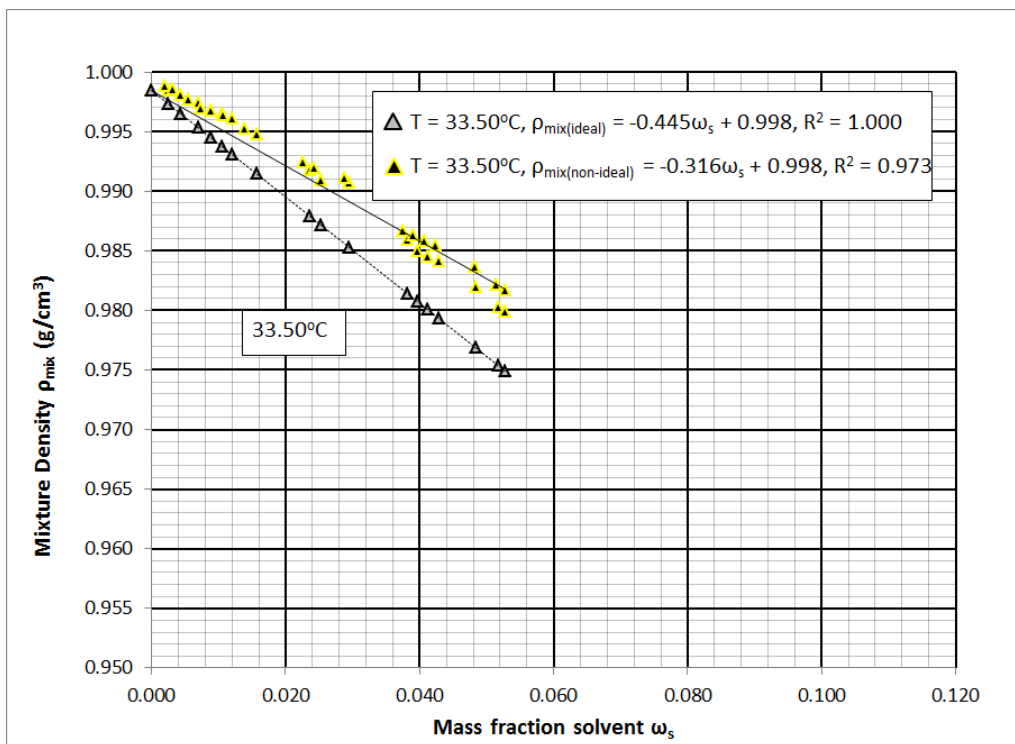


Figure 5-10 - Mixture density vs. solvent mass fraction (33.50°C)

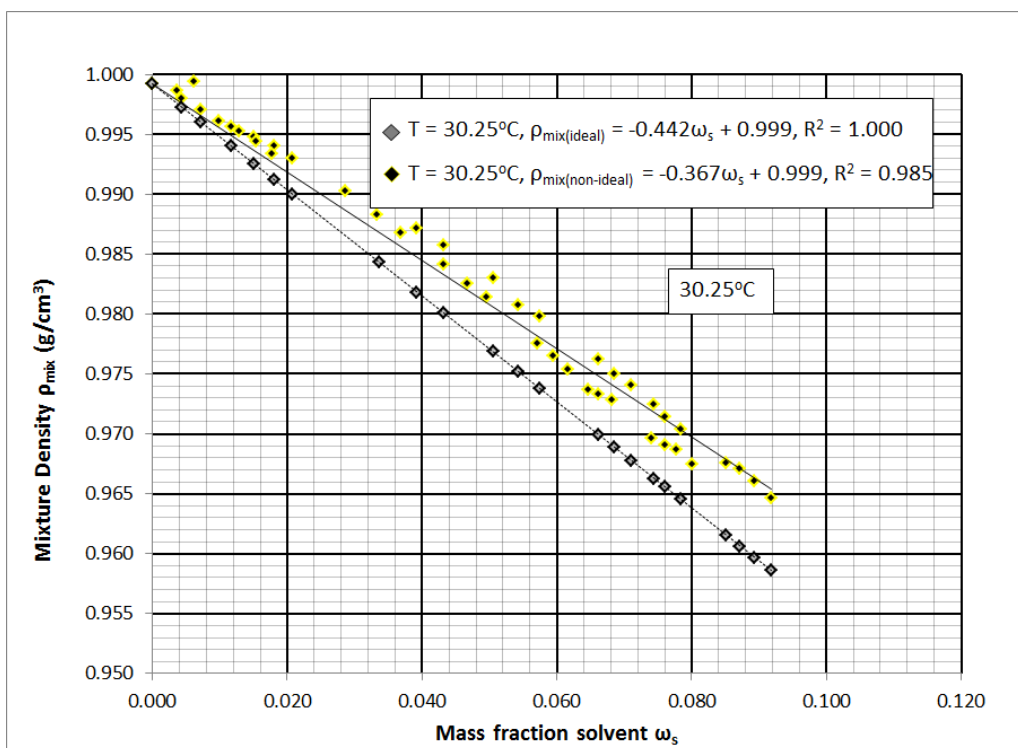


Figure 5-11 - Mixture density vs. solvent mass fraction (30.25°C)

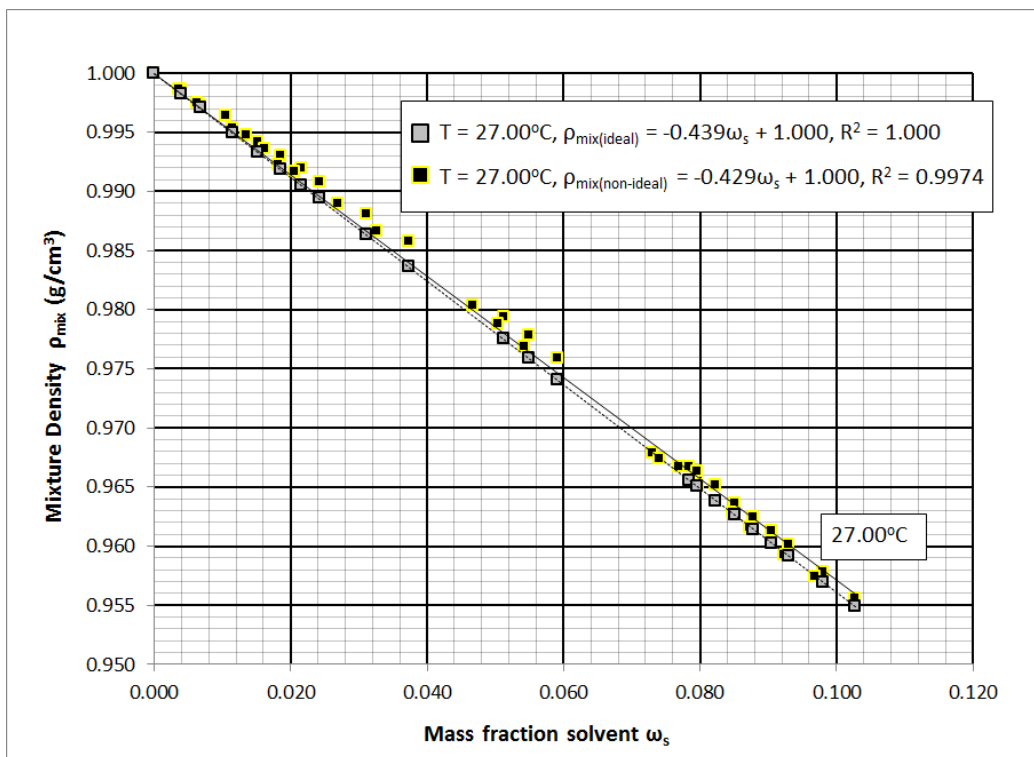


Figure 5-12- Mixture density vs. solvent mass fraction (27.00°C)

These graphs are consistent with **Figure 2-27** from Etminan *et al.* (2011). Assuming ideal mixing conditions over-estimates the real density reduction occurring (non-ideal mixing) between the bitumen and butane solvent. **Table 5-4** shows all experimental density results (ideal and non-ideal) obtained.

Table 5-4 - Ideal and non-ideal mixing density results

	<b>Ideal results</b>	<b>Non- ideal results</b>
<b>27.00°C</b>	$\rho_{\text{mix(ideal)}} = -0.439\omega_s + 1.000$	$\rho_{\text{mix(non-ideal)}} = -0.429\omega_s + 1.000$
<b>30.25°C</b>	$\rho_{\text{mix(ideal)}} = -0.442\omega_s + 0.999$	$\rho_{\text{mix(non-ideal)}} = -0.367\omega_s + 0.999$
<b>33.50°C</b>	$\rho_{\text{mix(ideal)}} = -0.445\omega_s + 0.998$	$\rho_{\text{mix(non-ideal)}} = -0.316\omega_s + 0.998$
<b>36.75°C</b>	$\rho_{\text{mix(ideal)}} = -0.449\omega_s + 0.998$	$\rho_{\text{mix(non-ideal)}} = -0.233\omega_s + 0.998$
<b>40.00°C</b>	$\rho_{\text{mix(ideal)}} = -0.452\omega_s + 0.997$	$\rho_{\text{mix(non-ideal)}} = -0.200\omega_s + 0.997$

At 27.00°C, the non-ideal mixing density equations are similar to the ideal equation (slopes of the graph). However as temperature increases the non-ideal slope deviates from the ideal slope with 40.00°C having the largest deviation. This deviation was previously illustrated in **Table 4-5** as the ideality coefficient deviated further from one as temperature increased. **Table 5-5** serves as a reminder of the coefficient values. This mirrors how the difference between ideal and non-ideal mixing conditions increases as temperature increases. The binary interaction parameter ( $k_{ij}$ ) from Peng-Robinson equation of state is a solid representation of mixing non-ideality (has a value of zero at ideal mixing conditions). The coefficient used in this thesis has a value of one at ideal mixing conditions. Deo *et al.* (1993) and Saryazdi *et al.* (2013) found that the binary interaction parameter (BIP) increases as temperature increases, hence the fact that the coefficient in this thesis deviates from one as temperature increases is in agreement with literature.

Table 5-5 - Non-ideal mixing specific volume expressions

	<b>Non-ideal mixing specific volume expressions (cm<sup>3</sup>/g)</b>
<b>27.00°C</b>	<b>0.992</b> $v_s - v_b$
<b>30.25°C</b>	<b>0.947</b> $v_s - v_b$
<b>33.50°C</b>	<b>0.900</b> $v_s - v_b$
<b>36.75°C</b>	<b>0.849</b> $v_s - v_b$
<b>40.00°C</b>	<b>0.824</b> $v_s - v_b$

## 5.4. Diffusivity results

This section reviews all the diffusivity results obtained from the experiments conducted. The method used to obtain the diffusivity functions is explained in **Section 2.2.3** in the literature review of James (2009) work and **Section 4.3**. Note that for each temperature, ideal and non-ideal diffusivity functions will be computed via Matlab. To obtain non-ideal diffusivity functions, the coefficients in the **Table 5-5** above will be incorporated into the diffusivity equations while for ideal diffusivity, the coefficients are not incorporated.

### 5.4.1. Diffusivity functions

The results are shown in **Table 5-6**. It should be noted that diffusivity functions are mathematical expressions for diffusion as functions of another term (mass fraction  $\omega_s$ ). Diffusion values are the numerical values obtained when ( $\omega_s$ ) is substituted into the diffusivity function. There is a clear trend of decreasing diffusion values (ideal and non-ideal) with increasing temperature. This is due to a reduction in solvent solubility in bitumen with increasing temperature, leading to less dilution solvent in bitumen as temperatures increases. However, at equal mass fractions ( $\omega_s$ ), the non-ideal diffusivity functions yield greater diffusion values than the ideal diffusivity functions. This means that assuming ideal mixing conditions under-estimates the magnitude of diffusion that occurs. This is because the occurrence of diffusion is driven by concentration gradient. However due to the over-estimation of density reduction in ideal mixing scenario, that concentration gradient is less for ideal mixing scenario compared to non-ideal mixing. Also, the difference between ideal and non-ideal diffusivity functions increases with increasing temperature (further discussed in **Section 5.4.3** in **Table 5-7**). This follows the previously observed pattern in **Section 5.3** of deviations from ideality increasing with higher temperatures.

Table 5-6 - Diffusivity functions for all temperatures (ideal and non-ideal)

	<b>Ideal Diffusivity <math>\times 10^6</math> (cm<sup>2</sup>/s)</b>	<b>Non-ideal Diffusivity <math>\times 10^6</math> (cm<sup>2</sup>/s)</b>
<b>27.00 °C</b>	$1.623\omega_s + 0.306$	$1.620\omega_s + 0.312$
<b>30.25 °C</b>	$0.843\omega_s + 0.799$	$0.884\omega_s + 0.851$
<b>33.50 °C</b>	$0.647\omega_s + 0.626$	$0.734\omega_s + 0.715$
<b>36.75 °C</b>	$0.456\omega_s + 0.423$	$0.546\omega_s + 0.532$
<b>40.00 °C</b>	$0.367\omega_s + 0.366$	$0.491\omega_s + 0.481$

James (2009) found diffusivity of butane solvent (24.90°C) in bitumen (26.30°C) to be **(4.780 $\omega_s$  + 4.910)  $\times 10^{-6}$  cm<sup>2</sup>/s** when assuming ideal mixing conditions. The experimental run for butane (24.00°C) in bitumen (27.00°C) is the closest match to James (2009) conditions and gives an ideal diffusivity of **(1.623 $\omega_s$  + 0.306)  $\times 10^{-6}$  cm<sup>2</sup>/s** and non-ideal diffusivity of **(1.620 $\omega_s$  + 0.312)  $\times 10^{-6}$  cm<sup>2</sup>/s**. Functions in this work yield less diffusion values than James (2009)'s which makes

sense given James (2009) operating conditions ensure considerably higher solubility of butane in bitumen (higher butane partial pressure and lower bitumen temperature). This is further illustrated in **Section 4.3.3** by James (2009) having a butane solubility limit ( $\omega_s^*$ ) of 0.6 mass fraction while the highest solubility limit achieved in this work (27.00°C) was 0.52 mass fraction. **APPENDIX I** contains full details of the diffusivity function results (ideal/non-ideal).

## 5.4.2. Butane solvent mass fraction profile and bitumen density profile

As part of the Matlab code, a predicted mass fraction (butane solvent) and density (bitumen) profile is obtained. This profile is available for ideal and non-ideal scenarios for a; temperatures and will show how the given parameter (bitumen density or butane solvent mass fraction) will change in relation to the height of the full bitumen fluid at different times.

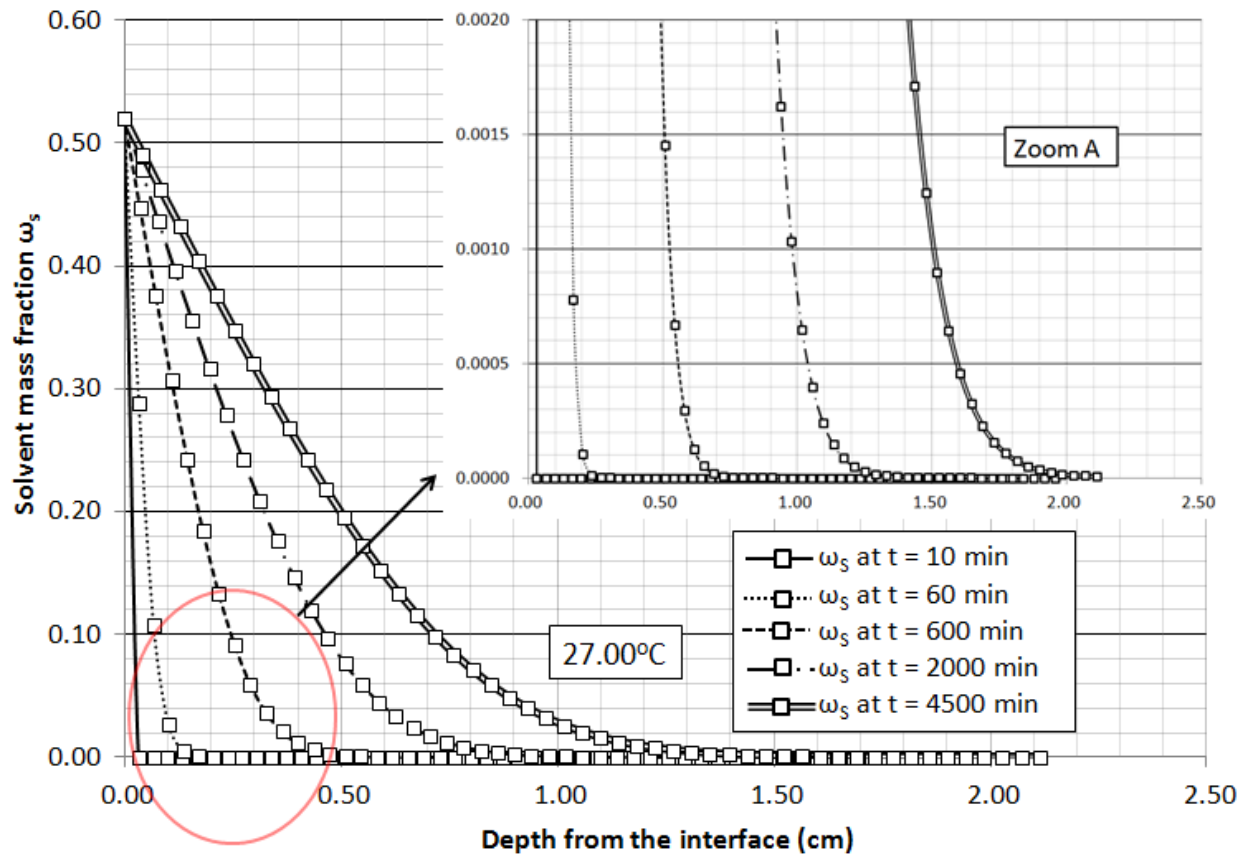


Figure 5-13 - Butane solvent mass fraction profile at 27.00°C (non-ideal)

**Figure 5-13** shows the predicted solvent mass fraction profiles for 27.00°C (non-ideal) at different times along with a magnified section of the graph. The figure clearly shows that the solvent mass fraction (concentration) at the bitumen solvent interface (depth from interface = 0) is kept at the solvent's solubility limit ( $\omega_s^*$ ) at the given temperature, i.e. 0.52 mass fractions. In the first 10 minutes, the solvent barely reaches 0.05 cm from the bitumen-butane solvent interface, hence the plateauing of the graph after 0.05 cm. At time 60 minutes, the butane solvent reaches a depth of 0.15 cm and the overall depth of the bitumen fluid increase due to swelling. As time passes, the mass fraction of butane solvent in the bitumen fluid keeps increasing as well as the overall bitumen fluid height due to swelling. It is not until after 4500 minutes that the butane solvent barely reaches the no-flux boundary at the bottom of the bitumen tube. This is clearly seen in the magnified part of the graph (Zoom A) as the 4500 minutes graph is the only one that does not completely plateau at solvent mass fraction of zero. **APPENDIX J** contains all the rest of the non-ideal solvent profiles at all temperatures.

**Figure 5-14** shows the bitumen density profiles for 27.00°C (non-ideal) at different times along with a magnified section of the graph (Zoom A). The significance of density 0.711 g/cm<sup>3</sup> at depth zero (bitumen-butane solvent interface) is the bitumen and butane solvent non-ideal mixture density ( $\rho_{\text{mix(non-ideal)}}$ ) when the butane solvent mass fraction is 0.52 (solubility limit  $\omega_s^*$ ). At 10 minutes, only the first 0.03 cm at the top of the bitumen fluid experiences density reduction. By 60 minutes, the first 0.24 cm at the top of the bitumen fluid experiences density reduction. As the experiment progresses, the density of the bitumen through the fluid keeps decreasing while the overall bitumen fluid height keeps increasing due to swelling of the bitumen. It is not until after 4500 minutes that there is an overall density reduction through the full bitumen fluid. This density reduction is from 1.0000 g/cm<sup>3</sup> to 0.9999 g/cm<sup>3</sup>. This is seen in the magnified version of the 4500 minutes graph (Zoom A) and these observations mirror the solvent mass fraction profile. **APPENDIX K** contains all the rest of the non-ideal density profiles at all temperatures.

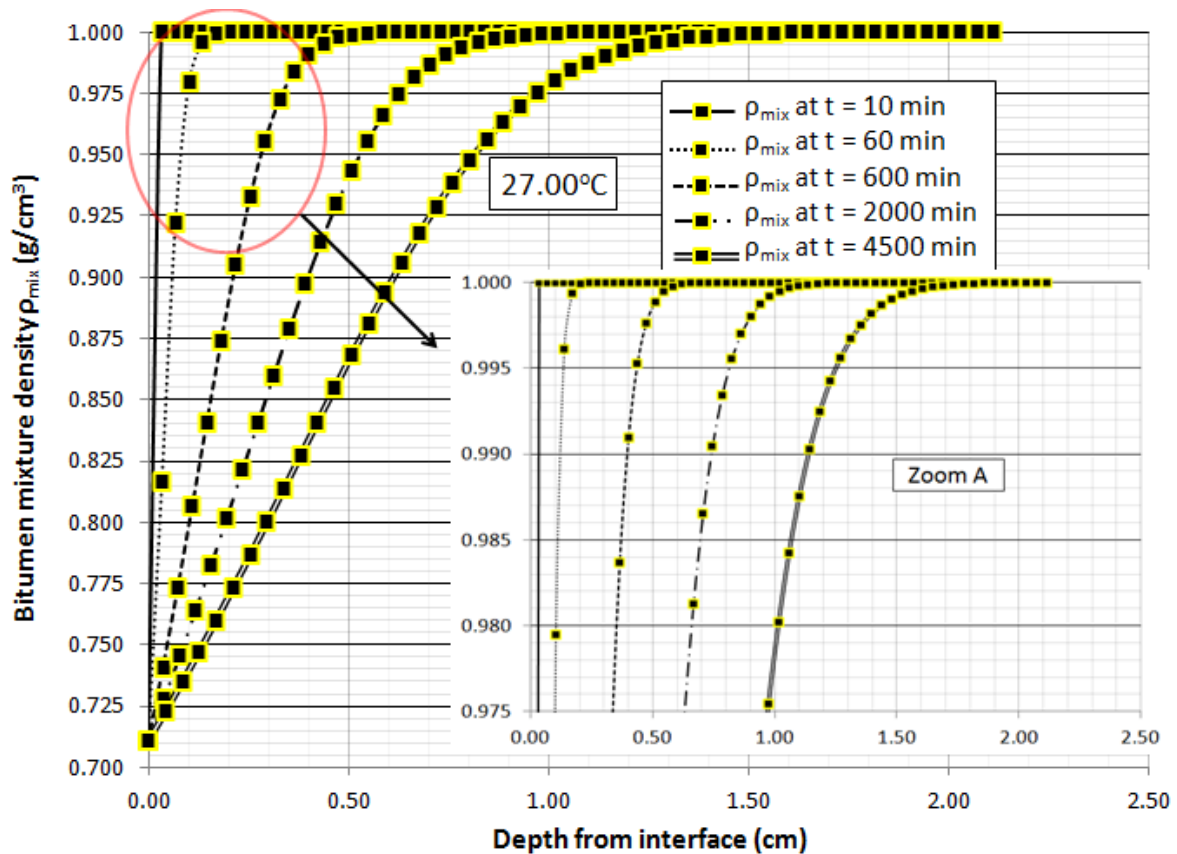


Figure 5-14 - Bitumen density profile at 27.00°C (non-ideal)

### 5.4.3. Ideal and non-ideal mixing comparisons

Figure 5-15, 5-16 and 5-17 below show graphs for ideal and non-ideal diffusivity functions at 27.00°C, 33.50°C and 40.00°C respectively. All graphs are plotted on the same scale for comparison for purposes. The difference between the graphs from temperature to temperature is explained with the help of upcoming **Table 5-7**.

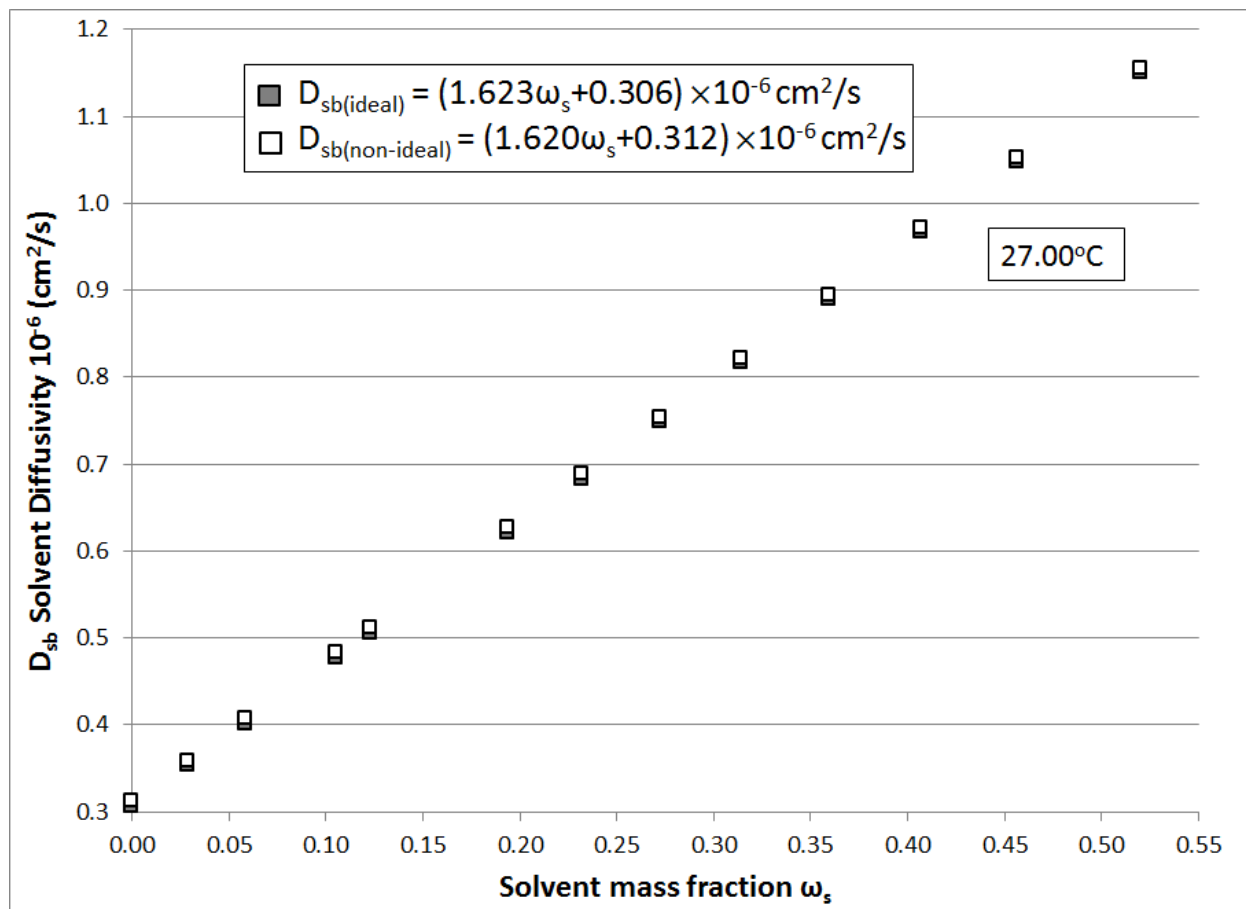


Figure 5-15- Solvent diffusivity functions at 27.00°C

The maximum solvent mass fraction (concentration) for each graph is dependent on the solubility limit ( $\omega_s^*$ ) for the given temperature. The solubility limits at the varying temperatures was tabulated in **Table 4-6**. Solvent mass fraction (concentration) in bitumen at a given temperature never exceeds the solubility limit. When the solvent mass fraction in the full bitumen fluid is at the given solubility limit, the full liquid is in equilibrium and diffusion stops. Reaching this equilibrium however is estimated to take approximately one to two weeks.

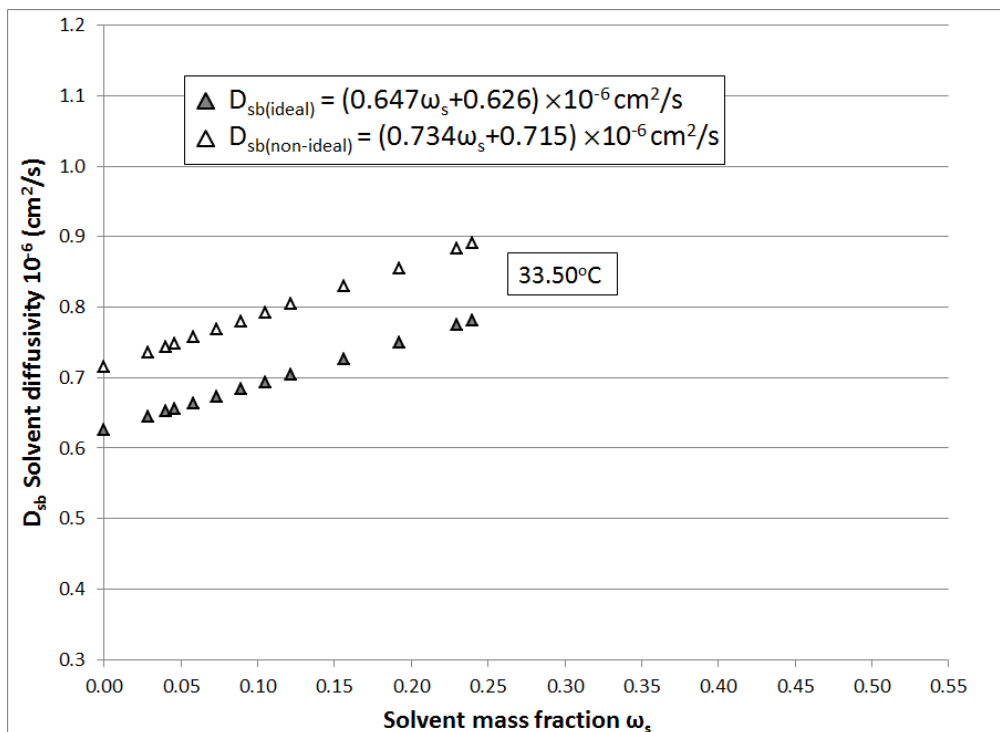


Figure 5-16 - Solvent diffusivity functions at 33.50°C

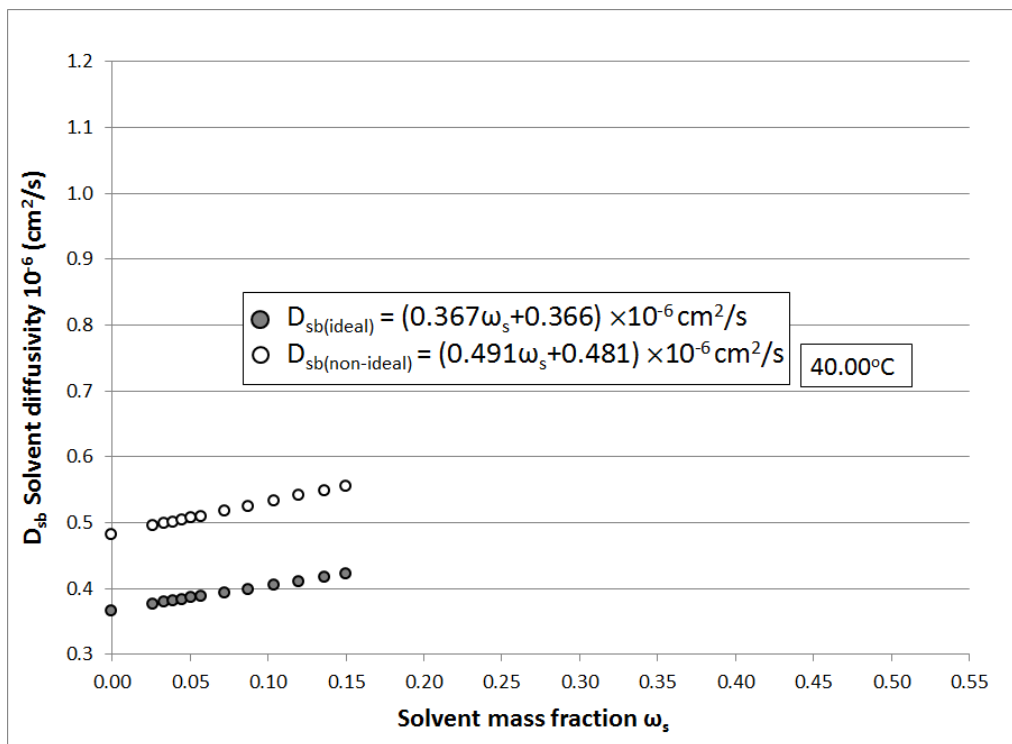


Figure 5-17 - Solvent diffusivity functions at 40.00°C

Aside from the non-ideal diffusion values being consistently greater than the ideal diffusion values, it is clear that as temperature increases, the difference between the ideal and non-ideal diffusion values becomes more significant. The highlighted parts of **Table 5-7** show the percentage difference between ideal and non-ideal diffusion values for all temperatures.

Table 5-7 - Table showing % difference between ideal and non-ideal diffusion values

Temperature (°C)	Ideal and Non-ideal diffusivity function comparisons			
		Diffusivity function	( $\omega_s = 0.15$ ) Diffusivity value $\times 10^6$ (cm <sup>2</sup> /s)	% diff from Ideal values
27.00	Ideal Diffusivity	$(1.623\omega_s+0.306)\times 10^{-6}$	0.549	
	Non-ideal Diffusivity	$(1.620\omega_s+0.312)\times 10^{-6}$	0.555	1.00
30.25	Ideal Diffusivity	$(0.843\omega_s+0.799)\times 10^{-6}$	0.925	
	Non-ideal Diffusivity	$(0.884\omega_s+0.851)\times 10^{-6}$	0.984	6.34
33.50	Ideal Diffusivity	$(0.647\omega_s+0.626)\times 10^{-6}$	0.723	
	Non-ideal Diffusivity	$(0.734\omega_s+0.715)\times 10^{-6}$	0.825	14.11
36.75	Ideal Diffusivity	$(0.456\omega_s+0.423)\times 10^{-6}$	0.491	
	Non-ideal Diffusivity	$(0.546\omega_s+0.532)\times 10^{-6}$	0.614	24.93
40.00	Ideal Diffusivity	$(0.367\omega_s+0.366)\times 10^{-6}$	0.421	
	Non-ideal Diffusivity	$(0.491\omega_s+0.481)\times 10^{-6}$	0.555	31.71

Using 27.00°C as an example, a butane solvent mass fraction  $\omega_s$  of 0.15 is selected for consistency. It is substituted into the ideal and non-ideal diffusivity functions as follows,

$$D_{sb(ideal)} = ((1.623 \times 0.15) + 0.306) \times 10^{-6} \times 10^6 = 0.5495 \text{ cm}^2/\text{s}$$

$$D_{sb(non-ideal)} = ((1.620 \times 0.15) + 0.312) \times 10^{-6} \times 10^6 = 0.5550 \text{ cm}^2/\text{s}$$

The percentage difference of non-ideal diffusivity value from the ideal diffusivity value is then found as,

$$\frac{|0.5495 - 0.5550|}{0.5495} \times 100 = 1.00\%$$

27.00°C has the lowest percentage difference (1.00%) while 40.00°C has the higher percentage difference (31.71%). This is due to the earlier explained deviation from ideality as temperature increases. This deviation from ideality is further illustrated in **Figure 5-18, 5-19** and **5-20**

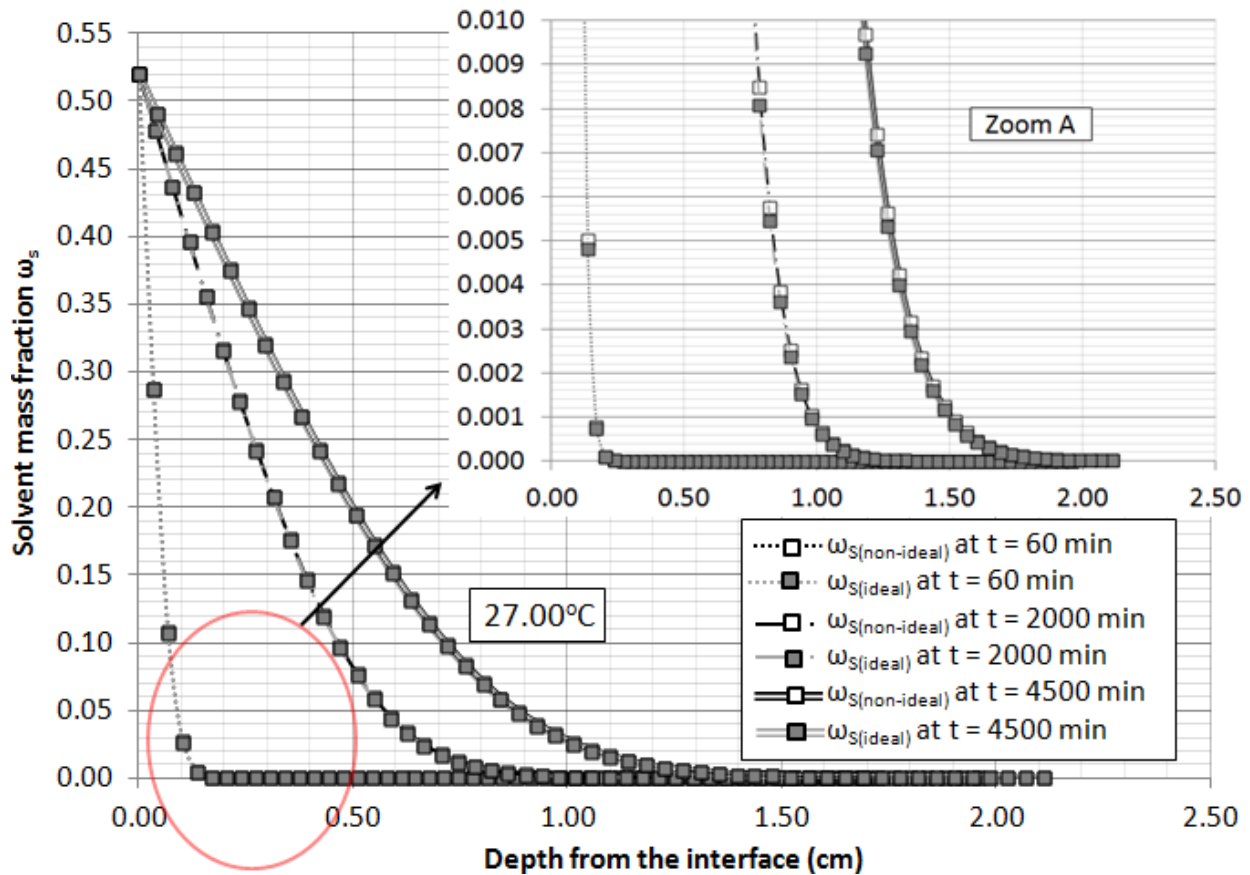


Figure 5-18 - Ideal and non-ideal butane solvent mass fraction profile at 27.00°C

**Figure 5-18** is butane solvent mass fraction/concentration profile at 27.00°C for ideal and non-ideal scenarios. In **Figure 5-18** the ideal and non-ideal profiles for the experimental times, predominantly overlap indicating similarities in their results. Looking at the zoomed profile (Zoom A) for **Figure 5-18**, the non-ideal solvent mass fraction is always greater than ideal. This is expected because the non-ideal diffusion is greater than ideal (more butane diffusing through

at every given stage). The same is true for **Figure 5-19** (ideal/non-ideal profile at 33.50°C) and **Figure 5-20** (ideal/non-ideal profile at 40.00°C). However the difference between the ideal and non-ideal profiles becomes more significant in both figures. All the profiles follow the same trend as the previously explained butane solvent concentration profile in **Section 5.4.2** in **Figure 5-13**.

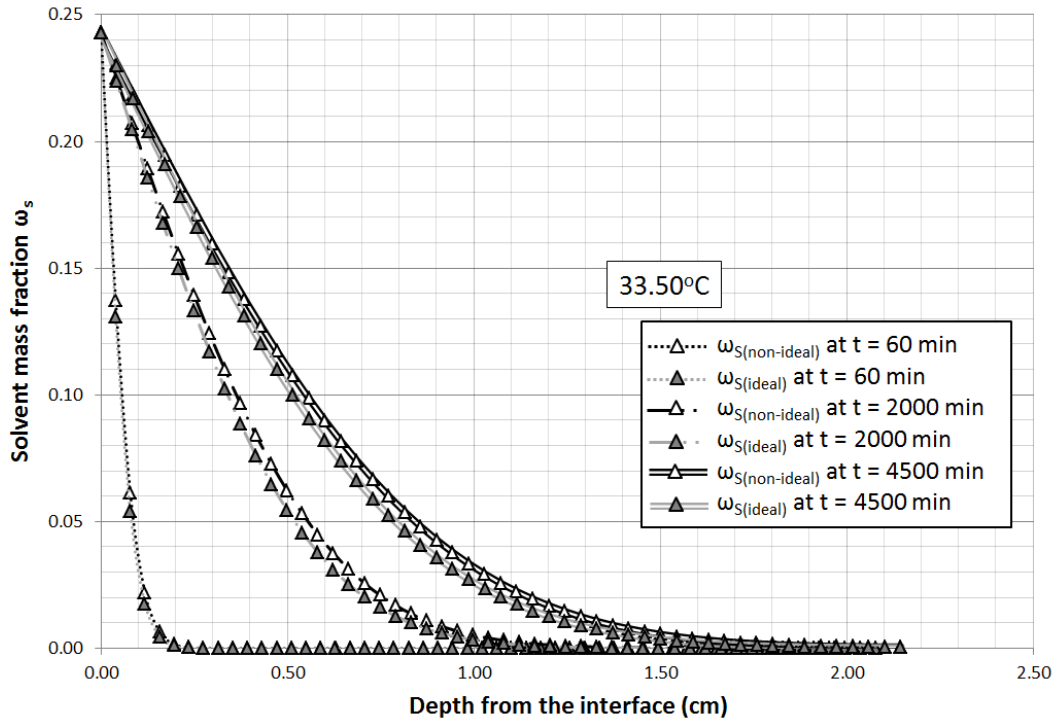


Figure 5-19 - Ideal and non-ideal butane solvent mass fraction profile at 33.50°C

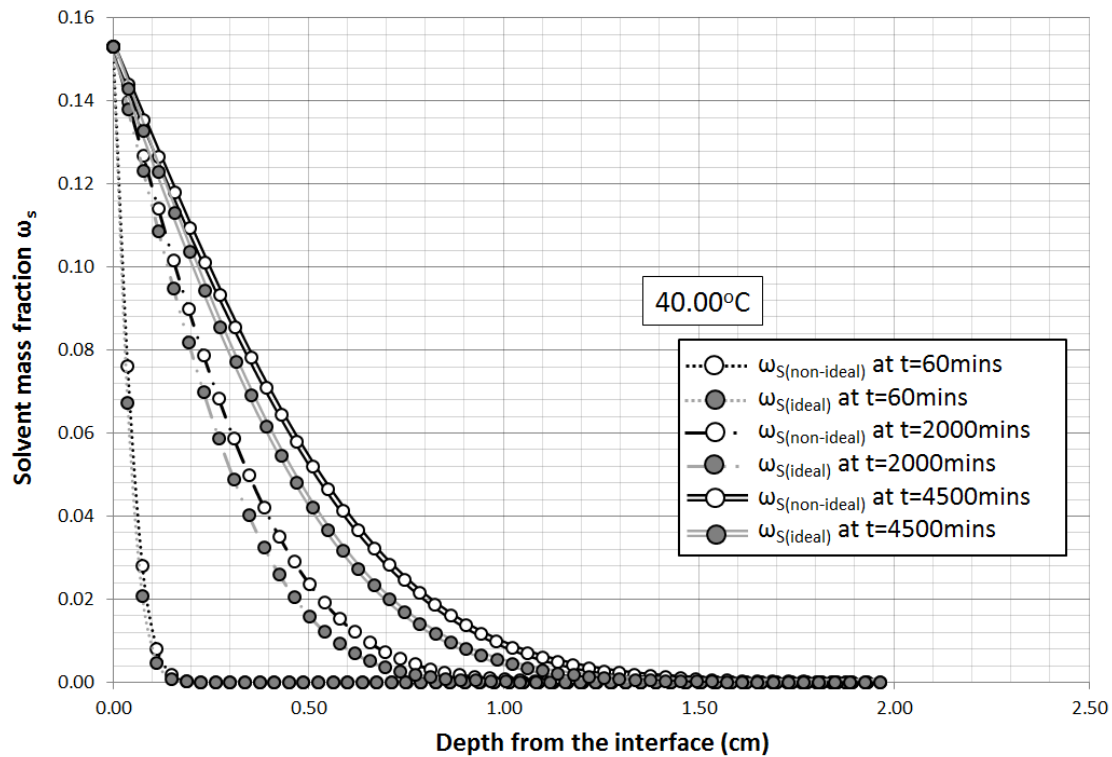


Figure 5-20 - Ideal and non-ideal butane solvent mass fraction profile at 40.00°C

As earlier stated in **Section 5.3**, assuming ideal mixing conditions over-estimates the density reduction that's occurs when butane solvent and bitumen mix. However, ideal mixing also underestimates diffusion values. **Figure 5-21** is the bitumen density profile at 27.00°C for ideal and non-ideal mixing scenario. At depth zero, the butane solvent mass fraction is at its highest value (solubility limit  $\omega_s^*$ ) and hence bitumen mixture density is at its lowest. As the depth increases, butane solvent mass fraction reduces and hence the bitumen density increases until it plateaus at the starting bitumen density (when solvent mass fraction is zero).

**Figure 5-21** shows that the mixing density of butane solvent and bitumen for ideal and non ideal mixing scenario gets as low as  $0.711 \text{ g/cm}^3$ . The ideal mixing density would be expected to be lower than the non-ideal but at 27.00°C the effects of ideality are almost non-existent (coefficient of 0.992), hence the similarities in the two values.

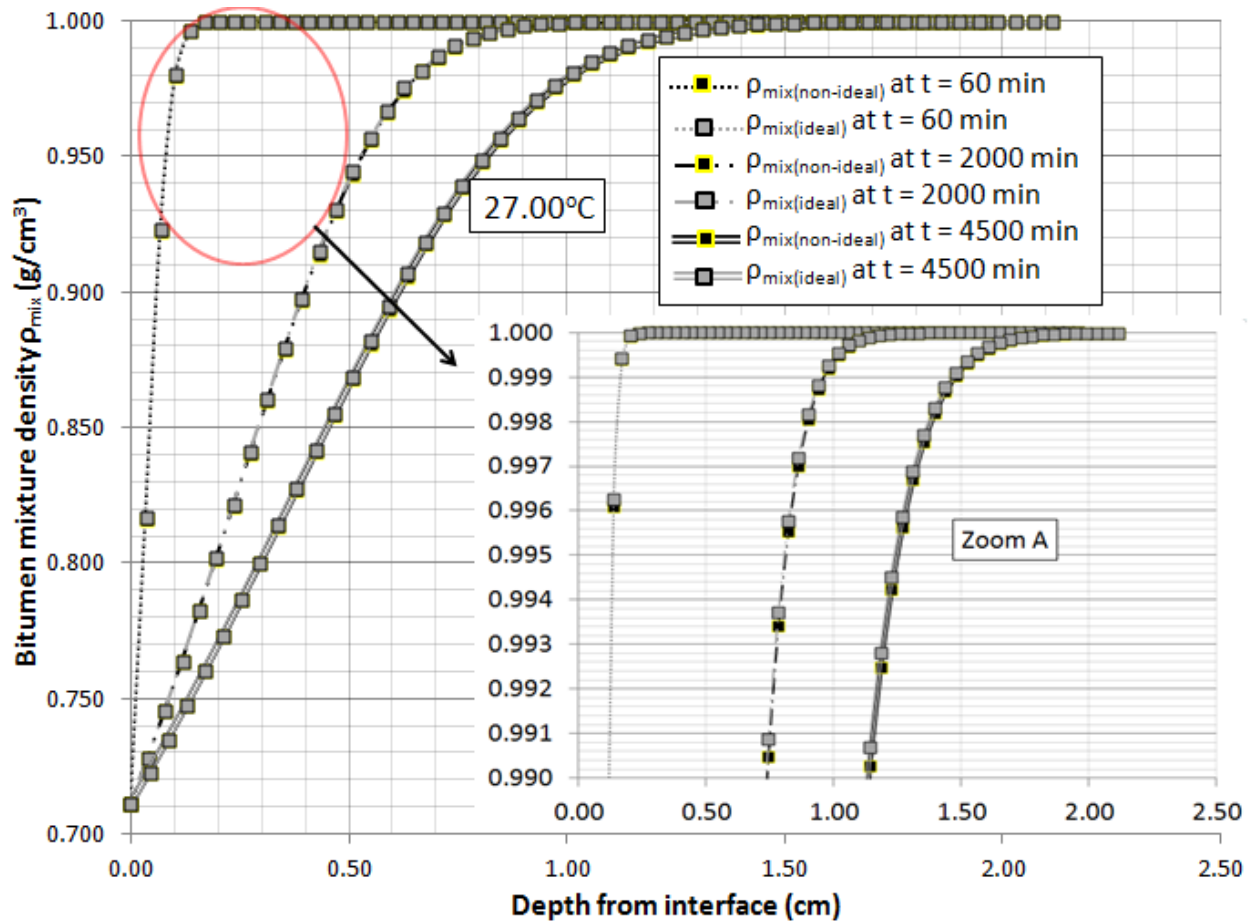


Figure 5-21 - Ideal and non-ideal bitumen density profile at 27.00°C

However, for 33.50°C in **Figure 5-22** (0.835 g/cm<sup>3</sup> ideal vs 0.878 g/cm<sup>3</sup> non-ideal) and 40.00°C in **Figure 5-23** (0.884 g/cm<sup>3</sup> ideal vs 0.921 g/cm<sup>3</sup> non-ideal) the effects of ideality significantly increase (0.900 for 33.50°C and 0.824 for 40.00°C). This ideality effect leads to a clear distinction between ideal and non-ideal mixing density values.

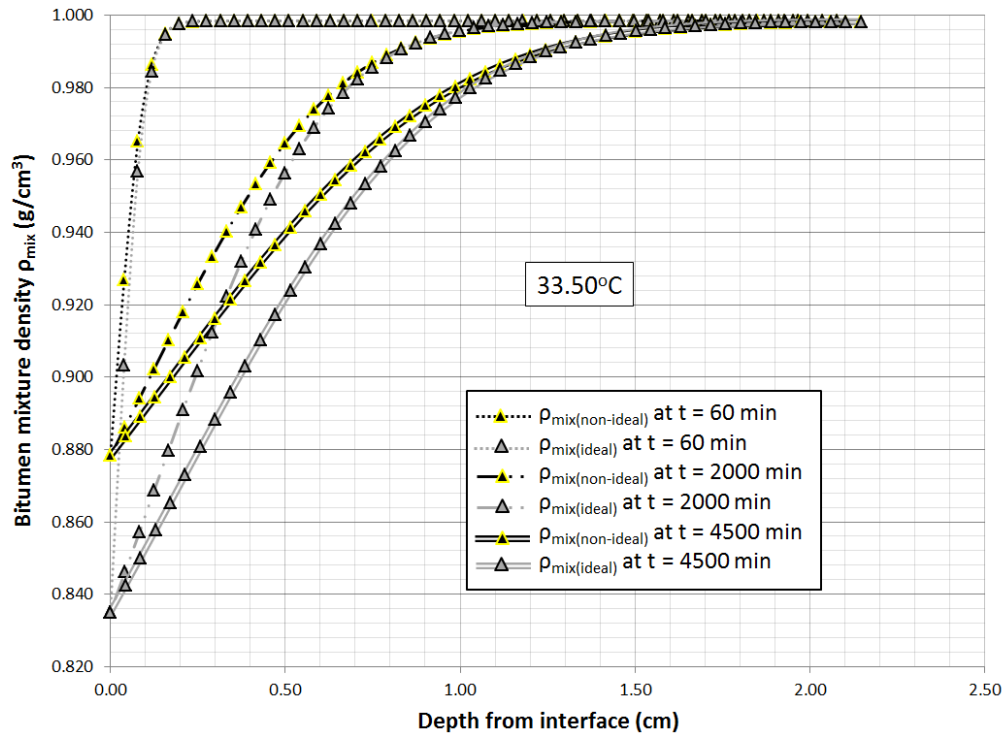


Figure 5-22 - Ideal and non-ideal bitumen density profile at 33.50°C

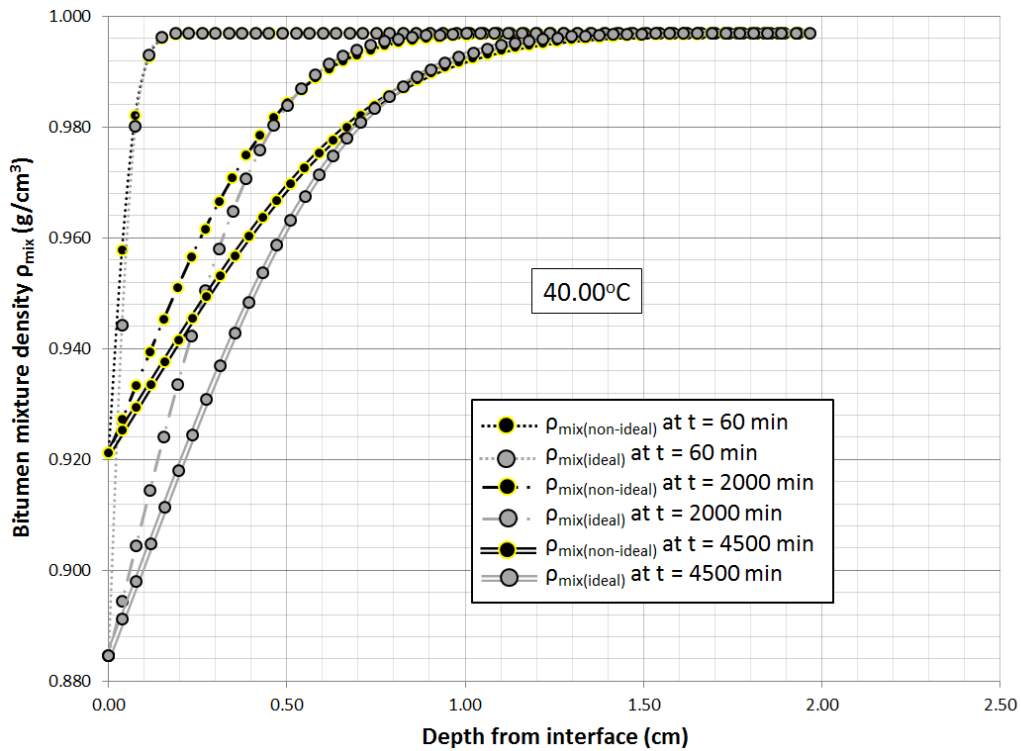


Figure 5-23 - Ideal and non-ideal bitumen density profile at 40.00°C

### 5.4.4. Temperature comparisons

Figure 5-24 shows the non-ideal diffusivity functions at varying temperatures. The figure confirms the earlier stated trend of decreasing diffusion with increasing temperature. All diffusivity functions are plotted to their solubility limits ( $\omega_s^*$ ) previously shown in Table 4-6.

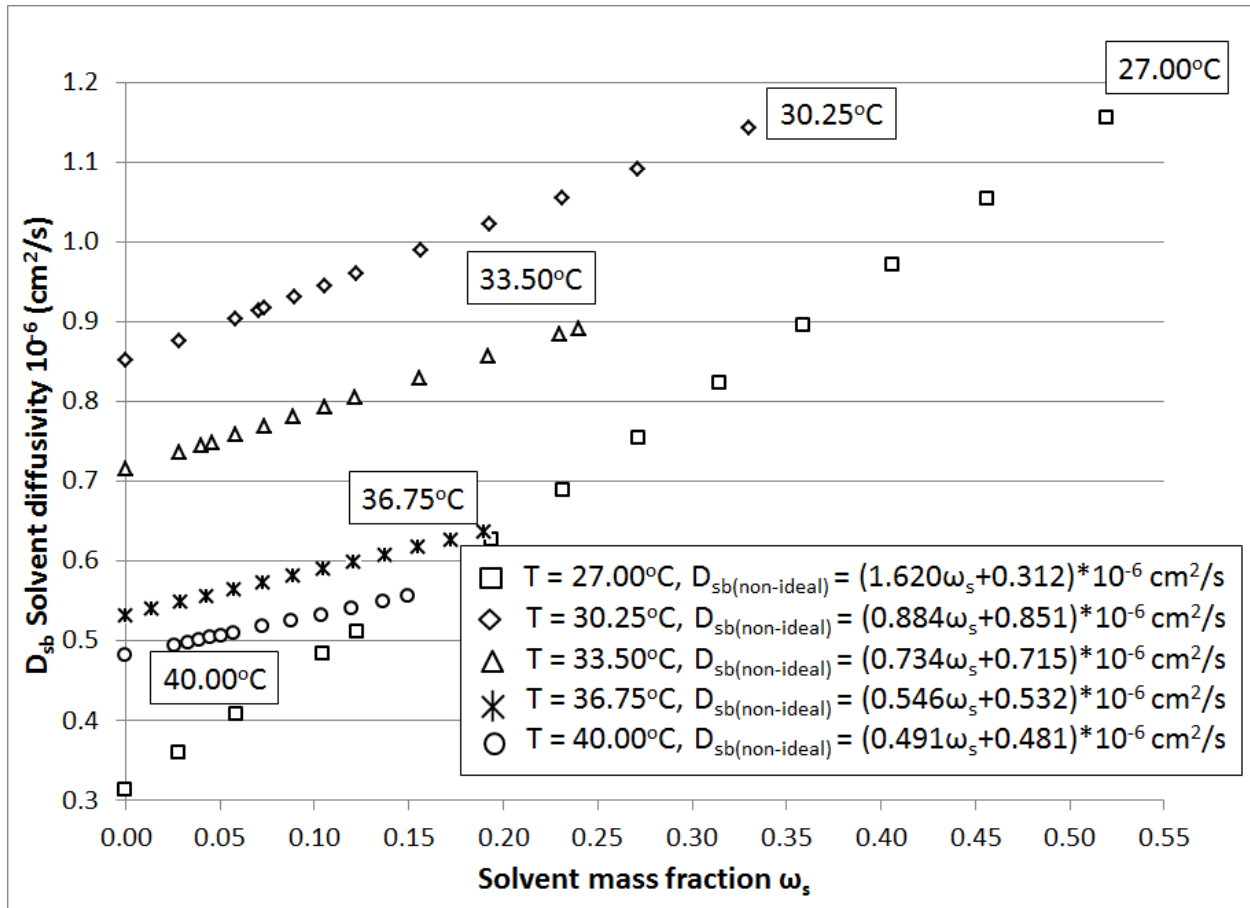


Figure 5-24- Non-ideal diffusivity functions at all temperatures

The trend of decreasing diffusion with increasing temperature is due to a reduction in butane solvent solubility in bitumen with increasing temperature, leading to less dilution solvent in bitumen as temperatures increases. However, the diffusivity function for 27.00°C stands out from the rest. It has a much steeper slope, gets to the highest solvent mass fraction (solubility limit  $\omega_s^*$ ), gets to the highest solvent diffusion value ( $D_{sb}$  at  $\omega_s^*$ ), but starts at the lowest initial solvent diffusion value ( $D_{sb}$  at  $\omega_s=0$ ). This can be explained due to the increasing bitumen

viscosity with decreasing temperature. 27.00°C (the lowest experimental temperature) subsequently has the highest bitumen viscosity. According to literature (Das and Butler 1996, Yazdani and Maini 2009), higher viscosities (from lower temperatures) impede the diffusion process leading lower diffusion values. However, lower temperatures also mean higher solubilities and hence higher diffusion values. When comparing the diffusivity function of 27.00°C to 30.25°C, the negative effects of higher viscosity at 27.00°C is not overcome until butane solvent mass fraction reaches approximately 0.50. This value keeps decreasing when comparing the 27.00°C diffusivity functions to the rest of the higher experimental temperatures. At 30.25°C, the negative effects of viscosity on butane solvent diffusion values are not enough to ever overcome the higher butane solvent solubility compared to the higher temperatures.

**Figure 5-25** shows non-ideal solvent profiles at 60 minutes for all temperatures. At depth zero all solvent profiles start at their varying solubility limits ( $\omega_s^*$ ) before plateauing 0. This is because at time 60 mins, the butane solvent has diffused a very short distance into the bitumen.

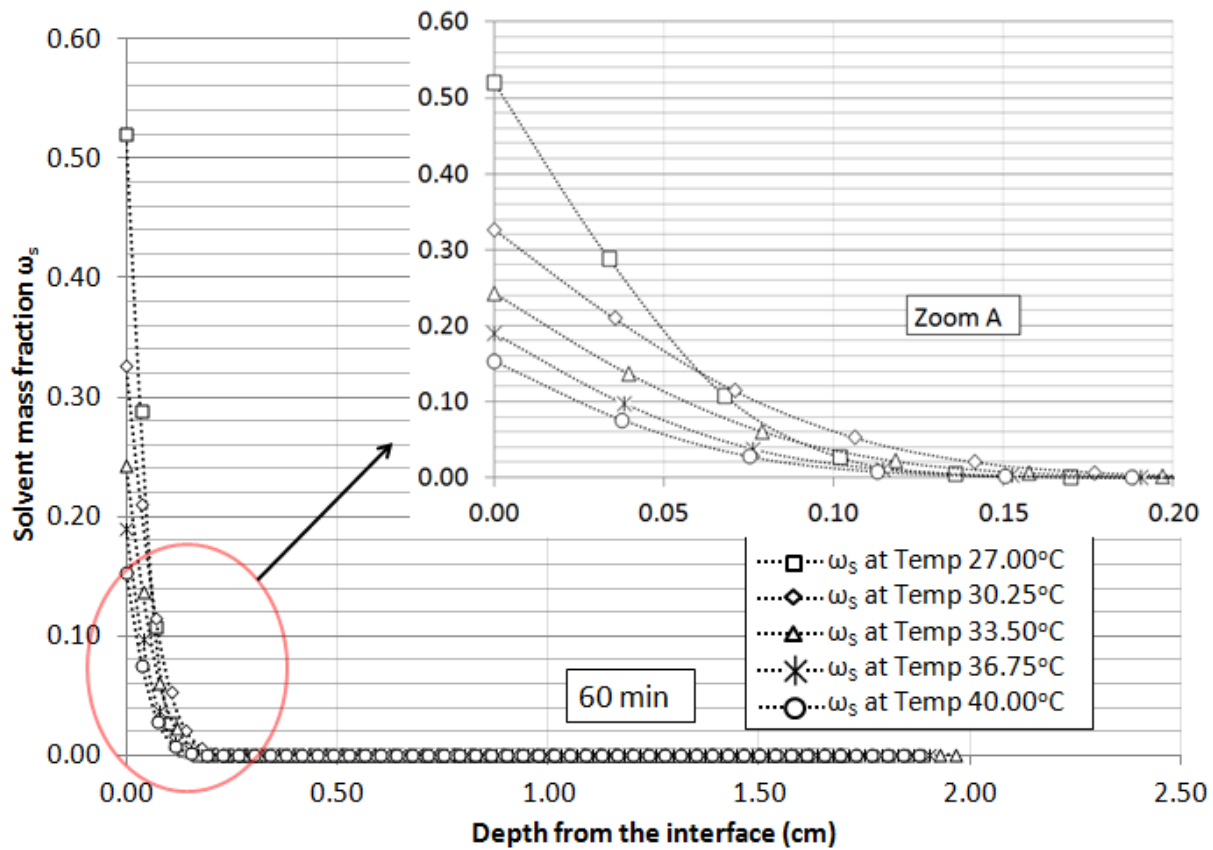


Figure 5-25 - Solvent mass fraction profile at 60 minutes for all temperatures

**Figure 5-26** shows non-ideal density profiles at 60 minutes for all temperatures. These density profiles start at the non-ideal bitumen mixture density with solvent at mass fraction solubility limit ( $\omega_s^*$ ). Zoom A shows that the concentration vs depth for 27.00°C is steeper than other temperatures. This is so that the 27.00°C profile can plateau above all the other profiles due to its higher density value at solvent mass fraction  $\omega_s = 0$  (bottom of bitumen tube). This is illustrated in Zoom B where all profiles plateau at their given density based on temperature and  $\omega_s = 0$ .

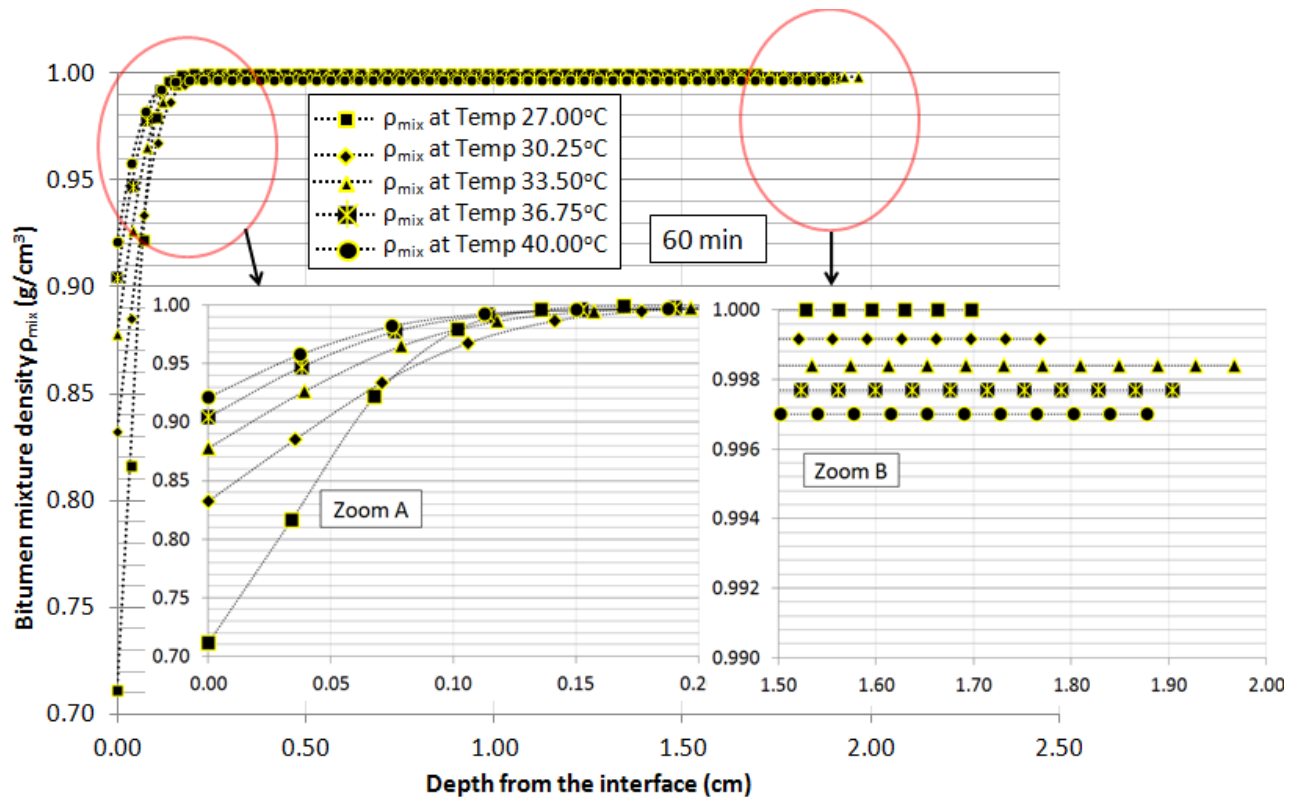


Figure 5-26 - Bitumen density profile at 60 minutes for all temperatures

**Figure 5-27** is the non-ideal solvent profile at 2000 minutes for all temperatures. It follows a trend to that explained in **Figure 5-25** for 60 minutes. However in time, i.e 2000 minutes, more solvent has diffused through the bitumen. With more solvent being diffused in, more density reduction is occurring for all temperatures hence a less steep profile (for solvent and density) compared to those for 60 minutes. This is also illustrated in **Figure 5-28** which is the non-ideal density profile at 2000 minutes for temperatures.

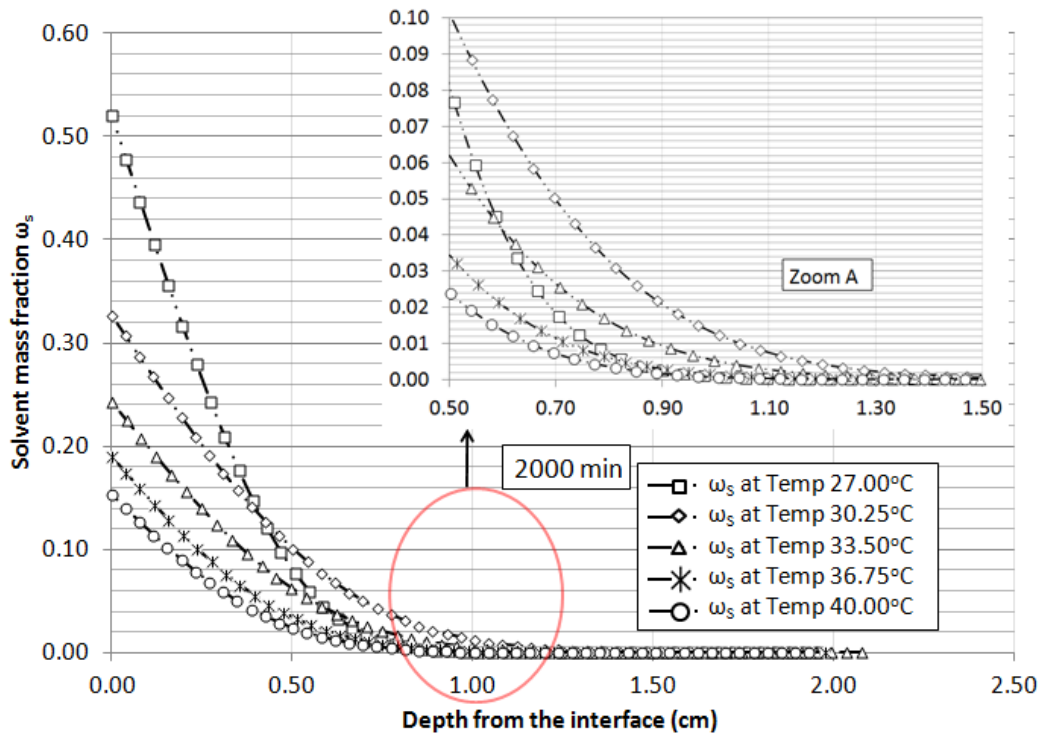


Figure 5-27 - Solvent mass fraction profile at 2000 minutes for all temperatures

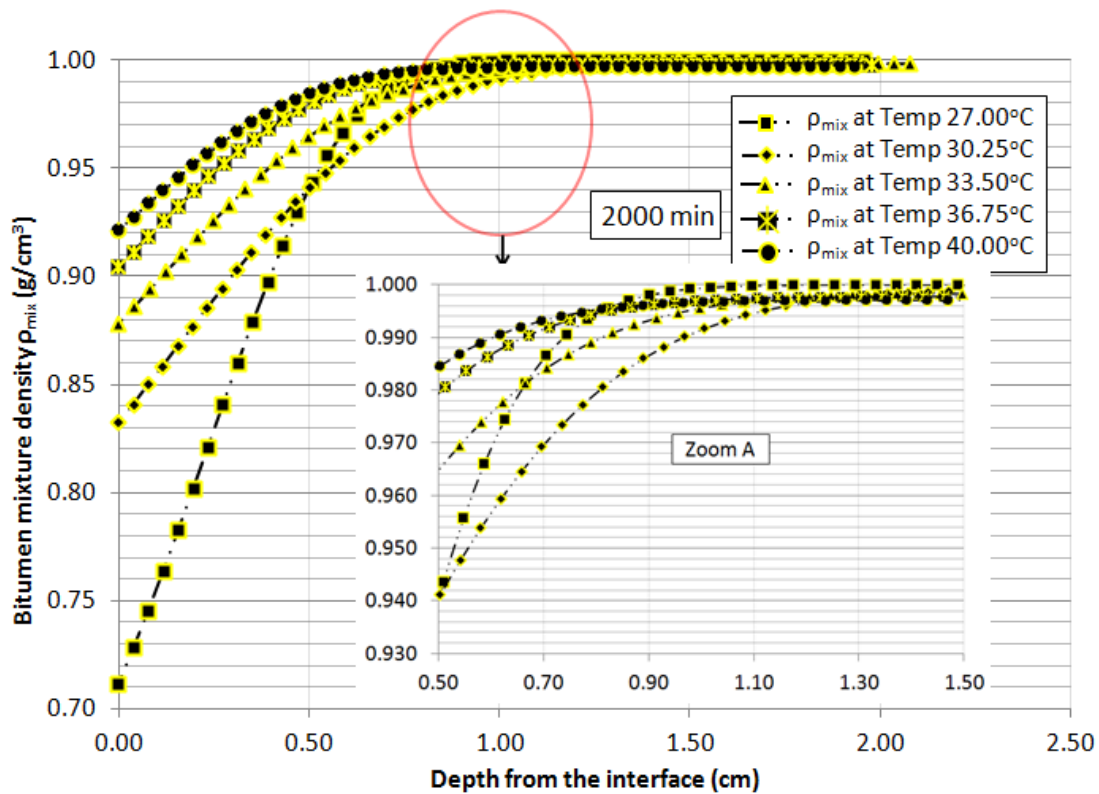


Figure 5-28 - Bitumen density profile at 2000 minutes for all temperatures

**Figure 5-29** is the solvent profile at 4500 minutes for all temperatures. As expected with more elapsed time for 4500 minutes, more solvent has diffused through the bitumen fluid, more density reduction occurring for all temperatures and less steep concentration and density profiles. 30.25°C is the only temperature that breaks the bitumen flux boundary. The flux boundary is a part of the bitumen fluid (usually at the bottom) that never comes in contact with butane solvent and hence maintains its original density at given temperature. Factors that increase the chances of the flux boundary being broken include: shorter bitumen depth (less distance to travel for solvent), higher solvent diffusion and lower viscosity (less impediment to solvent travel). These factors combine favourably for at 30.25°C and hence the flux boundary being broken as seen in Zoom A of the figure.

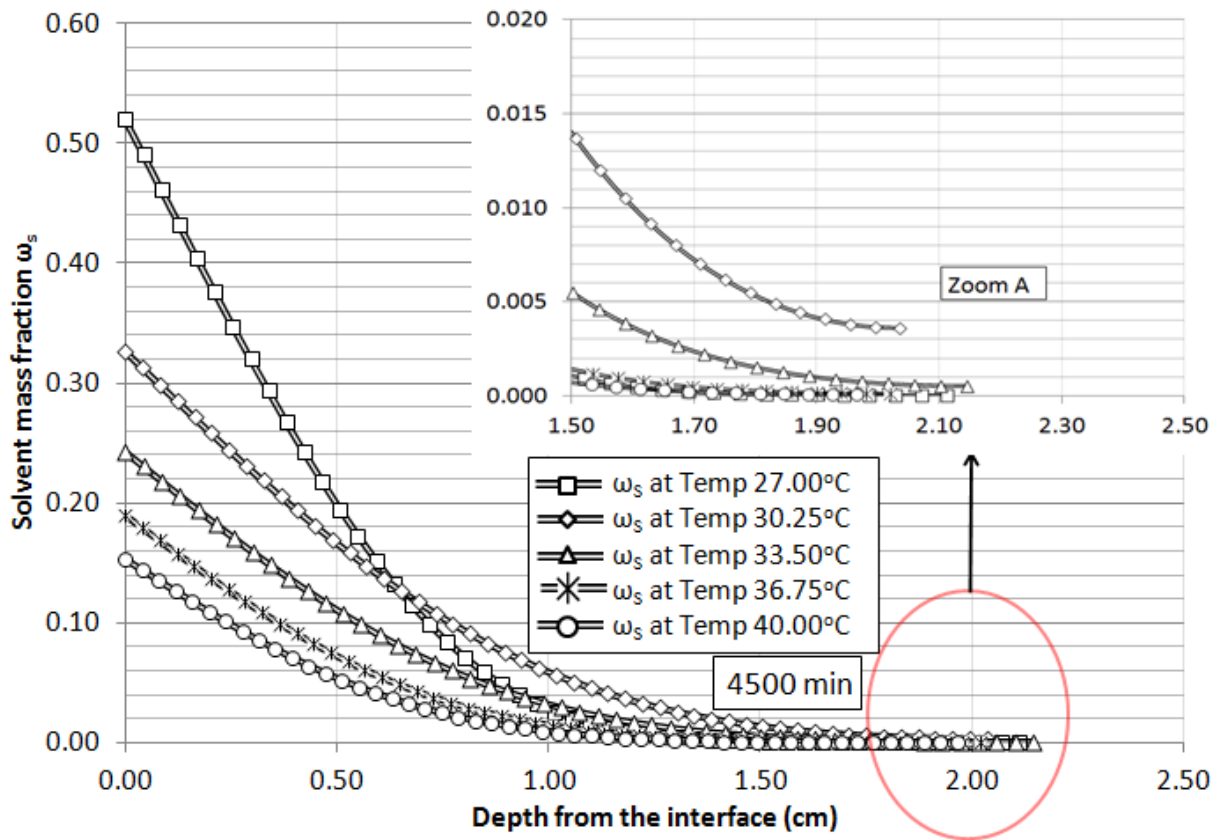


Figure 5-29 - Solvent mass fraction profile at 4500 minutes for all temperatures

Given the flux boundary is broken for 30.25°C, the density at the bottom of the tube for the same time should be considerably less than the normal density. **Figure 5-30** is the bitumen density

profile at 4500 minutes for all the temperatures. Normally 30.25°C should plateau in between the density of 27.00°C (1.000 g/cm<sup>3</sup>) and 33.50°C (0.998 g/cm<sup>3</sup>). However, due to the flux boundary being broken, 30.25°C plateaus below all the temperatures (0.997 g/cm<sup>3</sup>). This is illustrated in the zoomed part (Zoom A) of **Figure 5-30**. None of the other temperatures significantly break flux boundary and hence plateau at their typically expected densities.

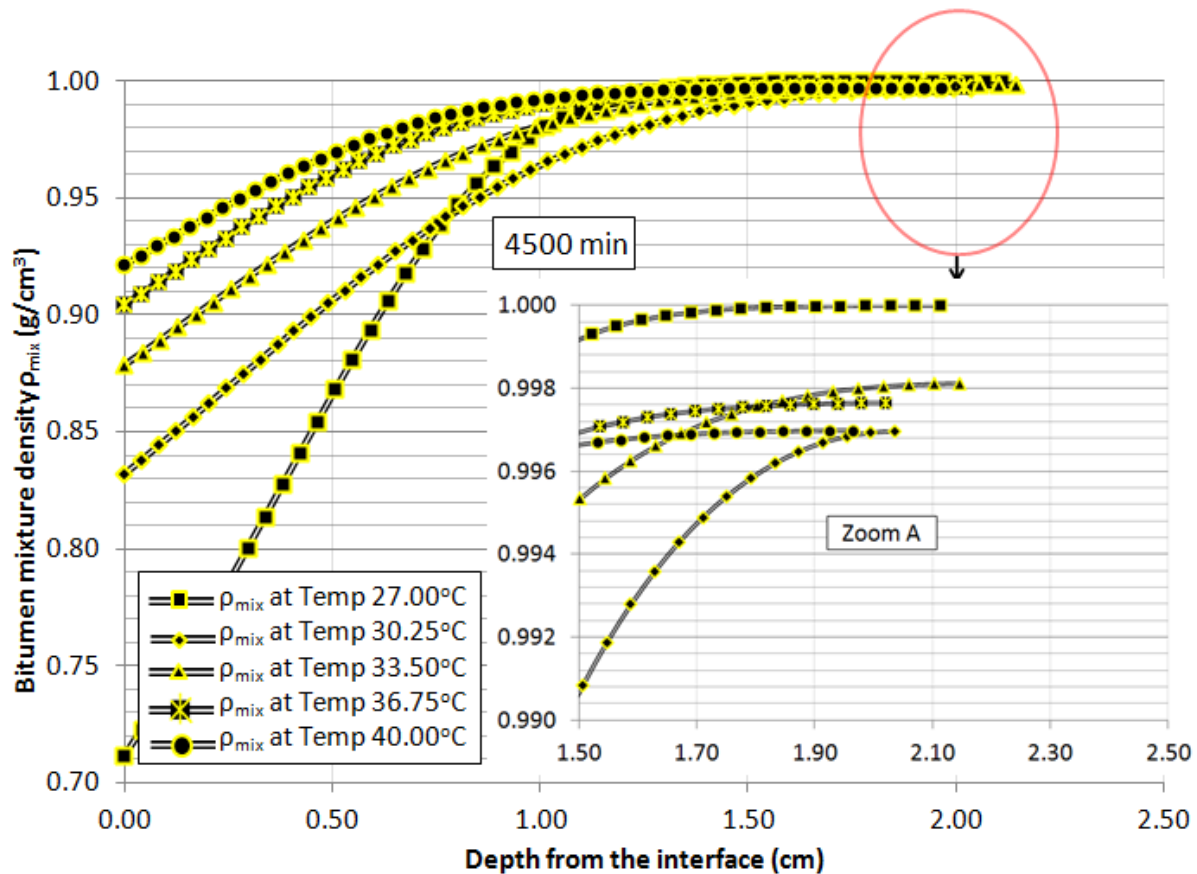


Figure 5-30 - Bitumen density profile at 4500 minutes for all temperatures

### 5.4.5. Diffusivity results validation

As stated earlier, the uniqueness of this method is the independent validation of the diffusivity function results. A macroscopic mass balance to predict the change in solvent height after ‘bitumen growth’ has been resolved for the full time duration. This counts as an independent validation because the experimental solvent height change values are not used in the model to determine the diffusivity.

**Figure 5-31** shows the predicted change in butane solvent height (ideal/non-ideal) and experimental change in butane solvent height vs time at 33.50°C over the entire experiment. The dashed line represents predicted values for ideal mixing scenario, the solid line represents predicted values for non-ideal mixing and the markers represents experimental data. Recollect that every single experimental run was duplicated hence the two sets of experimental data. The predicted values for non-ideal mixing clearly show a better fit with the experimental data than predicted values for ideal mixing scenario. The good fit between predicted non-ideal mixing scenario and experimental data validates the diffusivity functions obtained for this temperature.

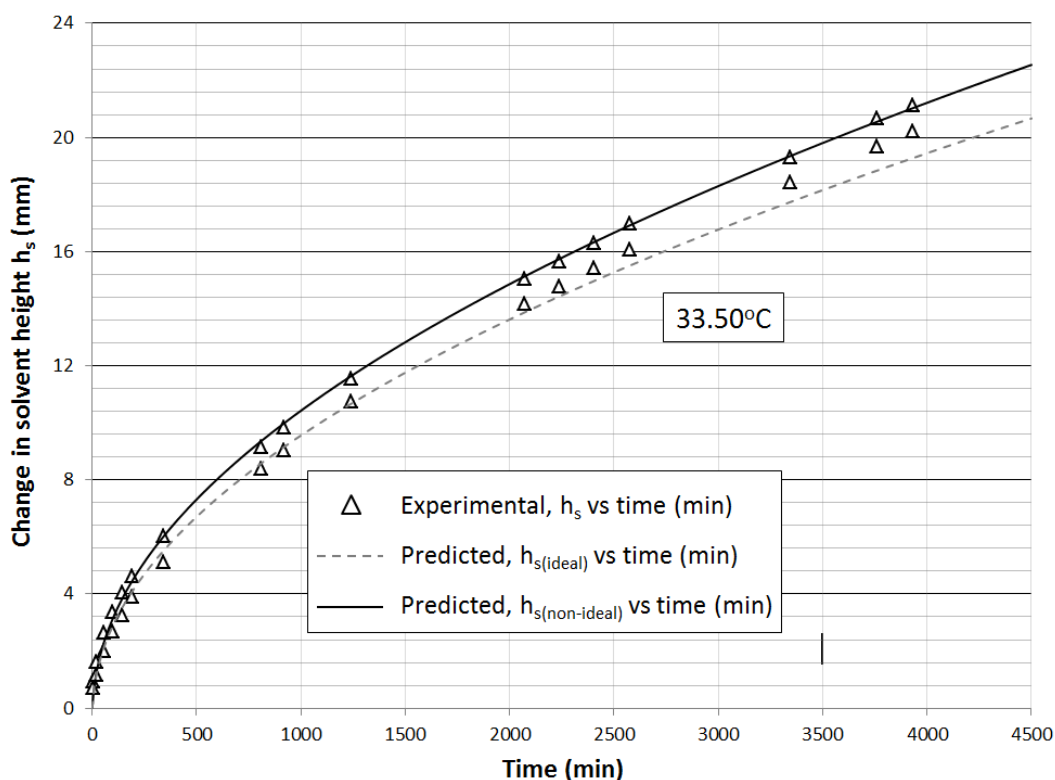


Figure 5-31 - Predicted and experimental change in solvent height vs time at 33.50°C

**Figure 5-32** shows the predicted change in butane solvent height (ideal/non-ideal) and experimental change in butane solvent height vs SRT at 33.50°C over the entire experiment. As expected the predicted non-ideal mixing shows a much better fit with the experimental data than the ideal mixing scenario.

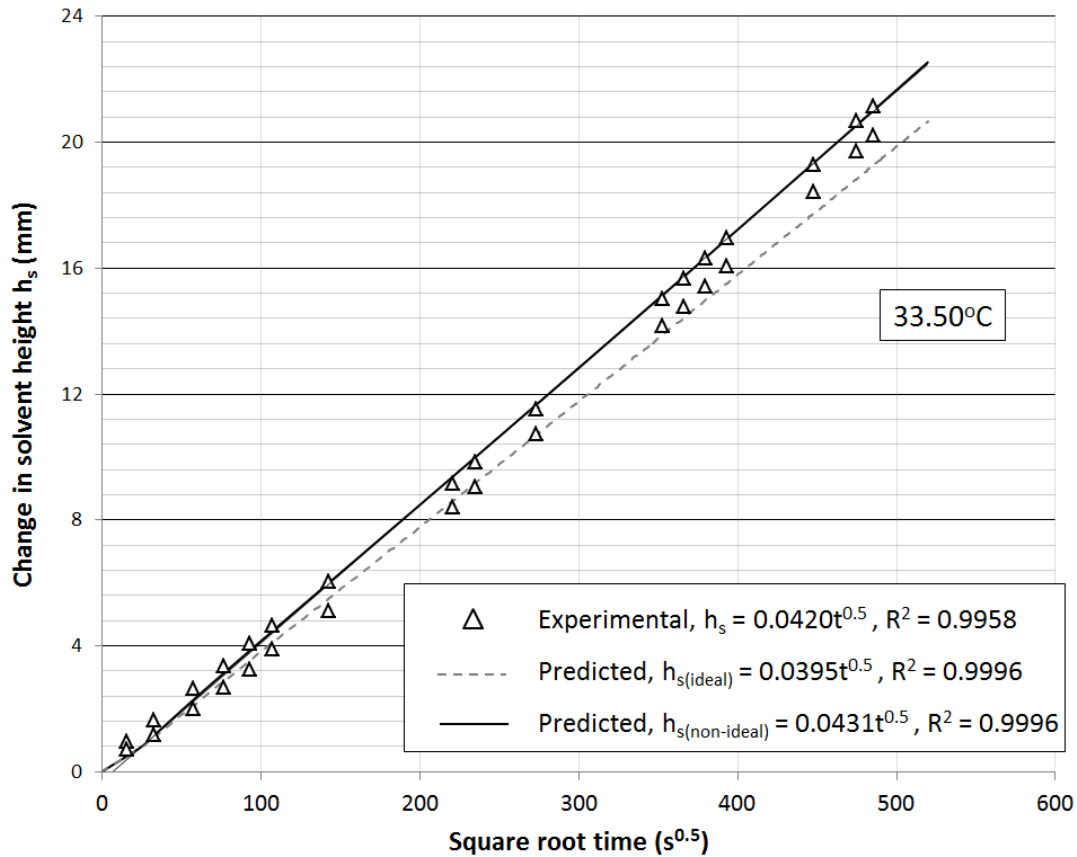


Figure 5-32 - Predicted and experimental change in solvent height vs SRT at 33.50°C

The validation works fine for temperatures 30.25°C, 33.50°C and 36.75°C. However the validations of 27.00°C and 40.00°C are not as clear. **Figures 5-33, 5-34, 5-35 and 5-36** show the validation plots for both these temperatures. The predicted non-ideal mixing values for both these temperatures fits well for the first 2000 minutes of the experiment but not so much for the rest of the experimental time. This lack of fit is more pronounced in 40.00°C more so than 27.00°C. This was due to technical issues encountered while conducting the experiments at those temperatures. Those issues are discussed in **Section 5.6**.

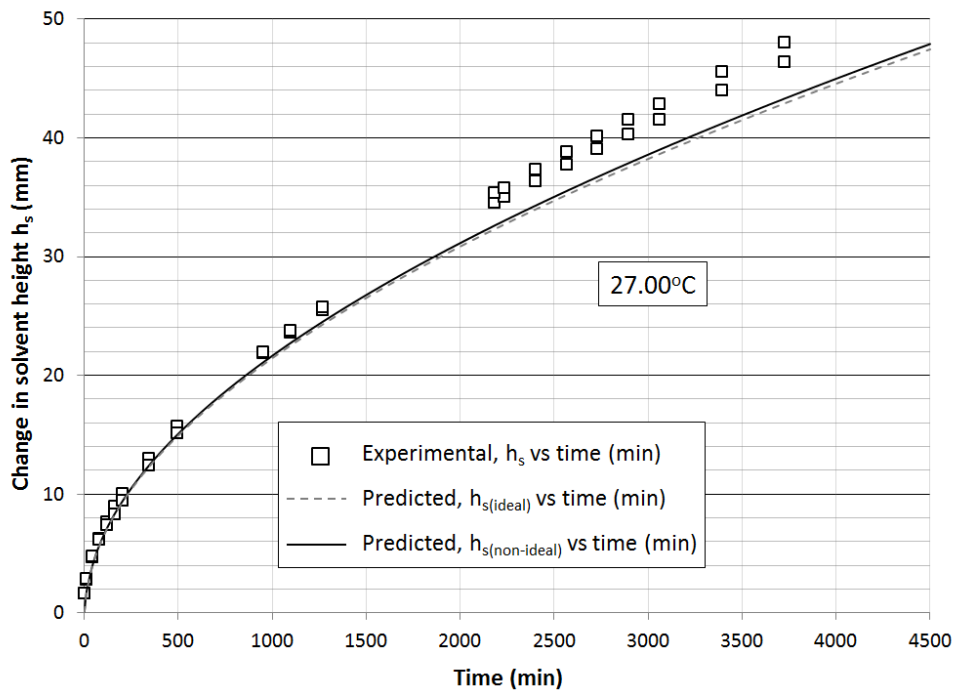


Figure 5-33- Predicted and experimental change in solvent height vs time at 27.00°C

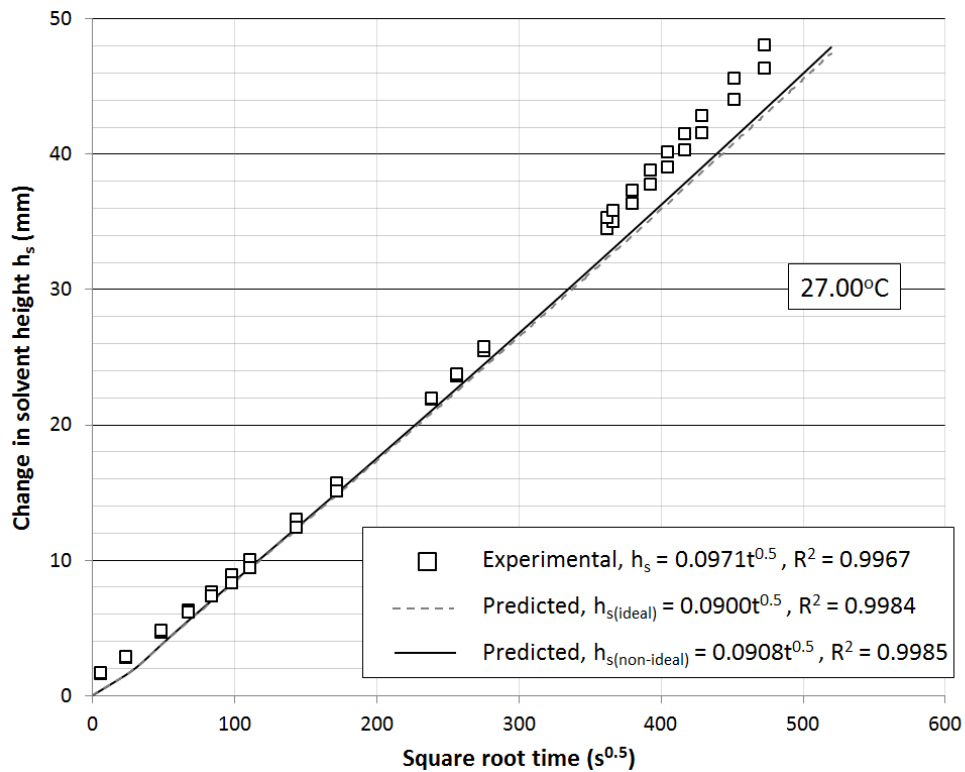


Figure 5-34 - Predicted and experimental change in solvent height vs SRT at 27.00°C

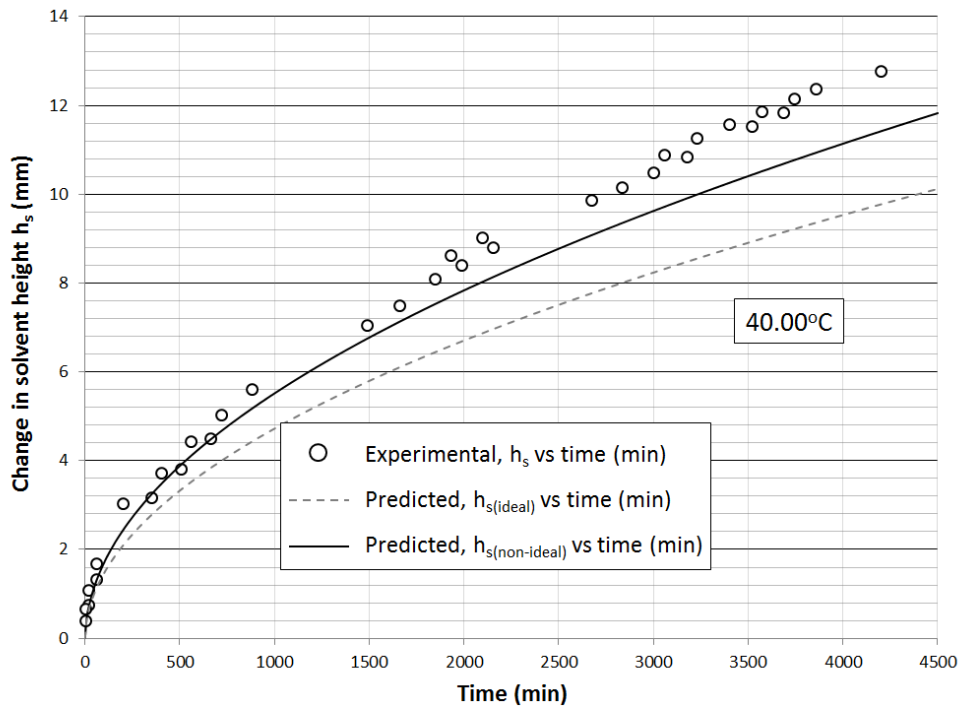


Figure 5-35 - Predicted and experimental change in solvent height vs time at 40.00°C

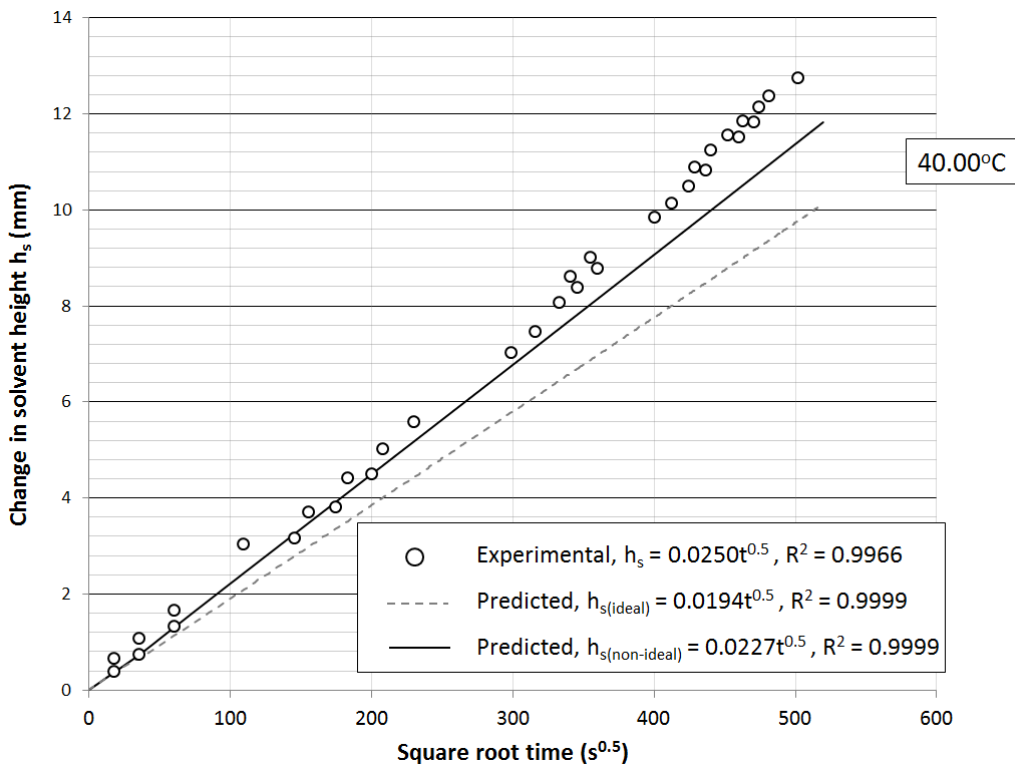


Figure 5-36 - Predicted and experimental change in solvent height vs SRT at 40.00°C

**Table 5-8** gives a list of predicted values (ideal/non-ideal) and experimental butane solvent change slopes for all temperatures. The predicted (ideal/non-ideal) slopes are then compared to experimental slopes using percentage difference. For each temperature, the predicted percentage difference closer to zero, signifies which is the better fit. For all temperatures, the highlighted column shows that the predicted non-ideal percentage differences are always closer to zero compared to the predicted ideal percentage differences.

Table 5-8 - Validation data for butane solvent height decrease at all temperatures

Butane height decrease vs. SRT graph data				
Temperature (°C)		Slope of graph (mm/s <sup>0.5</sup> )	% diff from Experimental values	R <sup>2</sup>
27.00	Experimental values	0.0971		0.9967
	Predicted ideal values	0.0900	7.31	0.9984
	Predicted Non-ideal values	0.0908	6.49	0.9985
30.25	Experimental values	0.0633		0.9992
	Predicted ideal values	0.0601	5.06	0.9992
	Predicted Non-ideal values	0.0623	1.58	0.9992
33.50	Experimental values	0.0420		0.9958
	Predicted ideal values	0.0395	5.95	0.9996
	Predicted Non-ideal values	0.0431	-2.62	0.9996
36.75	Experimental values	0.0302		0.9953
	Predicted ideal values	0.0257	14.90	0.9998
	Predicted Non-ideal values	0.0295	2.32	0.9998
40.00	Experimental values	0.0250		0.9966
	Predicted ideal values	0.0194	22.40	0.9999
	Predicted Non-ideal values	0.0227	9.20	0.9999

A brief overview of how the value in Table 5-8 is shown. Using 30.25°C as an example slope of graphs is given as follows;

$$\text{Experimental values} = 0.0633 \text{ mm/s}^{0.5}$$

$$\text{Predicted ideal values} = 0.0601 \text{ mm/s}^{0.5}$$

$$\text{Predicted non – ideal values} = 0.0623 \text{ mm/s}^{0.5}$$

The percentage difference of predicted value (ideal and non-ideal) from experimental value is then found as follows,

$$\text{MATLAB ideal \% diff} = \frac{|0.0601 - 0.0633|}{0.0633} \times 100 = 5.06\%$$

$$\text{MATLAB non - ideal \% diff} = \frac{|0.0623 - 0.0633|}{0.0633} \times 100 = 1.58\%$$

Bitumen is an input value in the validation equation, hence its predicted slope (ideal/non-ideal) is expected to be exactly the same as experimental data. The validation table is available in **APPENDIX L** along with the rest of the validation graphs.

## 5.5. Design expert correlation results

Design Expert (DE) software was used to analyze the experimental data to determine a correlation for predicting diffusivity function within the give temperature range (27°C – 40°C).

As stated in **Section 4.4**, input parameter (temperature) along with output parameters (butane slope, bitumen slope and ideality coefficient) were used in DE to form a correlation for predicting each of the output parameters for any given temperature within the range 27.00°C – 40.00°C. **Equations 4-23, 4-24 and 4-25** represent the models obtained for each of the output parameters. A real experiment at 28.50°C was conducted to test the robustness of the above models. The ANOVA tables from the DE results are in **APPENDIX H**.

### 5.5.1. Butane solvent decrease results

**Figure 5-37** shows the butane solvent decrease data vs SRT at 28.50°C. The experimental run encounters the same issues as others in regards to varying start times. The figure shows that a better data fit is achieved with a non-zero start time compared to a zero start time.

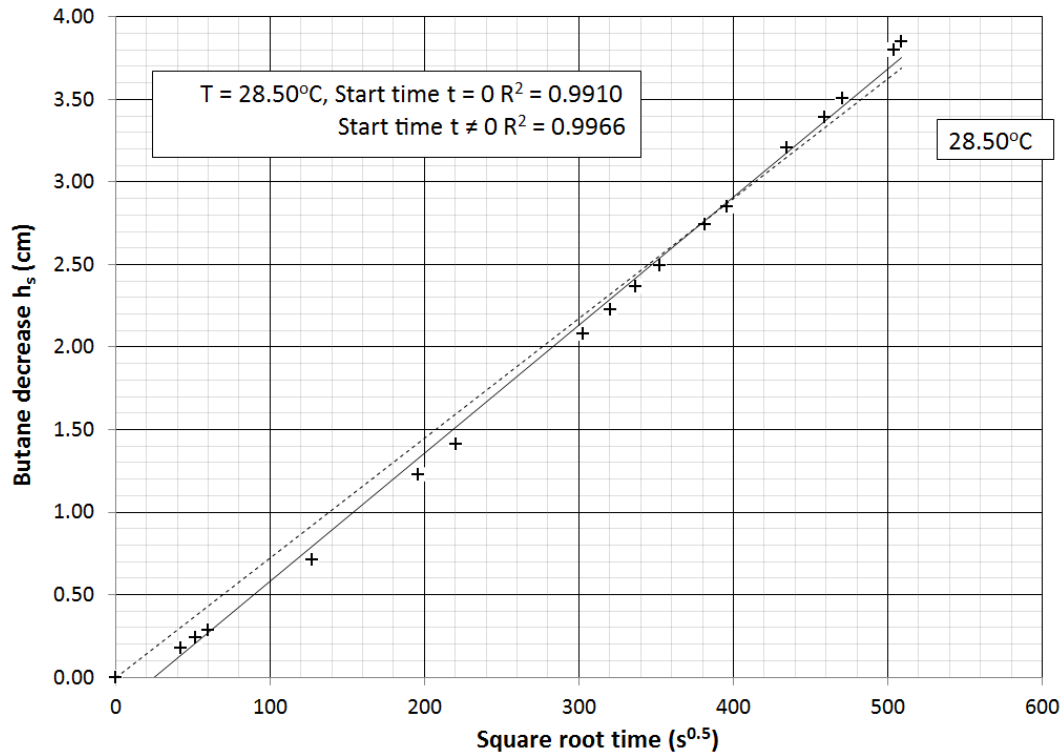


Figure 5-37 - Butane solvent decrease vs SRT for  $t = 0$  and  $t \neq 0$  at  $28.50^{\circ}\text{C}$

**Table 5-9** shows all the graph data for  $28.50^{\circ}\text{C}$ . The highlighted column indicates that the  $R^2$  value for  $t \neq 0$  ( $R^2 = 0.9966$ ) is greater than for  $t = 0$  ( $R^2 = 0.9910$ ). The experimental data is therefore shifted as explained in **Section 5.1** and the new data is plotted in **Figure 5-38**.

Table 5-9 - Butane solvent height decrease data ( $28.50^{\circ}\text{C}$ )

Butane height decrease vs. SRT graph data						
Temperature ( $^{\circ}\text{C}$ )	Experimental Start time (min)	Slope of graph ( $\text{cm}/\text{s}^{0.5}$ )	$R^2$	y intercept	x intercept	Start time (min)
28.50	t = 0	0.0072	0.9910	0.0000	0.00	0.00
	t $\neq$ 0	0.0077	0.9966	-0.1928	25.04	10.45

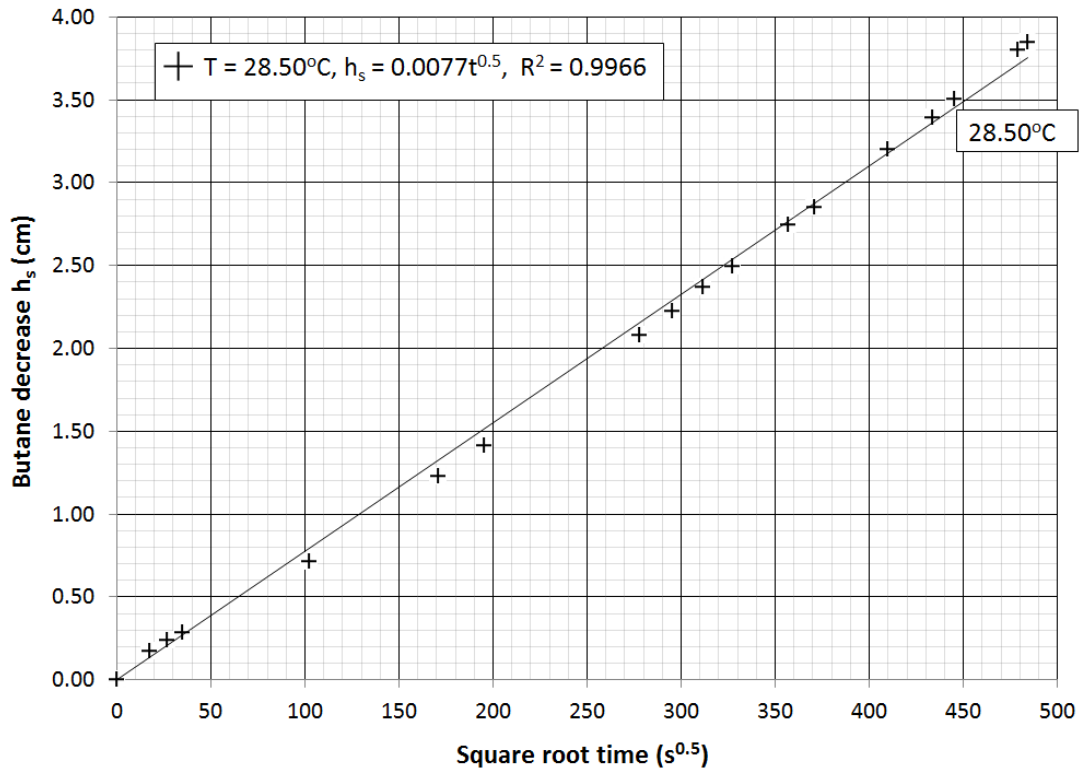


Figure 5-38 - Butane solvent height decrease vs. SRT (28.50°C)

Referring back to **Section 4.4, Equation 4-23** (obtained from Design Expert software) is utilized to compute the predicted butane slope value.

$$(\text{Butane slope})^{0.5} = 0.379 - [0.013 \times T] + [5.093 \times (10^{-5}) \times T^2] + [1.728 \times (10^{-6}) \times T^3]$$

Substituting in 28.50°C for T gives:

$$\begin{aligned} (\text{Butane slope})^{0.5} &= 0.379 - [0.013 \times 28.5] + [5.093 \times (10^{-5}) \times 28.5^2] \\ &\quad + [1.728 \times (10^{-6}) \times 28.5^3] \\ \text{Butane slope} &= \mathbf{0.0079 \text{ cm/s}^{0.5}} \end{aligned}$$

The experimental butane data and butane data obtained from the DE predicted slope are compared in **Figure 5-39**. If both were exactly the same, the equation of the graph should have a

slope of 1. The slope for this graph however is 1.0243. It is not a perfect fit but is good enough for use in this work.

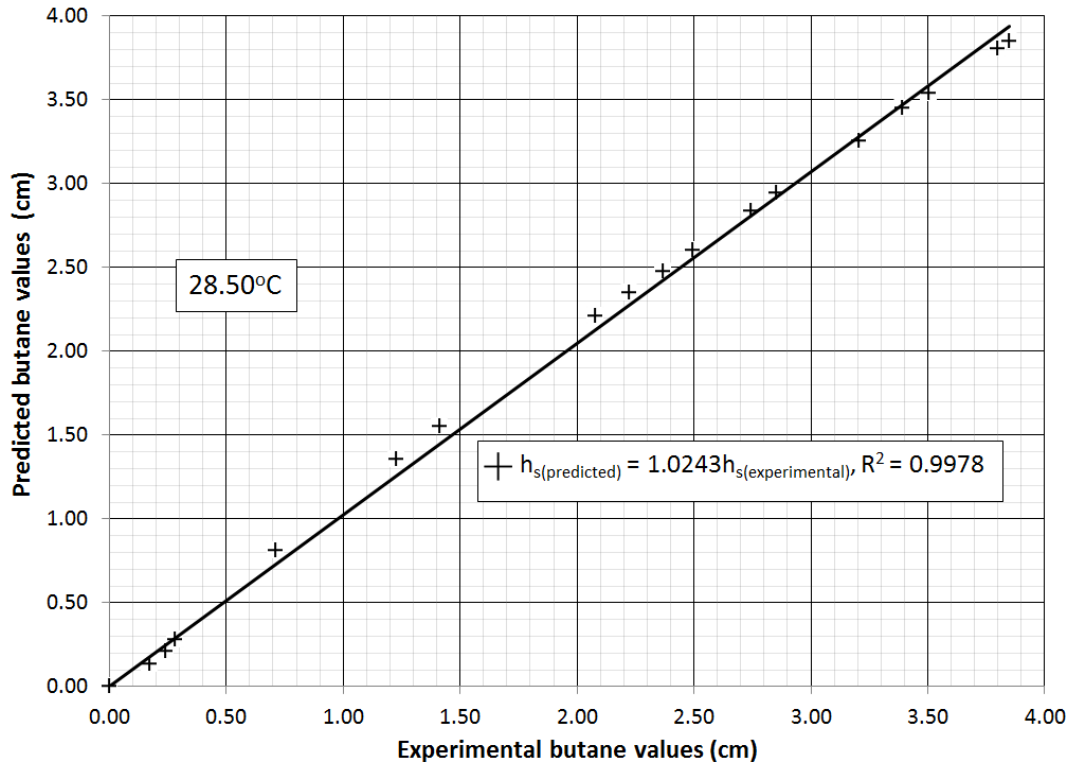


Figure 5-39 - Butane solvent decrease DE predicted vs experimental values (28.50°C)

Given temperature 28.50°C is in between 27.00°C and 30.25°C, the slope of the 28.50°C butane solvent graph (experimental and Design Expert predicted) should also be between the slope of 27.00°C and 30.25°C. This is illustrated in the highlighted part of **Table 5-10**.

Table 5-10 - Comparison of 28.50°C butane decrease graph data to other temperatures

Butane height decrease Experimental and Predicted SRT graph data						
Temperature (°C)	Start time (min)		Slope of graph (cm/s <sup>0.5</sup> )	R <sup>2</sup>	y intercept	x intercept
27.00	t = 0	Experimental values	0.0097	0.9967	0.00	0.00
28.50	t = 0	Experimental values	0.0077	0.9966	0.00	0.00
	t = 0	DE predicted values	0.0079	1.0000	0.00	0.00
30.25	t = 0	Experimental values	0.0063	0.9992	0.00	0.00

## 5.5.2. Bitumen increase results

Figure 5-40 shows the bitumen solvent increase data vs SRT at 28.50°C. The figure shows that a better data fit is achieved with a none zero start time compared to a zero start time.

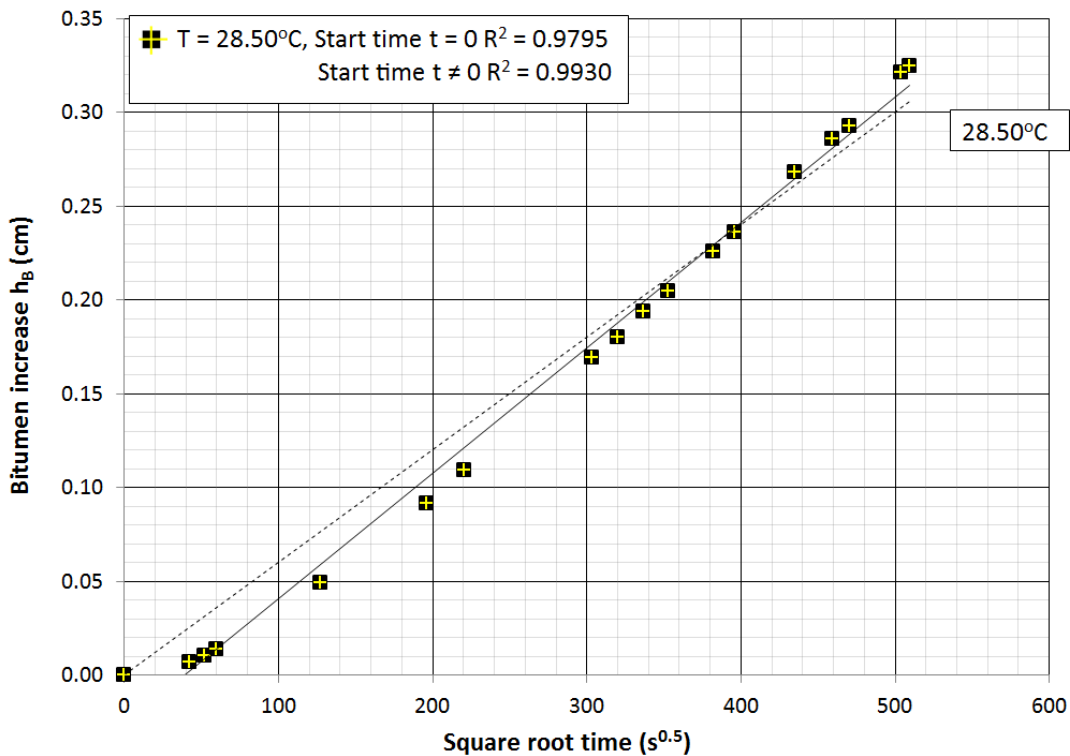


Figure 5-40 - Bitumen height increase vs SRT for t = 0 and t ≠ 0 at 28.50°C

**Table 5-11** shows all the graph data for 28.50°C. The highlighted column indicates that the  $R^2$  value for  $t \neq 0$  ( $R^2 = 0.9930$ ) is greater than for  $t = 0$  ( $R^2 = 0.9795$ ). The experimental data is therefore shifted as explained in **Section 5.2** and the new data is plotted in **Figure 5-41**.

Table 5-11 - Bitumen height increase graph data (28.50°C)

Bitumen height increase vs. SRT graph data						
Temperature (°C)	Experimental Start time (min)	Slope of graph (cm/s <sup>0.5</sup> )	R <sup>2</sup>	y intercept	x intercept	Start time (min)
28.50	t = 0	0.00060	0.9795	0.0000	0.00	0.00
	t ≠ 0	0.00067	0.9930	-0.0258	38.52	24.73

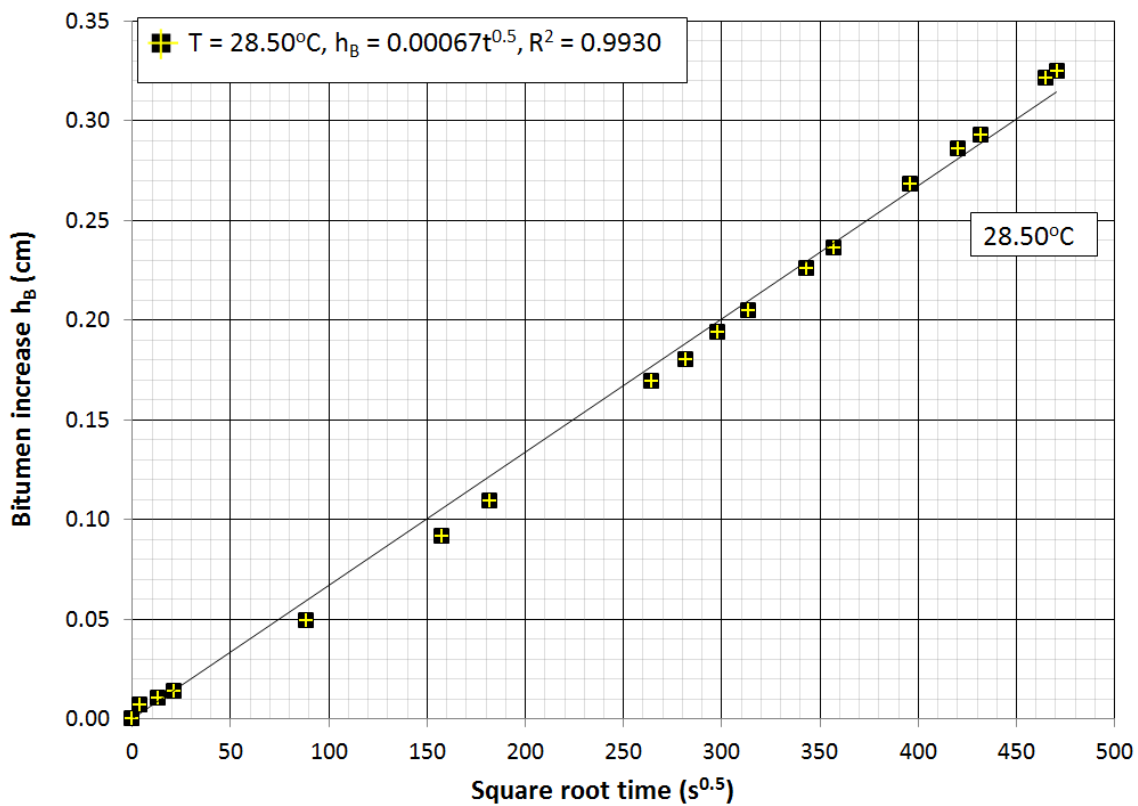


Figure 5-41 - Bitumen height increase vs SRT at 28.50°C

Referring back to **Section 4.4, Equation 4-24** (obtained from DE software) is utilized to compute the predicted bitumen slope value.

$$(\text{Bitumen slope})^{0.5} = 0.123 - [4.955 \times (10^{-3}) \times T] + [5.543 \times (10^{-5}) \times T^2]$$

Substituting in 28.50°C for T gives:

$$(\text{Bitumen slope})^{0.5} = 0.123 - [4.955 \times (10^{-3}) \times 28.5] + [5.543 \times (10^{-5}) \times 28.5^2]$$

$$\text{Bitumen slope} = \mathbf{0.00071 \text{ cm/s}^{0.5}}$$

The experimental bitumen data and bitumen data obtained from the DE predicted slope are compared in **Figure 5-42**. The slope for this graph is 1.0636 which is once again not a perfect fit, but is good enough for use in this work.

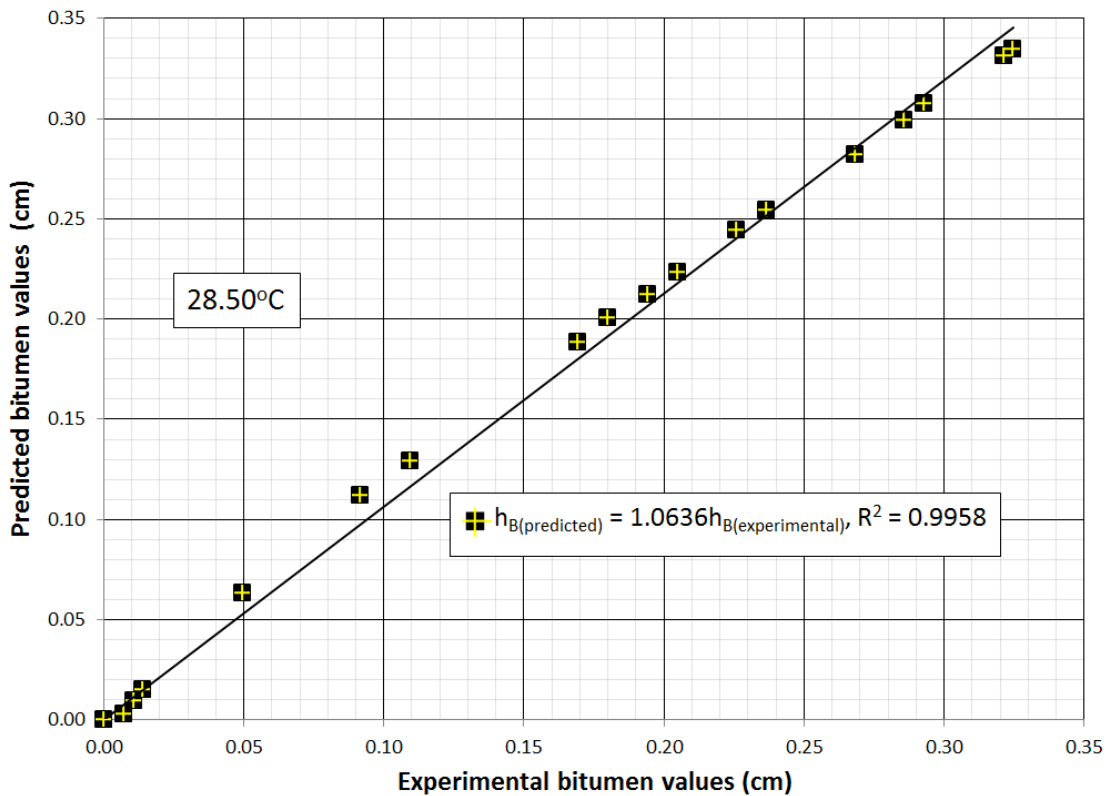


Figure 5-42 - Bitumen increase DE predicted vs experimental values (28.50°C)

The slope of the 28.50°C bitumen graph (experimental and Design Expert predicted) is also between the slope of 27.00°C and 30.25°C as illustrated in the highlighted part of **Table 5-12**.

Table 5-12 - Comparison of 28.50°C bitumen increase graph data to other temperatures

Bitumen height increase Experimental and Predicted SRT graph data						
Temperature (°C)	Start time (min)		Slope of graph (cm/s <sup>0.5</sup> )	R <sup>2</sup>	y intercept	x intercept
27.00	t = 0	Experimental values	0.00087	0.9934	0.00	0.00
28.50	t = 0	Experimental values	0.00067	0.9930	0.00	0.00
	t = 0	DE predicted values	0.00071	1.0000	0.00	0.00
30.25	t = 0	Experimental values	0.00056	0.9974	0.00	0.00

### 5.5.3. Non-ideal mixing results

**Figure 5-43** shows bitumen specific volume vs solvent mass fraction graph for 28.50°C. Using the method outlined in **Section 4.3.2** the ideality coefficient for 28.50°C is **0.977**.

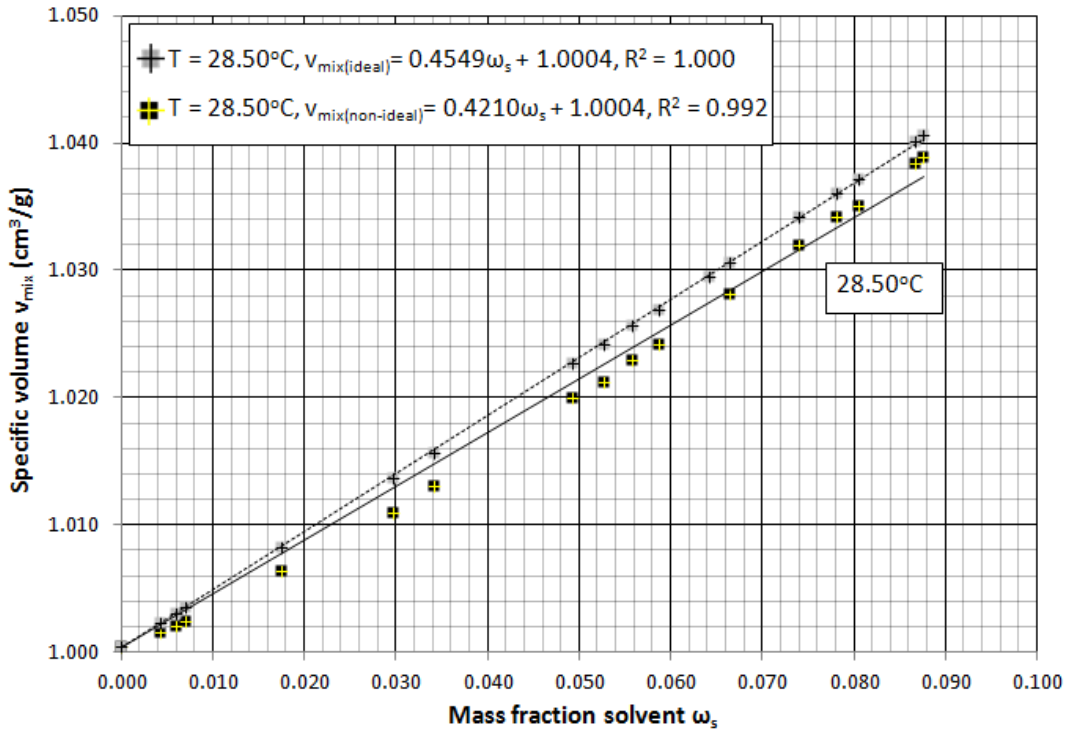


Figure 5-43 - Bitumen mixture specific volume plots for ideal and non-ideal mixing 28.50°C

Referring back to **Section 4.4, Equation 4-25** (obtained from DE software) is utilized to compute the predicted ideality coefficient at 28.50°C.

$$(Ideality)^3 = -2.13554 + [0.36648 \times T] - [0.013102 \times T^2] + [1.40606 \times (10^{-4}) \times T^3]$$

Substituting in 28.50°C for T gives:

$$\begin{aligned} (Ideality)^3 &= -2.13554 \\ &= +[0.36648 \times 28.50] - [0.013102 \times 28.50^2] \\ &\quad + [1.40606 \times (10^{-4}) \times 28.50^3] \end{aligned}$$

$$Ideality = \mathbf{0.973}$$

The ideality coefficient for 28.50°C (experimental and DE predicted) should also be between the ideality coefficient for 27.00°C and 30.25°C. This is illustrated in **Table 5-13**.

Table 5-13 - Non-ideal mixing expression (28.50°C) vs other temperatures

Non-ideal mixing expressions (cm <sup>3</sup> /g)		
	Experimental values	DE predicted values
27.00°C	$0.992v_s - v_b$	
28.50°C	$0.977v_s - v_b$	$0.973v_s - v_b$
30.25°C	$0.947v_s - v_b$	

### 5.5.4. Diffusivity results and validation

DE predicted and experimental diffusivity functions (ideal and non-ideal) are shown in **Table 5-14** below. At equal mass fractions ( $\omega_s$ ), the trend of non-ideal diffusivity functions yielding greater diffusion values than ideal diffusivity functions is observed. However, at equal mass fractions ( $\omega_s$ ) the DE predicted diffusivity functions yield greater diffusion values than the experimental diffusivity functions. This was expected given the DE predicted diffusivity gave a higher butane and bitumen height change slope (more diffusion occurring). **Figure 5-44** shows a comparison of all the functions on a graph.

Table 5-14 - Diffusivity results (28.50°C)

	Ideal Diffusivity $\times 10^6$ (cm <sup>2</sup> /s)		Non-ideal Diffusivity $\times 10^6$ (cm <sup>2</sup> /s)	
	Experimental	DE Predicted	Experimental	DE Predicted
<b>28.50°C</b>	$1.160\omega_s + 0.591$	$1.413\omega_s + 0.608$	$1.187\omega_s + 0.598$	$1.452\omega_s + 0.614$

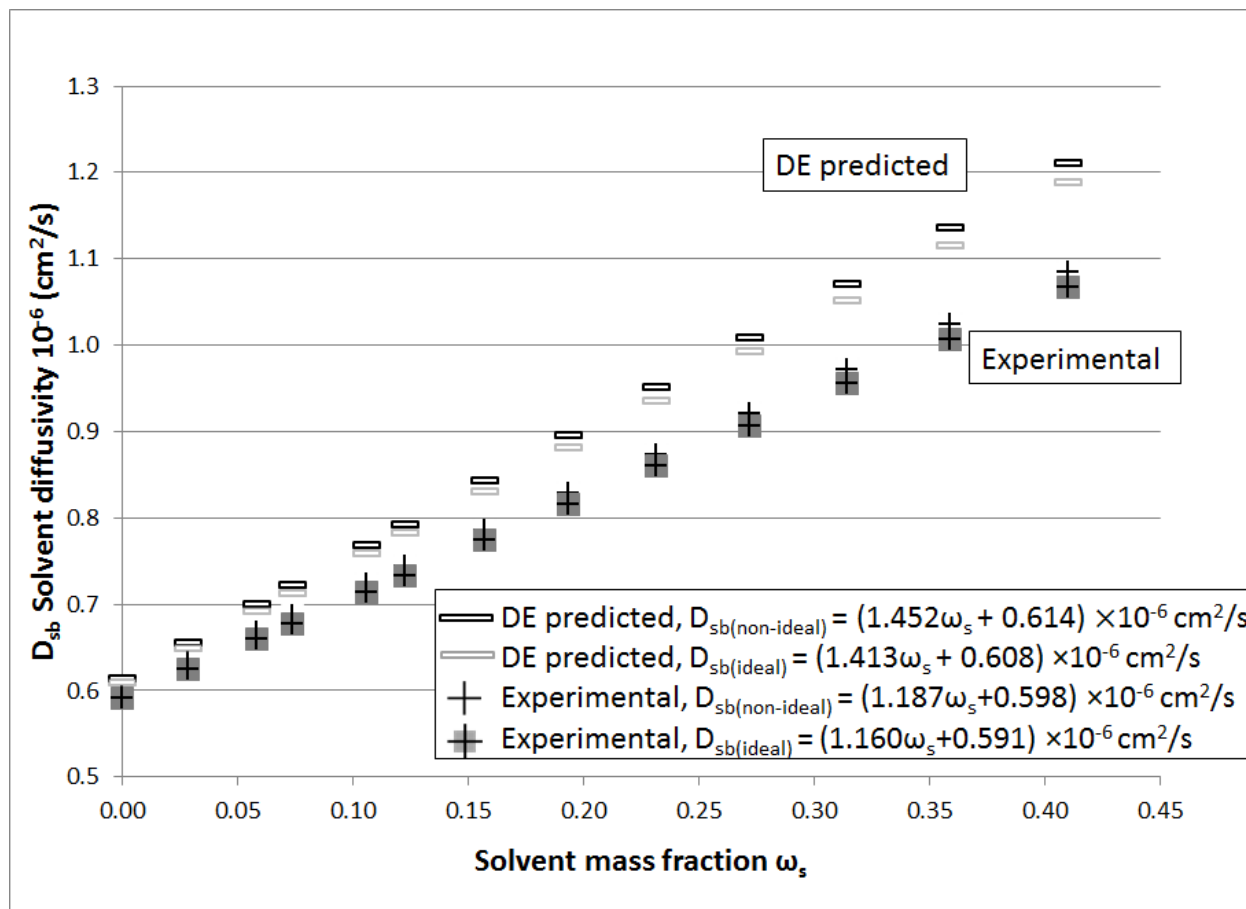


Figure 5-44 - Experimental and DE predicted diffusivity functions 28.50°C (ideal/non-ideal)

The diffusivity function at 28.50°C is expected to be in between the diffusivity function of 27.00°C and 30.25°C for both ideal and non-ideal scenarios. **Figures 5-45, 5-46** and **Table 5-15** show that is the case.

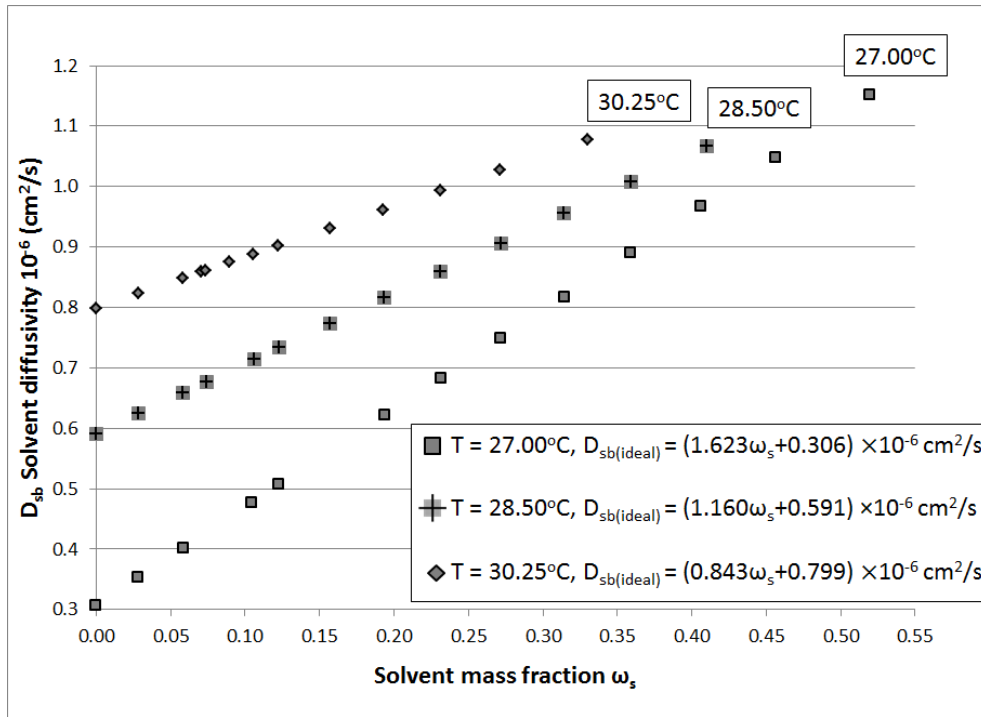


Figure 5-45- Comparison of 28.50°C diffusivity function to other temperature (ideal)

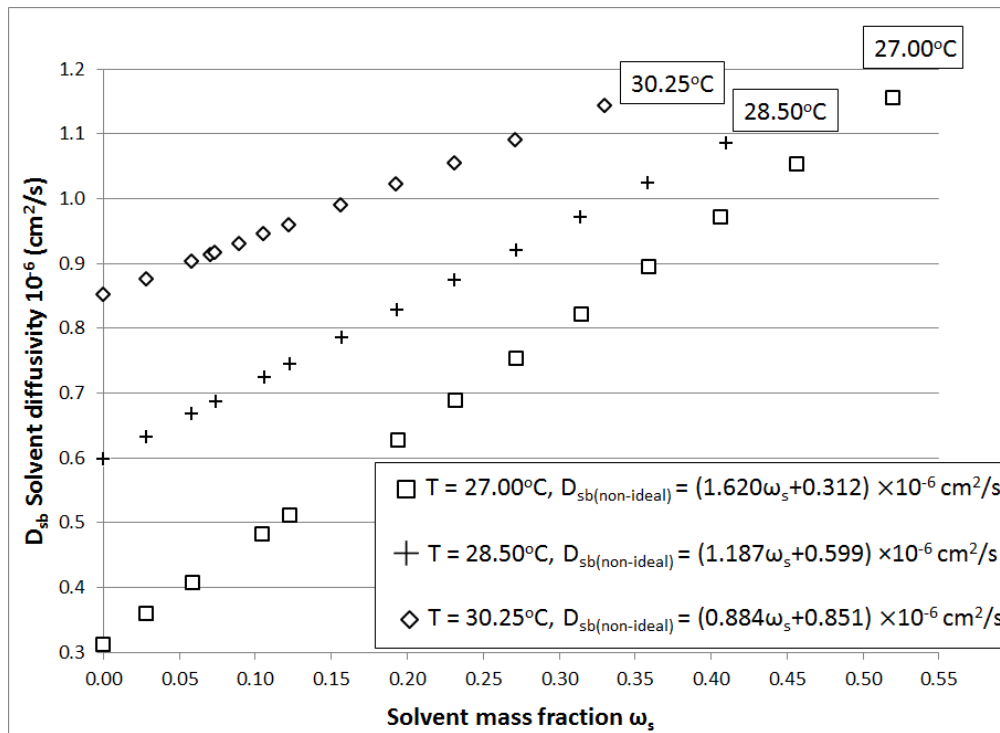


Figure 5-46 - Comparison of 28.50°C diffusivity function to other temperature (non-ideal)

Table 5-15 - Comparison of ideal/non-ideal diffusivity function deviation for 28.50°C

		Ideal and Non-ideal diffusivity function comparisons			
	Temperature (°C)		Diffusivity function	( $\omega_s = 0.15$ ) Diffusivity value $\times 10^6$ (cm <sup>2</sup> /s)	% diff from Ideal values
	27.00	Ideal Diffusivity	$(1.623\omega_s+0.306)\times 10^{-6}$	0.549	
		Non-ideal Diffusivity	$(1.620\omega_s+0.312)\times 10^{-6}$	0.555	1.00
Experimental	28.50	Ideal Diffusivity	$(1.156\omega_s+0.593)\times 10^{-6}$	0.766	
		Non-ideal Diffusivity	$(1.187\omega_s+0.598)\times 10^{-6}$	0.776	1.31
DE predicted	28.50	Ideal Diffusivity	$(1.413\omega_s+0.608)\times 10^{-6}$	0.820	
		Non-ideal Diffusivity	$(1.452\omega_s+0.614)\times 10^{-6}$	0.832	1.44
	30.25	Ideal Diffusivity	$(0.843\omega_s+0.799)\times 10^{-6}$	0.925	
		Non-ideal Diffusivity	$(0.884\omega_s+0.851)\times 10^{-6}$	0.984	6.34

The solvent profile for 28.50°C would also be expected to be wedged in between that of 27.00°C and 30.25°C solvent profiles at the same experimental times. This is confirmed by **Figures 5-47** below. The 28.50°C graph does not completely plateau at solvent mass fraction zero meaning that the flux boundary is partially broken at that temperature.

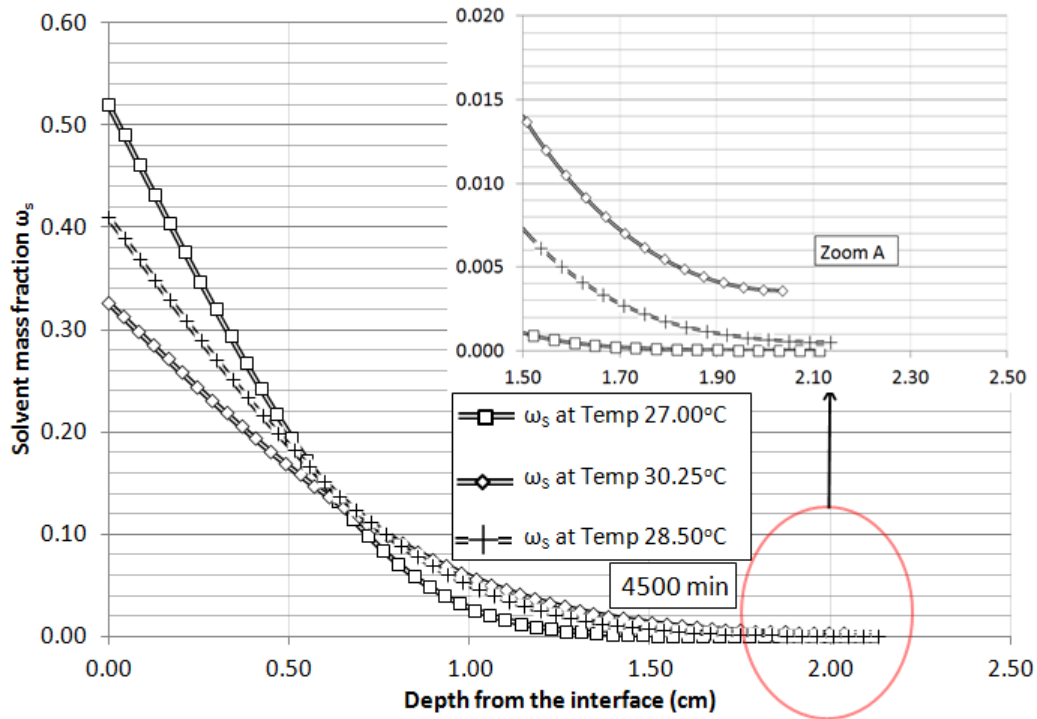


Figure 5-47 - Comparison of 28.50°C solvent profile to other temperatures (non-ideal)

Given the flux boundary for 28.50°C at 4500 minutes is slightly broken, the density profile is expected to plateau slightly below its normal bitumen density temperature (0.99956 g/cm<sup>3</sup>). **Figure 5-48** below shows it plateaus at 0.99917 g/cm<sup>3</sup>.

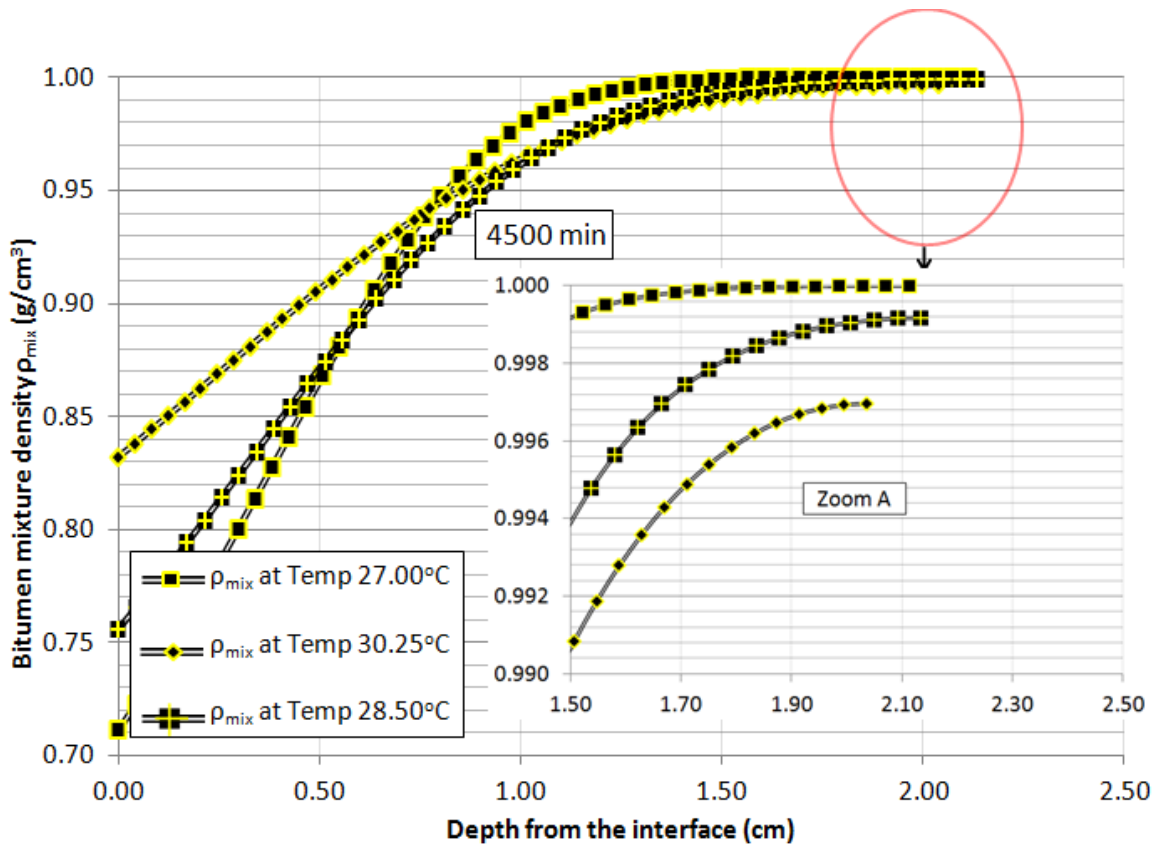


Figure 5-48 - Comparison of 28.50°C density profile to other temperatures (non-ideal)

Finally the diffusivity functions for both experimental are DE predicted diffusivities are validated in both **Figures 5-49** and **5-50**.

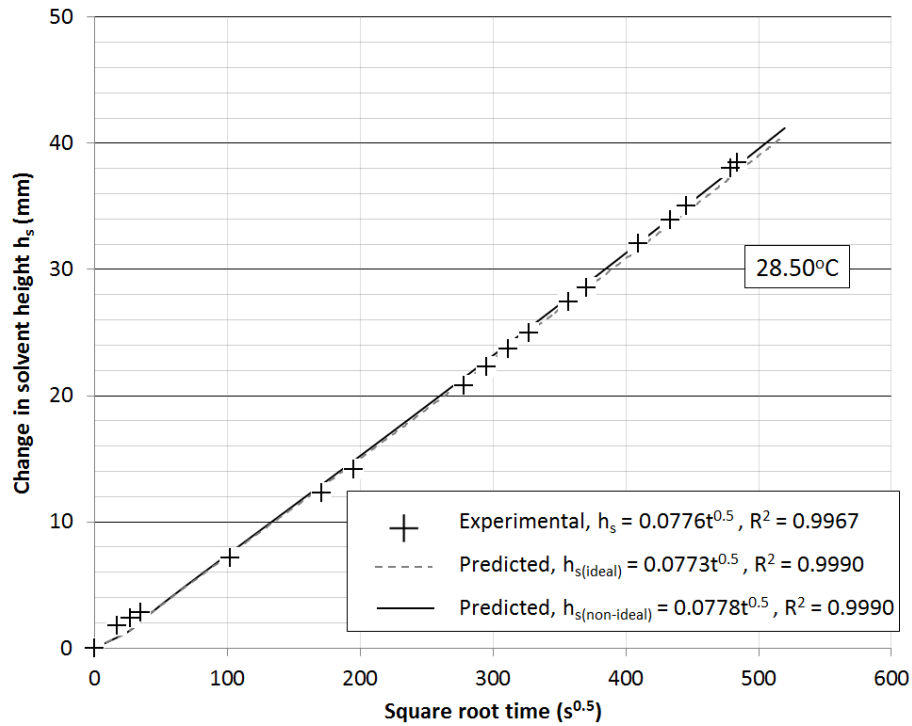


Figure 5-49 - Predicted and experimental change in solvent height vs SRT at  $28.50^\circ\text{C}$

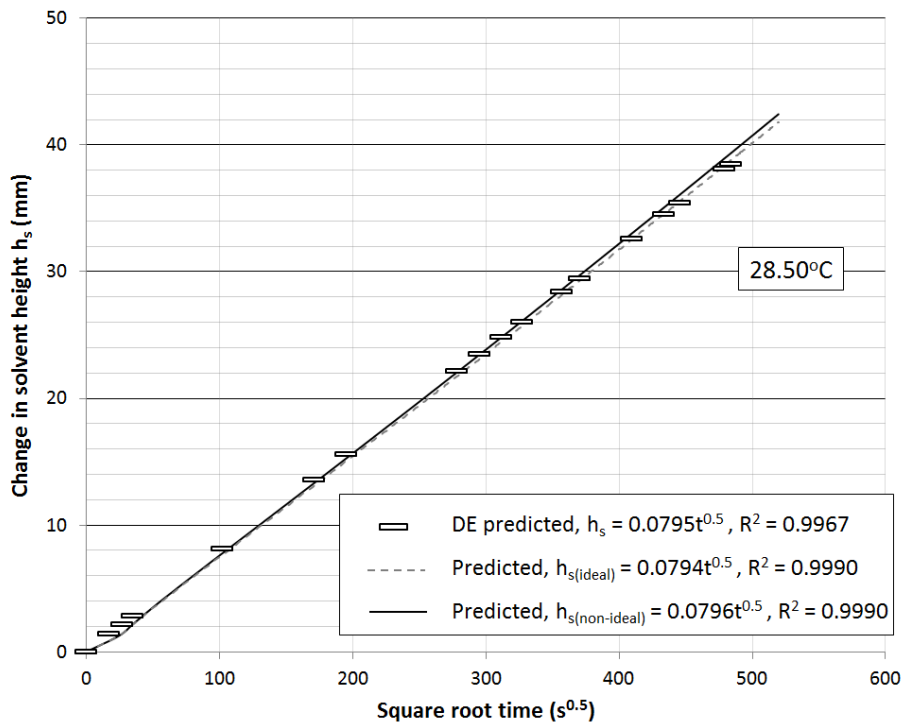


Figure 5-50 - Predicted and DE predicted change in solvent height vs SRT at  $28.50^\circ\text{C}$

## 5.6. Experimental Error

The purpose of this section is to review and analyze the experimental error encountered during the experiment. A major issue was the measurement of bitumen and butane set-up pre and post experiment. The weighing scale used had a precision of  $\pm 0.1$  g but many of the butane and bitumen masses calculated during the experiment had decimal places as low as 0.001 g (especially butane). A higher precision weighing scale would not have been big enough to accommodate the full weight of the butane/bitumen side. A weighing device which was big enough to accommodate the full weight of the butane or bitumen side, while also having high enough precision (0.001 g) was not available. This ultimately led to some inconsistencies while trying to match the final calculated weight of the bitumen mixture to the measured weight of bitumen mixture. Weight values also constantly fluctuated by  $\pm 0.1$  g during weighing. When these fluctuations occurred repeatedly, an average of the two values was taken.

The precision issues experienced while weighing the butane/bitumen masses post experiment prevents us from using those values as a way to confirm diffusivity data. However given the experimental data was independently validated, this is not seen as a problem. Another experimental issue was fluctuations in the bitumen (depending on run) and butane (24.00°C) water bath temperatures. 2 thermocouples were inserted in each water bath to monitor temperature over the duration of the experiment. Temperatures were logged every 5 minutes and **Table 5-16** below show the standard deviation for the temperatures recorded.

Table 5-16 - Standard deviations for temperature logging of all experimental runs

Temperature (°C)	Standard deviation for Butane temperature (°C)		Standard deviation for Bitumen temperature (°C)	
	Thermocouple 1	Thermocouple 2	Thermocouple 1	Thermocouple 2
27.00	0.096	0.110	0.122	0.156
33.50	0.077	0.079	0.077	0.084
36.75	0.068	0.064	0.082	0.083
40.00	0.121	0.127	0.154	0.173
28.50	0.064	0.060	0.073	0.076

Note: 30.25°C was not logged due to some technical difficulties

The standard deviations for the butane thermocouples are always lower than those of the bitumen thermocouples. This is because the butane water bath temperature (24.00°C) is closer to room temperature (25.00°C) compared to the bitumen temperatures (27.00°C - 40.00°C). This means deviations in room temperature do not have as much impact on the Butane water bath compared to the bitumen water bath.

The standard deviation values for the 27.00°C and 40.00°C are all significantly higher than the rest of the experimental runs. Fluctuations in room temperature and having to top-up the recirculatory water bath led to drops in the Plexiglass water bath temperature. This often led to spikes in pressure differential readings before values eventually stabilized. As stated in **Section 4.1**, pressure readings were not taken during this spiking period but error was most certainly incurred as a result of this issue. These spikes trickled down to the validation of the experiment discussed in **Section 5.4.5**.

**Figures 5-51** and **5-52** show a temperature vs time graph at 40.00°C, 36.75°C, 33.50°C and 27.00°C (30.25°C was not available due to technical issues). The data for 33.50°C shows a variation as high as +0.50°C early but mainly stays within ±0.20°C of its expected value. The data for 36.75°C consistently stays within ±0.20°C of its expected value. The data for 27.00°C

also shows one or two heavy temperature fluctuations in **Figure 5-51**. However, 40.00°C gets to a variance of  $\pm 0.50^\circ\text{C}$  on a few occasions. This was because at 40.00°C (highest experimental temperature), the water in the bitumen re-circulatory water bath evaporated at a very high rate making the addition of water multiple times essential. Pressure spikes were witnessed when the water was added. The pressure and temperature variations would have caused error in the recorded butane/bitumen change values and subsequently trickle down to diffusivity functions.

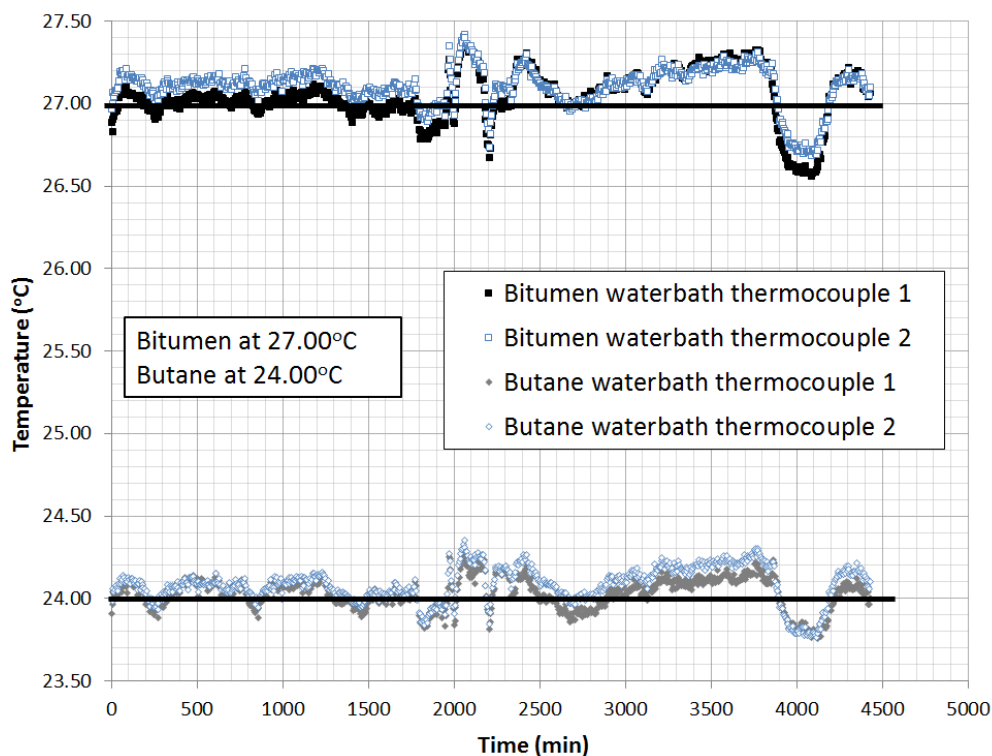


Figure 5-51 - Graph of temperature vs time for experiment (27.00°C bitumen and 24.00°C butane)

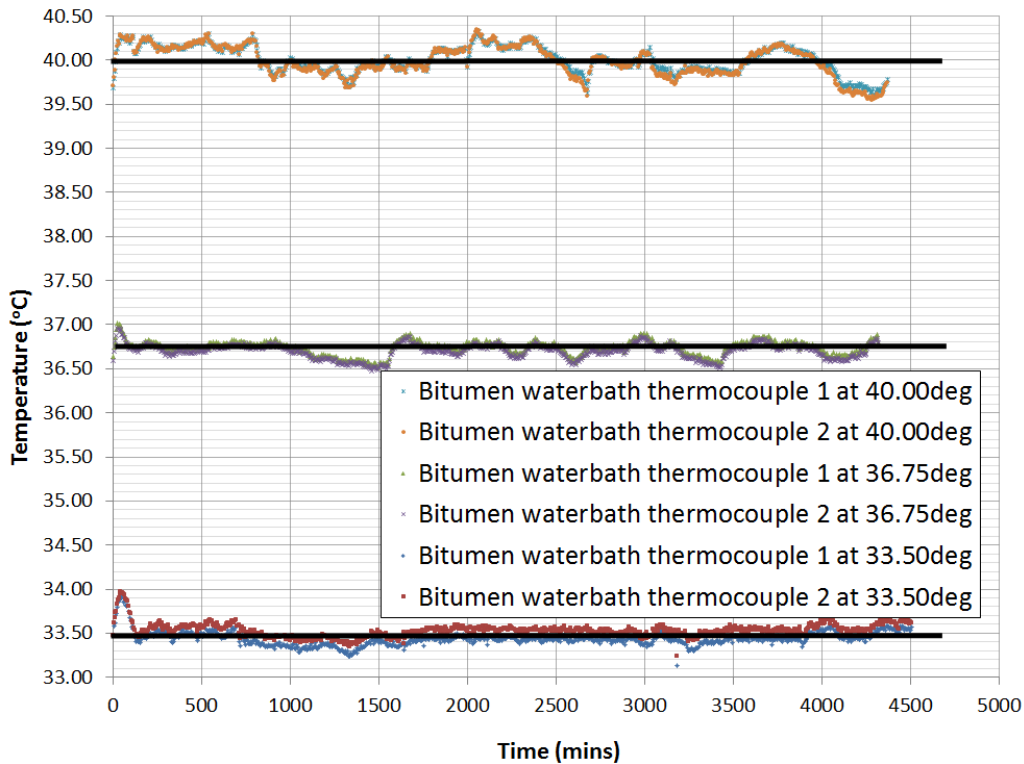


Figure 5-52 - Graph of temperature vs time for experiment (33.50°C, 36.75°C and 40.00°C bitumen)

**Figure 5-53** shows the temperature and differential pressure vs times graph for a typical experimental run (33.50°C). The temperature stays within its expected range. Save for a little spike approximately around time 1500 minutes and 3800 minutes the pressure also declines smoothly through the experiment. However **Figure 5-54** (27.00°C) and **5-55** (40.00°C) show significant pressure spikes. These pressure spikes are also clearly shown to coincide with quick changes in temperature. As can be seen, the circled areas show when the pressure spikes occur and how they always coincide with sudden increases or decreases in temperature. These spikes in pressure during the experiment are the cause of the validation issues for the 27.00°C (partially) and 40.00°C experimental runs.

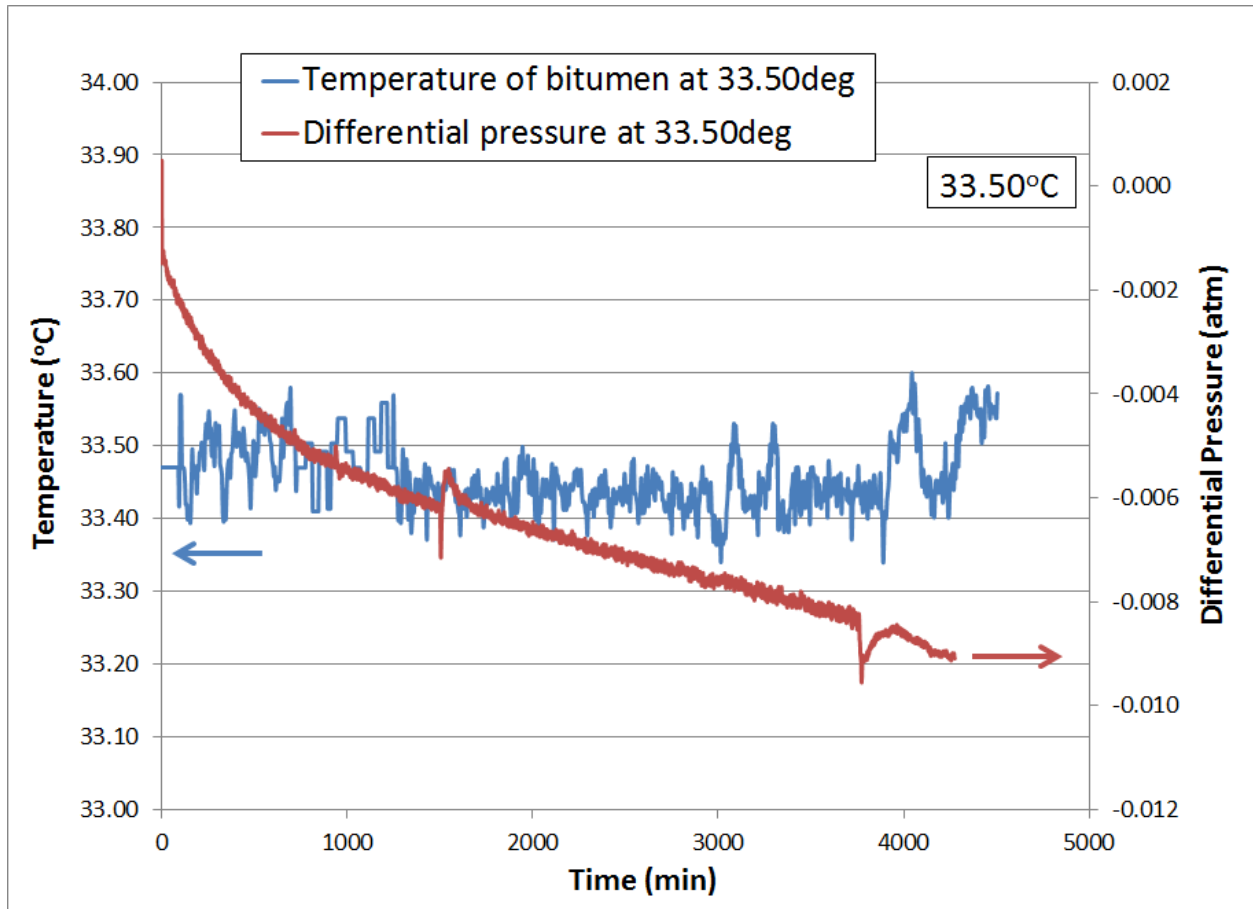


Figure 5-53 - Smooth pressure decline at 33.50°C

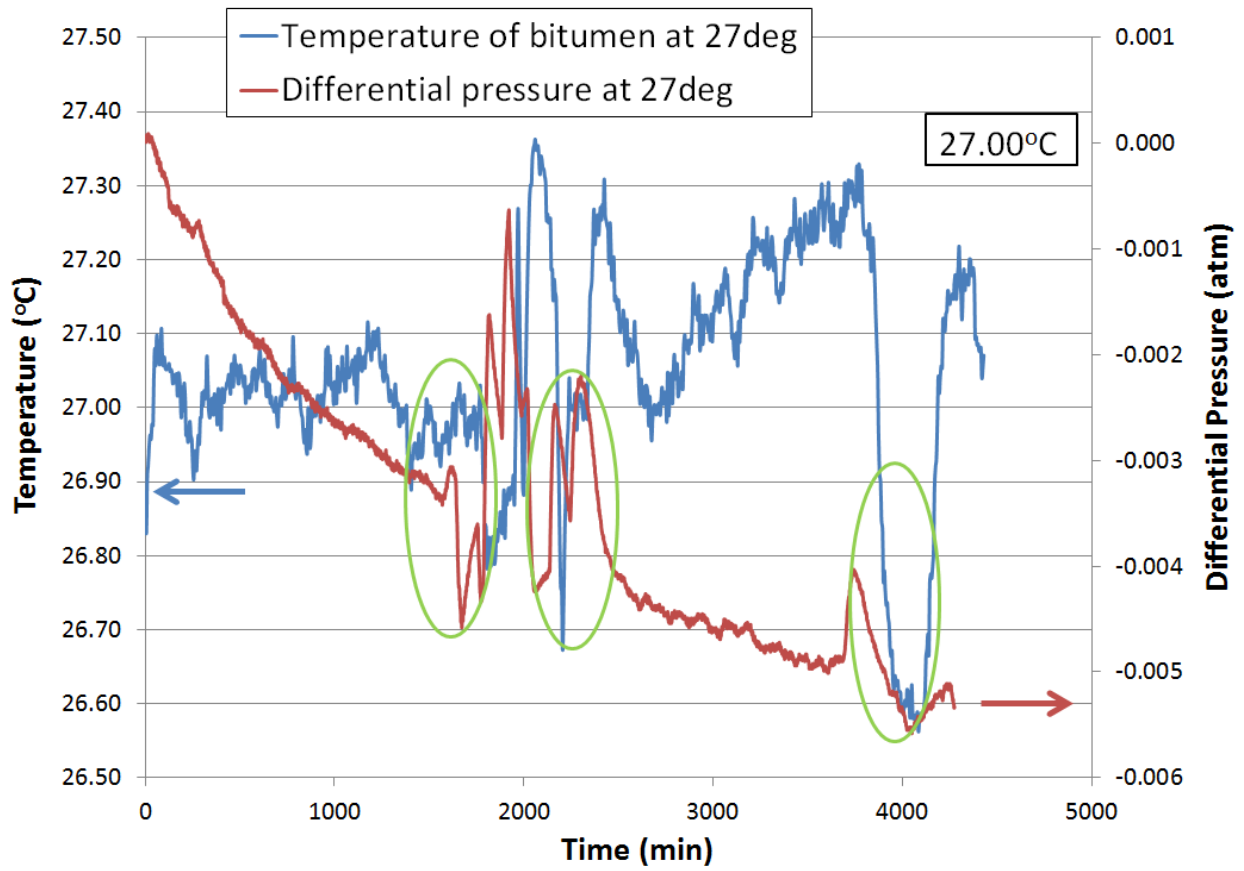


Figure 5-54 - Pressure spikes at 27.00°C

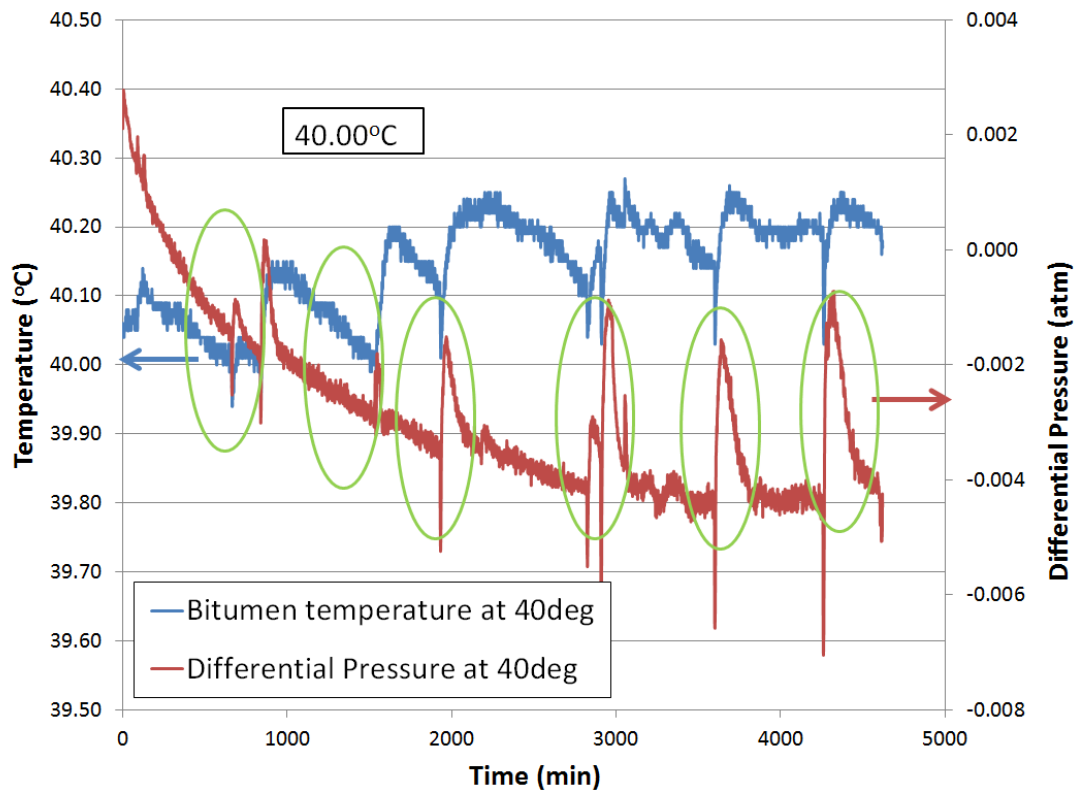


Figure 5-55 - Pressure spikes at 40.00°C

## 6) CONCLUSIONS AND RECOMMENDATIONS

### 6.1. Conclusions

- 1) The assumption of ideal mixing between bitumen and butane solvent over-estimates the density reduction when the fluids mix. Accounting for non-ideal mixing gives more accurate density reduction results
- 2) The deviation between ideal and non-ideal mixing density values increases as temperature increases. This is confirmed by majority of the literature in the field. As temperature tends to standard temperature (25.00°C), the effects of non-ideal mixing become exactly the same as ideal mixing
- 3) Results showed that the diffusion values decreased as temperature increased. In some other literature, diffusion has increased with increasing temperature but those scenarios had the live oil draining from the bitumen mainly with the help of the significant viscosity reduction that higher temperatures bring. Live oil draining allows for fresh new surface (hence higher concentration gradient) which favours more diffusion. This work has no oil draining so diffusion is predominantly governed by solvent solubility in the bitumen. This solvent solubility reduces with increasing system temperature.
- 4) According to literature (Das and Butler 1996, Yazdani and Maini 2009), higher viscosities (from lower temperatures) impede the diffusion process leading lower diffusion values. This effect was felt when comparing the 27.00°C and 30.25°C diffusivity functions. The positive diffusion effects of higher solubility at 27.00°C compared to 30.25°C, could not overcome negative diffusion effects of higher viscosity at 27.00°C compared to 30.25°C until about a mass fraction of 0.5 is reached for 27.00°C.
- 5) At the same mass fraction ( $\omega_s$ ) and temperature, all non-ideal mixing diffusion values were greater than ideal mixing diffusion values. This is because the occurrence of diffusion is driven by concentration gradient between the two fluids. However due to the over-estimation

of density reduction in ideal scenario, that concentration gradient is less for ideal scenario compared to non-ideal. Hence, the assumption of ideal mixing conditions between bitumen and butane by most literature clearly under-estimates diffusion values.

- 6) The deviation between ideal and non-ideal diffusion values also increased as temperature increased. This follows the same trend as the deviation between ideal and non-ideal mixing density results with temperature.
- 7) For all the validation data, the non-ideal diffusivity function always provided a better fit for the experimental data than the ideal diffusivity function. All but one of the diffusivity functions (40.00°C) were independently validated using the macroscopic mass balance to match the solvent growth. The reason for the lack of validation in the 40.00°C run was due to technical issues while running the experiment. The predicted non-ideal mixing values for both these temperatures fits well for the first 2000 minutes of the experiment but not so much for the rest of the experimental time. This lack of fit is more pronounced in 40.00°C than 27.00°C.
- 8) The predicted diffusivity function for 28.50°C obtained from the DE model showed a good fit with the 28.50°C experimental run. The model is therefore a strong model and can be used to predict diffusivity functions of butane at 24.00°C, within a given bitumen temperature range of 27.00°C - 40.00°C, while also accounting for non-ideal mixing and concentration dependency.

## 6.2. Recommendations

- 1) This work accounts for concentration dependency, non-ideal mixing and temperature dependency of diffusivity. However, it does not investigate the effect of pressure dependency on diffusivity. Experiments with varying solvent pressure and bitumen temperature would be useful. Given diffusion values increased with increasing solvent solubility (lower bitumen temperatures) the diffusion values would be expected to increase with if butane solvent vapor pressures values are increased.

- 2) Adding a NCG to the system would also make for interesting observations as current literature suggests that the NCG would hinder diffusion. However experimental run times will have to be significantly longer than those completed in this experiment to ensure detectable diffusion.
  
- 3) Performing experimental runs that allows the solvent to diffuse until equilibrium is reached (diffusion stops) would also give some interesting results. Some of such test runs were performed for these experiments but unfortunately, the solvent diffused through the bitumen and the gel. As minute as this diffusion is, equilibrium could never be reached using the current experimental set-up. Based on information from the test runs, equilibrium at 27.00°C bitumen temperature and 2.36 atm (34.65 psi) butane pressures would have been reached within approximately 14 days. Perhaps researching other intermediate fluids that the solvent does not remotely diffuse into would resolve this issue.

## 7) REFERENCES

Abukhalifeh, H., Lohi, A. and Upreti, S.R. 2009. A novel technique to determine concentration-dependent solvent dispersion in Vapex. *Energies* **2** (4): 851-72.

Alberta Energy. Alberta Energy: Facts and Statistics 2014  
<http://www.energy.gov.ab.ca/OilSands/791.asp>.

Alberta, Energy Resources Conservation Board 2013. Alberta's Energy Reserves 2012 and supply/demand outlook 2013-2022. Calgary, Alberta.

Ayub, M. 2009. The Role of Capillarity in the VAPEX Process. *Petroleum Science and Technology* **27** (10): 1020-32.

Behzadfar, E. and Hatzikiriakos, S. 2014. Diffusivity of CO<sub>2</sub> in Bitumen: Pressure-Decay Measurements Coupled with Rheometry. *Energy & Fuels* **28** (2): 1304-11. doi: 10.1021/ef402392r Washington American Chemical Society.

Bird, R.B., Stewart, W.E. and Lightfoot, E.N. 2002. Transport phenomena. New York: J. Wiley.

Boustani, A and Maini, B. 2001. The Role of Diffusion and Convective Dispersion in Vapour Extraction Process. *Journal of Canadian Petroleum Technology*. Volume 40. Issue 4. DOI 10.2118/01-04-05

Butler, R.M. and Mokrys, I.J. 1991. A New Process (VAPEX) For Recovering Heavy Oils Using Hot Water And Hydrocarbon Vapour. , Calgary, Alberta.

CAPP. Canada's Petroleum Resources - Canadian Association of Petroleum Producers 2014  
<http://www.capp.ca/energySupply/canadaPetroleumResources/Pages/default.aspx>.

Chatzis, I. September 2002. Pore scale phenomena of heavy oil recovery using vapor extraction. *This was presented at the Proceedings: International Symposium of Society of Core Analysts Monterey, CA.*

Chatzis, I., Fredrich, K. and Lohi, A. 2006. Investigation of the Effect of Inert Gas on Production History of Heavy Oil using VAPEX. *Presented at the 57th Annual Canadian International Petroleum Conference*, Calgary, Alberta.

Chordia, Mudit and Trivedi, Japan. 2010. Diffusion in Naturally Fractured Reservoirs- A-Review. Society of Petroleum Engineers

Civan, Faruk and Rasmussen, Maurice. 2001. Accurate Measurement of Gas Diffusivity in Oil and Brine Under Reservoir Conditions. Society of Petroleum Engineers

Cragoe, C.S. 1933. Changes in the Viscosity of Liquids with Temperature, Pressure and Composition. Washington, D.C. World Petroleum Congress.

Cuthiell, D. and Edmunds, N. 2013. Thoughts on Simulating the VAPEX Process. Journal of Canadian Petroleum Technology **52** (03): 192-203.

Cuthiell, D., McCarthy, C., Kissel, G. and Cameron, S. 2006. The Role of Capillarity in VAPEX. Petroleum Society of Canada.

Das, S.K. and Butler, R.M. 1994. Effect of Asphaltene Deposition on the Vapex Process: A Preliminary Investigation Using a Hele-Shaw Cell. The Journal of Canadian Petroleum Technology. **33** (6): 39. Montreal.

Das, S.K. and Butler, R.M. 1996. Diffusion Coefficients of Propane and Butane in Peace River Bitumen. Canadian Journal of Chemical Engineering **74** (6): 985-92.

Deo, M., Nutakki, R. and Orr Jr, F. 1993. Schmidt-Wenzel and Peng-Robinson Equations of State for CO<sub>2</sub>/Hydrocarbon Mixtures: Binary Interaction Parameters and Volume Translation Factors. SPE Advanced Technology Series **1** (2): 142-51. doi: 10.2118/18796-PA Society of Petroleum Engineers.

EIA. U.S. Energy Information Administration (EIA) 2014  
<http://www.eia.gov/countries/cab.cfm?fips=ve>.

EIA. Venezuela - U.S. Energy Information Administration (EIA) 2014  
<http://www.eia.gov/countries/country-data.cfm?fips=VE>.

EIA. Brazil - Analysis - U.S. Energy Information Administration (EIA) 2014  
<http://www.eia.gov/countries/cab.cfm?fips=BR>.

El-Haj, R.E. 2007. Experimental determination of solvent gas dispersion in vapex process. Toronto, Ontario. Digital Commons @ Ryerson.

Etminan, S.R., Maini, B.B. and Chen, Z. 2014. Determination of mass transfer parameters in solvent-based oil recovery techniques using a non-equilibrium boundary condition at the interface. Fuel **120** (1): 218-32.

Etminan, S.R., Haghghat, P., Maini, B.B. and Chen, Z.J. 2011. Molecular Diffusion and Dispersion Coefficient in a Propane-Bitumen System: Case of Vapour Extraction (VAPEX) Process. Vienna, Austria. Society of Petroleum Engineers.

Etminan, S.R., Maini, B., Hassanzadeh, H. and Chen, Z.J. 2009. Determination of Concentration Dependent Diffusivity Coefficient in Solvent Gas Heavy Oil Systems. New Orleans, Louisiana. Society of Petroleum Engineers.

Frauenfeld, T.W., Jossy, C., Bleile, J., Krispin, D. and Ivory, J. 2013. Experimental and Economic Analysis of the Thermal Solvent and Hybrid Solvent Processes. *Journal of Canadian Petroleum Technology* **48** (11): 55-62.

Friedrich, K. 2006. Effects of a non-condensable gas on the Vapex process. M.A.Sc. dissertation, University of Waterloo (Canada), Canada.

Ghanavati, M., Hassanzadeh, H. and Abedi, J. 2014a. Critical review of mutual diffusion coefficient measurements for liquid solvent + bitumen/heavy oil mixtures. *Canadian Journal of Chemical Engineering* **92** (8): 1455-66.

Ghanavati, M., Hassanzadeh, H. and Abedi, J. 2014b. Application of Taylor dispersion technique to measure mutual diffusion coefficient in hexane + bitumen system. *AIC AICHE Journal* **60** (7): 2670-82.

Haghighat, P. and Maini, B.B. 2013. Effect of Temperature on VAPEX Performance. *Journal of Canadian Petroleum Technology* **52** (06).

Haghighat, P., Maini, B.B. and Abedi, J. 2013. Experimental and Numerical Study of VAPEX at Elevated Temperatures. Calgary, Alberta. Society of Petroleum Engineers.

Haskett, W.J. and Brown, P.J. 2005. Evaluation of Unconventional Resource Plays. Dallas, Texas. Society of Petroleum Engineers.

Hayduk, W. and Cheng, S.C. 1971. Review of relation between diffusivity and solvent viscosity in dilute liquid solutions. *Chemical Engineering Science* **26** (5): 635-46.

Hirschfelder, J.O., Curtiss, C.F., Bird, R.B. and University of Wisconsin., Naval Research Laboratory 1954. Molecular theory of gases and liquids. New York: Wiley.

Irani, M. and Gates, I.D. 2013. Understanding the Convection Heat-Transfer Mechanism in Steam-Assisted-Gravity-Drainage Process. *SPE JOURNAL* **18** (6) doi: 10.2118/167258-PA Society of Petroleum Engineers.

James, L. and Chatzis, I. 2005. Core analysis issues in Heavy Oil Recovery using VAPEX. *This paper was prepared for presentation at the International Symposium of the Society of Core Analysts*, Toronto, Canada.

James, L., Chatzis, I. and Spirou, C. 2003. VAPEX Production Rates in Porous Media Models and Solvent Chamber Growth Rate. *Presented at the Proceedings from the Canadian International Petroleum Conference*, Calgary, Alberta.

James, L.A., Rezaei, N. and Chatzis, I. 2007. VAPEX, Warm VAPEX and Hybrid VAPEX - The State of Enhanced Oil Recovery for In Situ Heavy Oils in Canada. **47**. Calgary, Alberta. *Journal of Canadian Petroleum Technology*.

James, L. and Chatzis, I. 2004. Details of gravity drainage of Heavy oil during vapour extraction. *Presented at the International Symposium of the Society of Core Analysts*, Abu Dhabi, UAE.

James, L.A. 2003. A closer look at VAPEX, University of Waterloo [Dept. of Chemical Engineering], Waterloo, Ont.

James, L.A. and Chatzis, I. 2007. Mass Transfer Coefficients in Vapour Extraction (VAPEX). Calgary, Alberta. Society of Petroleum Engineers. Society of Petroleum Engineers.

James, L.A. 2009. Mass transfer mechanisms during the solvent recovery of heavy oil. PHD thesis dissertation, University of Waterloo, Ontario, Ottawa.

Jiang, Q. 1997. Recovery of heavy oil and bitumen using vapex process in homogeneous and heterogenous reservoirs. PHD dissertation dissertation, University of Calgary, Alberta.

Landau, H.G. 1950. Heat Conduction in a Melting Solid. Quarterly of Applied Mathematics. Page 81-94

David Law. A New Heavy Oil Recovery Technology to Maximize Performance and to Maximize Performance and Minimize Environmental Impact 2014 <http://www.spe.org/dl/docs/2011/Law.pdf>.

Leahy-Dios, A. and Firoozabadi, A. 2007. A Unified Model for Diffusion Coefficient Prediction in Non-Ideal Petroleum Fluids. Society of Petroleum Engineers.

Lobe, V.M. 1973. A model for the viscosity of liquid-liquid mixtures. Masters of Science dissertation, University of Rochester.

Lunn, S. 2013. Water Use in Canada's Oil-Sands Industry: The Facts. doi: 10.2118/156676-PA Society of Petroleum Engineers.

Luo, H. and Kantzas, A. 2008. Investigation of diffusion coefficients of heavy oil and hydrocarbon solvent systems in porous media. *Presented at the SPE Symposium on Improved Oil Recovery*. Tulsa, Oklahoma, April 2008

Morrow, A.W., Mukhametshina, A., Aleksandrov, D. and Hascakir, B. 2014. Environmental Impact of Bitumen Extraction with Thermal Recovery. Society of Petroleum Engineers.

Mukhametshina, A., Morrow, A.W., Aleksandrov, D. and Hascakir, B. 2014. Evaluation of Four Thermal Recovery Methods for Bitumen Extraction. Society of Petroleum Engineers.

Nasr, T.N. and Ayodele, O.R. 2005. Thermal Techniques for the Recovery of Heavy Oil and Bitumen. *Presented at the Fourth SPE International Improved Oil Recovery Conference in Asia Pacific (IIORC 2005)*, Kuala Lumpur, Malaysia.

Nenniger, J.E. and Dunn, S.G. 2008. How Fast is Solvent Based Gravity Drainage? Petroleum Society of Canada.

Okazawa, T. 2009. Impact of concentration-dependence of diffusion coefficient on VAPEX drainage rates. *Journal of Canadian Petroleum Technology* **48** (2): 47-54.

Peng, D.Y. and Robinson, D.B. 1976. A New Two-Constant Equation of State. *Industrial & Engineering Chemistry Fundamentals* **15** (1): 59-64.

Rajnauth, J. 2012. Is It Time to Focus on Unconventional Resources? Society of Petroleum Engineers.

Rezaei, N., Mohammadzadeh, O., James, L.A. and Chatzis, I. 2014. Experimental Investigation of the VAPEX Process in Vuggy Porous Media. *SPE Journal* **19** (01): 101-8.

Riazi, M.R. 1996. A new method for experimental measurement of diffusion coefficients in reservoir fluids. *Journal of Petroleum Science and Engineering* **14** (3-4): 235-50. doi: [http://dx.doi.org.qe2a-proxy.mun.ca/10.1016/0920-4105\(95\)00035-6](http://dx.doi.org.qe2a-proxy.mun.ca/10.1016/0920-4105(95)00035-6).

Saryazdi, F., Motahhari, H., Schoeggl, F.F., Taylor, S.D. and Yarranton, H.W. 2013. Density of Hydrocarbon Mixtures and Bitumen Diluted with Solvents and Dissolved Gases. *Energy & Fuels* **27** (7): 3666-78.

Schramm, L.L., Kramers, J.W. and Isaacs, E.E. 2010. Saskatchewan's Place in Canadian Oil Sands. *Journal of Canadian Petroleum Technology* **49** (11): 12-21.

Shu, W.R. 1984. A Viscosity Correlation for Mixtures of Heavy Oil, Bitumen, and Petroleum Fractions. doi: 10.2118/11280-PA Society of Petroleum Engineers.

Speight, J.G. .2013a. Heavy oil production processes. In . Oxford; Waltham, MA: Gulf Professional Publishing. <http://library.books24x7.com/toc.aspx?bookid=50964>.

Speight, J.G. .2013b. Oil sand production processes. In . Oxford; Waltham, MA: Gulf Professional Publishing. <http://library.books24x7.com/toc.aspx?bookid=50965>.

Stickler, A. 2009. Economic Comparison of In Situ Tar Sands Extraction Technologies: N-Solv and Steam Assisted Gravity Drainage. *Presented at the Presented to 2nd Annual Global Petroleum Conference*, Stampede Park, Calgary, Alberta.

Tharanivasan, A.K., Yang, C. and Gu, Y. 2006. Measurements of Molecular Diffusion Coefficients of Carbon Dioxide, Methane, and Propane in Heavy Oil under Reservoir Conditions. *Energy and Fuels* **20** (6): 2509-17.

Upreti, S.R., Lohi, A., Kapadia, R.A. and El-Haj, R. 2007. Vapor Extraction of Heavy Oil and Bitumen: A Review. *Energy and Fuels* **21** (3): 1562-74.

Upreti, S.R. and Mehrotra, A.K. 2002. Diffusivity of CO<sub>2</sub>, CH<sub>4</sub>, C<sub>2</sub>H<sub>6</sub> and N<sub>2</sub> in Athabasca bitumen. The Canadian Journal of Chemical Engineering **80** (1): 116-25. doi: 10.1002/cjce.5450800112 Hoboken Wiley Subscription Services, Inc., A Wiley Company.

USGS. Related Petroleum Studies, USGS (U.S. Geological Survey) -ERP (Energy Resources Program) 2014 <http://energy.cr.usgs.gov/oilgas/addoilgas/>.

Vargas-Vasquez, S. and Romero-Zeran, L.B. 2007. The Vapor Extraction Process: Review. Petroleum Science and Technology **25** (11): 1447-63. doi: 10.1080/10916460500528979 Taylor & Francis.

Vassilellis, G.D. 2009. Roadmap To Monetization Of Unconventional Resources. Society of Petroleum Engineers.

Wen, Y., Bryan, J. and Kantzas, A. 2013. Estimation of Diffusion Coefficients in Bitumen Solvent Mixtures as Derived From Low Field NMR Spectra. Journal of Canadian Petroleum Technology **44** (04).

Wen, Y., Bryan, J. and Kantzas, A. 2003. Evaluation of Bitumen-Solvent Properties Using Low Field NMR. Petroleum Society of Canada.

Wen, Y. and Kantzas, A. 2006. Evaluation of Heavy Oil/Bitumen- Solvent Mixture Viscosity Models. doi: 10.2118/06-04-04 Petroleum Society of Canada.

Wen, Y. and Kantzas, A. 2004. Evaluation of Heavy Oil/Bitumen-Solvent Mixture Viscosity Models. Petroleum Society of Canada.

Wen, Y., Kantzas, A. and Wang, G.J. 2004. Estimation of Diffusion Coefficients in Bitumen Solvent Mixtures Using X-Ray CAT Scanning and Low Field NMR. Petroleum Society of Canada.

Yang, C. and Gu, Y. 2006. A New Method for Measuring Solvent Diffusivity in Heavy Oil by Dynamic Pendant Drop Shape Analysis (DPDSA). Society of Petroleum Engineers Journal **11** (1): 48-57.

Yang, C. and Gu, Y. 2003. A New Method for Measuring Solvent Diffusivity in Heavy Oil by Dynamic Pendant Drop Shape Analysis (DPDSA). Society of Petroleum Engineers doi: 10.2118/84202-MS.

Yang, C. and Gu, Y. 2005. Effects of Heavy Oil-Solvent Interfacial Tension on Gravity Drainage in the vapor extraction (VAPEX) Process. Society of Petroleum Engineers.

Yazdani, A. and Maini, B. 2009. The effective diffusion/dispersion coefficient in vapor extraction of heavy oil. Petroleum Science and Technology **27** (8): 817-35.

Yazdani, A. and Maini, B.B. 2010. Measurements and Modelling of Phase Behaviour and Viscosity of a Heavy Oil/Butane System. doi: 10.2118/132484-PA Society of Petroleum Engineers.

Y. Yildirim. Application of Vapex (Vapour extraction) process on Carbonate reservoirs  
<http://etd.lib.metu.edu.tr/upload/3/1206366/index.pdf>.

Zhang, Y.P., Hyndman, C.L. and Maini, B.B. 2000. Measurement of gas diffusivity in heavy oils. *Journal of Petroleum Science and Engineering* **25** (1-2): 37-47.

# **APPENDIX**

## **APPENDIX A - Bitumen assay characteristics**

### **Bitumen Analysis**

<b>Temperature</b>	<b>Density</b>
15°C	1.012 g/ml
22°C	1.001 g/ml
40°C	0.997 g/ml
70°C	0.978 g/ml

### **Fractions (SAPA analysis by ARC)**

Saturates = 22.4 mass%

Aromatics = 30.8 mass%

Polars = 29.4 mass%

Asphaltenes = 17.4 mass%

Notes: Since the fractions are solubility classes not compounds this analysis is only useful when comparing fractions separated in the same manner – it is not comparable to SARA. Asphaltenes are precipitated first with the addition of excess pentane.

### **Carbon-Hydrogen-Nitrogen-Sulphur**

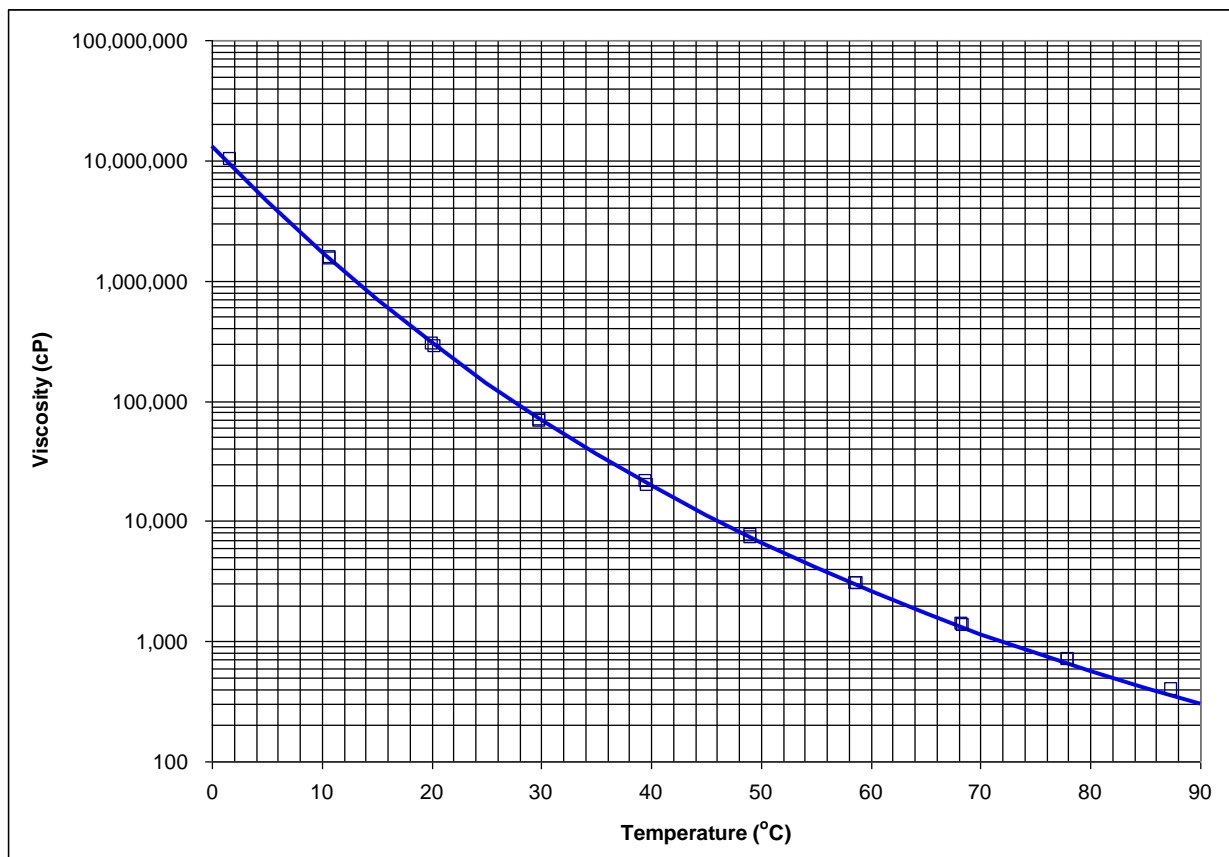
Carbon = 83.62 mass% (ASTM D5291)

Hydrogen = 9.57 mass% (ASTM D5291)

Nitrogen = 0.39 mass% (ASTM D5291)

Sulphur = 5.25 mass% (ASTM D1552)

**Molecular Weight = 557 g/mol (ASTM D2503)**



Appendix - A1: Viscosity correlations

Appendix - A2: Bitumen Assay

<b>Component</b>		<b>Boiling Point (°C)</b>	<b>Normalized Weight Percent</b>	<b>Cumulative Weight Percent</b>
< Octane	≤C7	≤98	0.0	0.0
Octane	C8	126	0.0	0.0
Nonane	C9	151	0.0	0.0
Decane	C10	174	0.0	0.0
Undecane	C11	196	0.7	0.7
Dodecane	C12	216	1.0	1.7
Tridecane	C13	235	1.3	3.0
Tetradecane	C14	254	1.6	4.6
Pentadecane	C15	271	1.8	6.4
Hexadecane	C16	287	1.9	8.3
Heptadecane	C17	302	2.1	10.4
Octadecane	C18	316	2.3	12.7
Eicosane	C20	344	4.8	17.5
Docosane	C22	369	4.5	22.0
Tetracosane	C24	391	4.4	26.4
Hexacosane	C26	412	4.0	30.4
Octacosane	C28	431	4.1	34.5
triacontane	C30	449	4.0	38.5
Dotriacontane	C32	466	3.3	41.8
Tetratriacontane	C34	481	2.9	44.7
Hexatriacontane	C36	496	2.7	47.4
Octatriacontane	C38	509	2.5	49.9
Tetracontane	C40	522	2.4	52.3
Dotetracontane	C42	534	2.0	54.3
Tetratetracontane	C44	545	1.9	56.2
Hexatetracontane	C46	556	1.8	58.0
Octatetracontane	C48	566	1.6	59.6
Pentacontane	C50	575	1.5	61.1
Dopentacontane	C52	584	1.5	62.6
Tetrapentacontane	C54	592	1.3	63.9
Hexapentacontane	C56	600	1.3	65.2
Octapentacontane	C58	608	1.3	66.5

Hexacontane	C60	615	1.2	67.7
Dohexacontane	C62	622	1.2	68.9
Tetrahexacontane	C64	629	1.3	70.2
Hexahexacontane	C66	635	1.1	71.3
Octahexacontane	C68	641	1.2	72.5
Heptacontane	C70	647	1.2	73.7
Doheptacontane	C72	653	1.3	75.0
Tetraheptacontane	C74	658	1.1	76.1
Hexaheptacontane	C76	664	1.2	77.3
Octaheptacontane	C78	670	1.1	78.4
Octacontane	C80	675	1.1	79.5
Dooctacontane	C82	681	1.1	80.6
Tetraoctacontane	C84	686	1.0	81.6
Hexaoctacontane	C86	691	1.1	82.7
Octaoctacontane(C88)	C88	695	0.9	83.6
Nonacontane	C90	700	1.0	84.6
Dononacontane	C92	704	0.9	85.5
Tetranonacontane	C94	708	0.9	86.4
Hexanonacontane	C96	712	0.8	87.2
Octanonacontane	C98	716	0.9	88.1
Hectane	C100	720	0.9	89.0
Hectane +	C100+	> 720	10.4	99.4

## APPENDIX B - Troubleshooting

### Non ideality

Normally when measuring diffusion in VAPEX systems, the bitumen height change is used to measure the progression of the experiment. This change signifies the amount of butane that has diffused into the bitumen. However, both butane and bitumen are hydrocarbons and do not mix ideally. Still, difficulty with taking in-situ measurements makes it extremely hard to account for ideality.

A differential pressure transmitter was used with the following specifications;

- Model PD-33X pressure transmitter

- Range: 1.4503 psi differential
- Accuracy:  $\pm 7.25 * 10^{-4} \text{psi} + 7.25 * 10^{-5} \frac{\text{psi}}{\text{psi static line pressure}}$
- Max static line pressure: 725 psi
- Resolution:  $2.9 * 10^{-5}$  psi

One side of the transmitter accounts for butane gas pressure and the other side accounts for butane gas pressure plus bitumen liquid pressure. The difference is the hydrostatic pressure of bitumen which is dependent on bitumen height where  $P = \Delta \rho gh$ .

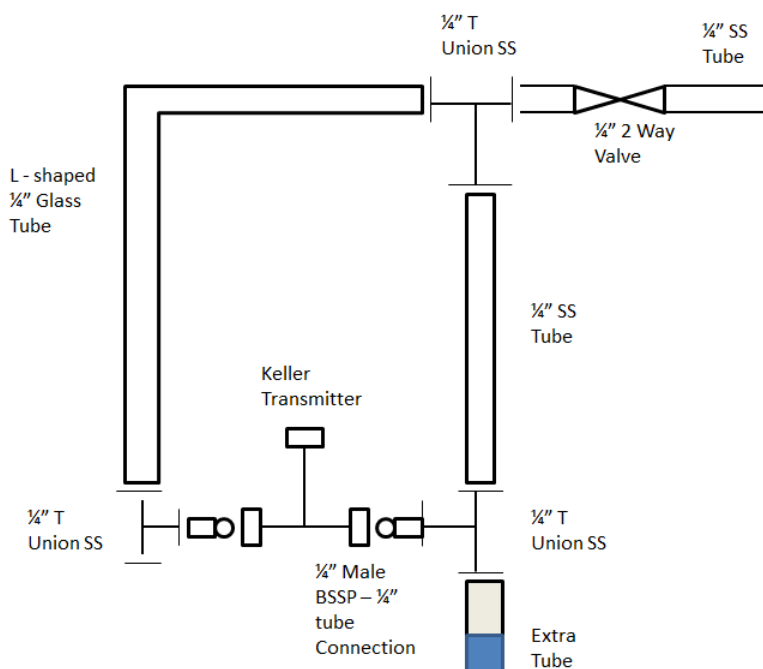
With consistent logging of pressure and bitumen height values, the bitumen phase density can be calculated (which are non-ideal values) and used to validate the amount of butane diffused into the bitumen. A normal pressure transmitter cannot be used because the pressure changes observed are too small (1-10 Pa or 0.000145 psi over a few minutes). Most available pressure transmitters today do not possess such high precision.

It is best not to let bitumen come in contact with the diaphragm of the differential pressure transmitter. The bitumen is extremely sticky and will create a mess on the diaphragm and possibly damage it. An intermediate fluid is therefore necessary between the bitumen and the differential pressure transmitter diaphragm. It is recommended that such a fluid must have a higher density than the bitumen to ensure it holds it up. It must be largely inert and fully capable of transmitting pressure values from the bitumen through to the transmitter. Also the fluid should have a low enough viscosity to flow while loading it but high viscosity to maintain its shape integrity through the experiment. Colgate toothpaste was used in this experiment.

## Monitoring the butane

Initially the plan was to install a differential transmitter under the butane as well. The butane height pressure would be measured and with the constant density, height values can be logged into the computer system as often as every second.

Unfortunately, as seen the below set-up **Appendix - B3** the system requires two sides immersed in the same water. As a result, there will always be condensation in the opposite side of the set-up leading to erroneous butane height values. Multiple runs showed that there was always condensed butane liquid in the extra tube side. An easy fix could be to use a normal pressure transmitter (leading to just the one end needed) but again pressure transmitters with the needed precision are hardly available given the miniscule pressure changes that will be observed.



Appendix - B3: Two sided butane set-up

Utilizing a heating coil around the second side is not feasible either as this creates a temperature gradient in the water. There could be a valve closing the other side but this defeats the whole purpose of the differential pressure transmitters as gas needs to get to the negative side of the transmitter.

All these issues led to the use of an L-shape tube for the butane with no pressure transmitter connected to it. The height of the butane is easily monitored with the cathetometer. The butane

height decreases during the experiment but the density does not change, leaving little to worry about ideality wise.

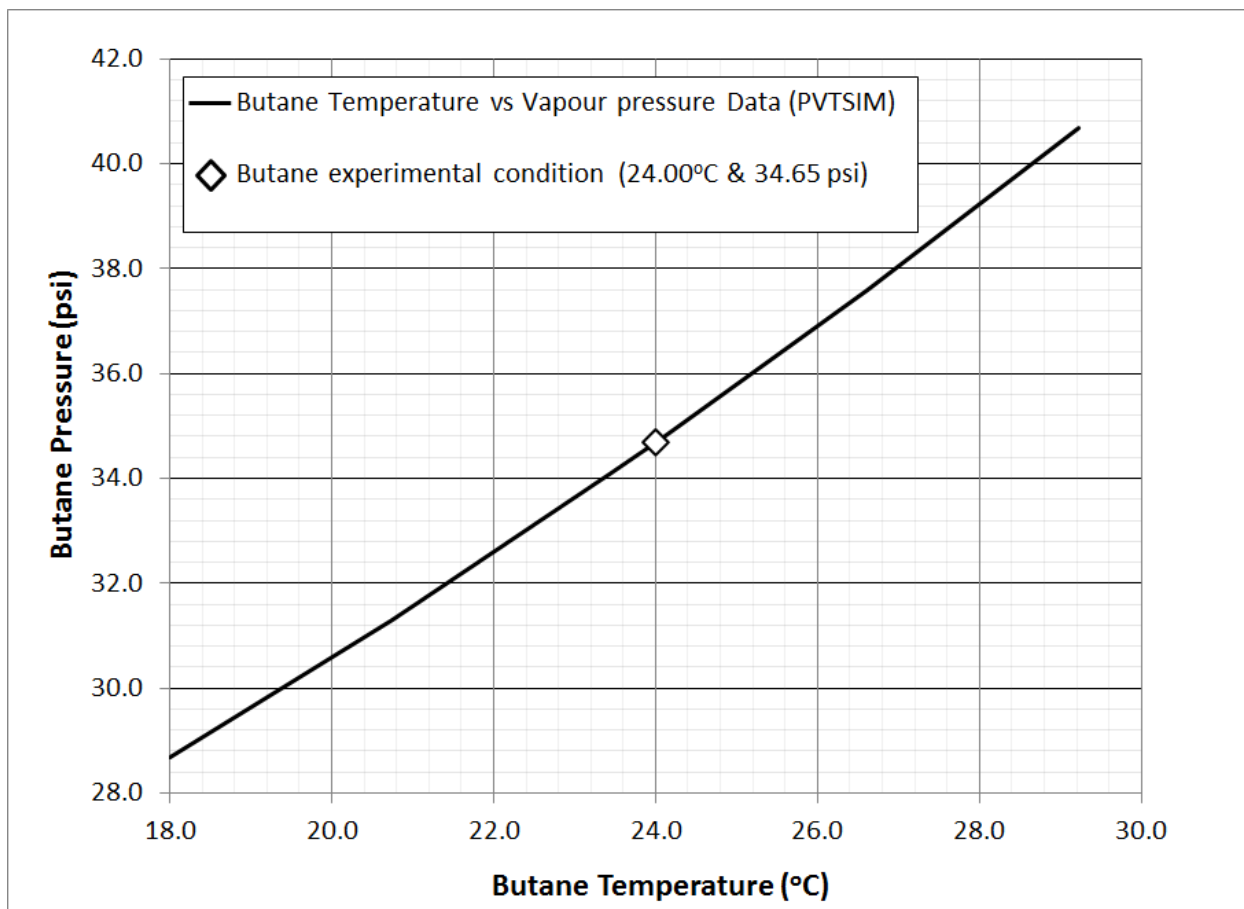
## Purity of butane

When VAPEX was first being considered, the thought was to add non-condensable gas (NCG) to reduce the amount of expensive pure solvent being used and reduces the chances of solvent condensation due to the elevated pressure that the NCG provides. However, a reduction in solvent (butane) purity leads to a reduction of the butane solubility of the butane in the bitumen. This is because solubility is a function of the partial pressure of the diffusing gas component and not total pressure of the gas mixture. This leads to significantly less diffusion occurring and given how slow the diffusion is under the best conditions, this leads to extremely low values (2-3 mm) of bitumen height change over as much as a week. Such miniscule values are almost impossible to track even with the best equipment. The solubility of the solvent in the bitumen is a function of the partial pressure of the solvent and not total gas mixture pressure.

It is therefore advisable to keep purity levels of butane high to ensure that significant and clearly detectable diffusion occurs, preferably purity values that give a solubility of 80% and above.

## Butane vapor pressure vs. bitumen temperature

The partial pressure of the butane and the bitumen temperature are the two most important parameters affecting diffusion as they are both directly responsible for the solubility of the butane in the bitumen. The butane vapor pressure is a function of the butane temperature, the higher the temperature, the higher the vapor pressure (**Appendix – B4**) and resulting solubility. The bitumen temperature works conversely because as it increases, butane solubility in bitumen decreases and so does the diffusion



Appendix - B4: PVTsim butane solvent temperature vs vapour pressure graph

The bitumen temperature must be kept greater than the butane temperature (if the partial pressure is equal to the vapour pressure) or the butane will condense on any surface at a temperature less than the butane liquid temperature. In fact it is advisable to have the bitumen system at least 3°C higher to ensure no condensation occurs. Also, the middle region of the experimental set-up (space between the Plexiglass water baths) is kept a 3°C higher to avoid condensation.

One would assume that varying the butane and bitumen temperatures over a certain range (always at least 3°C difference between both) and obtaining subsequent diffusion coefficient values would create a good correlation of diffusion at varying conditions. However, the solubility problem is once again an obstacle at moderately low butane temperatures and

moderately high bitumen temperatures. The solubility of the solvents is just too low to effectively track changing bitumen height and therefore diffusivity.

It is advisable to maximise the butane temperature, keep it constant through the experiment and vary bitumen value (minimum value being 3°C higher than the butane temperature). Getting as many thermocouple wires to measure temperature at various parts of the experiment will help a great deal.

### Bitumen and gel interaction

Given the slight compressibility of the gel used (toothpaste), the interface between the bitumen and gel goes down briefly at the start of the experiment. It is imperative to keep track of this to ensure correct values for bitumen height. The gel fluid height has to be visible in the glass tube to ensure the changing interface is visible. The bitumen falling does stain the walls of the glass tube but butane pressure later ensures all the bitumen on the walls goes into the liquid making a clear readable height.

Creating a vacuum in the bitumen also pulls up the bitumen giving false bitumen height but after half an hour of the experiment running, the bitumen height starts to clear up and be readable with meniscus stains on the glass walls.

The gel provides a huge advantage when transitioning from one experimental run to the other. The system is constantly required to be air tight, so always having to dismantle the set and re-tighten would be extremely tedious; especially given the system is a combination of steel and glass parts (the glass could easily break on tightening). The experimental set-up does not need to be washed either, all that is needed is the bitumen glass tube taken out, gel topped up (since some gel is taken out with the glass tube), a new glass tube used and bitumen loaded. Preliminary runs were executed to see if the gel held its structure during and after experimental runs. The gel always held its structure. The butane is completely emptied out between experimental runs and loaded with fresh pure butane.

## APPENDIX C - Starting experimental values

Appendix - C5: Starting experimental parameters

		27.00°C		30.25°C		33.50°C		36.75°C		40.00°C		28.50°C
		Sample 1	Sample 2	Sample 1								
Butane Solvent	Density in butane tube (g/cm <sup>3</sup> )	0.565	0.565	0.565	0.565	0.565	0.565	0.565	0.565	0.565	0.565	0.565
	Density in bitumen tube (g/cm <sup>3</sup> )	0.561	0.561	0.557	0.557	0.553	0.553	0.549	0.549	0.545	0.545	0.559
	**Area of tube (cm <sup>2</sup> )	0.083	0.083	0.112	0.112	0.112	0.112	0.112	0.112	0.112	0.112	0.950
Bitumen	Starting measured mass (g)	1.90	2.10	1.95	2.15	2.40	2.30	2.40	2.15	2.20	2.30	2.15
	Density (g/cm <sup>3</sup> )	1.000	1.000	0.999	0.999	0.998	0.998	0.998	0.998	0.997	0.997	1.000
	Area of tube (cm <sup>2</sup> )	1.207	1.207	1.207	1.207	1.207	1.207	1.207	1.207	1.207	1.207	1.207

\*\*Note: 27.00°C and 28.50°C experiments were the last two runs and tubes used differed from previous due to availability of solvent tubing

## APPENDIX D - Bitumen/Butane density and pressure calculations

### Non-ideal mixture density

Shown below in **Appendix – D6** is table used to calculate non-ideal density/real density, real specific volume and equivalent mass over a certain time period for the experiment. The highlighted row is used in our sample calculation.

Appendix - D6: Sample calculation for non-ideal density

Column Number	1	2	3	4	5	6	7	8	9	10	11	12	13
	Given Time	Minutes	Diff pressure (atm)	Diff Pressure (Pa)	ΔPressure (Pa)	Real Pressure (Pa)	Bitumen Height (cm)	Full Hydrostatic Height (cm)	Δ Bitumen Height (cm)	Δ Bitumen Density (g/cm <sup>3</sup> )	Real bitumen density (g/cm <sup>3</sup> )	Real bitumen specific volume (cm <sup>3</sup> /g)	Real Mass Bitumen (g)
DAY 1	7pm	0	0.00019	19	0	0	1.6169	6.4169	0.0000	0.000	0.999	1.001	1.950
	7.30pm	30	0.00016	16	-3	0	1.6245	6.4245	0.0076	-0.001	0.998	1.002	1.957
	8pm	60	-0.00001	-1	-20	-1	1.6320	6.4320	0.0151	-0.002	0.997	1.003	1.964
	9pm	120	-0.00029	-29	-49	-3	1.6434	6.4434	0.0265	-0.004	0.996	1.004	1.975
	10pm	180	-0.00056	-57	-76	-5	1.6510	6.4510	0.0341	-0.004	0.995	1.005	1.982
	11pm	240	-0.00093	-94	-113	-8	1.6586	6.4586	0.0417	-0.005	0.994	1.006	1.990
	12am	300	-0.00111	-112	-132	-9	1.6661	6.4661	0.0492	-0.006	0.993	1.007	1.997
	6am	660	-0.00222	-225	-244	-17	1.6964	6.4964	0.0795	-0.010	0.989	1.011	2.026

Time is given in minutes (column 2) and every value is calculated until the end of the experiment (4320 minutes). Given that the starting experimental time (column 1) is 7pm and the sample calculation time is at 6am, the time elapsed in minutes is 660 minutes.

Diff pressure (column 3) represents the differential pressure reading on the Keller transmitter at the given time (-0.00222 atm). The value is converted to Pascals (column 4) using the factor below.

$$Pressure (Pa) = Pressure(atm) * 101325 \quad A-1$$

$$-0.00222 * 101325 = -225 Pa$$

Column 3 shows a reduction in differential pressure values as the experiment progresses. One would expect differential pressure values to increase given bitumen height increase as time proceeds. But the increase in bitumen height is more than offset by the reduction in bitumen density due to diffusion of the butane solvent.

At every given time, the differential pressure reading, represents the hydrostatic pressure of the full liquid (butane dissolved, bitumen and gel). However, the differential pressure transmitter is zero'd at the start of the experiment and we assume the butane does not dissolve in the gel.

Therefore, any changes in hydrostatic pressure are a result of the butane diffusing into the bitumen. We then consistently subtract the differential pressure readings at every time point from the starting differential pressure reading at 0 minutes. This gives us the pressure change/ $\Delta$  pressure (column 5) experienced due to swelling of bitumen from diffusion of butane.

$$\Delta \text{ Pressure} = \text{Pressure (at time } t) - \text{Pressure (at time } 0) \quad \text{A-1}$$

$$-224.94 - (19.25) = -\mathbf{244 \text{ Pa}}$$

The Keller differential transmitters used has a different calibration from real pressure values. These readings have to be normalized to give real pressure values. The reduction factor for both transmitters (used in the above table) was calculated to be 0.0708. The value is multiplied by the  $\Delta$  pressure value to give real pressure values (column 6).

$$\text{Real pressure value} = \Delta \text{ Pressure} * \text{reduction factor} \quad \text{A-2}$$

$$-244.19 * 0.0708 = -\mathbf{17 \text{ Pa}}$$

The next column is the bitumen height (column 7) at the given time. This value is calculated from the images from the camera. They are analyzed in Paint software using pixel numbers (explained in **Section 4.2**). The full hydrostatic height (**6.4964 cm** column 8) is the full height of the liquid in the system (bitumen liquid + gel). This directly correlates to pressure differential values in the transmitter. Given the gel height (4.8 cm) is assumed constant, the only changes in this column are a result of bitumen height changes.

The  $\Delta$  height (column 9) is the difference in height between bitumen at any given time and initial bitumen height at time zero minutes. Given starting bitumen height is 1.6169 cm:

$$\Delta \text{ height} = \text{height (at time } t) - \text{height (at time } 0) \quad \text{A-3}$$

$$\Delta \text{ height} = 1.6964 - 1.6169$$

$$= \mathbf{0.0795 \text{ cm}}$$

The change in bitumen density or  $\Delta$  density, (in column 10) represents the change in density due to the hydrostatic pressure change and increase in bitumen height. This is calculated by:

$$P_1 = \rho_1 g h_1 \quad \text{A-4}$$

$$P_2 = \rho_2 g h_2 \quad \text{A-5}$$

Subtracting both sides from each other,

$$P_1 - P_2 = \rho_1 g h_1 - \rho_2 g h_2$$

$$\frac{P_1 - P_2}{g} = \rho_1 h_1 - \rho_2 h_2 ,$$

Knowing that  $(\rho_2 = \rho_1 + \Delta\rho)$  and  $(h_2 = h_1 + \Delta h)$  we get,

$$\frac{P_1 - P_2}{g} = \rho_1 h_1 - [(\rho_1 + \Delta\rho)(h_1 + \Delta h)]$$

$$\frac{P_1 - P_2}{g} = \rho_1 h_1 - (\rho_1 h_1 + \rho_1 \Delta h + \Delta\rho h_1 + \Delta\rho \Delta h)$$

$$\frac{P_1 - P_2}{g} = \rho_1 h_1 - \rho_1 h_1 - \rho_1 \Delta h - \Delta\rho h_1 - \Delta\rho \Delta h$$

$$\frac{P_1 - P_2}{g} = -\rho_1 \Delta h - \Delta\rho h_1 - \Delta\rho \Delta h$$

$$\frac{P_1 - P_2}{g} = -\rho_1 \Delta h - \Delta\rho (h_1 + \Delta h)$$

$$\Delta\rho = \left( \frac{1}{h_1 + \Delta h} \right) \left[ -\rho_1 \Delta h - \left( \frac{P_1 - P_2}{g} \right) \right] \quad \text{A-6}$$

Where,  $h_1$  = hydrostatic height of the gel and bitumen at time 0 minutes (6.4169 cm)

$\Delta h$  = height change at given time (0.0795 cm)

$\rho_1$  = initial bitumen density at time 0 minutes (0.999 g/cm<sup>3</sup>)

$g$  = acceleration due to gravity (981 cm/s<sup>2</sup>)

$P_1 - P_2$  = real differential pressure change at given time (-17.29 Pa)

$\Delta\rho$  = Changing density values. Note that the toothpaste density is not used because it is assumed to remain constant while bitumen density changes due to the diffusion. Also the differential transmitter is zero'd at the start of experiment so any pressure change is solely due to changing bitumen density

$$\Delta\rho = \left( \frac{1}{6.4169 \text{ cm} + 0.0795 \text{ cm}} \right) [(-0.999 \text{ gcm}^{-3} * 0.0795 \text{ cm}) - \left( \frac{-17.29 \text{ Pa}}{981 \text{ cm/s}^2} \right)]$$

$$\Delta\rho = -\mathbf{0.010 \text{ gcm}^{-3}}$$

Column 11 is the real or non-ideal density of the bitumen mixture at time 't'. This bitumen mixture density is given as the addition of  $\Delta\rho$  at time (t) and Bitumen mixture density at time (t=0):

$$\textit{Real bitumen mixture density} = \Delta\rho + \textit{Bitumen mixture density (t = 0)}$$

$$\rho_{mix (non-ideal)} = \Delta\rho + \rho_B \quad \text{A-7}$$

$$-0.010 + 0.999 = \mathbf{0.989 \text{ gcm}^{-3}}$$

Column 12 is the real or non-ideal specific volume of the bitumen mixture at time 't'. This bitumen mixture is given as the inverse if the real bitumen mixture density:

$$\textit{Real bitumen mixture specific volume} = \frac{1}{\textit{Real bitumen mixture density}}$$

$$v_{mix (non-ideal)} = \frac{1}{\rho_{mix (non-ideal)}} \quad \text{A-8}$$

$$\frac{1}{0.990} = \mathbf{1.011 \text{ cm}^3 \text{g}^{-1}}$$

Column 13 is the mass of the bitumen phase at the given time. This is calculated by multiplying the density, cross sectional area of the bitumen tube and height of bitumen.

$$\text{Mass} = \text{Area} * (\text{bitumen height}) * \rho$$

A-9

$$1.207 \text{ cm}^2 * (1.6964 \text{ cm}) * 0.989 \text{ gcm}^{-3} = \mathbf{2.026 \text{ g}}$$

### Ideal mixture density

**Appendix - D7** for this section covers the way to calculate ideal density of the bitumen. Column 13 is the mass at time  $t$  for the non-ideal bitumen scenario

Appendix - D7: Sample calculations for ideal density

13	14	15	16	17	18	19	20	21	22
Real Mass Bitumen (g)	$\Delta$ Butane heighty (cm)	Area butane tube (cm <sup>2</sup> )	Volume butane diffused (cm <sup>3</sup> )	Moles butane diffused	Mass butane diffused (g)	Mass fraction butane ( $\omega_s$ )	Mole fraction butane $w_s$	Ideal bitumen Mixture density (g/cm <sup>3</sup> )	Ideal bitumen specific volume (cm <sup>3</sup> /g)
1.950	0.0000	0.112	0.000	0.000	0.000	0.000	0.000	0.999	1.001
1.957	0.1360	0.112	0.015	0.000	0.009	0.004	0.041	0.997	1.003
1.964	0.2230	0.112	0.025	0.000	0.014	0.007	0.065	0.996	1.004
1.975	0.3620	0.112	0.041	0.000	0.023	0.012	0.101	0.994	1.006
1.982	0.4680	0.112	0.052	0.001	0.030	0.015	0.127	0.993	1.008
1.990	0.5650	0.112	0.063	0.001	0.036	0.018	0.150	0.991	1.009
1.997	0.6540	0.112	0.073	0.001	0.041	0.021	0.169	0.990	1.010
2.026	1.0700	0.112	0.120	0.001	0.068	0.034	0.250	0.984	1.016

The next value (**1.0700** cm in column 14) is the height change of the butane at time  $t$  compared to time 0 minutes. The cross sectional area of the butane tube (column 15) comes next and is calculated as:

$$\text{Cross sectional Area of butane tube} = \pi r^2$$

A-10

$$\text{Cross sectional Area of butane tube } A_S = \pi * (0.189 \text{ cm})^2$$

$$A_S = \mathbf{0.112 \text{ cm}^2}$$

This area is multiplied by the change in butane height to get the volume of butane liquid (column 16) that has been converted to vapor and diffused into the bitumen in that time frame.

$$\text{Volume of butane } V_S = \text{Area} * \text{height} \quad \text{A-11}$$

$$\text{Volume of butane } V_S = 0.112 \text{ cm}^2 * 1.0700 \text{ cm}$$

$$\text{Volume of butane } V_S = \mathbf{0.120 \text{ cm}^3}$$

The next two columns compute the moles (column 17) and mass of butane (column 18) contained in the above volume. The number of butane is obtained by dividing volume of butane lost (butane diffused into bitumen) by molar volume of butane at butane temperature (24.00°C). The molar volume of butane (102.87 cm<sup>3</sup>/mol) at 24.00°C is obtained from PVTsim. The mass is obtained by multiplying volume of butane lost (butane diffused into bitumen) by density of butane at butane temperature (24.00°C). The density of butane (0.565 g/cm<sup>3</sup>) at 24.00°C is also obtained from PVTsim.

$$\# \text{ of butane moles} = \frac{\text{Volume}}{\text{Molar volume}} \quad \text{A-12}$$

$$\# \text{ of butane moles} = \frac{0.1200 \text{ cm}^3}{102.87 \text{ cm}^3/\text{mol}}$$

$$\# \text{ of butane moles} = \mathbf{0.001 \text{ mols}}$$

$$\text{Mass} = \text{Volume} * \text{density} \quad \text{A-13}$$

$$\text{Mass} = 0.12 \text{ cm}^3 * 0.565 \text{ gcm}^{-3}$$

$$\text{Mass} = \mathbf{0.068 \text{ g}}$$

The butane mass fraction/concentration  $\omega_s$  (column 19) becomes the above calculated mass of butane divided by the sum of mass of butane and starting experimental mass of bitumen.

$$\text{Mass fraction } \omega_s = \frac{\text{butane mass}}{\text{butane mass} + \text{bitumen mass}} \quad \text{A-14}$$

$$\text{Mass fraction } \omega_s = \frac{0.068 \text{ g}}{0.068 \text{ g} + 1.95 \text{ g}}$$

$$\text{Mass fraction } \omega_s = \mathbf{0.034}$$

Similarly, the butane mole fraction  $\omega_s$  (column 20) becomes the above calculated moles of butane divided by the sum of moles of butane and starting experimental moles of bitumen.

$$\text{Mole fraction} = \frac{\text{\# of butane moles}}{\text{\# of butane mole} + \text{\# of bitumen mole}} \quad \text{A-15}$$

$$\text{mole fraction} = \frac{0.0012}{0.0012 + 0.0035}$$

$$\text{mole fraction} = \mathbf{0.250}$$

The ideal bitumen mixture density (column 21) of the bitumen and butane is computed as follows:

*Ideal mixture density*

$$= (\text{Butane density} * \text{Butane mass fraction}) + (\text{Bitumen density} * \text{Bitumen mass fraction})$$

$$\rho_{\text{mix}(\text{ideal})} = (\rho_s * \omega_s) + (\rho_B * (1 - \omega_s)) \quad \text{A-16}$$

$$\begin{aligned} \rho_{\text{mix}(\text{ideal})} &= (0.557 \text{ g cm}^{-3} * 0.034) + (0.999 \text{ g cm}^{-3} * (1 - 0.034)) \\ &= \mathbf{0.984 \text{ g cm}^{-3}} \end{aligned}$$

Finally, the ideal bitumen mixture specific volume (column 22) is computed as:

$$\text{Ideal bitumen specific volume} = \frac{1}{\text{Ideal mixture density}}$$

$$v_{\text{mix}(\text{ideal})} = \frac{1}{\rho_{\text{mix}(\text{ideal})}} \quad \text{A-17}$$

$$\frac{1}{0.984} = 1.016 \text{ cm}^3 \text{ g}^{-1}$$

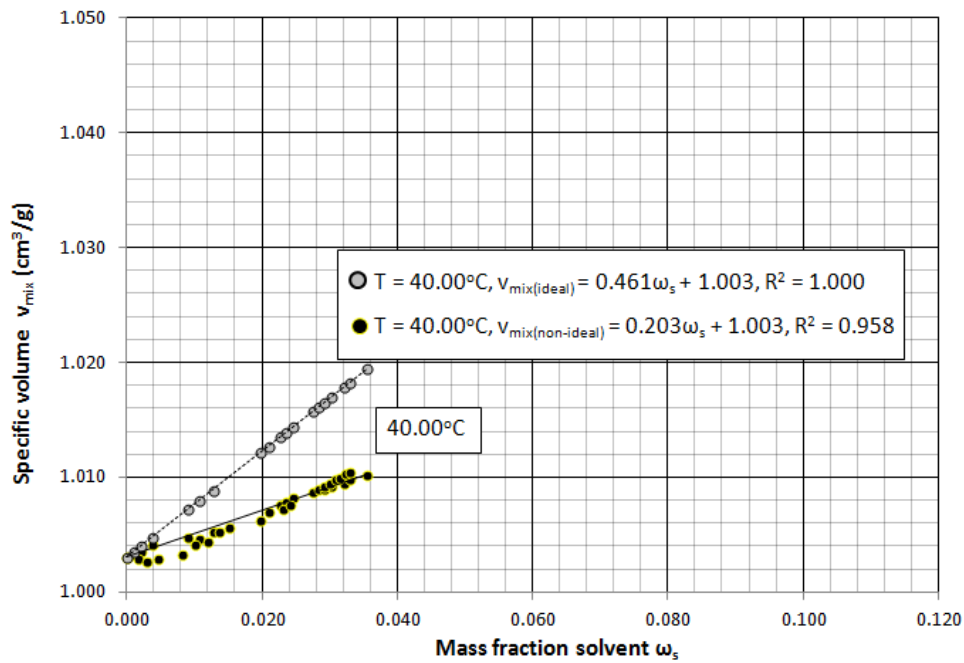
Note: All values from column 11 (real mixture density  $\rho_{\text{mix}}$ ), column 12 (real mixture specific volume  $v_{\text{mix}}$ ), column 19 (solvent mass fraction  $\omega_s$ ), column 21 (ideal mixture density  $\rho_{\text{mix(ideal)}}$ ) and column 22 (ideal mixture specific volume  $v_{\text{mix(ideal)}}$ ) are later used to plot graphs applied in **Section 4.3.2** and **5.3**

## APPENDIX E - Bitumen height analysis table

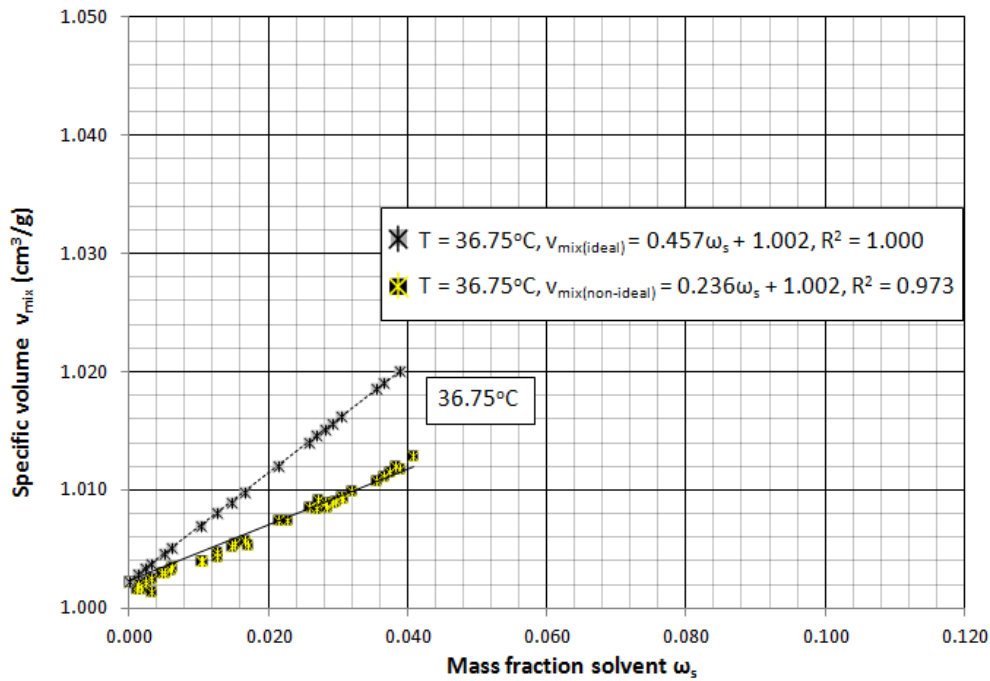
Appendix - E8: Bitumen height analysis

		Bitumen initial height analysis			
		Height analysis using bitumen mass values (cm)	Height analysis using scaling of bitumen height (cm)	Average value (cm)	Value used (cm)
27.00°C	Sample 1	1.5743	1.5743	1.5743	1.5743
	Sample 2	1.7410	1.7390	1.7400	1.7400
30.25°C	Sample 1	1.6169	1.6169	1.6169	1.6169
	Sample 2	1.8657	1.8657	1.8657	1.8657
33.50°C	Sample 1	1.9915	1.9915	1.9915	1.9915
	Sample 2	1.9082	1.9088	1.9085	1.9085
36.75°C	Sample 1	1.9930	1.9928	1.9929	1.9929
	Sample 2	1.7853	1.7853	1.7853	1.7853
40.00°C	Sample 1	1.8282	1.8282	1.8282	1.8282
	Sample 2	1.9111	1.9115	1.9113	1.9113

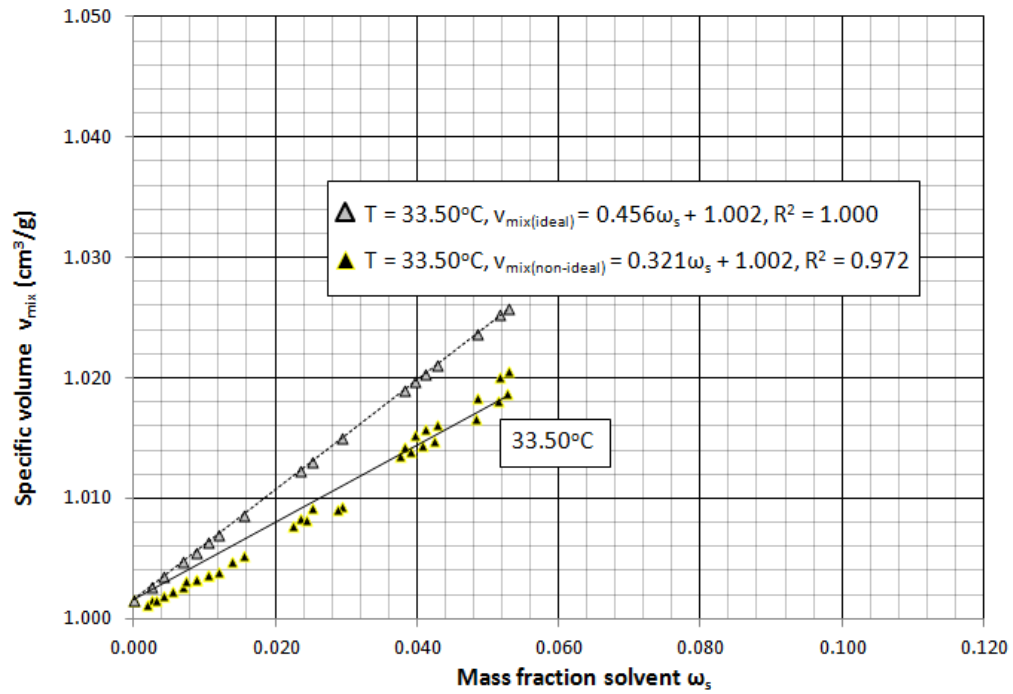
## APPENDIX F - Specific volume graphs (all temperatures)



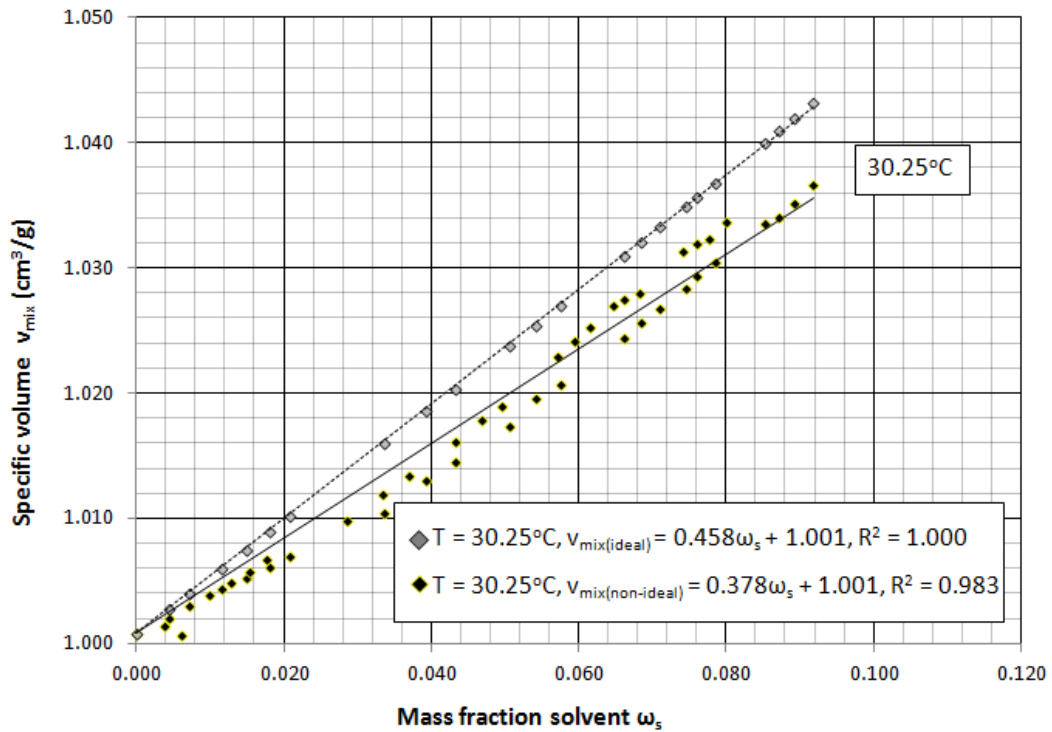
Appendix - F9: Bitumen mixture specific volume plots for ideal and non-ideal mixing 40.00°C



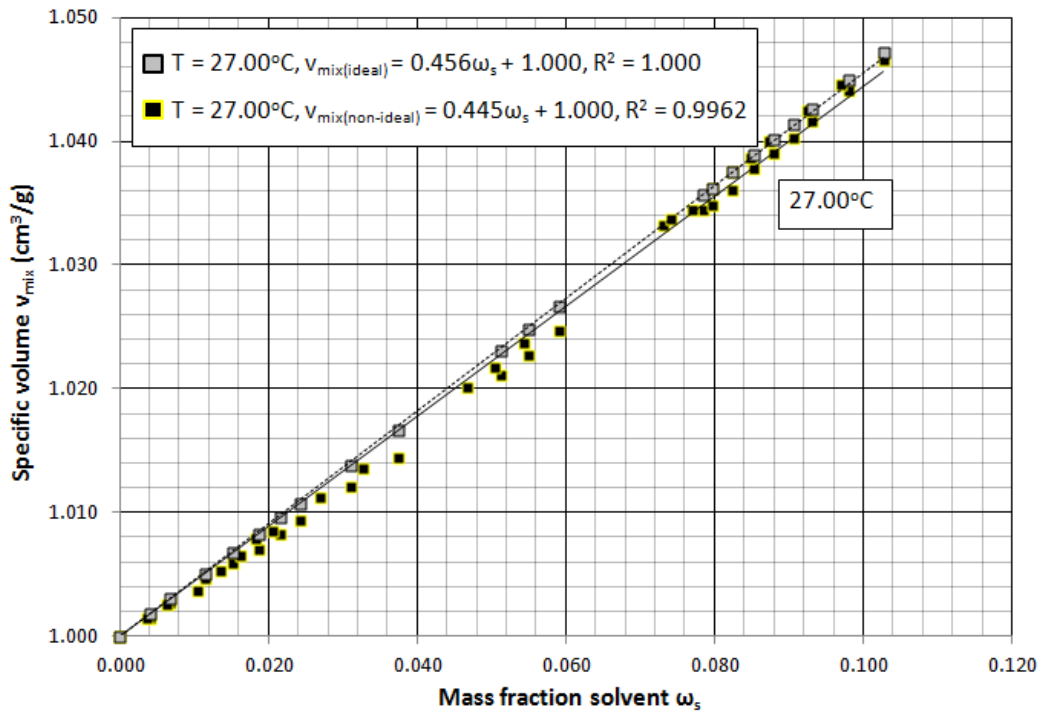
Appendix - F10: Bitumen mixture specific volume plots for ideal and non-ideal mixing 36.75°C



Appendix - F11: Bitumen mixture specific volume plots for ideal and non-ideal mixing 33.50°C



Appendix - F12: Bitumen mixture specific volume plots for ideal and non-ideal mixing 30.25°C



Appendix - F13: Bitumen mixture specific volume plots for ideal and non-ideal mixing  $27.00^\circ\text{C}$

## APPENDIX G - Butane/Bitumen changes as function of time calculations

### Butane

The real start time is found by using the equation of the ( $t \neq 0$ ) trendline. For  $27.00^\circ\text{C}$ , that equation is,

$$y = 0.0097t^{0.5} - 0.3517$$

A-18

Where (0.0097) is the slope of the graph and (-0.3517) is the y-intercept of the graph. The SRT start time (x-intercept from **Table 5-1**) can be found by equating y to zero and finding  $t^{0.5}$ ,

$$0 = 0.0097t^{0.5} - 0.3517$$

$$0.3517 = 0.0097t^{0.5}$$

$$\frac{0.3517}{0.0097} = t^{0.5}$$

$$t^{0.5} = 36.26s^{0.5}$$

This value is directly subtracted from all 27.00°C SRT experimental values to give a trendline that will pass through zero. Other corresponding x-intercept values for other temperature are identically computed and used to give trendlines that will pass through zero. The new graph with all trendlines passing through zero is shown in **Figure 5-3**. This data is what is used to eventually calculate diffusivity.

To get the real start time in minutes from **Table 5-1**, the above compute SRT start time is converted back to minutes by squaring and dividing by 60,

$$\frac{(36.26)^2}{60} = 21.91mins$$

Other real start times are calculated similarly.

**Figure 5-3** shows all the new trendlines at various temperatures going through zero. The slopes are tabulated in **Appendix - G14** along with other data. It should be noted that all R<sup>2</sup> values are greater than 0.99 thereby showing a great fit for the data. These slopes are also later used in Design Expert (DE) software (**Section 5.5**) for further analysis.

Appendix - G14: Butane solvent height decrease graph data (all temperatures)

Butane height decrease vs. SRT graph data						
Temperature (°C)	Experimental Start time (min)	Slope of graph (cm/s <sup>0.5</sup> )	R <sup>2</sup>	y intercept	x intercept	Start time (min)
27.00	t = 0	0.0097	0.9967	0.0000	0.00	0.00
30.25	t = 0	0.0063	0.9992	0.0000	0.00	0.00
33.50	t = 0	0.0042	0.9958	0.0000	0.00	0.00
36.75	t = 0	0.0030	0.9953	0.0000	0.00	0.00
40.00	t = 0	0.0025	0.9966	0.0000	0.00	0.00

### Bitumen table

The real start time is found by using the equation of the ( $t \neq 0$ ) trendline. For 27.00°C, that equation is,

$$y = 0.00087t^{0.5} - 0.0360$$

A-19

Where (0.00087) is the slope of the graph and (-0.0360) is the y-intercept of the graph. The SRT start time (x-intercept from **Table 5-2**) can be found by equating y to zero and finding  $t^{0.5}$ ,

$$0 = 0.00087t^{0.5} - 0.0360$$

$$0.0360 = 0.00087t^{0.5}$$

$$\frac{0.0360}{0.00087} = t^{0.5}$$

$$t^{0.5} = 41.33s^{0.5}$$

This value is directly subtracted from all 27.00°C SRT experimental values to give a trendline that will pass through zero. Other corresponding x-intercept values for other temperature are identically computed and used to give trendlines that will pass through zero. The new graph with all trendlines passing through zero is shown in **Figure 5-3**. This data is what is used to eventually calculate diffusivity.

To get the real start time in minutes from **Table 5-1**, the above compute SRT start time is converted back to minutes by squaring and dividing by 60,

$$\frac{(41.33)^2}{60} = 28.47mins$$

Other real start times are calculated similarly.

**Figure 5-6** shows all the new trendlines at various temperatures going through zero. The slopes are tabulated in **Appendix - G15** along with other data. It should be noted that all  $R^2$  values are greater than 0.99 (apart from at 40.00°C) thereby showing a great fit for the data. These slopes are also later used in Design Expert (DE) software (**Section 5.5**) for further analysis.

Appendix - G15: Bitumen height increase graph data (all temperatures)

Bitumen height increase vs. SRT graph data						
Temperature (°C)	Experimental Start time (min)	Slope of graph (cm/s <sup>0.5</sup> )	R <sup>2</sup>	y intercept	x intercept	Start time (min)
27.00	t = 0	0.00087	0.9934	0.0000	0.00	0.00
30.25	t = 0	0.00056	0.9974	0.0000	0.00	0.00
33.50	t = 0	0.00037	0.9981	0.0000	0.00	0.00
36.75	t = 0	0.00024	0.9956	0.0000	0.00	0.00
40.00	t = 0	0.00018	0.9886	0.0000	0.00	0.00

# APPENDIX H - Design expert ANOVA tables

## Butane table

Transform: Square Root Constant: 0  
ANOVA for Response Surface Cubic model

Analysis of variance table [Partial sum of squares - Type III]					
Source	Sum of Squares	df	Mean Square	F Value	p-value Prob > F
Model	3.114E-003	3	1.038E-003	3.836E+005	< 0.0001
A-Temperature	3.384E-004	1	3.384E-004	1.251E+005	< 0.0001
A <sup>2</sup>	1.576E-004	1	1.576E-004	58250.34	< 0.0001
A <sup>3</sup>	1.014E-007	1	1.014E-007	37.47	0.0009
Residual	1.624E-008	6	2.706E-009		
Lack of Fit	1.624E-008	1	1.624E-008		
Pure Error	0.000	5	0.000		
Cor Total	3.114E-003	9			

The Model F-value of 383575.77 implies the model is significant. There is only a 0.01% chance that an F-value this large could occur due to noise.

Values of "Prob > F" less than 0.0500 indicate model terms are significant. In this case A, A<sup>2</sup>, A<sup>3</sup> are significant model terms.

Values greater than 0.1000 indicate the model terms are not significant. If there are many insignificant model terms (not counting those required to support hierarchy), model reduction may improve your model.

User Std. Dev.	2.198E-004	R-Squared	1.0000
Std. Dev.	5.202E-005	Adj R-Squared	1.0000
Mean	0.069	Pred R-Square	1.0000
C.V. %	0.075	Adeq Precision	1473.805
PRESS	3.604E-008		

Factor	Coefficient Estimate	df	Standard Error	95% CI Low	95% CI High	VIF
Intercept	0.065	1	2.564E-005	0.065	0.065	
A-Temperature	-0.025	1	6.990E-005	-0.025	-0.025	9.03
A <sup>2</sup>	9.491E-003	1	3.932E-005	9.395E-003	9.587E-003	1.00
A <sup>3</sup>	4.747E-004	1	7.755E-005	2.849E-004	6.644E-004	9.03

Final Equation in Terms of Coded Factors:

$$\begin{aligned} \text{Sqrt(Butane slope)} = & \\ & +0.065 \\ & -0.025 * A \\ & +9.491E-003 * A^2 \\ & +4.747E-004 * A^3 \end{aligned}$$

The equation in terms of coded factors can be used to make predictions about the response for given levels of each factor. By default, the high levels of the factors are coded as +1 and the low levels of the factors are coded as -1. The coded equation is useful for identifying the relative impact of the factors by comparing the factor coefficients.

Final Equation in Terms of Actual Factors:

$$\begin{aligned} \text{Sqrt(Butane slope)} = & \\ & +0.37925 \\ & -0.013034 * \text{Temperature} \\ & +5.09293E-005 * \text{Temperature}^2 \\ & +1.72839E-006 * \text{Temperature}^3 \end{aligned}$$

## Bitumen table

Transform: Square Root Constant: 0  
ANOVA for Response Surface Quadratic model

Analysis of variance table [Partial sum of squares - Type III]					
Source	Sum of Squares	df	Mean Square	F Value	p-value Prob > F
Model	3.349E-004	2	1.675E-004	12133.65	< 0.0001
A-Temperature	3.253E-004	1	3.253E-004	23571.76	< 0.0001
A <sup>2</sup>	9.599E-006	1	9.599E-006	695.55	< 0.0001
Residual	9.661E-008	7	1.380E-008		
Lack of Fit	9.661E-008	2	4.830E-008		
Pure Error	0.000	5	0.000		
Cor Total	3.350E-004	9			

The Model F-value of 12133.65 implies the model is significant. There is only a 0.01% chance that an F-value this large could occur due to noise.

Values of "Prob > F" less than 0.0500 indicate model terms are significant. In this case A, A<sup>2</sup> are significant model terms.

Values greater than 0.1000 indicate the model terms are not significant. If there are many insignificant model terms (not counting those required to support hierarchy), model reduction may improve your model.

User Std. Dev.	5.041E-004	R-Squared	0.9997
Std. Dev.	1.175E-004	Adj R-Squared	0.9996
Mean	0.020	Pred R-Square	0.9995
C.V. %	0.58	Adeq Precision	250.715
PRESS	1.646E-007		

Factor	Coefficient Estimate	df	Standard Error	95% CI Low	95% CI High	VIF
Intercept	0.019	1	5.789E-005	0.019	0.019	
A-Temperature	-8.066E-003	1	5.254E-005	-8.190E-003	-7.942E-003	1.00
A <sup>2</sup>	2.342E-003	1	8.881E-005	2.132E-003	2.552E-003	1.00

Final Equation in Terms of Coded Factors:

$$\begin{aligned} \text{Sqrt(Bitumen slope)} = & \\ & +0.019 \\ & -8.066E-003 * A \\ & +2.342E-003 * A^2 \end{aligned}$$

The equation in terms of coded factors can be used to make predictions about the response for given levels of each factor. By default, the high levels of the factors are coded as +1 and the low levels of the factors are coded as -1. The coded equation is useful for identifying the relative impact of the factors by comparing the factor coefficients.

Final Equation in Terms of Actual Factors:

$$\begin{aligned} \text{Sqrt(Bitumen slope)} = & \\ & +0.12287 \\ & -4.95504E-003 * \text{Temperature} \\ & +5.54341E-005 * \text{Temperature}^2 \end{aligned}$$

## Ideality table

Transform: Power Lambda: 3 Constant: 0

ANOVA for Response Surface Cubic model

Analysis of variance table [Partial sum of squares - Type III]

Source	Sum of Squares	df	Mean Square	F Value	p-value Prob > F
Model	0.23	3	0.078	3899.05	< 0.0001
A-Temperatu	0.034	1	0.034	1693.92	< 0.0001
A <sup>2</sup>	3.305E-003	1	3.305E-003	165.71	< 0.0001
A <sup>3</sup>	6.710E-004	1	6.710E-004	33.64	0.0012
Residual	1.197E-004	6	1.994E-005		
Lack of Fit	1.197E-004	1	1.197E-004		
Pure Error	0.000	5	0.000		
Cor Total	0.23	9			

The Model F-value of 3899.05 implies the model is significant. There is only a 0.01% chance that an F-value this large could occur due to noise.

Values of "Prob > F" less than 0.0500 indicate model terms are significant. In this case A, A<sup>2</sup>, A<sup>3</sup> are significant model terms.

Values greater than 0.1000 indicate the model terms are not significant.

If there are many insignificant model terms (not counting those required to support hierarchy), model reduction may improve your model.

Std. Dev.	4.466E-003	R-Squared	0.9995
Mean	0.75	Adj R-Squared	0.9992
C.V. %	0.60	Pred R-Square	0.9989
PRESS	2.656E-004	Adeq Precision	147.541

Factor	Coefficient Estimate	df	Standard Error	95% CI Low	95% CI High	VIF
Intercept	0.72	1	2.201E-003	0.72	0.73	9.03
A-Temperature	-0.25	1	6.001E-003	-0.26	-0.23	9.03
A <sup>2</sup>	0.043	1	3.376E-003	0.035	0.052	1.00
A <sup>3</sup>	0.039	1	6.657E-003	0.022	0.055	9.03

Final Equation in Terms of Coded Factors:

$$\begin{aligned} (\text{Ideality})^3 = & \\ & +0.72 \\ & -0.25 * A \\ & +0.043 * A^2 \\ & +0.039 * A^3 \end{aligned}$$

The equation in terms of coded factors can be used to make predictions about the response for given levels of each factor. By default, the high levels of the factors are coded as +1 and the low levels of the factors are coded as -1. The coded equation is useful for identifying the relative impact of the factors by comparing the factor coefficients.

Final Equation in Terms of Actual Factors:

$$\begin{aligned} (\text{Ideality})^3 = & \\ & -2.13554 \\ & +0.36648 * \text{Temperature} \\ & -0.013102 * \text{Temperature}^2 \\ & +1.40606E-004 * \text{Temperature}^3 \end{aligned}$$

## APPENDIX I - Matlab code & diffusivity function results

### fD<sub>sb</sub>

```
% Diffusion of Butane in Bitumen
%
% by Lesley James, 20088392
% Supervisor: Dr. I Chatzis
% Quality Assurance: Dr. M.A. Ioannidis
%
% Name: fDsb.m
% Version: 3.0
% Date Created: 20-Mar-03
% Last Updated: 14-Mar-09
%
% List of Versions, dates and descriptions
% 1.0 20-Mar-03 Creation
% 2.0 12-May-03 Add Co-efficient variables for use in
% Optimisation Program (Dsb_Opt.m)
% 3.0 14-Mar-09 Tidy unused and obsolete diffusivity functions
%
% Description of program
% This function solves the bogus Diffusivity function
```

```
function Dsb = fDsb(B)
global rhoS rhoB nA1 nA2 nA3 nE2 nE3 p MWS MWB
```

```
Dsb=p(1)*B+p(2);      % Linear diffusivity to optimise for the
coefficients
```

## frho

```
%-----
% Diffusion of Butane in Bitumen
%
% by Lesley James, 20088392
% Quality Assurance: Dr. M.A. Ioannidis
% Updated by: Evulukwu Ebubechi
%
% Name:          frho.m
% Version:       1.0
% Date Created:  20-Mar-03
% Last Updated:  14-Dec-14
%
%
% Description of program
%   This function solves the mixture density function
%-----
```

```
function rho = frho(A)
global vS vB
```

```
rho = (1/((1*A*vS) + ((1-A)*vB)));
```

Note: parts bolded and highlighted vary depending on ideal/non-ideal experimental run

## Optimisation

```
%-----
% Diffusion of Butane in Bitumen
%
% by Lesley James, 20088392
% Quality Assurance: Dr. M.A. Ioannidis
% Updated by: Evulukwu Ebubechi
%
% Name:          Optimisation.m
% Version:       2.0
% Date Created:  Fall 2008
% Last Updated:  14-Dec-14
%
% List of Versions, dates and descriptions
%   1.0    Fall 2008    Creation
%   2.0    14-Mar-09   Tidy and delete unused variables
%
% Description of program
%   This shell optimises the one-dimensional diffusion of solvent into
bitumen.
%   It calls wS_xt_ode_dim_OBJ1.m and minimises the objective function
%   using lsqnonlin
```

```

clc
clear all
close all
global p times

p0 = [1e-6 1e-6];
lb = [1E-8 1E-8];
ub = [1E-04 1E-04];

times = linspace(0, 270000, 450); % for 26-Aug-08 and both, every 10 min up
to 4500 min

%options=optimset('MaxFunEvals',1000,'MaxIter',150,'LargeScale','on');
%[p,fval]=fmincon(@wS_xt_ode_dim_OBJ1,p0,A,b,Aeq,beq,lb,ub,[],options,tfrom,t
to)

options=optimset('MaxIter',400, 'MaxFunEvals',1200,'LargeScale','on',
'Display','iter', 'TolFun',1E-08, 'TolX',1E-08);

%TolFun - Termination tolerance on the function value [ positive scalar ]
%TolX -Termination tolerance on X [ positive scalar ]
%Display - to display output for every iteration, 'iter'
%MaxFunEvals - specifies the maximum number of log-likelihood objective
function evaluations. The default value is 100 times the number of
parameters
%estimated in the model.

[p,resnorm, residual, exitflag, output]=lsqnonlin(@wS_xt_ode_dim_OBJ1, p0,
lb, ub, options)

```

Note: parts bolded and highlighted vary depending on experimental run trial and error

## fsystem\_ode\_dim

```

%-----
% Diffusion of Butane in Bitumen
%
% by Lesley James, 20088392
% Quality Assurance: Dr. M.A. Ioannidis
% Updated by: Evulukwu Ebubechi
%
% Name:          fsystem_ode_dim.m
% Version:       6.0
% Date Created:  05-Mar-03
% Last Updated:  09-Dec-14
%
% List of Versions, dates and descriptions
% 1.0    06-Mar-03    Creation
% 2.0    21-Mar-03    Organisation + solution of ode for no change in
%                    interface
% 3.0    16-Aug-06    Name change and boundary condition
% 4.0    05-Dec-07    Make ode dimensionless over height of bitumen
% 5.0    20-Feb-08    Replace Vv, dxsvdt and dxsdt with new dxsdt

```

```

%      6.0      09-Mar-09  Do not set dwSt=zeros, insert "dummy" variable to
approximate dxSdt on RHS of (4)
%      7.0      09-Dec-14  Adding non-ideality coefficients (bolded and
highlighted in code

%              at end, reset "dummy" to new value of dxSdt
%              (LHS of (4))
%      Description of program
%      This function solves the discrete version of the Continuity eqtn
%      taking into account bulk swelling, a convection term due to density
%      changes and the fact that density and the diffusion coefficient are
%      dependent on the mass fraction of the solvent in the bitumen.
%-----

function dwSdt = fsystem_ode_dim(times, wS)
global z vB vS deltaxi p MWS MWB dummy

% Dimensionless segment thickness
deltaxi = 1/z;

% (2) Mass Average Velocity - comment out if you want to look at effect of
diffusion only
Vf = zeros(z+1,1);
Vfsum = zeros (z+1,1);
Vm = zeros (z+1,1);

Vf(1) = 0;

Vf(z+1)=(fDsb(wS(z+1))/wS(z+2))*((3*frho(wS(z+1))-
4*frho(wS(z))+frho(wS(z-1)))/2*deltaxi))*((3*wS(z+1)-4*wS(z)+wS(z-
1))/2*deltaxi)+(frho(wS(z+1))/wS(z+2))*((3*fDsb(wS(z+1))-
4*fDsb(wS(z))+fDsb(wS(z-1)))/2*deltaxi))*((3*wS(z+1)-4*wS(z)+wS(z-
1))/2*deltaxi)+(frho(wS(z+1))*fDsb(wS(z+1))/wS(z+2))*((2*wS(z+1)-
5*wS(z)+4*wS(z-1)-wS(z-2))/(deltaxi^2));

for r=2:z
    Vf(r) = (fDsb(wS(r))/wS(z+2))*((frho(wS(r+1))-frho(wS(r-
1)))/(2*deltaxi))*((wS(r+1)-wS(r-
1))/(2*deltaxi))+frho(wS(r))/wS(z+2))*((fDsb(wS(r+1))-fDsb(wS(r-
1)))/(2*deltaxi))*((wS(r+1)-wS(r-
1))/(2*deltaxi))+frho(wS(r))*fDsb(wS(r))/wS(z+2))*((wS(r+1)-2*wS(r)+wS(r-
1))/(deltaxi^2));

    Vfsum(r)=Vf(r)+Vfsum(r-1);
end

Vm(1) = 0;
Vm(z+1) = ((1*vS)-vB)*(((1/(2*z))*Vf(1)+Vf(z+1)))+(1/z)*Vfsum(z);

for s=2:z
    Vm(s) = ((1*vS)-vB)*((((s-1)*deltaxi)/(2*(s-
1)))*Vf(1)+Vf(s))+((((s-1)*deltaxi)/(s-1))*Vfsum(s-1));
end

```

```

% (3) The Continuity Equation
% Boundary Conditions
% (a) At node z+1, i.e. the solvent bitumen interface, there is no
% change in solvent concentration wrt time. At time t > 0 the interface
% concentration (wS(z+1)) has reached equilibrium (wS*) for the given
% pressure and temperature conditions.

%   wS(z+1) = 0.6;   % The solvent mass fraction instantaneously reaches
%                   % equilibrium at the interface.
dwSdt(z+1) = 0;

% (b) There is no flux at the end wall of the bitumen. So that the
% change in solvent mass fraction wrt change in position is zero at the
% end wall. Equation 3.27

dwSdt(1) = (2*fDsb(wS(1))/(wS(z+2))^2)*(wS(2) - wS(1))/(deltaxi^2);

if round(times)==0
    dummy=0;
end

% Nodes greater than 1 and less than z+1 can be expressed with the discrete
% derivative of the general continuity equation.

for i=2:z
    % The change in solvent mass fraction wrt time is represented as the
    % following form taking into account swelling and convection

    dwSdt(i) = ((i-1)*deltaxi/wS(z+2))*((wS(i+1)-wS(i-1))/2*deltaxi)*(dummy)+
(1/wS(z+2))*((wS(i+1)-wS(i-1))/2*deltaxi)*((fDsb(wS(i))/(frho(wS(i)*wS(z+2))))*((frho(wS(i+1))-
frho(wS(i-1)))/2*deltaxi) + ...
(1/wS(z+2))*((fDsb(wS(i+1))-fDsb(wS(i-1)))/2*deltaxi) - Vm(i)) +
(fDsb(wS(i))/wS(z+2)^2)*(wS(i+1)-2*wS(i)+wS(i-1))/(deltaxi^2));

end

% (4) New material balance development of xS (Increase in Bitumen Height),
28-Mar-08
% dxSdt is stored in the dwSdt(z+2) column and xS in the wS(z+2) column.

b = 1;
a = 0;

fa = ((frho(wS(1)))^2)*dwSdt(1);
fb = ((frho(wS(z+1)))^2)*(-1/wS(z+2))*dummy*((3*wS(z+1)-4*wS(z)+wS(z-1))/(2*deltaxi))+dwSdt(z+1));

fi = 0;
fsum = 0;

```

```

for j=2:z
    fi = ((frho(wS(j)))^2)*(-(deltaxi*(j-1)/wS(z+2))*dummy*(wS(j+1)-wS(j-1))/(2*deltaxi))+dwSdt(j));
    fsum = fsum + fi;
end

integral = ((b-a)/(2*z))*(fa+fb)+((b-a)/z)*fsum; %had fi, changed to fsum
(06-Mar-09)

dwSdt(z+2) = (fDsb(wS(z+1))/wS(z+2))*(3*wS(z+1)-4*wS(z)+wS(z-1))/(2*deltaxi) - ((vB-1*vS)*(wS(z+2))/frho(wS(z+1)))*integral;

% No moving boundary - if you want to look at effect of no swelling,
% comment out the above expression for dwSdt(z+2) and use the following.

dummy=dwSdt(z+2);

%dwSdt(z+2)
%for q=1:52
%    dxSdt(q) = dwSdt(q);
%end
%dxSdt=dwSdt(1,z+2);
%disp('comming out')
%pause
dwSdt=dwSdt';
%%%%%%%%%%%%%%%%%%%%%%%%%%%%%%%%%%%%%%%%%%%%%%%%%%%%%%%%%%%%%%%%%%%%%%%%
%%%%%%%%%%%%%%%%%%%%%%%%%%%%%%%%%%%%%%%%%%%%%%%%%%%%%%%%%%%%%%%%%%%%%%%%

```

Note: parts bolded and highlighted vary depending on ideal/non-ideal experimental run

## wS xt ode dim OBJ1

```

function f = wS_xt_ode_dim_OBJ1(par, times)
global p vS vB z times MWS MWB

p=par;

%-----
% Diffusion of Butane in Bitumen
%
% by Lesley James, 20088392
% Quality Assurance: Dr. M.A. Ioannidis
% Updated by: Evulukwu Ebubechi

% Name:          wS_xt_ode_dim_OBJ1.m
% Version:       10.0
% Date Created:  05-Mar-03
% Last Updated:  14-Dec-14
%
% List of Versions, dates and descriptions
% 1.0    05-Mar-03    Creation
% 2.0    21-Mar-03    Organisation + solution of ode for no change in
%                    interface
% 3.0    30-Mar-03    Add functionality for a change in bitumen

```

```

%
%      4.0      14-Apr-03      interface height
%      Add convergence functionality by resetting the
%      initial concentration profile to the result of
%      the previous ode and obtaining an acceptable
%      tolerance.
%      5.0      24-Apr-03      Following Grogan's method, if xS_new is not
%      within the desired tolerance than the initial
%      concentration profile is set to the previous
%      result and the xS_old is set to the previous
%      xS_new.
%      6.0      07-Jun-03      Implemented trapezoidal rule for finding the
%      change in mass and height.
%      7.0      24-Jul-06      Change directories for writing files
%      7.1      26-Jul-06      Added file extensions (.csv) to output files.
%      8.0      03-Nov-08      New Flux Boundary condition, see changes to
%      lines 125, 127, 129, 136 and in
%
fssystem_ode_dim_BC2.m
%      9.0      09-Mar-09      Change ode23s to ode45
%      10.0     14-Mar-09      Tidy and delete unused variables
%      11.0     14-Dec-14      Change experimental parameters and excel
directories

%      Description of program
%      This function is used by Optimisation.m to solve the discrete version
of the Continuity eqtn
%      taking into account bulk swelling, a convection term due to density
%      changes and the fact that density and the diffusion coefficient are
%      dependent on the mass fraction of the solvent in the bitumen.
%-----
%-----

% This program finds the relationship of Diffusivity & density
% as a function of solvent concentration of butane in bitumen with respect
% to depth and time.

% (1) Experimental Results
% Read experimental results from the given Worksheet found in the listed
Excel Workbook
% ('Workbook', 'Worksheet') found in the Directory listed. The experimental
results
% must be copied into this file name (Workbook) or the name listed below must
be changed.
% The data contained in the worksheet must start in cell A1 (without header
titles) as the
% command below will read the entire sheet starting at cell A1.

%-----
%      Diffusion of Butane in Bitumen
%
%      cd 'C:\Users\admin\Desktop\Diffusion code\Lesley\Ideal'

```

```

Decrease in Solvent Height (mm)
[dHS_Exp] = xlsread('26,3c','Imported Butane 1');

Increase in Bitumen Height (mm)
[dHB_Exp] = xlsread('26,3c','Imported Bitumen 1');

% Extract the experimental times in seconds
[t_dHS_Exp] = (dHS_Exp(:,1)).^2; % The experimental times for
recording the height of the Solvent (s)
[t_dHB_Exp] = (dHB_Exp(:,1)).^2; % The experimental times for
recording the height of the Bitumen (s)

% Extract the experimental heights in mm
[h_dHS_Exp] = dHS_Exp(:,2); % The experimental times for recording the
height of the Solvent (s)
[h_dHB_Exp] = dHB_Exp(:,2); % The experimental times for recording the
height of the Bitumen (s)

% (3) Variable Declaration
%global vS vB n

% (3a) Input Variables
z = 50; % Number of segments
mB = 1.583; % Mass of bitumen
AS = 0.0855; % Cross sectional area of new glass tubes for the
solvent (cm^2)
AB = 1.207; % Cross sectional area of the bitumen (cm^2)

% (3b) Miscellaneous variables
rhoW = 1.0; % Density of pure water (g/cm^3).

% (3c) Pure Solvent (butane) Properties
TS = 24.0; % Temperature of the solvent (oC)
rhoS = 0.57132; % Density of pure liquid solvent at the bitumen
temperature (butane) (g/cm^3).
rhoSS = 0.57295; % Density of pure liquid solvent at the solvent
temperature (butane) (g/cm^3).
vS = 1/rhoS; % Mass specific volume of liquid butane (cm^3/g).
muS = 0.15645; % Viscosity of liquid butane corrected for the
bitumen temperature (cP)
MWS = 58.123; % Molecular weight of butane (g/gmol).
SGS = rhoS/rhoW; % The specific gravity of butane.

% (3d) Pure Bitumen Properties
rhoB = 1.0004; % Density of pure bitumen (g/cm^3).
vB = 1/rhoB; % Mass specific volume of bitumen (cm^3/g).
muB = 238441; % Bitumen viscoity (cP) at 26.3oC after Karen re-ran
mu for degassed bitumen
TB = 26.3; % Temperature of the bitumen (oC)
MWB = 557; % Molecular weight of bitumen (g/gmol).
SGB = rhoB/rhoW; % The specific gravity of bitumen.

```

```

L = mB/(rhoB*AB); % Original height of bitumen

% (4) Solve simultaneously the set of Equations
% (4a) Initial Solvent Mass Fraction
    wS_init = zeros(1,z+2); % Mass fraction of solvent in the

wS_init(z+1) = 0.60; % Instantaneously the wS at the interface
reaches equilibrium.
wS_init(z+2) = L; % Set the initial xS to the wS(n+2) position
%times = linspace(0, 46000, 1000);

% (4b) Call the ODE
% options = odeset('RelTol', 1e-03, 'AbsTol', 1e-4);
[t, wS] = ode45('fsystem_ode_dim', times, wS_init);
% wS_init); with time intervals
[j,k] = size(wS); % j times (rows) and k positions including dummy
q=k-1; % The last i value is the dummy wS, i.e. xS_new

% (5) Record the ODE Results and Analyse
% (5a) Initialization of the ODE output solvent mass fraction (wS)
% and the functions dependent upon it

% Output matrix for Dsb wrt time and position
    Dsb_tx = zeros(j, q);

% Output matrix for rho wrt time and position
    rho_tx = zeros(j, q);

% The height of each nodal point throughout the depth of the bitumen layer
% (no flux boudary =0)
    xS_t = zeros(j,1);
    x_t = zeros(j,q);
    xS_xt=zeros(j,q);

% Rewrite the solvent mass fractions into a new array for plotting purposes
    wS_t = zeros(j, 1);

% Mole Fraction
    MoleS_t=zeros(j,q);

% The solvent mass over depth of the bitumen wrt time
    mS_t = zeros(j, q);

% The total mass of solvent diffused into the bitumen at each time
% (integrated)
    mS_tot = zeros(j,1);

% The change in height of the solvent due to diffusion into the bitumen
    hS_tot = zeros(j,1);

% The change in height of the solvent due to diffusion into the bitumen
    hS_tot_delta = zeros(j,1);

```

```

% The change in height of the bitumen mixture
hB_tot_delta = zeros(j,1);

% The change in height of the bitumen mixture
hB_tot = zeros(j,1);

% The mass fraction of solvent diffused
wS_tot = zeros(j,1);

% Computation of the convection term
Convection = zeros(j,q);

% Computation of the diffusion term
Diffusion = zeros(j,q);

% Record the sum of the solvent masses in node positions 2:i-1 for use in
% trapezoidal rule
Sum_rhoS_t = zeros(j,1);

% The solvent mass over depth of the bitumen wrt time
mS_t = zeros(j, q);
rhoS_t_trap = zeros (j, q);

% Initialise the time in minutes
t_min = zeros(j,1);

% Initialise the experimental heights
Exp_dhS = zeros(j,1);
Exp_dhB = zeros(j,1);

% (5b) Step through the times and positions recording the output parameters.
for h = 1:j %time steps
    for i=1:q %position steps

        % Determine the diffusivity dependent on the solvent mass
        % fraction (wS)
        Dsb_tx(h,i) = fDsb(wS(h,i));

        % Determine the mixture density at each node dependent on the
        % solvent mass fraction (wS)
        rho_tx(h,i) = frho(wS(h,i));

        % The size of the individual node segment
        delta_xS = (wS(h,k)/z);

        % The nodal positions starting from the no flux boundary
        x_t(h,i) = delta_xS*(i-1);

        % The nodal position at the no flux boundary is zero
        x_t(h,1) = 0;
    end
end

```

```

% Rewrite the solvent mass fractions into a new array for
% plotting purposes.
wS_t(h,i) = wS(h,i);

%Mole Fraction array
MoleS_t(h,i) = (wS_t(h,i)/MWS)/((wS_t(h,i)/MWS)+(1-
wS_t(h,i))/MWB));

% The mass of solvent in a differential segment
rhoS_t_trap(h,i) = AB*delta_xS*rho_tx(h,i)*wS(h,i);

% For each time step sum the mass of solvent from the 2nd to
% the next to last node to resolve the overall mass of solvent
% diffused into the bitumen
if i~=2
    if i==(k-1)
        Sum_rhoS_t(h) = Sum_rhoS_t(h) + rhoS_t_trap(h,i);
    end
end

end

% Capture the change in height of the bitumen mixture explicitly (mm)
xS_t = wS(h,k);
hB_tot_delta(h) = ((wS(h,i+1) - L)*10); % in milimetres

for i=1:q-1

    % The mass of solvent in a differential segment
    mS_t(h,i) =
AB*(rho_tx(h,i)*wS(h,i)+rho_tx(h,i+1)*wS(h,i+1))*delta_xS/2;

end

% Change the time into minutes for plotting
t_min(h) = t(h)/60;

% The change in the mass of butane diffused into the bitumen for each
% time t
mS_tot(h) = sum(mS_t(h,:));

% The total mass fraction at time t
wS_tot(h) = mS_tot(h)/(mS_tot(h)+mB);

% Capture the change in height of the bitumen mixture explicitly (cm)
hB_tot(h) = wS(h,k);

% The change in butane height (mm)
hS_tot(h) = (mS_tot(h)/(rhoSS*AS))*10;

% The change in butane height (mm)
hS_tot_delta(h) = (mS_tot(h)/(rhoSS*AS))*10;

```

```

% The experimental change in bitumen and solvent heights computed from
% the curve fit of the experimental data
Exp_dhB(h) = 0.0244*sqrt(t(h));
Exp_dhS(h)=0.1602*sqrt(t(h));

end

% Prepare Xi matrix
Xi = zeros(j,q);

for h = 1:j
    for i = 1:q
        Xi(h,i) = x_t(h,i)/x_t(h,k-1);
        xS_xt(h,i)=x_t(h,q)-x_t(h,i);
    end
end

% (6) Objective Function
% (6a) Minimise the SSE

%f=abs((Exp_dhB-hB_tot_delta)/Exp_dhB)+abs((Exp_dhS-hS_tot)/Exp_dhS);
f=abs((Exp_dhB-hB_tot_delta)/Exp_dhB);
%f=abs((Exp_dhS-hS_tot)/Exp_dhS);

hold off

% (8) Write comma separated files for the following variables for Icappsrvt1
csvwrite('C:\Documents and Settings\la2james\My Documents\Diffusion\Matlab
Results 2008\t.csv',t)
csvwrite('C:\Documents and Settings\la2james\My Documents\Diffusion\Matlab
Results 2008\t_min.csv',t_min)
csvwrite('C:\Documents and Settings\la2james\My Documents\Diffusion\Matlab
Results 2008\Dsb_tx.csv',Dsb_tx)
csvwrite('C:\Documents and Settings\la2james\My Documents\Diffusion\Matlab
Results 2008\rho_tx.csv',rho_tx)
csvwrite('C:\Documents and Settings\la2james\My Documents\Diffusion\Matlab
Results 2008\x_t.csv',x_t)
csvwrite('C:\Documents and Settings\la2james\My Documents\Diffusion\Matlab
Results 2008\xS_t.csv',xS_t)
csvwrite('C:\Documents and Settings\la2james\My Documents\Diffusion\Matlab
Results 2008\xS_xt.csv',xS_xt)
csvwrite('C:\Documents and Settings\la2james\My Documents\Diffusion\Matlab
Results 2008\Xi.csv',Xi)
csvwrite('C:\Documents and Settings\la2james\My Documents\Diffusion\Matlab
Results 2008\wS_t.csv',wS_t)
csvwrite('C:\Documents and Settings\la2james\My Documents\Diffusion\Matlab
Results 2008\wS.csv',wS)
csvwrite('C:\Documents and Settings\la2james\My Documents\Diffusion\Matlab
Results 2008\MoleS_t.csv',MoleS_t)
csvwrite('C:\Documents and Settings\la2james\My Documents\Diffusion\Matlab
Results 2008\mS_t.csv',mS_t)

```

```

csvwrite('C:\Documents and Settings\la2james\My Documents\Diffusion\Matlab
Results 2008\mS_tot.csv',mS_tot)
csvwrite('C:\Documents and Settings\la2james\My Documents\Diffusion\Matlab
Results 2008\hS_tot.csv',hS_tot)
csvwrite('C:\Documents and Settings\la2james\My Documents\Diffusion\Matlab
Results 2008\hB_tot.csv',hB_tot)
csvwrite('C:\Documents and Settings\la2james\My Documents\Diffusion\Matlab
Results 2008\wS_tot.csv',wS_tot)
csvwrite('C:\Documents and Settings\la2james\My Documents\Diffusion\Matlab
Results 2008\hB_tot_delta.csv',hB_tot_delta)
csvwrite('C:\Documents and Settings\la2james\My Documents\Diffusion\Matlab
Results 2008\Exp_dhB.csv',Exp_dhB)
csvwrite('C:\Documents and Settings\la2james\My Documents\Diffusion\Matlab
Results 2008\Exp_dhS.csv',Exp_dhS)

```

Note: parts bolded and highlighted vary depending on experimental run

## 27.00°C ideal

output =

```

firstorderopt: 6.7773e-04
iterations: 20
funcCount: 63
cgiterations: 0
algorithm: 'trust-region-reflective'
message: [1x415 char]
Number of iterations: 20
Number of function evaluations: 63
P: 1.62253E-06
Number of iterations: 3.06452E-07
Number of function evaluations: Sum of squared residuals at solution: 0.0137505

```

## 27.00°C non-ideal

output =

```

firstorderopt: 0.0092
iterations: 16
funcCount: 51
cgiterations: 0
algorithm: 'trust-region-reflective'
message: [1x415 char]
Number of iterations: 16
Number of function evaluations: 51
P: 1.62036E-06
Number of iterations: 3.11999E-07
Number of function evaluations: Sum of squared residuals at solution: 0.0129484

```

## 30.25°C ideal

output =

```

firstorderopt: 7.8061e-04
iterations: 11
funcCount: 36

```

cgiterations: 0  
algorithm: 'trust-region-reflective'  
message: [1x415 char]  
Number of iterations: 11  
Number of function evaluations: 36  
P: **8.42601E<sup>-07</sup>**  
Number of iterations: **7.98569E<sup>-07</sup>**  
Number of function evaluations: Sum of squared residuals at solution: 0.0210707

### 30.25°C non-ideal

output =  
firstorderopt: 0.0012  
iterations: 12  
funcCount: 39  
cgiterations: 0  
algorithm: 'trust-region-reflective'  
message: [1x415 char]  
Number of iterations: 12  
Number of function evaluations: 39  
P: **8.83794E<sup>-07</sup>**  
  
Number of iterations: **8.51128E<sup>-07</sup>**  
Number of function evaluations: Sum of squared residuals at solution: 0.0163218

### 33.50°C ideal

output =  
firstorderopt: 0.0069  
iterations: 11  
funcCount: 36  
cgiterations: 0  
algorithm: 'trust-region-reflective'  
message: [1x415 char]  
Number of iterations: 11  
Number of function evaluations: 36  
P: **6.47256E<sup>-07</sup>**  
Number of iterations: **6.26044E<sup>-07</sup>**  
Number of function evaluations: Sum of squared residuals at solution: 0.0305356

### 33.50°C non-ideal

output =  
firstorderopt: 0.0025  
iterations: 11  
funcCount: 36  
cgiterations: 0  
algorithm: 'trust-region-reflective'  
message: [1x415 char]  
Number of iterations: 11

Number of function evaluations: 36

P: **7.34443E<sup>-07</sup>**

Number of iterations: **7.14686E<sup>-07</sup>**

Number of function evaluations: Sum of squared residuals at solution: 0.019785

### 36.75°C ideal

output =

firstorderopt: 0.0055

iterations: 11

funcCount: 36

cgiterations: 0

algorithm: 'trust-region-reflective'

message: [1x415 char]

Number of iterations: 11

Number of function evaluations: 36

P: **4.56324E<sup>-07</sup>**

Number of iterations: **4.22576E<sup>-07</sup>**

Number of function evaluations: Sum of squared residuals at solution: 0.0417347

### 36.75°C non-ideal

output =

firstorderopt: 0.0076

iterations: 13

funcCount: 42

cgiterations: 0

algorithm: 'trust-region-reflective'

message: [1x415 char]

Number of iterations: 13

Number of function evaluations: 42

P: **5.46299E<sup>-07</sup>**

Number of iterations: **5.31826E<sup>-07</sup>**

Number of function evaluations: Sum of squared residuals at solution: 0.0218285

### 40.00°C ideal

output =

firstorderopt: 0.0057

iterations: 13

funcCount: 42

cgiterations: 0

algorithm: 'trust-region-reflective'

message: [1x415 char]

Number of iterations: 13

Number of function evaluations: 42

P: **3.67085E<sup>-07</sup>**

Number of iterations: **3.65682E<sup>-07</sup>**

Number of function evaluations: Sum of squared residuals at solution: 0.0473623

### 40.00°C non-ideal

output =

firstorderopt: 0.0048  
iterations: 11  
funcCount: 36  
cgiterations: 0  
algorithm: 'trust-region-reflective'  
message: [1x415 char]

Number of iterations: 11

Number of function evaluations: 36

P: **4.90677E<sup>-07</sup>**

Number of iterations: **4.80693E<sup>-07</sup>**

Number of function evaluations: Sum of squared residuals at solution: 0.0225671

### 28.50°C ideal (experimental)

output =

firstorderopt: 0.0034  
iterations: 13  
funcCount: 42  
cgiterations: 0  
algorithm: 'trust-region-reflective'  
message: [1x415 char]

Number of iterations: 13

Number of function evaluations: 42

P: **1.16052E<sup>-06</sup>**

Number of iterations: **5.91083E<sup>-07</sup>**

Number of function evaluations: Sum of squared residuals at solution: 0.0195693

### 28.50°C non-ideal (experimental)

output =

firstorderopt: 0.0053  
iterations: 12  
funcCount: 39  
cgiterations: 0  
algorithm: 'trust-region-reflective'  
message: [1x415 char]

Number of iterations: 12

Number of function evaluations: 39

P: **1.18692E<sup>-06</sup>**

Number of iterations: **5.97641E<sup>-07</sup>**

Number of function evaluations: Sum of squared residuals at solution: 0.0175477

## 28.50°C ideal (DE predicted)

output =

firstorderopt: 0.0049

iterations: 13

funcCount: 42

cgiterations: 0

algorithm: 'trust-region-reflective'

message: [1x415 char]

Number of iterations: 13

Number of function evaluations: 42

P: **1.41302E<sup>-06</sup>**

Number of iterations: **6.08486E<sup>-07</sup>**

Number of function evaluations: Sum of squared residuals at solution: 0.017115

## 28.50°C non-ideal (DE predicted)

output =

firstorderopt: 0.0043

iterations: 13

funcCount: 42

cgiterations: 0

algorithm: 'trust-region-reflective'

message: [1x415 char]

Number of iterations: 13

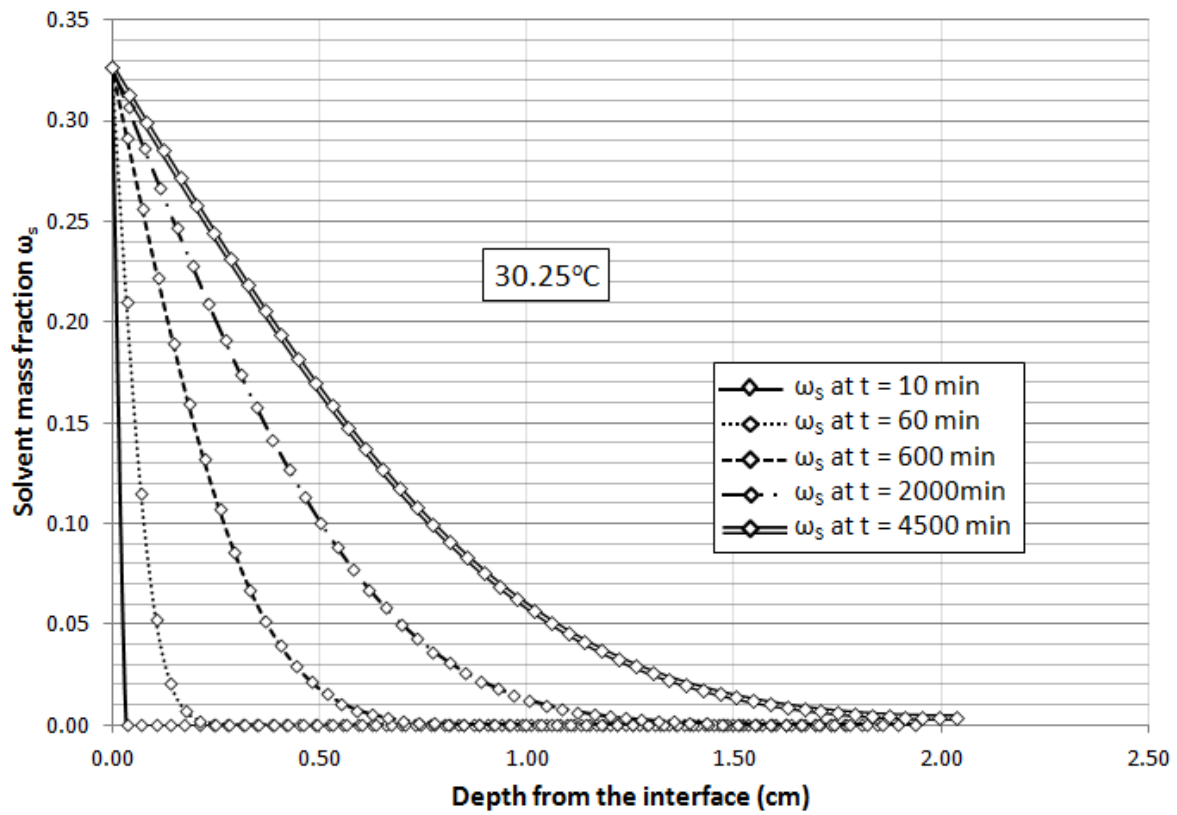
Number of function evaluations: 42

P: **1.45127E<sup>-06</sup>**

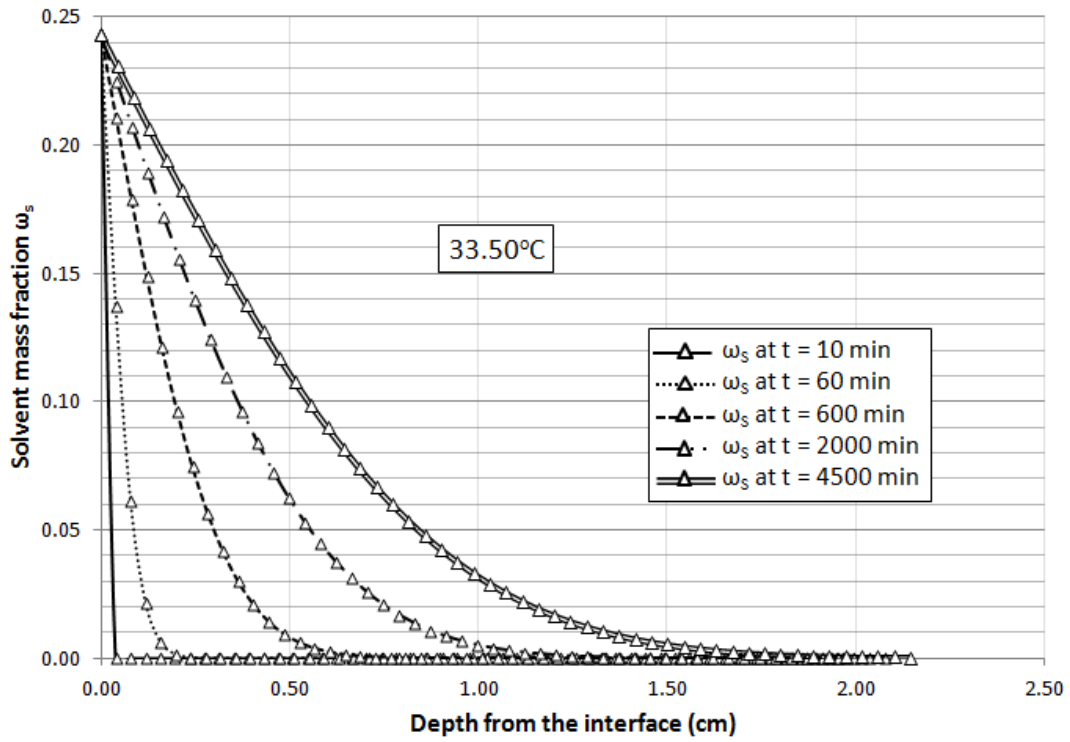
Number of iterations: **6.13672E<sup>-07</sup>**

Number of function evaluations: Sum of squared residuals at solution: 0.0149401

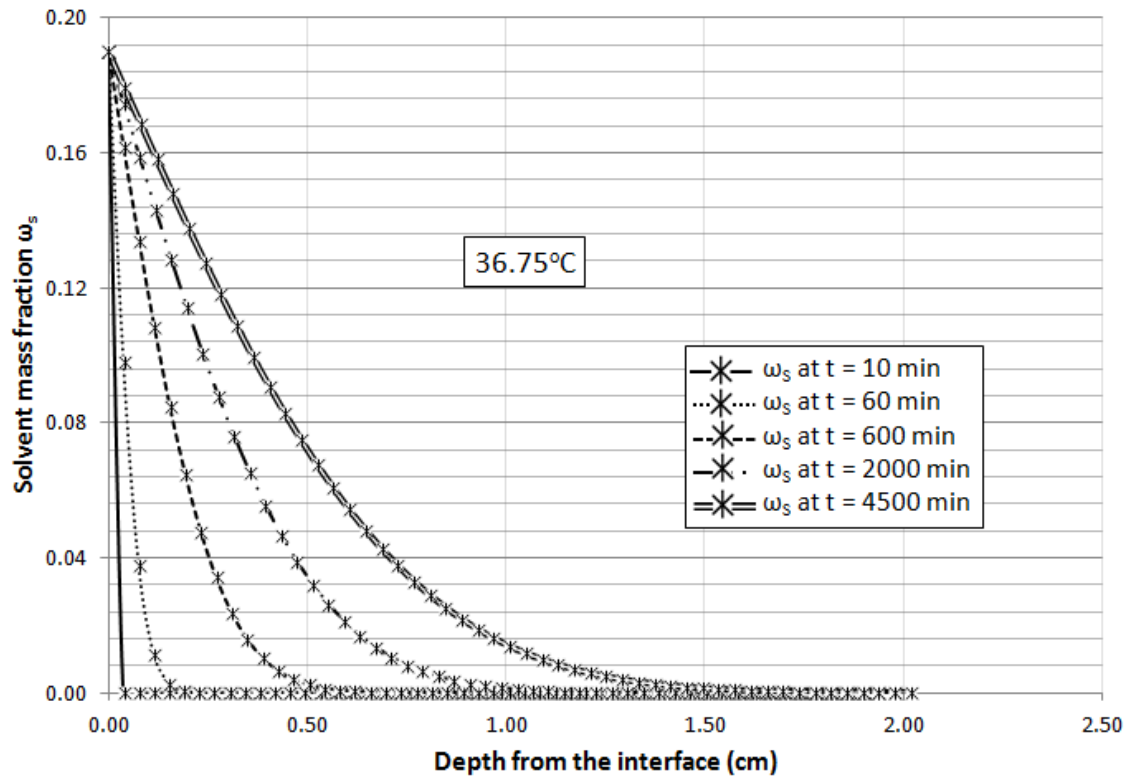
## APPENDIX J - Solvent concentration profiles (non-ideal)



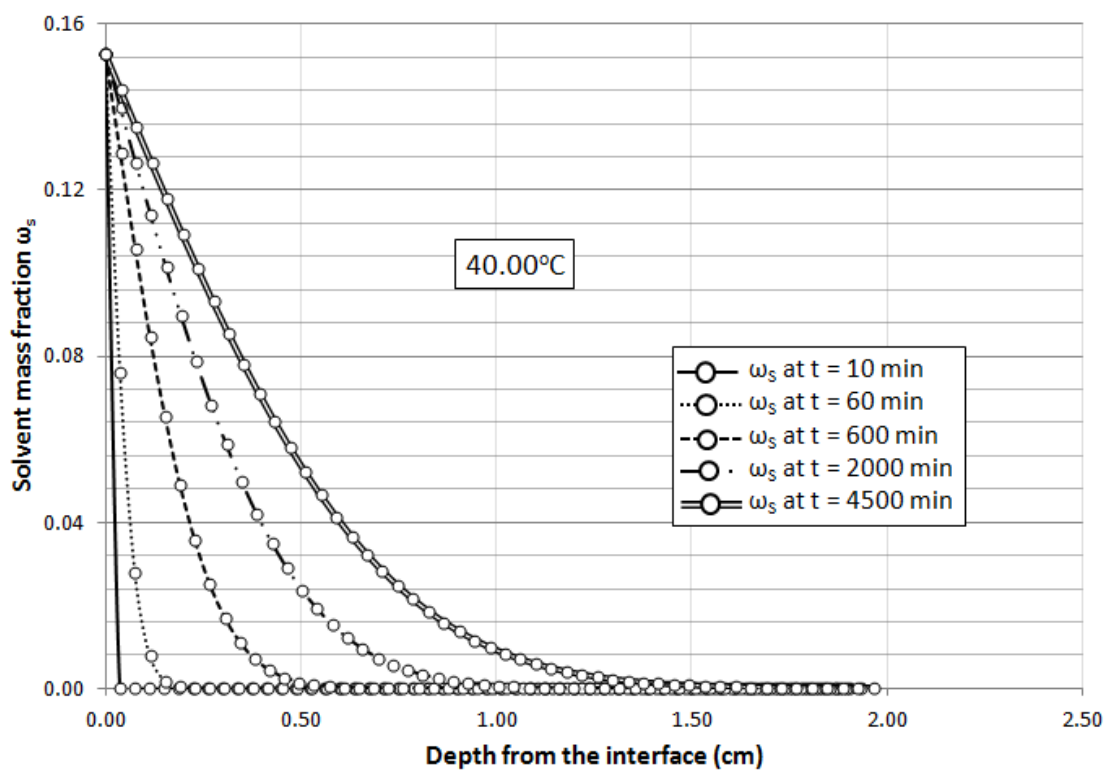
Appendix - J16: Butane solvent mass fraction profile at 30.25°C (non-ideal)



Appendix - J17: Butane solvent mass fraction profile at 33.50°C (non-ideal)

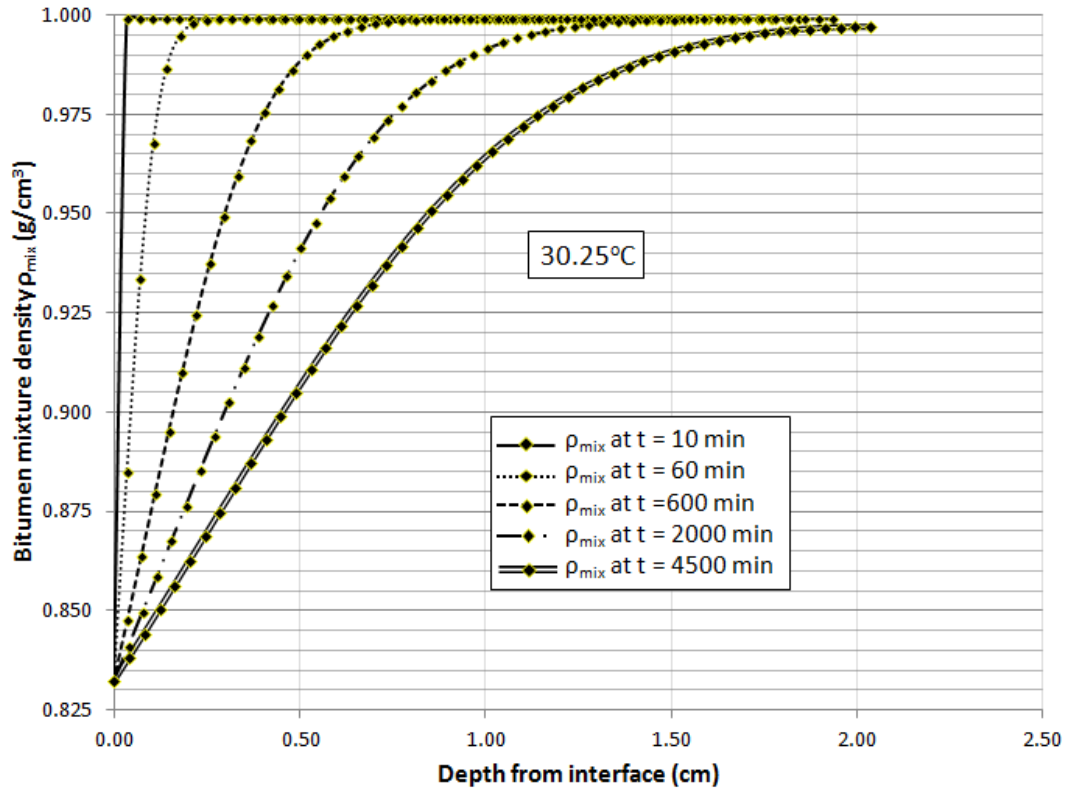


Appendix - J18: Butane solvent mass fraction profile at 36.75°C (non-ideal)

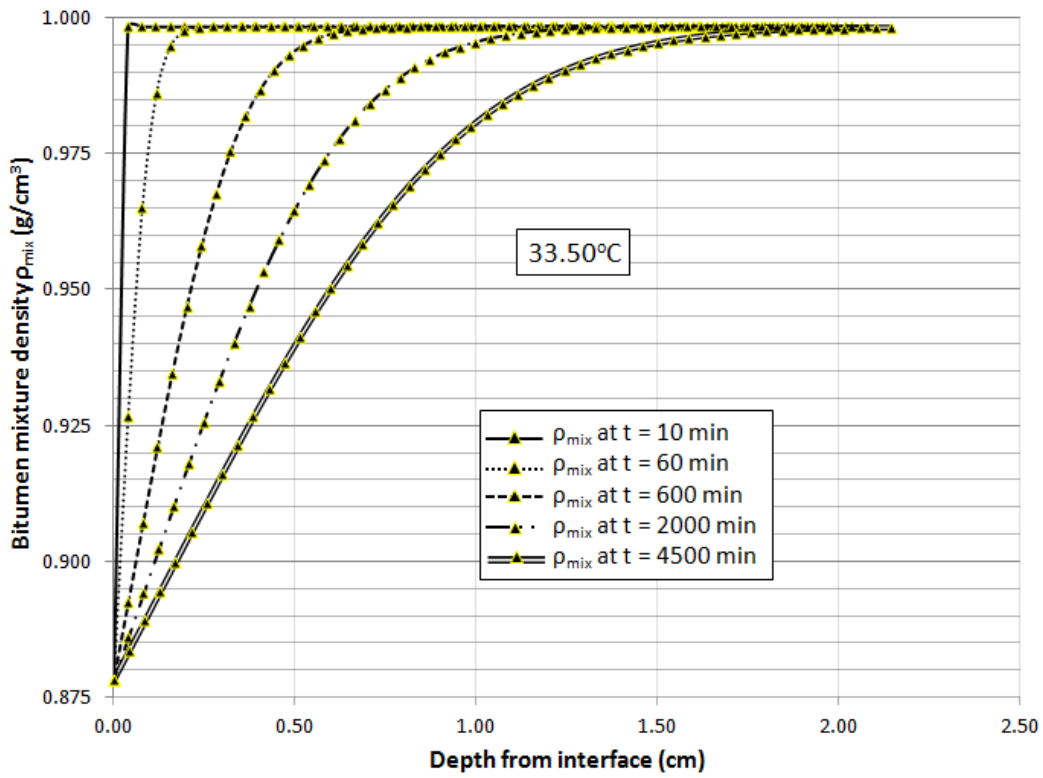


Appendix - J19: Butane solvent mass fraction profile at 40.00°C (non-ideal)

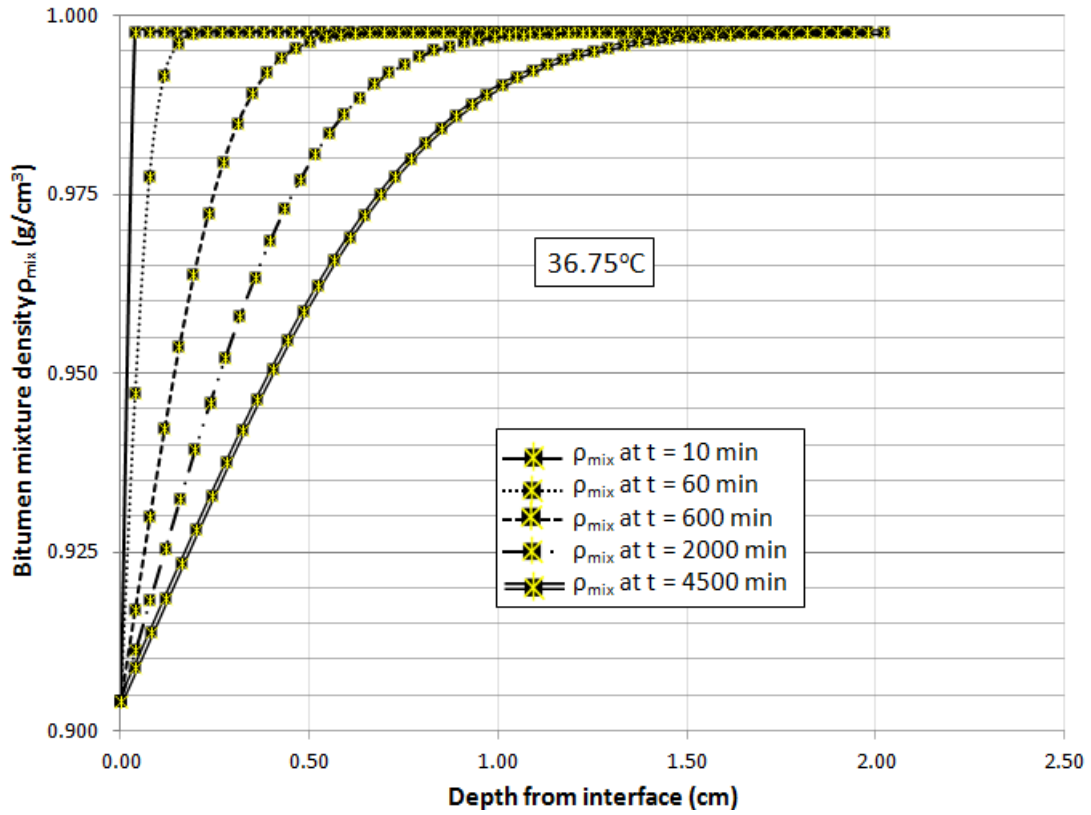
## APPENDIX K - Density profiles (non-ideal)



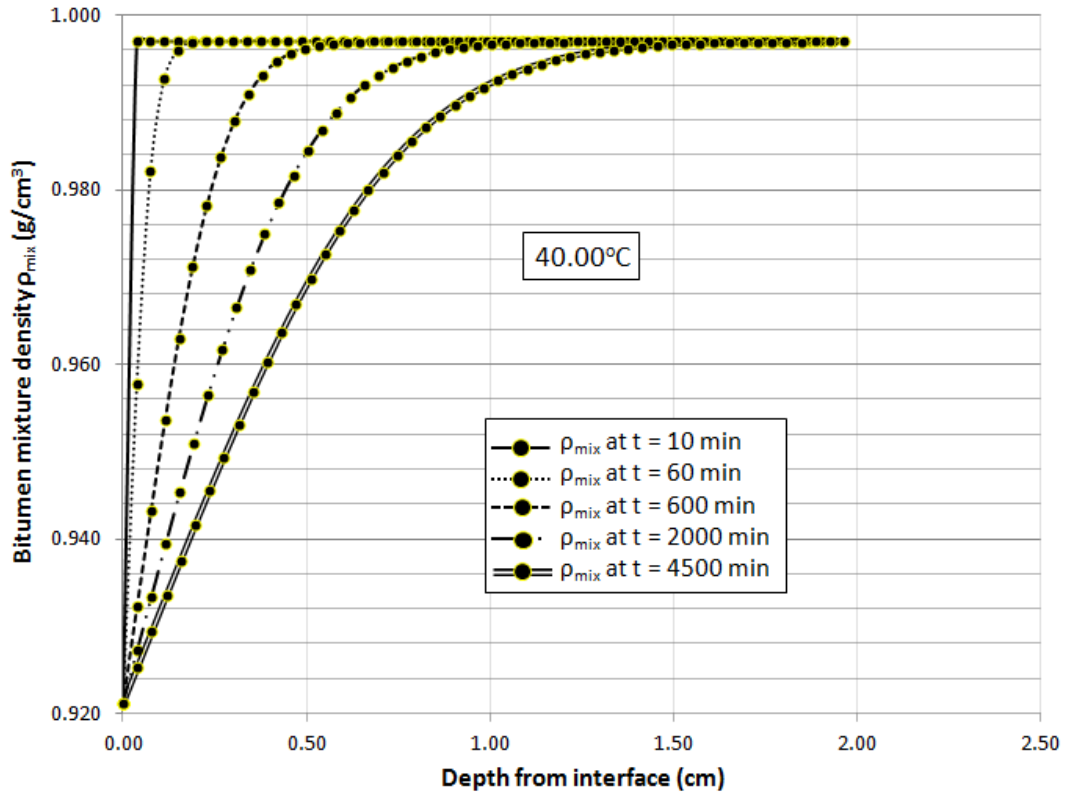
Appendix - K20: Bitumen density profile at 30.25°C (non-ideal)



Appendix - K21: Bitumen density profile at 33.50°C (non-ideal)

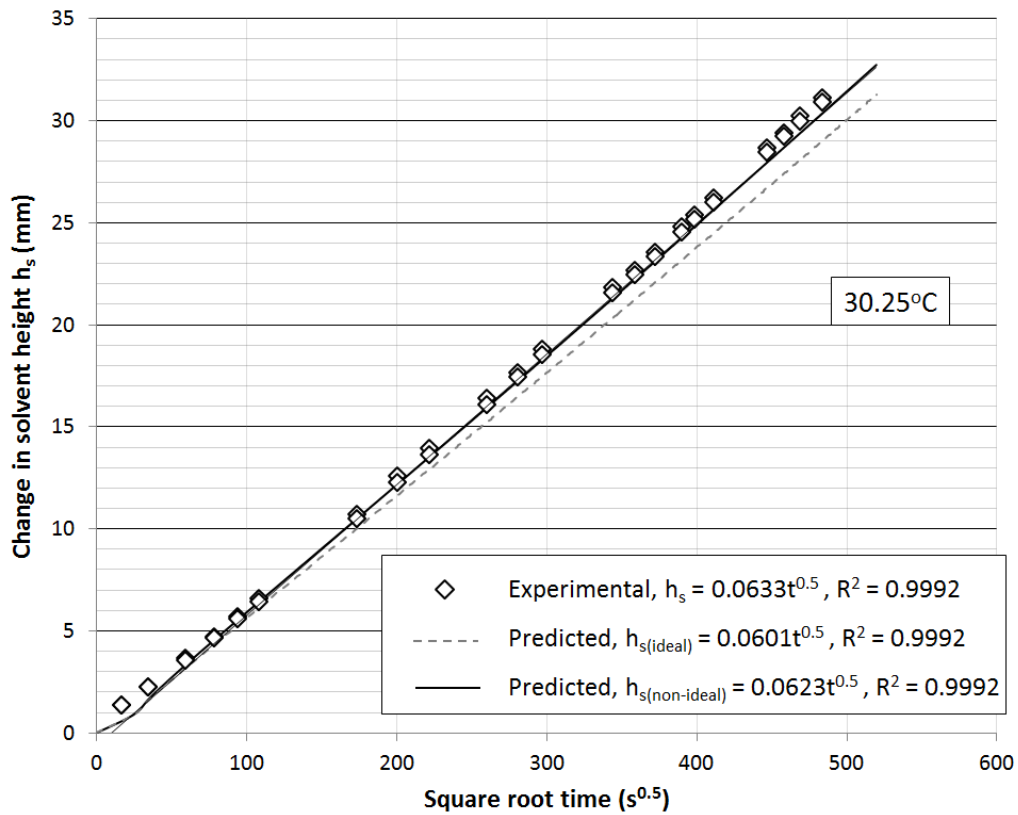


Appendix - K22: Bitumen density profile at 36.75°C (non-ideal)

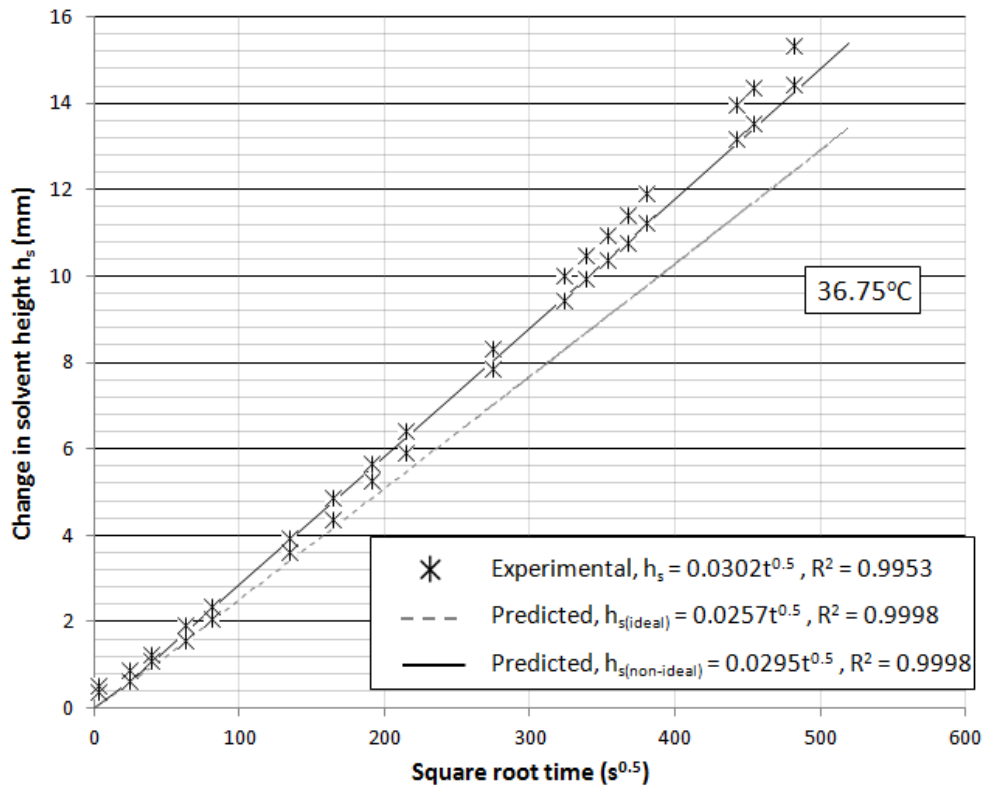


Appendix - K23: Bitumen density profile at 40.00°C (non-ideal)

## APPENDIX L - Extra Validation temperatures data



Appendix - L24: Predicted and experimental change in solvent height vs SRT at 30.25°C



Appendix - L25: Predicted and experimental change in solvent height vs SRT at 36.75°C

Appendix - L26: Validation data for bitumen height increase at all temperatures

Bitumen height increase vs. SRT graph data				
Temperature (°C)		Slope of graph (mm/s <sup>0.5</sup> )	% diff from Experimental values	R <sup>2</sup>
27.00	Experimental values	0.0087	0.0000	0.9934
	Predicted ideal values	0.0087	0.0000	0.9990
	Predicted Non-ideal values	0.0087	0.0000	0.9991
30.25	Experimental values	0.0056	0.0000	0.9974
	Predicted ideal values	0.0056	0.0000	0.9987
	Predicted Non-ideal values	0.0056	0.0000	0.9989
33.50	Experimental values	0.0037	0.0000	0.9981
	Predicted ideal values	0.0037	0.0000	0.9982
	Predicted Non-ideal values	0.0037	0.0000	0.9987
36.75	Experimental values	0.0024	0.0000	0.9956
	Predicted ideal values	0.0024	0.0000	0.9978
	Predicted Non-ideal values	0.0024	0.0000	0.9986
40.00	Experimental values	0.0018	0.0000	0.9886
	Predicted ideal values	0.0018	0.0000	0.9976
	Predicted Non-ideal values	0.0018	0.0000	0.9986